Antonio Rendón Romero

Fibre Optic Sensors with Biologically Active Coatings for the Detection of Cells

Centre for Engineering Photonics
School of Aerospace, Transport and Manufacturing

PhD Thesis

Academic Year: 2015 - 2019

Supervisors: Prof. Stephen W. James
Prof. Ralph P. Tatam
Dr. Matthew Partridge

May 2019

This thesis is submitted in partial fulfilment of the requirements for the Degree of Doctor of Philosophy

Abstract

The purpose of this thesis is to develop a rapid, sensitive and selective optical sensor for *Campylobacter jejuni* detection as it is the most common cause of foodborne illness in humans. The optical sensor platform was based on the optical fibre long period grating (LPG). The LPG fabrication technique chosen was the point-by-point method, involving the UV irradiation of photosensitive doped optical fibre. This technique allows the tailoring of the sensor platform to the requirements of the application. Polyclonal antibodies were selected as the material which can selectively immobilise bacterial cells on to the surface of the fibre optic. Methodologies for reliable and repeatable coating of this material (antibodies) onto the surface of the sensor platform were developed. Two methods to integrate the antibodies to the surface of the fibre, adsorption and covalent binding, were explored. Bovine serum albumin was selected as the material to block the sites on the surface of the fibre not covered by the antibodies, with the aim to prevent non-specific adsorption. The sensor was tested in a direct assay using bacterial samples at different concentrations. The sensitivity of the sensor was evaluated using different concentrations of the target bacteria in a direct assay and multiple repetitions, achieving a limit of detection of 10^4 and 10^3 CFU/mL (colony-forming unit (CFU), a measure of viable cells in a sample) for the sensor created using adsorption and covalent binding of antibodies, respectively. The selectivity of the sensor was explored by testing the sensor against different bacteria in a direct assay and multiple repetitions. The response of the sensor was 100% for *Campylobacter jejuni* (target bacteria), 22.77% for *Listeria monocytogenes*, 9.47% for *Salmonella typhimurium* and 3.01% for *Escherichia coli*. The enhancement of the sensitivity of the sensor using cell staining was explored. Cell staining induces a change in the refractive index of the cell, enhancing the signal detected, improving the limit of detection by one order of magnitude to 10^2 CFU/mL.

Acknowledgments

First of all, I would like to express my sincere gratitude to my supervisor, Prof. Stephen James for his invaluable support, help, patience and guidance throughout the entire project. I also appreciate the support and guidance from Dr. Matthew Partridge, especially in the very first experiments and lab work. I would like to thank sincerely Prof. Ralph Tatam for his support, direction and suggestions that undoubtedly helped me to improve the work. I am grateful for the fact that thanks to the support of my three supervisors I never walked without a compass in the path of the PhD.

I want to thank Stephen Staines for his help, fabricating many of the items used in this thesis. I also acknowledge Noor Masdor and Prof. Ibtisam Tothill for providing the bacterial cells and the antibodies for the development of this work as well as Roberta D'Aurelio for sharing the lab and some of her chemical reagents.

I am also grateful to all members of the Centre for Engineering Photonics for the fellowship and excellent work environment. My special thanks to James Barrington, Nick Davis, Alex Tothill and Evangelos Rigas, with whom I not only shared office and laboratories, but also honoured me with their friendship.

I gratefully acknowledge funding from the Mexican National Council for Science and Technology (CONACYT) and the Centre for Engineering Photonics from Cranfield University.

Last but not least, I would like to thank the unconditional support from my wife, my parents, my siblings and my friends. The culmination of this thesis would have been impossible without their encouragement.

Dedicated to my parents and Regina

Contents

List of Figures

List of Tables

List of Acronyms

ACS American Chemical Society.

AFM Atomic force microscopy.

AM Amplitude mask.

APTES 3-Aminopropyl-triethoxysilane.

APTMS 3-Aminopropyl-trimethoxysilane.

ATP Adenosine triphosphate.

ATR Attenuated total reflection.

BSA Bovine serum albumin.

CFU Colony-forming unit.

DAPI 4',6-diamidino-2-phenylindole.

DDA 3,3'-dithiodiglycolig acid.

DI De-ionized.

DNA Deoxyribonucleic acid.

EDC N-(3-dimethylaminodipropyl)-N'-ethylcarbodiimide.

ELISA Enzyme-linked immunosorbent assay.

ESEM Environmental scanning electron microscope.

Fab Fragment antibody.

FBG Fibre Bragg grating.

Fc Fragment crystallizable.

FFT Fast Fourier transform.

GA Glutaraldehyde.

HPLC High-performance liquid chromatography.

IBD Inflammatory bowel disease.

Ig Immunoglobulin.

IPA Isopropyl alcohol, isopropanol.

LPG Long period grating.

LPS Lipopolysaccharide.

MARDI Malaysian Agricultural Research and Development Institute.

MIP Molecularly imprinted polymer.

MPTMS (3-Mercaptopropyl) trimethoxysilane.

MRSA Methicillin-resistant *Staphylococci aureus*.

MSSA Methicillin-sensitive *Staphylococci aureus*.

MZI Mach-Zehnder interferometer.

NA Numerical aperture.

Nd:YAG Neodymium-doped yttrium aluminium garnet.

NHS N-hydroxy-succinimide.

NHSS N-hydroxy-sulfosuccinimide.

OCT Optical coherence tomography.

PBS Phosphate buffered saline.

PCR Polymerase chain reaction.

PFU Plaque forming unit.

PI Propidium iodide.

PLA Polylactic acid.

PMTP Phase matching turning point.

PTFE Polytetrafluoroethylene.

QCM Quartz crystal microbalance.

RE Recognition element.

RIA Radioimmunoassay.

RMS Root mean square.

RNA Ribonucleic acid.

SELEX Systematic evolution of ligands by exponential enrichment.

SPR Surface plasmon resonance.

TFG Tilted fibre grating.

TIR Total internal reflection.

TNBS 2,4,6-Trinitrobenzene sulfonic acid.

UK United Kingdom.

USA United States of America.

Chapter 1

Introduction

1.1 Rationale, aims and objectives for this research

Campylobacteriosis is one of the most commonly reported bacterial infections in humans [1]. It is caused mainly by four species of *Campylobacter*: *upsaliensis*, *lari*, *coli* and *jejuni*, collectively referred to as *Campylobacter* species (spp). Of these species, *Campylobacter jejuni* is the most reported in human diseases [2]. The main route of transmission is foodborne, via undercooked meat and meat products, as well as raw contaminated milk [3]. Contaminated water and ice are also sources of campylobacteriosis [4]. Although campylobacteriosis is considered to be a mild illness, it can be mortal for children and the elderly, with fatality rates ranging from 0.01% to 8.8%, depending on the country [5, 6]. As an example, in the United States of America (USA) the estimated annual number of illnesses related with *Campylobacter* spp. was 845,024, with 8,463 hospitalizations and 76 deaths [7]. Furthermore, the sequels that may occur after campylobacteriosis include Guillain-Barré syndrome [8], reactive arthritis [9] and irritable bowel syndrome [10]. A summary of the clinical importance of *Campylobacter* spp. in both gastrointestinal and extragastrointestinal infections in humans is presented in Table 1.1.

Furthermore, the annual economic cost of treating campylobacteriosis, including hospitalization costs, in developed countries such as Switzerland (€45 million [12]), the United Kingdom (UK) (£50 million [13]) and the USA ($1,560 million USD [7]) has increased in the last decade [14], becoming greater in developing countries with a higher occurrence rate [15]. Fig. 1.1 summarises the global incidence and prevalence of campylobacteriosis (detailed information can be found in [14]).

A mean concentration of 9 x 10^4 CFU/mL (colony-forming unit (CFU), a measure of viable cells in a sample) has been determined to be the dose of *C. jejuni* required for a human to develop campylobacteriosis [16]. However, a human experimental study revealed that doses as low as 800 CFU can cause the illness in young healthy adults [17]. Taking into consideration the high contamination level of *Campylobacter jejuni* in poultry products (approximately 10^3 CFU/g [18, 19], 10^3-10^4 CFU/plate [20], 5x10^8 CFU/mL [21]), unpasteurized milk (6.4x10^7 CFU/mL [21]) and water (10^3-3.2x10^8 CFU/mL [22]), contaminated food can provide the necessary doses to develop the disease in humans.

Methods currently employed to detect *Campylobacter* in water samples or food

Table 1.1: Clinical repercussions of *Campylobacter* species on human health. Modified from [11]. Abbreviations used: (IBD) Inflammatory bowel disease, (−) No associated disease in humans has been reported.

Campylobacter spp.	Gastrointestinal diseases	Extragastrointestinal condition
C. avium	–	–
C. canadensis	–	–
C. coli	Gastroenteritis, acute cholecystitis	Bacteremia, sepsis, meningitis, spontaneous abortion
C. concisus	Gastroenteritis, IBD, Barrett esophagitis	Brain abscess, arthritis
C. cuniculorum	–	–
C. curvus	Gastroenteritis, elcerative colitis, liver abscess, Barrett esophagitis	Bacteremia, bronchial abscess
C. fetus	Gastroenteritis	Abscess, meningitis, bacteremia, vertebral osteomyelitis, cellulitis, septic abortion
C. gracilis	Crohn's disease, ulcerative, colitis, peridontitis	Head and neck infection, brain abscess
C. hominis	Crohn's disease, ulcerative colitis	Bacteremia
C. helveticus	Diarrhea	No association reported
C. hyointestinalis	Diarrhea	Fatal septicemia
C. insulaenigrae	Gastroenteritis, abdominal pain, diarrhea and vomiting	Septicemia
C. jejuni	Gastroenteritis, IBD, celiac disease, acute cholecystitis	Guillain-Barré syndrome, sepsis, Miller-Fisher syndrome, bacteremia, meningitis, reactive arthritis, urinary tract infection and hemolytic uremic syndrome
C. lanienae	–	–
C. lari	Gastroenteritis	Pacemaker infection and bacteremia
C. mucosalis	Gastroenteritis	No association reported
C. perioridis	–	–
C. rectus	Gastroenteritis, Crohn's disease, ulcerative colitis	Necrotizing soft tissue infection, empyema thoracis
C. showae	Crohn's disease, ulcerative colitis	Intraorbital abscess
C. sputorum	Gastroenteritis	Axillary abscess
C. subantarcticus	–	–
C. troglodytis	–	–
C. upsaliensis	Gastroenteritis	Breast abscess, bacteremia, spontaneous abortion
C. ureolyticus	Gastroenteritis, Crohn's disease, ulcerative colitis, oral and perianal abscesses	Soft tissue abscesses, ulcers, arthritis, gangrenous lesions of the lower limb
C. volucris	–	–

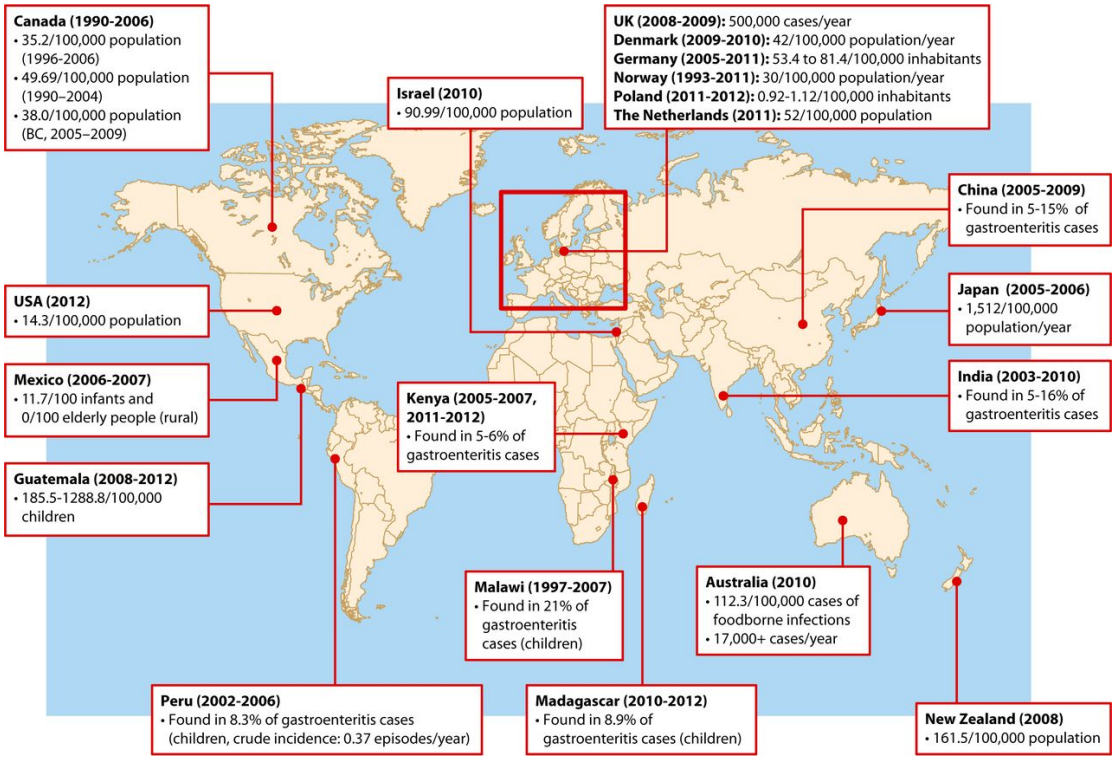

Figure 1.1: Global incidence and prevalence of campylobacteriosis. Image from [14].

can take several days to produce results and involve a precise process requiring highly trained staff [5]. The research gap is the lack of a rapid, sensitive and selective bacterial sensor for *Campylobacter jejuni*. In this project, this has been addressed by developing an optical fibre based bacterial sensor. Optical sensors offer a faster alternative to traditional methods for bacterial detection thanks to ease of integration of recognition elements with the sensing platform and the ability to measure directly the receptor-analyte interaction. Among the most explored fibre-optic sensing platforms for chemical and biological applications are long period gratings (LPGs). The transmission spectrum of an LPG is sensitive to target analyte induced changes in the optical properties of a recognition element bound to the surface of the fibre. In this case, the recognition element is rabbit polyclonal antibody against *Campylobacter jejuni*. As is demonstrated in this thesis, the use of antibodies as recognition elements provides high selectivity and sensitivity, which can be further enhanced by using cell staining protocols.

The aim of this project is to combine fibre optic sensors with biologically active coatings for the sensitive and selective detection of bacterial cells and to develop methods for enhancing the sensitivity using approaches such as cell staining.

The specific objectives for the research are:

1. Fabrication and characterisation of the LPG sensing platform.
2. Selection of a suitable recognition element.
3. Development of a methodology for the reliable and repeatible deposition of the recognition element.

4. Evaluation of the sensor's response at different concentrations of *Campylobacter jejuni* cells with a direct assay.

5. Establish the sensitivity, limit of detection and selectivity.

6. Explore the enhancement of the sensitivity of the sensor using cell staining methods.

The intellectual contributions of this project include the methodologies developed for coating the surface of the sensing platform with polyclonal antibody against *Campylobacter jejuni*, the sensitive and selective detection of the bacterial cells at concentration as low as 10^3 CFU/mL, which matches the requirements for the detection of harmful concentrations of the bacteria, and the bacterial staining of the cells attached onto the surface of the optical fibre, which enhanced the limit of detection by an order of magnitude to 10^2 CFU/mL.

1.2 Structure of the thesis

This thesis begins with a description of the rationale, aims and objectives for this research (Chapter 1). Following the introduction, Chapter 2 provides reviews of the literature pertinent to the various technologies exploited in this thesis. First, a review of the methods for bacterial detection is reported. Then, as the selected sensing platform, a review of long period gratings (LPGs) is described. Subsequently, a review of the most widely used recognition elements for the development of sensors for bacterial detection and a review of the methods to immobilize them on the surface of the sensing platform are presented. To finish the review chapter, different methods for cell staining, emphasizing their suitability for staining *C. jejuni* cells, are presented. Since this thesis involves a multidisciplinary topic, in addition to reviewing the prior work in the respective areas, the review chapter describes key procedures, introduces the terminology employed in the different research areas and defines concepts used in the subsequent chapters. Following the literature review, three experimental chapters related to the fabrication of the optical fibre sensing platform, the functionalization of the surface of the optical fibre and the testing of the performance of the sensor against the target and non-target bacteria are presented (Chapter 3, 4 and 5). Finally, the conclusions of the thesis and an outlook for future work are presented in Chapter 6.

The content of the individual chapters of this thesis is as follows:

Chapter 1 contains the rationale, aims and objectives for this research and a description of the structure of this thesis.

Chapter 2 provides an overview of the established methods, both traditional and modern, for bacterial detection, emphasizing the detection of *Campylobacter jejuni*. Within the modern methods, a review of LPGs, as a promising sensing platform, is provided. This chapter also reviews the main elements and the different strategies employed to accomplish surface coating for the development of sensors for bacterial detection. Finally, a review of cell staining methods, as a means to enhance the sensitivity of the sensor, is provided.

Chapter 3 describes the fabrication of LPGs by the point-by-point technique and the development of software for the analysis of the experimental data.

Chapter 4 covers the different stages of the fabrication of the sensor, including the cleaning of the surface of the fibre, surface activation and surface coating. This chapter also presents the design and optimization of the sample container used to accommodate the LPG sensor for the incubation stages.

Chapter 5 presents the experimental results of the bacterial detection using a direct assay. The responses of the sensor to different concentrations of the target bacteria (*Campylobacter jejuni*) are presented. The specificity of the sensor, investigated by testing the sensor against non-target bacteria, is presented. The sensitivity of the sensor, enhanced by bacterial staining, is evaluated.

Chapter 6 summarises the results and conclusions of this research. An outlook for future work and further improvements is proposed.

A flow chart of the thesis structure is depicted in Fig. 1.2.

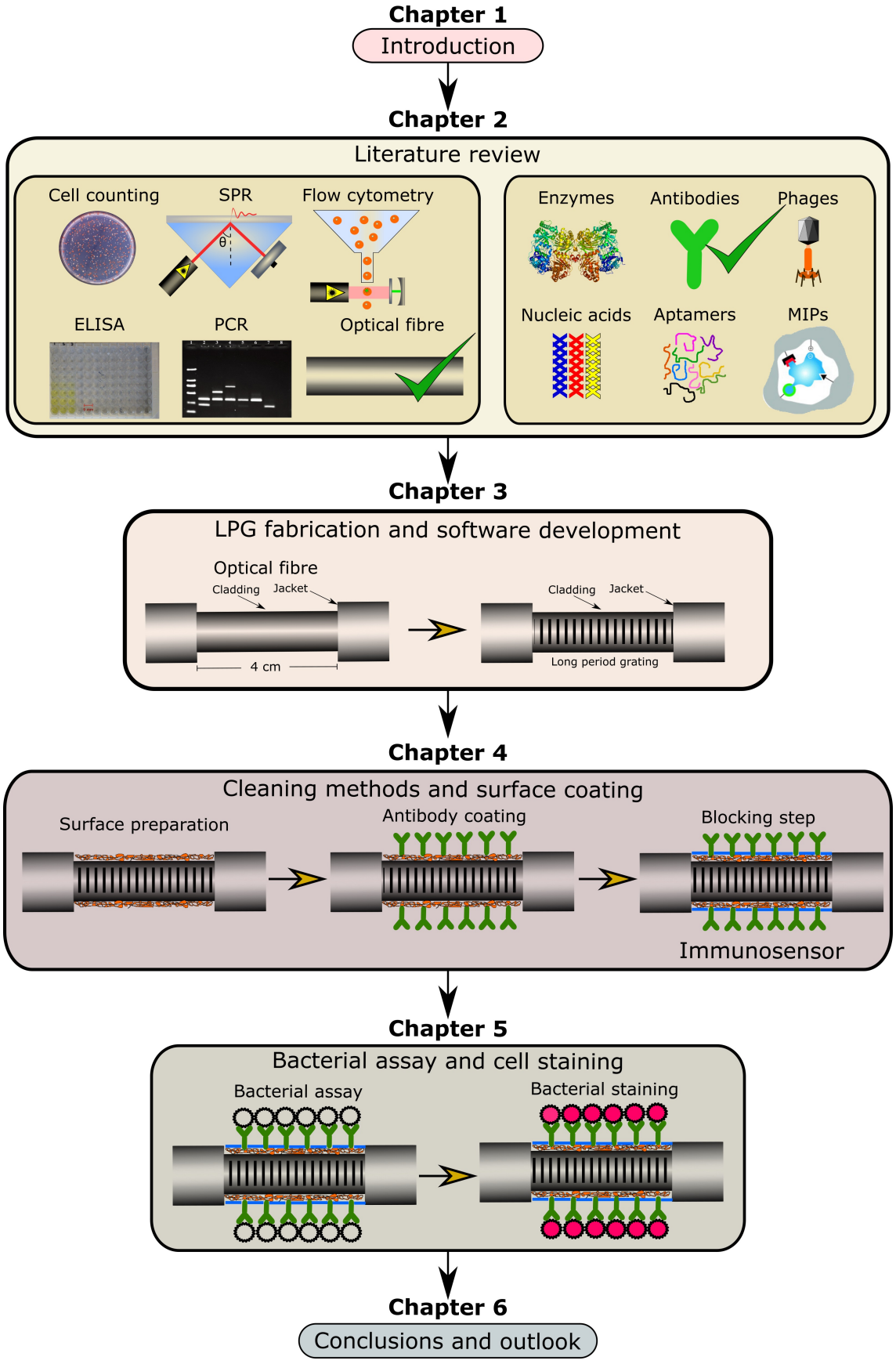

Figure 1.2: Structure of the thesis.

Chapter 2

Literature Review

2.1 *Campylobacter jejuni*: The target bacteria

The *Campylobacter* genus consists, to date, of 25 species (listed in Table 1.1), two provisional species (*C. Dolphin* and *C. Prairie Dog*) and 8 subspecies. *Campylobacter* species are Gram-negative and morphologically diverse bacteria, as they can present spiral, rod, or curved shapes [11]. Spherical forms (coccoid shapes) are common in old cultures. *Campylobacter* species have an approximate size of 0.2 to 0.8 by 0.5 to 5 μm, can present or not, unipolar or bipolar flagellae, and do not present spores [14]. Particularly, *C. jejuni* present bipolar flagellae and capsule [23, 24]. Depending on the species, *Campylobacter* can grow under anaerobic or aerobic conditions [11]. *Campylobacter* exhibit a slow growth (72-96 h for primary isolation), growing better between 37°C and 42°C [1]. Despite having a minimum growth temperature of 30°C and a maximum of 46°C, *Campylobacter* can be active at low temperature and be capable of surviving under refrigeration. For instance, *C. jejuni* cells, shown in Fig. 2.1, exhibit metabolic activity such as oxygen consumption, catalase activity, adenosine triphosphate (ATP) generation and protein synthesis even at 4°C [25]. On the other hand, despite having a moderate cold resistance, *Campylobacter jejuni* is more sensitive to heat, acid and drying than other food-borne bacteria [26].

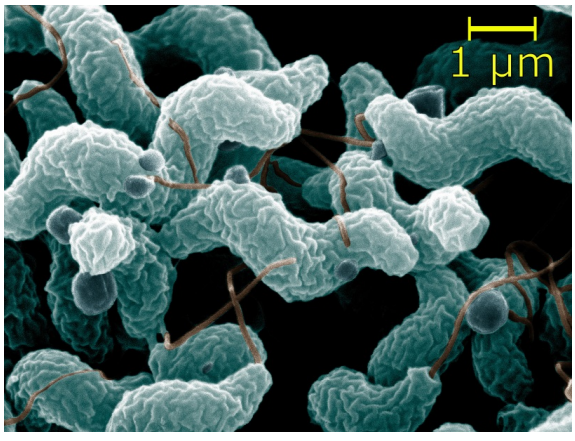

Figure 2.1: Digitally coloured scanning electron microscope image of *Campylobacter jejuni* bacterial cells. Photo from [27].

Reports of the clinical impact of *Campylobacter* on human health date back to circa 1938, when *Vibrio jejuni* (nowadays known as *Campylobacter jejuni*) provoked an outbreak due to its presence in raw milk [28]. However, cases of abortion in pregnant ewes associated with *Vibrio fetus* were reported in 1913 [29], and cases of intestinal disorders in cows associated with *Vibrio jejuni* were reported later in 1931 [30]. In 1963, the genus *Campylobacter* was proposed and defined as a Gram-negative, curved and motile bacteria with a strictly respiratory metabolism, which produces no acid in media with carbohydrates, and which has deoxyribonucleic acid (DNA) with content between 29 and 36% of nitrogenous bases guanine-cytosine. Unlike *Campylobacter*, the genus *Vibrio* comprises bacteria that ferment glucose and contain DNA with guanine-cytosine content between 40 and 53% [29]. Nowadays, *Campylobacter jejuni* is one of the most reported causes of diarrhea illness in humans [25], with poultry being the main source of the infection [3]. The symptoms usually occur within the first 24-72 h after ingestion [14]. The illness lasts an average of 6 days, with over 80% of patients reporting fever and muscular spasms [11]. Despite efforts to control the transmission of pathogens, the prevalence of *Campylobacter*-related infections has increased globally. The rise may be due to, but not limited to, the ability to detect the bacteria and the failure to prevent its transmission effectively [14].

2.2 Review of methods for bacterial detection

The cell is the fundamental unit of structure and function in all living organisms. Despite their countless beneficial functions, cells also can be harmful or be part of pathogenic organisms. Consequently, there is a vast demand for fast and cost-effective analytical techniques to detect and monitor a wide range of cells in clinical, environmental and industrial applications [31]. Biosensors are promising tools for the rapid and accurate detection of pathogens and other biomolecular interactions in these fields [32, 33]. A biosensor can be defined as a device that measures the interaction between the recognition element (also known as bioreceptor) and the target analyte through the transducer, which transforms the interaction to a measurable signal that is converted into a readout or display by the signal processing system [34]. In the development of a sensor for biochemical applications, the selection of the solid support, i.e. the transducer's surface, for the further deposition of the biochemical material that will act as recognition element is an important step [33]. In general, desirable properties of the solid support are a high surface-to-volume ratio, high protein-binding capacity, compatibility with and insolubility in the reaction medium, high mechanical and chemical stability, recoverability after use and conformational flexibility [35].

For the aims of this project, a comprehensive literature review has been carried out. As the published literature related to pathogen bacteria is extensive, this review was focused on the detection, identification and quantification aspects of the established methods for bacterial detection, especially the detection of *Campylobacter jejuni*.

In this section, the main methods for cell detection will be reviewed, including both traditional and modern methods. Table 2.1 summarizes the main methods used

for cell detection.

Table 2.1: Overview of the main methods for cell detection

Traditional methods	Culturing		
	Microscopic examination		
Modern methods	Immunological methods	ELISA	
	Nucleic acid assays	PCR	
	Optical methods	Optical fibre based sensors	Gratings
		Other techniques (Non-optical fibre based sensors)	Flow cytometry ATP bioluminescence SPR

2.2.1 Traditional methods

Traditional cell detection procedures, such as culture, direct counting and microscopic examination, have the advantages of being very sensitive and of being capable of providing both quantitative and qualitative details of the specimen [36]. On the other hand, these methods are time consuming (up to 1 week), since organisms have to be isolated, i.e. transferred from their ecological niche (e.g. water stream), transient vehicle (e.g. food), or storage medium (e.g. stock culture), into a growth-permitting laboratory medium [37]. The inoculated medium is then incubated under optimum growth conditions and for a suitable length of time to allow cell multiplication, resulting in a culture of the organism. Further biochemical assessment must be completed for identification [38, 39, 40]. Additionally, these microbial methods must be performed by skilled personnel [41]. Bacterial pathogens detected in water, food, blood, tissues and other body fluids are generally present at concentrations below 10^3 colony-forming unit (CFU) per millilitre or gram [42]. CFU is a unit used in microbiology to estimate the number of viable (capable of living and reproducing) cells in a sample. When CFUs are unable to reproduce under suitable conditions, they are indicated as killed or inactivated. A colony represents an aggregate of cells derived from a single progenitor cell. [43]. However, CFU is not a measure for individual cells as a colony is usually formed by a conglomerate of them. Simple microbiological cultures, such as direct plating on selective media agar, are not able to detect these values due to the interference of the matrix (water, blood, etc.), or

the inherent detection limitation of the technique. In this case, it is necessary to enrich the sample with the pathogen of interest to levels detectable by the analytical method [44].

The prevalence of pathogen bacteria in chickens purchased from retail outlets in England between 1998 and 2000 was studied using direct enumeration methods [45]. Concisely, *Campylobacter* spp. and *Salmonella* samples from 241 whole raw chickens were isolated from the carcass and packaging. The isolation of *Campylobacter* spp. was then enriched at 37°C for 48 h using a modified Exeter Broth containing Nutrient broth, *Campylobacter* Growth Supplement, *Campylobacter* Selective Supplement and lysed defibrinated horse blood. The confirmation was carried out by examination of cell morphology using Gram-staining and microscopy. The study found higher levels of *Campylobacter* spp. in the carcass than in neck-skin samples, being *C. jejuni* in 98% of them, with only 2% of the samples containing *C. coli*. The limits of detection for *Campylobacter* spp. by direct enumeration was 500 CFU for the neck-skin samples and entire packing, while for the carcass plus neck-skin samples it was 600 CFU.

Recent advances in microbiology, chemistry and other disciplines have resulted in the development of more rapid and less expensive methods for cell detection, with a progressive advance in terms of sensitivity and accuracy. These methods are also called modern, rapid or/and alternative methods.

2.2.2 Immunological methods

The immune system consists of proteins, cells and organs that are concerned with defence of the individual, primarily against the threat of disease caused by infectious organisms, called pathogens, such as bacteria, viruses, parasites and fungi. Lymphocytes are a type of white blood cell that form part of the immune system. One specific kind of lymphocyte, called the B lymphocyte, is responsible for the production of glycoproteins that have the ability to recognise foreign molecules on the surface of pathogens. These glycoproteins are called immunoglobulins or more colloquially, antibodies [46]. For further information about antibodies, please refer to section 2.4.2.
Briefly, immunological methods are based on the attachment of a specific antibody to a specific molecule, termed an antigen [47]. Immunoassay refers to the qualitative and quantitative determination of antigen and antibody in a sample by immunological reaction [48]. In other words, immunoassays make specific and sensitive measurements of target analytes by exploiting the high specificity of the antibody-antigen interaction [49].

ELISA

The enzyme-linked immunosorbent assay (ELISA) is the most representative example of an immunological test and relies on the use of specific antibodies to bind the target antigen, and on the detection system to indicate the presence and quantity of antigen binding.

It was developed in 1971 by Engvall and Perlman [50]. They purposed the ELISA method by labelling the antigen with a suitable enzyme instead of a radioactive isotope, in order to determine the levels of IgG in rabbit serum. At that time, radioimmunoassay (RIA) techniques for the quantitative determination of antigen were in apogee. They were based on radioactively labelled antigen and antibodies, covalently attached to cellulose or gel [51]. However, the drawbacks were the high cost of equipment and the short half-lives of the antibodies labelled with radioactive isotopes. Around the same time, techniques for labelling antibodies with enzymes were described for immunohistochemistry applications [52]. Engvall and Perlman modified the RIA method by labelling antibodies with an enzyme for a serological assay. The advantages of this method were that the antibody-enzyme conjugation was stable and the equipment required was simpler than that needed for radioactivity studies.

In the ELISA, the enzymes catalyse chemical reactions involving substrates. A substrate is a substance that is affected by the action of a catalyst; for example, the substance upon which an enzyme acts in a biochemical reaction [53]. A substrate is called colorimetric (also called chromogenic) if it produces a coloured product when it reacts with an enzyme. The immobilization of the target antigen is usually done in 96-well polystyrene plates, shown in Fig. 2.2. The substrate binds to the active site of the enzyme, and an enzyme-substrate complex is formed. By the action of the enzyme, the substrate is transformed into a product, is released from the active site and is free to receive another substrate. The coloured readout produced by the enzyme is read typically on a spectrophotometer operating with wavelength range 400-600 nm [54].

ELISA can be performed with a number of modifications to the basic concept: direct, indirect, sandwich and competitive.

Direct ELISA. The direct ELISA is considered to be the fastest and simplest type of assay. In this test, the target antigen is adsorbed onto a well plate, and the rest of binding sites in the well plate not covered by the target antigen are then blocked with another protein, usually bovine serum albumin (BSA). In a separate reaction, the antibody is linked to an enzyme, usually alkaline phosphatase, horseradish peroxidase, or β-galactosidase. Then, the plate is incubated with the enzyme-conjugated antibody, followed by a washing step to remove the excess of (or non-bound) enzyme-conjugated antibody. Finally, a substrate (o-phenyldiamine dihydrochloride for peroxidase, or p-nitrophenyl phosphate for alkaline phosphatase) is added and then catalyzed by the enzyme, producing a coloured readout. This assay is used to test specific antibody-antigen reactions. Fig. 2.3 illustrates the ELISA direct assay.

The direct assay, compared with other ELISA assays, possesses the advantages of being fast and simple, as it has fewer steps and inherent null cross-reactivity with other antibodies, as only one antibody is involved in the process. The disadvantages of the direct assay are its inflexibility, as each target analyte needs a specific antibody, and the reduced sensitivity of the test, since there is no signal amplification as no secondary antibody is used.

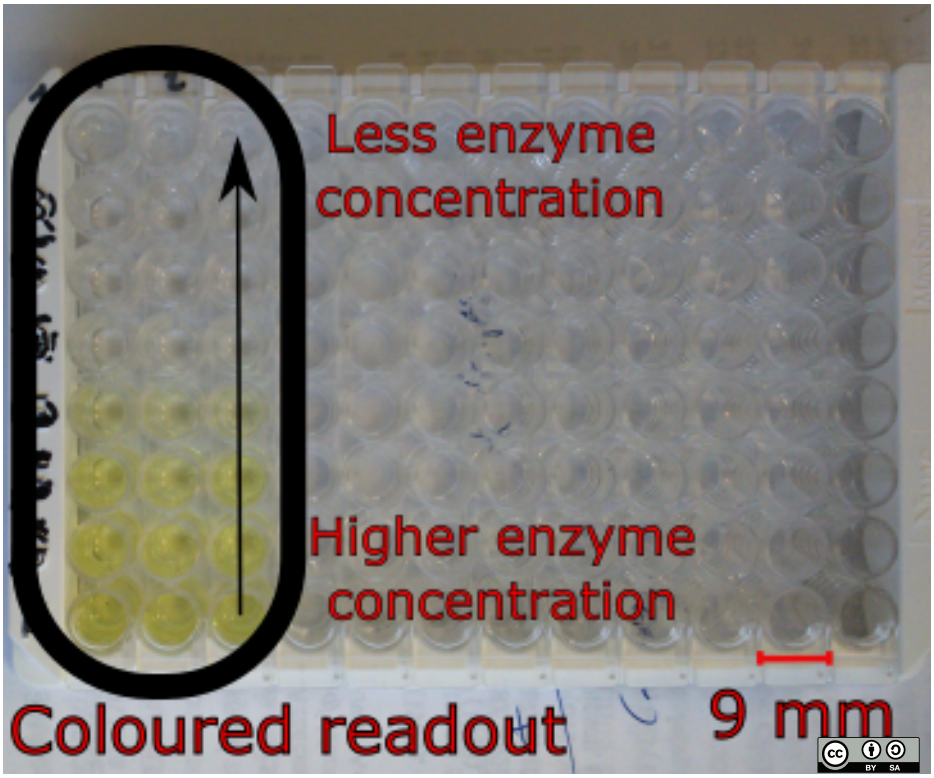

Figure 2.2: ELISA test in a 96-well plate

Indirect ELISA. In the indirect ELISA, the detection of the target analyte is carried out with one more step than is involved in the direct assay. First, the target analyte is adsorbed onto a well plate and then the surface is blocked against non specific binding. The primary antibody is added to the well to bind the target analyte. In a separate reaction, the secondary antibody is labeled with the enzyme. The well is washed to remove the unbound primary antibody and then the enzyme-conjugated secondary antibody is added to bind the primary antibody. Finally, the well is washed and a substrate is added, which is catalyzed by the enzyme and produces a coloured signal. Fig. 2.4 shows the ELISA indirect assay.

The advantages of indirect ELISA are its high sensitivity, as more than one enzyme-conjugated secondary antibody can bind the primary antibody, and greater flexibility, since a single enzyme-conjugated secondary antibody can be used with different primary antibodies. Within the disadvantages of the indirect ELISA are the possibility of cross-reactivity, as the secondary antibody can bind the target antigen, and a longer procedure than the direct assay.

Sandwich ELISA. The sandwich ELISA quantifies the target antigen between two layers of antibodies, as shown in Fig. 2.5. For this reason, the target antigen must have at least two epitopes to bind the different antibodies. First, the capture antibody is immobilized onto the surface of a well plate and then the surface is blocked against non specific binding with a protein, usually bovine serum albumin. In a separate reaction, the detection antibody is linked with an enzyme. The sample containing the target antigen is added to the well plate. The well plate is washed

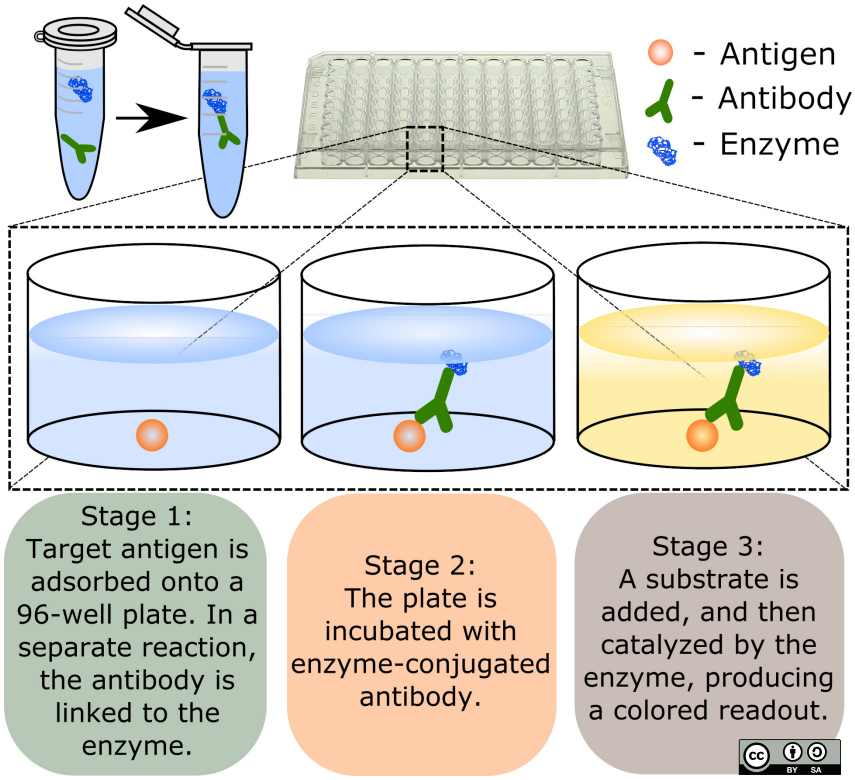

Figure 2.3: ELISA direct assay

with a suitable buffer to remove the unbound antigen. From this step, the sandwich assay can be performed in two ways: direct and indirect. For the direct method, the enzyme-conjugated detection antibody is added to the well plate to bind the antigen. Finally, a substrate is added to the well plate and then catalyzed by the enzyme, producing a coloured signal. On the other hand, in the indirect method, an unlabeled antibody specific for the target antigen is added to the well plate. The plate is washed and then the enzyme-conjugated secondary antibody is added. The unbound antibody is washed. Finally, a substrate is added and then catalyzed by the enzyme, producing a coloured readout.

Magliulo *et al.* [55] reported a sandwich enzyme immunoassay for the detection of *Escherichia coli*, *Yersinia enterocolitica*, *Salmonella typhimurium* and *Listeria monocytogenes* using monoclonal antibodies specific for each bacteria. The limit of detection achieved for each bacteria was in the range of 10^4-10^5 CFU/mL. In the same way, Lilja *et al.* [56] described the detection of *Campylobacter* spp. using ELISA in a sandwich format with two different polyclonal antibodies. The reagents were supplied in a ready-to-use kit and all the steps were performed in an automated instrument (EiaFoss Campylobacter System, Foss Electric, DK 3400). The reported limit of detection was 10^5CFU/mL in about 24 hours. However, in the reported ELISA method, the assay detected thermophilic *Campylobacter* spp. without distinguishing between the different species. For the specific detection of *C. jejuni*, conventional techniques such as culture or amplification techniques such as the polymerase chain reaction (see Sec. 2.2.3) need to be performed, adding at least a couple of days to the overall experimental time.

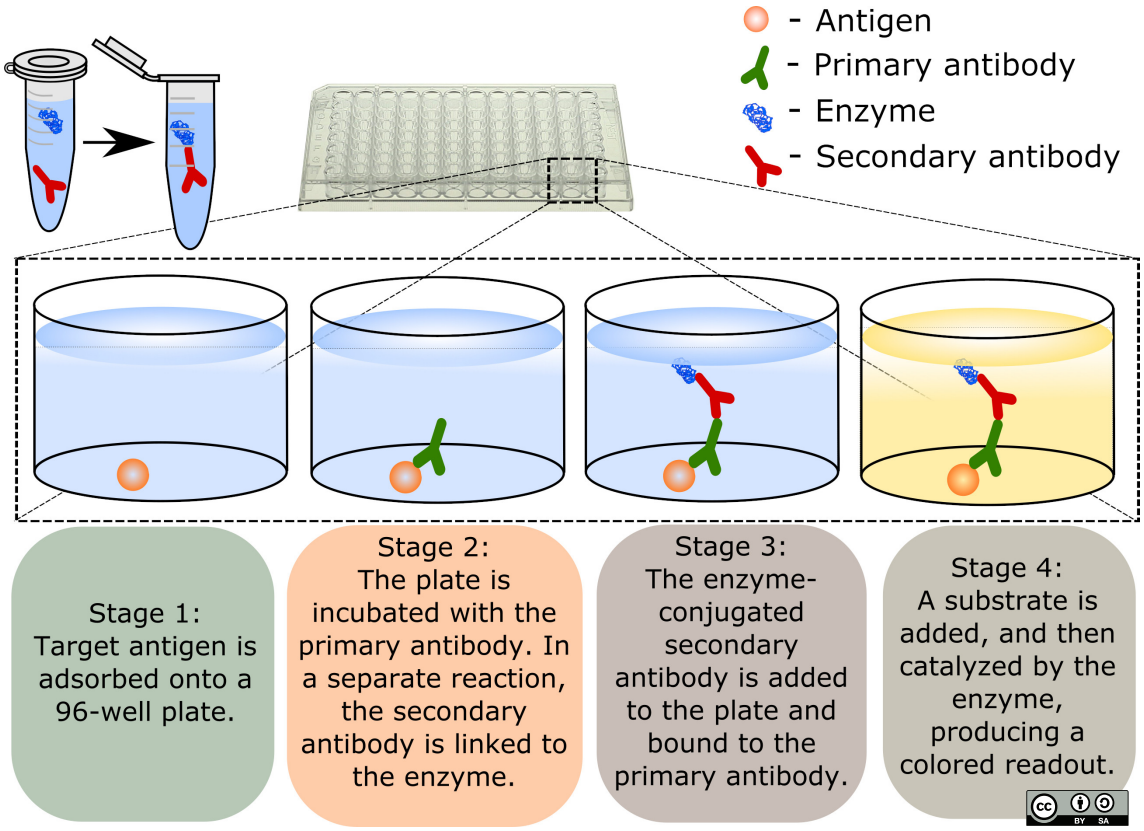

Figure 2.4: ELISA indirect assay

The advantages of sandwich ELISA are its high sensitivity, being 2-5 times more sensitive than the direct or indirect assays [54], high specificity, since two antibodies are involved in the attachment of the target analyte, and great flexibility, as both direct and indirect capture can be performed. The main disadvantage of this method is the possible occurrence of cross-reactivity between the antibodies.

Competitive ELISA The competitive ELISA, also known as inhibition ELISA, is mainly employed to quantify the amount of an antigen (present in both the sample and attached onto the plate) that competes for the binding to the primary antibody. In the competitive ELISA, the target antigen is adsorbed onto a well plate. The excess is washed off and the surface is blocked against non specific binding. In a separate reaction, unlabeled primary antibody is incubated with the sample containing the same target antigen as that incubated onto the plate. At this point, two cases can be observed: i) more antigen in the sample than antibody; and, ii) more antibody than antigen in the sample. If the amount of antigen present in the sample is more than the amount of antibody added, it is more likely that the antigen in the sample captures the antibody, leaving only a small amount of free antibodies to be captured by the antigens attached to the well and vice versa. Later on, the sample containing the primary antibody is added to the well plate. In a separate reaction, the secondary antibody is labelled with an enzyme. The enzyme-conjugated secondary antibody is added to the well and bound to the primary antibody. The unbound antibodies are then washed off. Finally, a substrate is added to the well and

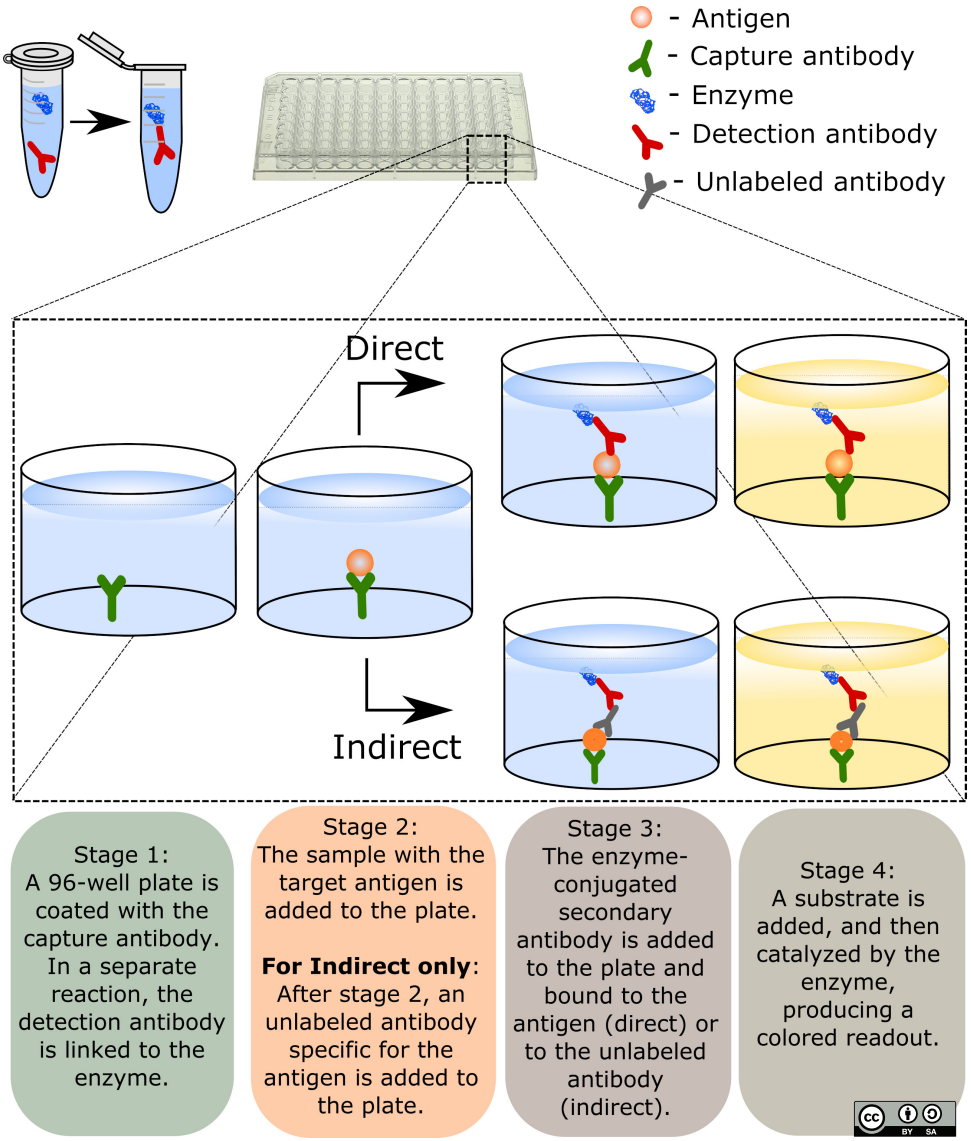

Figure 2.5: ELISA sandwich assay

catalyzed by the enzyme, producing a coloured readout, which depends on the the amount of enzyme available for the reaction. Note that in the competitive ELISA, unlike the other assays, the weaker the signal, the larger the presence of antigen in the sample. In other words, the larger presence of antigen in the sample (more antigen than antibodies in the sample) implies less available primary antibodies to bind the antigen attached to the well plate. This means that after adding the secondary antibody to the well, only a small amount of the two-antibody complex is present in the well. Thus, the amount of enzyme to catalyze the substrate is small and, as a result, the signal is weak. Fig. 2.6 shows an example of the ELISA competitive assay.

The competitive ELISA has a number of advantages that make it an attractive method for bacterial detection, such as its high sensitivity, specificity and flexibility. The high specificity of ELISA is a result of the use of two antibodies to capture and detect the target analyte. In addition, this assay format is highly flexible, as

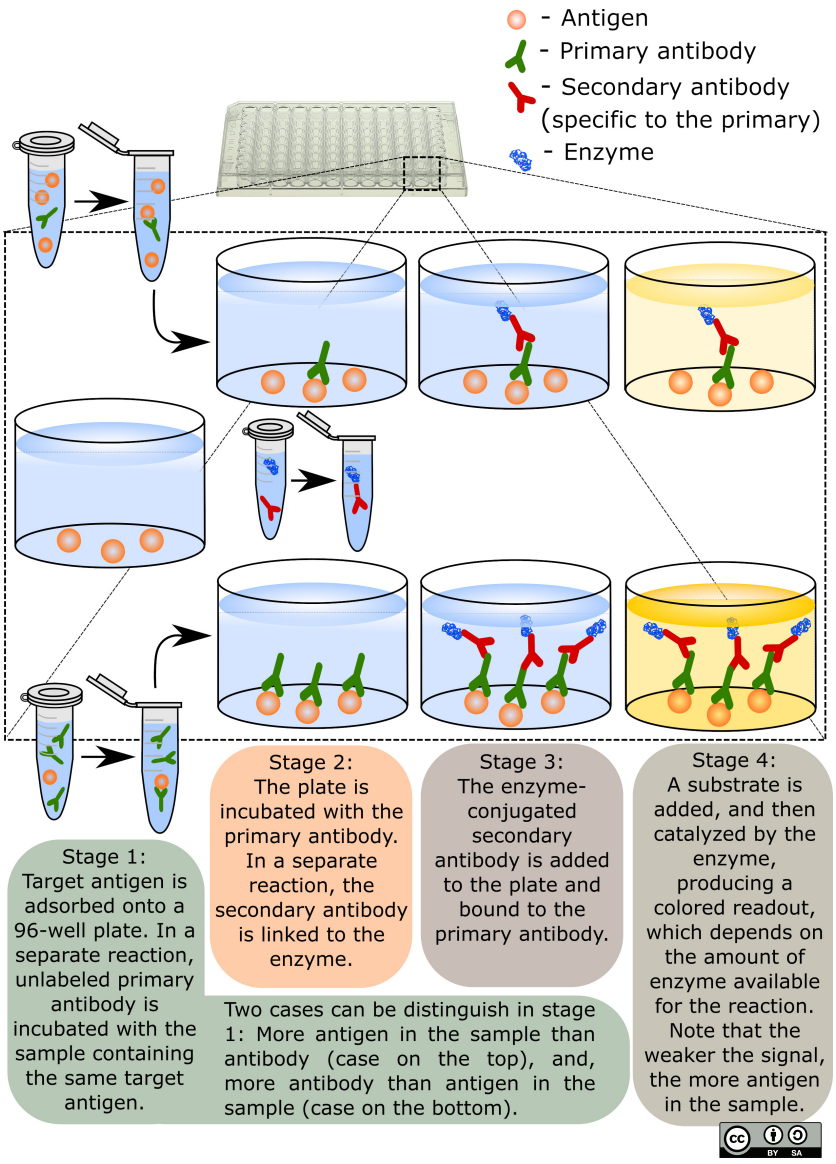

Figure 2.6: ELISA competitive assay

direct, indirect and sandwich formats can be implemented. Furthermore, competitive ELISA has been shown to be more sensitive than indirect ELISA [57]. Finally, the competitive assay is suitable for impure samples, since the target bacteria does not require sample processing. On the other hand, the competitive ELISA shows the same limitations as the base ELISA, as each format can be adapted to the competitive assay.

A competitive ELISA in a direct format for the detection of *Campylobacter jejuni* in poultry samples, using immunomagnetic separation to isolate the target bacteria, was reported by Che *et al.* [58]. Briefly, magnetic beads of different sizes and functional groups were coated with primary (rabbit anti-*C. jejuni*) and secondary (sheep anti-rabbit IgG) antibody. Bacterial samples in the concentration range from 10^3 to 10^8 CFU/mL were incubated in a competitive format and then the magnetic separation was carried out. The electrochemical signal was measured with an electrode modified

with tyrosinase to detect the presence of the phenol generated by the conjugated bacteria. The limit of detection was calculated to be 2.1 x 10^4 CFU/mL.
Competitive ELISA in the indirect format has been performed for the detection of *C. jejuni*, reaching a limit of detection in the range of 5.0 x 10^4-3.2 x 10^6 CFU/mL [59]. Hochel *et al.* [60] reported the immobilization of *Campylobacter jejuni* cells in a well plate. Bacterial detection was achieved using polyclonal chicken IgY and rabbit anti-IgY antibody-horseradish peroxidase conjugate at concentrations of 10 μg/mL and 8 μg/mL, respectively.

Even though immunological methods are faster than traditional methods, they are still time-consuming, since typical enrichment of pathogens takes 16-24 hours [48], and the complete assay around 52 hours [56, 61].

2.2.3 Nucleic acid methods

The use of nucleic acid-based methods to detect bacteria offers a reduced time to diagnosis, accurate and reliable results with increased sensitivity and selectivity over traditional techniques [62]. The development of nucleic acid assays for bacterial detection is based on the isolation of species-specific DNA [63].

PCR

Polymerase chain reaction (PCR) is an amplification technique developed by Mullis *et al.* in 1986, which reproduces multiple copies of a DNA sequence from a DNA fragment, and is representative of nucleic acid assays [64]. Broadly, a thermal cycler is used to generate repeating cycles of heating and cooling to make many copies of a DNA fragment. First, the temperature is raised up to 95 °C to denature the DNA, in other words causing the two strands of DNA to separate. When the temperature is decreased (55 °C), short DNA sequences bind and complementarily matches the target DNA sequence, enriching with the new DNA material. When the temperature is slightly increased (72 °C), an enzyme, commonly Taq (Thermis aquaticus) DNA polymerase, synthetizes and expands the DNA sequence creating an amplified DNA target and completes the first cycle, which is then repeated several times. The advantages of this technique are its high sensitivity, specificity and rapidity (compared with traditional methods) [65]. The assay provides results in 2 days and the reported limits of detection for *Campylobacter jejuni* are in the range between 10^1-10^5 CFU/mL [58, 66, 67], which can be reduced to 10-100 CFU/mL [63, 65] if sample pre-enrichment is carried out. Usually, the limit of detection of PCR techniques is related to the enrichment [58, 67]. However, many limitations are present. One of them is the generation of false positives due to its sensitivity to environmental contaminants, which demands a confirmation test from a traditional method, increasing the overall test duration [68]. In addition, the use of PCR for the detection of pathogenic cell is complicated and requires highly trained staff [39]. One more disadvantage of PCR assays is the high cost of the equipment (prices ranging from ∼$32,000 USD [69] to ∼$195,000 USD [70]) and the inability to distinguish between viable and non-viable cells, since DNA is intrinsically present in cells [71]. Compared with ELISA, PCR shows a higher sensitivity[72, 73, 57]

(See Table 2.3). Winters *et al.* reported the detection of *Campylobacter jejuni* in artificially contaminated food [66]. Briefly, *C. jejuni* cells were grown on plates using a biphasic system of Brucella agar overlayed with Brucella broth for 24-48 h at 42 °C. Food samples, including pre-cooked turkey breast, pre-cooked chicken breast, raw turkey and a selection of fruits and vegetables, were inoculated with the bacteria immediately after purchase. A sample solution was taken from the washed food and used for the PCR assay. The reaction was carried out in an Ericomp Powerblock thermocycler as follows: one cycle of 95 °C for 3 min; 40 cycles of 95 °C for 1 min, 56 °C for 1 min, 72 °C for 1 min and one cycle of 72 °C for 3 min. Then, a 10 μL sample was taken and electrophoresed at 90 V for 90 minutes. The amplified products were stained and visualized. The limit of detection of the PCR detection in meat, fruits and vegetables was 1 x 10^3 CFU/mL.

2.2.4 Optical methods

Optical sensors combine the recent advances in optics and optoelectronics with well established analytical techniques [74]. More specifically, optical sensors use light as the stimulus and are able to detect changes in the intensity of light as it passes through or refracts from a sampling system in response to the recognition element and the target analyte binding [49]. In general, the most notable advantages of optical sensors compared with other sensing platforms are the high sensitivity, the rapidity and the immunity to electromagnetical interference [75, 74]. For example, optical sensors can detect the small changes in the refractive index of the sample, or its optical thickness, that results from binding of bacteria to the recognition element immobilized on the sensing platform [76]. In addition, optical sensors allow direct and label-free assays for the detection of bacteria [76]. This is in contrast to electrochemical immunosensors, where the signal is visualized indirectly via an auxiliary reaction by a labeling compound, since antibodies are usually not electrochemically active within the desired potential range [77]. Unlike potentiometric sensors, where the difference between two potentials is measured, optical sensors do not require a reference signal. Additionally, due to the optical nature of the signal, it is not subject to electromagnetic interferences by, for example the static electricity of the body or the surface potentials of the sensor head [78]. Another advantage of optical sensors over electrochemical sensors is the low cost of optical fibres compared to the cost of electrodes [78]. Also, optical fibre sensors allow remote sensing which can be performed in ultra-clean rooms or in dangerous environments [78]. On the other hand, the major disadvantage of optical sensors is the size and high cost of the equipment used for some approaches. In addition, some instruments are suitable only for laboratory conditions and are susceptible to physical damage [74].

In this section, the optical methods used for the detection of cells will be discussed. A wider comparison of other sensing platforms such as optical, electrochemical, magnetic and colorimetric that were not considered appropriate for the scope of this review can be found in [79, 76].

Non-optical-fibre based sensors

In this section, sensors based on flow cytometry, ATP bioluminescence and surface plasmon resonance will be described.

Flow cytometry

Cytometry is a process for measuring the physical and chemical characteristics of biological cells [80]. In flow cytometry, the measurements are made as the cells pass through the flow cytometer in a fluid stream. Even though acoustic and electrical properties can be measured, the estimation of optical properties is the most common in flow cytometry [80] due to the low cost of light sources, energy-efficiency and the compact size of the equipment [81]. In optical flow cytometry, cells are labelled in solution with a non-fluorescent marker that is inserted into the cell and adhered by enzymatic activity to produce a fluorescing substrate. The labelled sample is injected into a fluid that passes through a sensing medium in a flow cell. Light is focused on the sensing zone and causes the cells to emit a pulse of fluorescence, which is collected by lenses and focused onto photodetectors, as shown in Fig. 2.7. The collected light provides information about the cell [82]. For the tracking of cells *in vivo*, if required, the cells can be additionally labelled with antibodies to distinguish between different bacterial species [83]. The major advantage of this technique is its ability to measure the properties of a large number of single cells in a short time frame. Typically, results are obtained within 2 hours, with a limit of detection of 100 CFU/mL [61]. A drawback of the technique is that it requires a suspension of single cells, with minimum clumps and debris [84].

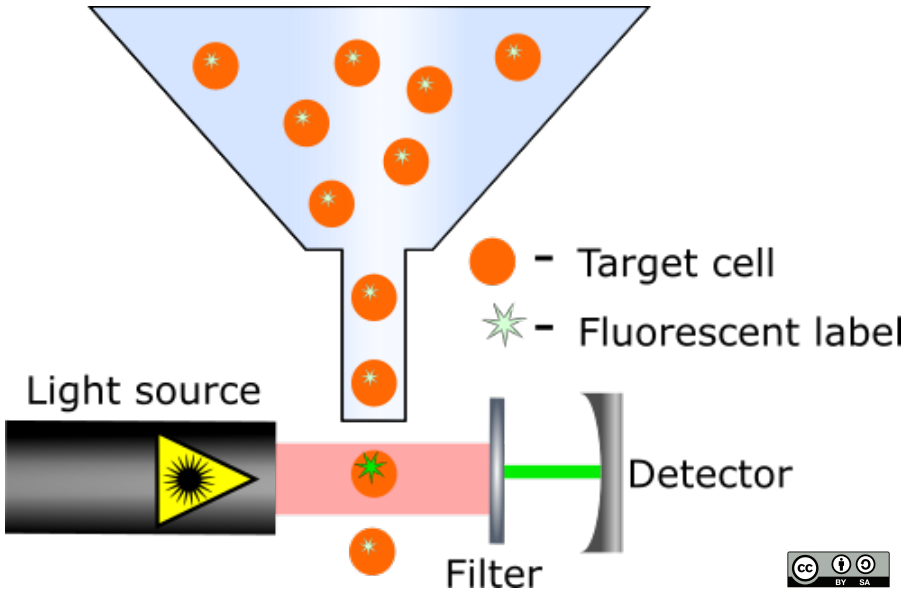

Figure 2.7: Simplified schematic of a flow cytometer.

Mixter *et al.* reported the use of flow cytometry to identify murine cell subsets that retained *C. jejuni* after intraperitoneal injection [83]. Briefly, mice were intraperitoneal injected with *C. jejuni* cells and then euthanized. Suspensions from

spleen and liver were used for CFU determination and flow cytometry detection. For the cytometry studies, bacterial cells were labeled with tagged antibodies. The average number of *C. jejuni* recovered from the spleen and liver was 5 x 10^7 and 2.5 x 10^8 CFU per homogenate.

ATP bioluminescence

Luminescence-based techniques for the detection of pathogenic bacteria [85, 86, 87, 88, 89] and environmental contaminants [90, 91, 92] are widely used in the industrial sector, where continuous monitoring of biochemical pollution is important [93]. The main advantages of luminescence-based techniques are their sensitivity, rapidity, the simplicity of the equipment required, and the high detectability, as photons are produced in the dark by a chemical reaction and are therefore easily and efficiently measurable without any background signal, such as that derived from the photoexcitation source in photoluminescence [94]. Bioluminescence is the emission of light by an organism as a result of a biochemical reaction. In contrast to fluorescence and phosphorescence, bioluminescence reactions do not require the initial absorption of electromagnetic radiation by a molecule or pigment to emit light [95].

The first recorded detailed observations of luminescence date from Aristotle (384-322 BCE (Before Common Era)), who recognized the self-luminosity of bioluminescent organisms and that it was not accompanied by heat [96]. The first specific and complete record of bioluminescent organisms was produced by Pliny the Elder (23-79 CE) in his Naturalis Historia. In his work, there are detailed descriptions of bioluminescent animals such as glowworms, fireflies, purple jellyfish and lantern fish [96]. Later, in 1667, Boyle discovered the requirement for oxygen for the emission of light [97] from an observation that began at his kitchen with a chicken carcase displaying bright spots of bluish-green light [98]. Fig. 2.8 shows an example of a chicken carcase contaminated with bioluminescent bacteria.

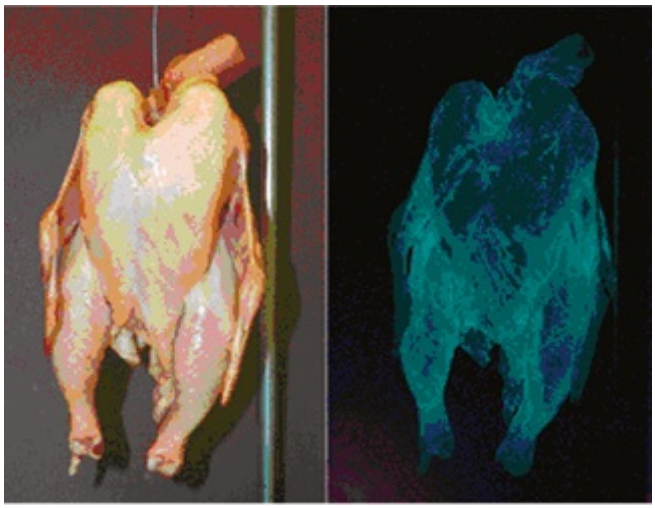

Figure 2.8: Chicken carcase contaminated with a bioluminescent bacteria at room light (left) and with lights off (right). Modified image from [98].

Bioluminescent systems produce light through the oxygenation of a substrate,

typically luciferin, and an enzyme, luciferase. Bioluminescent reactions vary among organisms but can be explained as a luciferase catalyzed production of an excited intermediate from oxygen and luciferin that emits light when returning to its ground state [98]. The requirement for Adenosine triphosphate (ATP) as a substrate was established in 1968 by Chapelle and Levin [99], and, since then, it has been used to develop bioluminescent assays for ATP quantification [94]. ATP is present in all living cells and, in the presence of oxygen, D-luciferin and magnesium ions, the enzyme luciferase uses energy from ATP to oxidise D-luciferin and to produce light. The quantity of light, measured by lumenometers, is proportional to the quantity of ATP and depends on both the type of bacteria and the metabolic state of the organism. This technique is up to 30% faster than traditional techniques and the limit of detection in a filtered sample is 100 cells/100 mL [100]. In addition, ATP bioluminescence, unlike flow cytometry, can be used to screen both filterable and non-filterable samples [61]. However, the majority of current ATP-based systems commercially available are qualitative [61]. In order to produce quantitative results, additional techniques have to be used.

The luciferin-luciferase bioluminescence reaction was used to estimate cell numbers of *Campylobacter jejuni* and *C. coli* in broth cultures by Ng *et al.* [89]. The estimation was based on a linear relationship between cell numbers and ATP levels. The sensitivity of this reaction for *Campylobacter* spp. in both brucella medium or modified K broth was 10^4 to 10^5 CFU/mL. Using *Escherichia coli* as a reference bacteria, the sensitivity of the reaction was 10^3 to 10^4 CFU/mL. The better performance for the detection of *E. coli* may be due to higher levels of intracellular ATP per cell.

Kassem *et al.* constructed bioluminescent *Campylobacter* strains and used them to monitor the survival of these pathogens in chicken litter material [87]. Briefly, they inserted shuttle plasmids carrying the luminescence genes (*luxCDABE*) into *C. jejuni* and *C. coli* to construct bioluminescent strains of these pathogens. The strains (7×10^6 CFU/mL of *C. jejuni* and 6×10^6 CFU/mL of *C. coli*) were spiked into samples of litter collected from different enclosures that had previously contained broiler chickens. Their results revealed that *Campylobacter* spp. survived for at least 20 days in litter.

Fukuda and co-workers reported a bioluminescent enzyme immunoassay (BEIA) using biotinylated firefly luciferase for the detection of *Salmonella* in naturally contaminated chicken meat samples [86]. More specifically, *Salmonella* cells were pre-enriched and incubated for 24 h at 36°C. Anti-*Salmonella* monoclonal antibody, which recognizes the core polysaccharide region of *Salmonella* lipopolysaccharide (LPS) and biotinylated firefly luciferase, was diluted in phosphate buffered saline (PBS) and placed on microplates. Then, *Salmonella* samples were added to the plates. After, biotinylated antibody was incubated in the plate. Finally, streptavidin-biotinylated luciferase BLU-Y complex was added to the microplates for 15 min. After a final washing step, each plate was placed in a tube for the luminometer. The limit of detection reported was 7.3×10^2 CFU/mL, which is comparable with that achieved by PCR assays.

Despite the fact that bacterial detection with luminescent techniques are relatively fast and sensitive, they present some limitations. For instance, ATP results should

not be interpreted as surrogate indicators for the presence of microbial pathogens, since some cleaning agents used in the process can enhance or decrease the light signal [93]. Also, correlations of ATP with microbial counts expressed as colony forming units (CFU) for different species of bacteria varies from 0.64 to 0.99, which indicates that pre-treatment of the sample has to be performed [93]. In addition, the amount of ATP depends on the stress levels of the cells, which can cause decreases of up to 90% [101]. Furthermore, as the light signal is not stable over time, the light-emitting species are subject to diffusion phenomena in solution, causing a loss in resolution [102]. Finally, when the cell is labeled with an enzyme, special care must be taken to keep the enzyme activity constant, considering temperature and buffer solution [94].

Surface Plasmon Resonance

Surface plasmon resonance (SPR) sensors are optical sensing devices that use a type of electromagnetic field, the surface plasmon, to measure changes in the refractive index of the surrounding medium [103]. An SPR device for biosensing purposes measures the change in refractive index as a result of the binding of the antigen molecule to an immobilized antibody (or enzyme) on the surface of metal films such as gold or silver [104]. The SPR phenomenon was studied theoretically by Zenneck in 1907 [105, 106], but was used for first time as a chemical sensor by Liedberg *et al.* in 1983 [107]. SPR is the electromagnetic phenomenon that occurs when incident light excites electrons in a dielectric-metal interface; and due to this excitation, electrons oscillate and generate electromagnetic waves that propagate along the surface of the metal layer, which are known as surface plasmons [108, 39]. There are three widely used methods to excite SPR: i) prism coupling, ii) waveguide coupling, and iii) grating coupling. Between these methods, the most common, and the one which exhibits the best sensitivity, is prism coupling [109, 110, 108], shown in figure 2.9. Prism coupling offers an instrumental contribution to the sensitivity of SPR sensors due to the dispersion of glasses constituting prism couplers, which is much smaller than the dispersion of surface plasmons on a metal-dielectric interface. This instrumental contribution to sensitivity by a prism coupler is larger by an order of magnitude than that for a grating coupler [104]. SPR by prism coupling is based on total internal reflection where the incident light interacts with the thin metal layer, generating an evanescent wave which propagates along the interface with a propagation constant which can be adjusted to match that of surface plasmons of similar frequency by controlling the angle of incidence, wavelength, intensity, phase or polarization [111, 105]. The matching method that involves controlling the angle of incidence is known as attenuated total reflection (ATR). The matching is determined by measuring the coupling strength at a fixed wavelength and multiple angles of incidence. At a certain angle, the light is not totally reflected but it is coupled to the surface plasmons, causing a reduction in the reflected intensity; as a consequence the intensity of the light reflected which is detected by the photodetector decreases [112]. There are two configurations to excite surface plasmons by prism coupling and the attenuated total reflection method: the Kretschmann geometry [113] and the Otto geometry [114]. In the Kretschmann geometry of the ATR method (Fig.

2.9a), incident light propagating in the prism is partially reflected at the interface between the prism and a thin metal layer. The other part of the light propagates in the metal, decaying exponentially in direction perpendicular to the interface, which is referred to as evanescent wave. If the thickness of the metal layer is thin enough (less than 100 nm for visible and near-infrared light), the evanescent wave penetrates through the metal layer and couples to surface plasmons at the outer boundary of the metal [104]. This method has been found to be very suitable for sensing, since the coupling is sensitive to the refractive index of the medium surrounding the metal later, and has become the most widely used geometry in SPR sensors [115]. On the other hand, in the Otto geometry (Fig. 2.9b), a prism with refractive index n_{prism} is interfaced with a dielectric-metal waveguide that consists of a dielectric layer with refractive index $n_{dielectric}$ ($n_{prism} > n_{dielectric}$) and a thickness of typically few microns, followed by a thin metal layer. In other words, there is a gap (dielectric) between the prism and the metal layer. This configuration is difficult to implement and it is more suitable for studying single-crystal metal surfaces and adsorption on them [105].

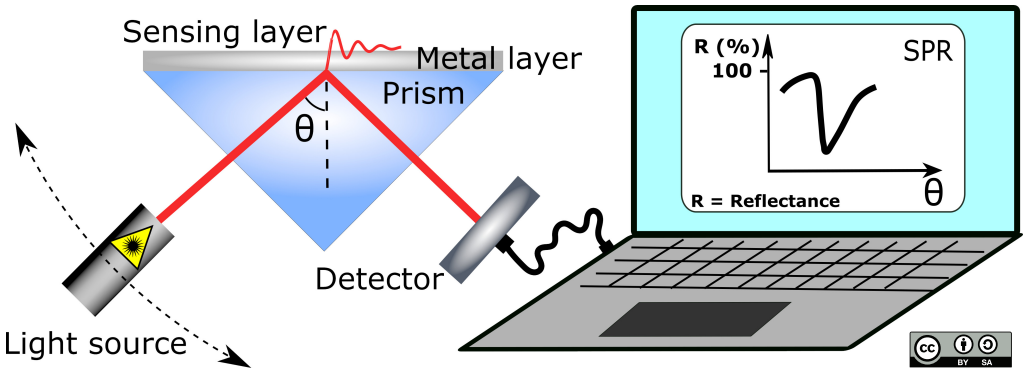

(a) Kretschmann configuration.

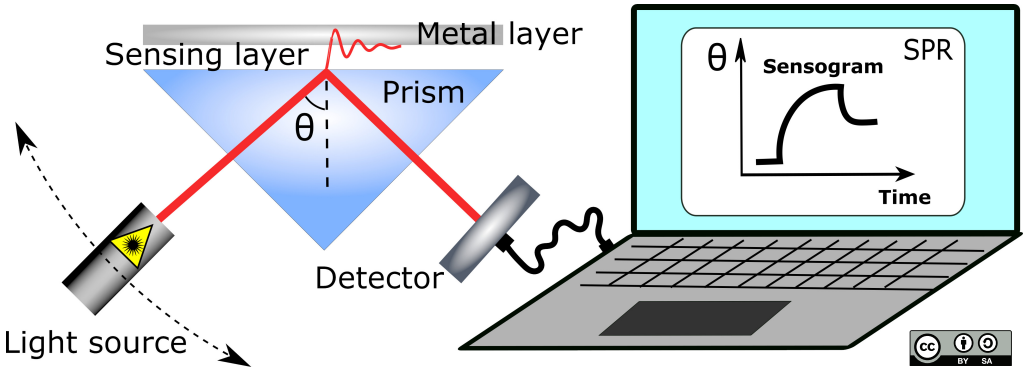

(b) Otto configuration.

Figure 2.9: Excitation of surface plasmons by prism configurations.

Analogously, for SPR sensors with wavelength modulation, the phase matching is determined by measuring the coupling at a fixed angle of incidence and multiple wavelengths. For SPR sensors exploiting intensity modulation, the matching is measured at a fixed wavelength and fixed angle of incidence. Similarly, for SPR sensors exploiting polarization modulation, the phase matching is determined by measuring changes in polarization at fixed angle of incidence and fixed wavelength. Finally, for SPR sensors with phase modulation, the coupling is determined by

measuring the shift in phase of the light at fixed angle of incidence and fixed wavelength [111]

Taylor *et al.* reported the detection of *E. coli* with a prism-based SPR sensor operating in the angle configuration [116]. Monoclonal antibodies were attached to a self-assembled monolayer of alkanethiols on a gold sensing surface. The limit of detection achieved was 10^6 CFU/mL for viable cells. If pre-treatment of the cells was carried out, the limit of detection can be lowered by two orders of magnitude. However, a sandwich assay and the use of a sophisticated sensor equipped with two channels (one for sensing and one as a reference) are necessary for the indirect detection of bacteria. Similarly, Taylor and coworkers [117] reported the detection of *C. jejuni* in apple juice using polyclonal rabbit antibody and biotinylated polyclonal antibody in a customized SPR sensor in the Kretschmann geometry. They reported a limit of detection of 1.1 x 10^5 CFU/mL.

The detection of *C. jejuni* using a commercially available SPR machine (SPR-4, Sierra Sensors, Germany) with the use of amine coated gold sensor chips was reported by Masdor et al. [118]. Briefly, rabbit polyclonal antibody (50, 70, 100 and 150 μg/mL) was covalently attached onto the surface of the gold coated chip by injection for 3 min at a flow rate of 25 μL/min. *C. jejuni* cells at concentrations from 1 x 10^4 to 1 x 10^9 CFU/mL were injected for 3 min. The limit of detection achieved with a direct assay was 8 x 10^6 CFU/mL. The sensitivity of the sensor was enhanced with a sandwich assay achieving a limit of detection of 4 x 10^4 CFU/mL.

SPR biosensors present some limitations. First, an inherent specificity drawback. If the sample contains a high concentration of non-target molecules, the response of the sensor may conceal a specific response produced by low levels of target analyte [111]. Second, like other sensors that rely on the measurement of changes in refractive index, as SPR is sensitive to interference of external parameters such as temperature or non-specific adsorption on the sensor surface [111]. Finally, the major drawback of SPR is the short penetration of the evanescent wave into the sensing zone ($\approx$100 nm) which complicates the detection of large analytes such as cells [119].

Optical-fibre based sensors

An optical fibre is a cylindrical waveguide, made of glass or plastic, that consists of central part known as the core, with refractive index n_{core}, surrounded by the cladding, with refractive index $n_{cladding}$. In order to create guidance conditions for light, the refractive index of the core must be higher than that of the cladding. The cladding in turn is usually surrounded by a protective buffer coating for mechanical and environmental protection. The material and dimensions of the core and cladding determine the optical attenuation and modal dispersion of the fibre. A schematic representation of an optical fibre is shown in Fig. 2.10

The idea of guiding light through a thin and long dielectric goes back to 1841 when Colladon showed that a thin stream of water could guide and bend light [120]. However, this contribution is commonly given to Tyndall who performed the experiment thirteen years later, in 1854 [120]. After the laser invention in 1960, the potential benefits of transmitting information using light were valued and, six years later, the coupling of lasers with optical fibres for long distance communication was achieved. In 1970, Maurer and co-workers from the Corning Glass Works produced

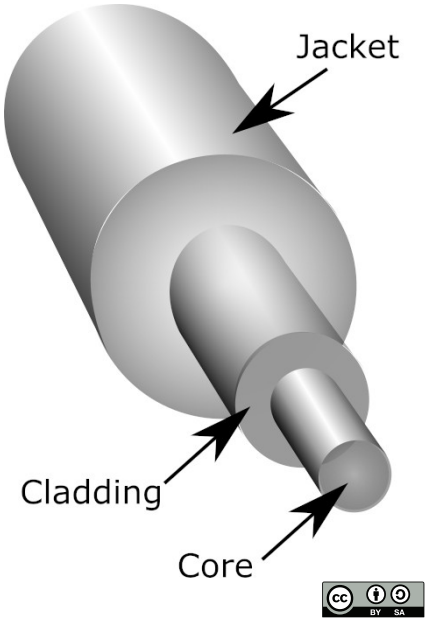

Figure 2.10: Schematic of a fibre optic

a silica fibre able to transmit signals with an attenuation of 20 dB/Km. In the following 20 years, the attenuation of the transmitted signal reached approximately 0.16 dB/Km [121], making it suited for long distance communication systems.

The most established and widespread material for fibre optic fabrication is silica (SiO_2). Silica can be doped with a range of materials to alter its refractive index and absorption and emission properties. Optical fibres can be categorised according to the refractive index profile (step-index and graded-index) and the number of modes that can propagate (single-mode and multi-mode). Based on previous distinctions, there are three types of fibres of interest for communications and sensing [122]: i) step-index multimode fibres, ii) step-index single-mode fibres, and iii) graded-index multimode fibres. A schematic of these fibres is shown in Fig. 2.11.

The physical operating principle of an optical fibre is total internal reflection (TIR). Assuming this, the light trajectory is determined by interference and reflection. Electromagnetic waves that satisfy these two transmission requisites are called modes. In other words, modes are a discrete set of electromagnetic fields that can propagate in the fibre. The interference condition requires that rays propagating in the core overlap themselves to obtain constructive interference. The reflection condition requires that the angle of propagation within the fibre, θ, must be larger than the critical angle for total internal reflection, i.e. $\theta > arcsin(n_{clad}/n_{core})$. The critical acceptance angle is related to an essential property of the fibre, the numerical aperture (NA), defined as the sine of the largest angle that an incident ray can have for TIR.

$$NA = \sqrt{n_{core}^2 - n_{clad}^2}. \tag{2.1}$$

The propagating properties of a fibre can be explained by the normalized frequency, ν, which is a structural parameter rather than a frequency. This property is defined

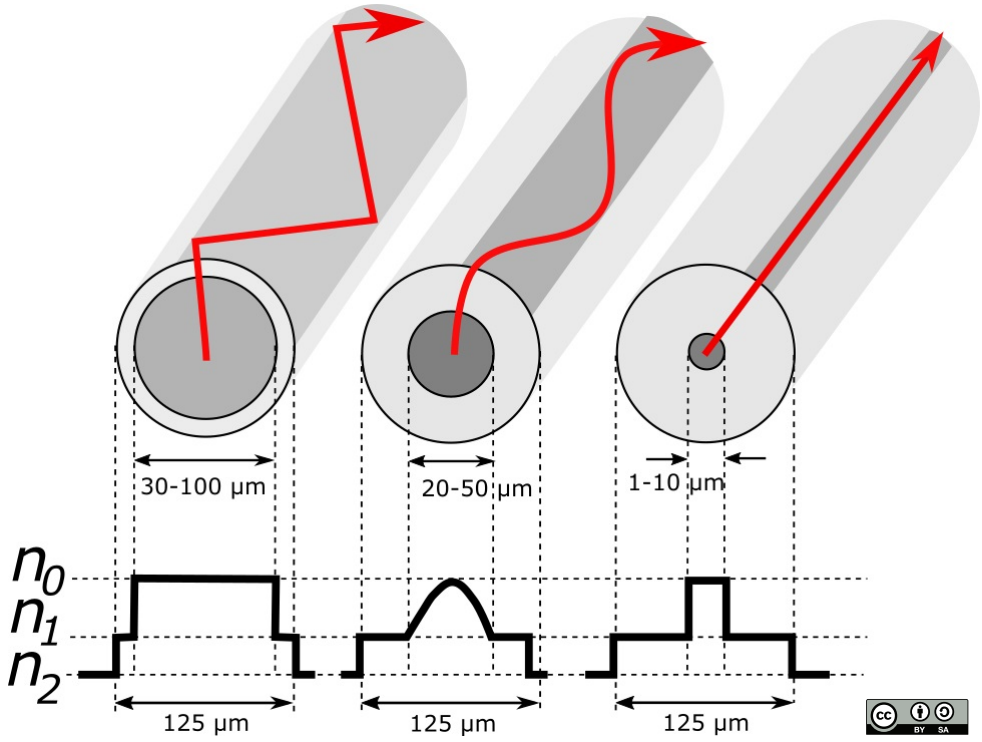

Figure 2.11: Schematic of refractive index profiles and dimension of cross sections of a step-index multimode fibre, graded-index multimode fibre and step-index single-mode fibre respectively

as

$$\nu = 2\pi \left(\frac{a_{core}}{\lambda}\right) \sqrt{n_{core}^2 - n_{clad}^2} = 2\pi \left(\frac{a_{core}}{\lambda}\right) NA, \tag{2.2}$$

where a_{core} is the radius of the core, and determines, among other factors, the number of modes that a fibre can support. An optical fibre is single-mode when only the fundamental mode is propagated, which is the case when $\nu \leq 2.405$ [123].

Multi-mode fibres have a core diameter that is large compared to the wavelength, which allows the propagation of several modes, defined by different transverse intensity distributions and propagation constants [122]. Modes can be distinguished as guided modes and radiation modes. The guided modes are restricted to the core and propagate energy along the fibre. Meanwhile, radiation modes carry energy out of the core and the energy is rapidly dissipated. Each guided mode has its own velocity and can be further decomposed into orthogonal linearly polarized components [124].

Fibre optic biosensors are optical fibre-derived devices which use optical fields to measure biological species such as cells, proteins, and DNA [125]. In this type of sensors, the light needs to interact with the surrounding environment. As light is usually confined to the core, the interaction of the light with the surrounding environment is promoted, for example, by removing the cladding or tapering the fibre. Optical fibre sensors possess advantages that include immunity to electromagnetic interference, compact size, lightweight, large bandwidth, high sensitivity, capacity to be multiplexed [75], the absence of a requirement for an external reference probe, unlike potentiometric sensors [126], and, in some cases, self calibration, which is an important feature for continuous monitoring applications [127, 128]. In addition,

optical fibres can be made of glass which is a solid silicon compound that is widely used in biological applications as a sensor solid support thanks to its favourable features as: being chemically inert, an insulator, transparent and having low fluorescence emission [129].

Gratings. Optical fibres were fabricated originally with the main objective of propagating a signal over a long distance. However, the use of fibre-optics for sensor applications started in the middle of the 1970's [130]. The properties of the light propagating in the fibre are influenced by the surrounding environment and by probing these properties (for example intensity, phase, polarization, etc.) sensors can be created. In 1978, Hill *et al.* reported the first observations of photosensitivity in Ge-doped core optical fibre and the fabrication of the first gratings. Such photosensitivity was manifested by light-induced refractive-index changes in the core of the waveguide [131]. It was not until 1989, when first in-fibre Bragg gratings, inscribed by illuminating the core from the side of the fibre with coherent UV radiation, were reported, providing new ways to make measurements of temperature and strain by monitoring the shift in the Bragg wavelength of the in-fibre grating structure [132].

A new type of fibre grating was introduced in 1996 by Vengsarkar *et al.*: the long-period grating (LPG) [133]. LPGs were initially developed for use as band-rejection filters. However, LPGs also have remarkable opportunities as fibre optic bio-sensors. The central wavelengths of the resonance bands that are characteristics of the transmission spectra of an LPG depend critically on the index difference between the modes propagating in the core and the cladding, and hence any variation caused by strain, temperature, or changes in the external refractive index can cause large wavelength shifts in the resonances [134]. The first evidence of biomolecule detection using an LPG sensor was reported in 2000 [135]. Briefly, an LPG fabricated with the point-by-point method (see Sec. 2.3.2) was coated with antibody (goat anti-human IgG) for the detection of antigen (human IgG), showing a limit of detection of 2 μg/mL.

Fibre gratings consist of a periodic perturbation of the refractive index of the core or/and cladding. Such periodic alteration creates a perturbation in the guidence conditions and consequently a change in the transmitivity of the light for certain wavelengths [136]. Fibre gratings can be classified according to the period of the grating as i) short-period gratings or fibre Bragg gratings (FBGs), and ii) long-period gratings (LPGs) [137].

FBGs have a sub-micron period (typically 0.25-0.6 μm [138, 139]) and sensing zone length of the order of millimiters (1-5 mm [140, 141, 142, 143]). The FBG acts as a narrow-band reflection-filter coupling light from the forward-propagating mode to the backward-propagating mode which happens at certain wavelength, also called the Bragg wavelength (λ_B) [109]:

$$\lambda_B = 2n_{eff}\Lambda, \tag{2.3}$$

where n_{eff} is the effective refractive index of the core mode and Λ is the period of the grating. In Fig. 2.12 the schematic of FBG operation is shown.

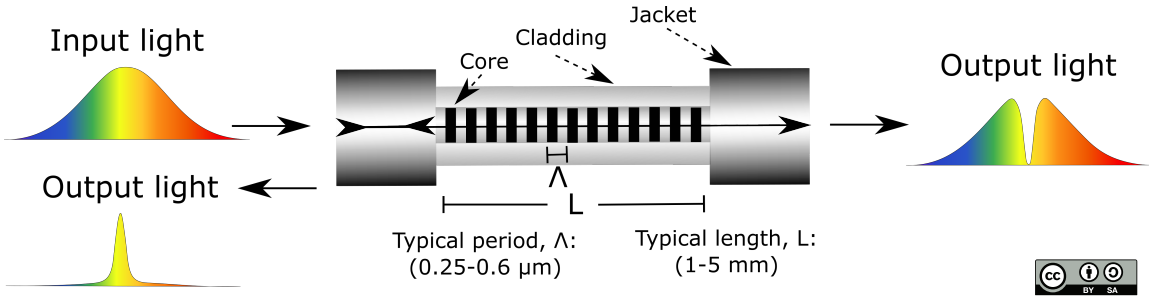

Figure 2.12: Schematic of the operation of an FBG.

FBGs have been used as optical sensors due to their high sensitivity to parameters such as pressure, vibration, temperature and bending [144]. However, standard FBGs are not sensitive to the surrounding refractive index [145]. Hence, FBGs are not suitable to be used as surrounding refractive index sensor [146], i.e. as a biochemical sensor. Since any biochemical reaction or interaction results in a change in the refractive index of the medium [147], the core of the section of the optical fibre containing the FBG has to be exposed to the surrounding medium, so that changes in the surrounding refractive index can influence the effective index of the propagating modes and thus cause a change in the reflected Bragg wavelength. The core can be exposed by polishing the cladding [109] or by etching, as reported Zhou *et al.* [145], who described a glucose sensor able to detect changes of 5% and 0.5% (for a deeper etching) of sugar concentration. Another configuration employed in the development of sensors for biochemical applications is the tilted fibre grating (TFG) [148, 149]. A TFG is similar to a regular FBG, but the grating planes are tilted relative to the fibre axis, as shown in Fig. 2.13. The tilted grating promotes coupling between

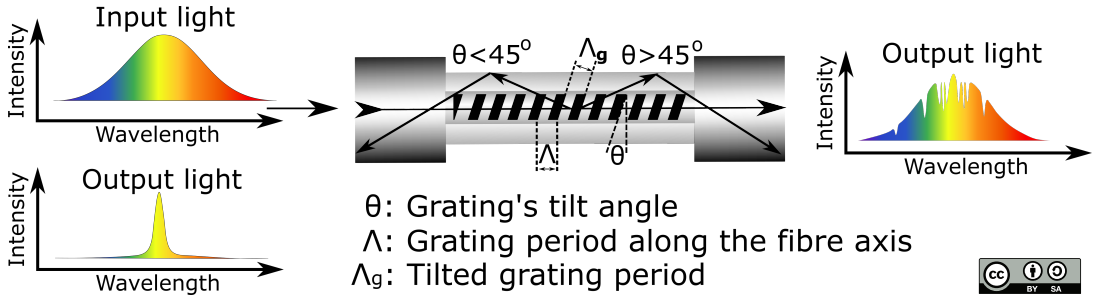

Figure 2.13: Schematic of the operation of a TFG.

the core and the cladding modes at wavelengths that satisfy the phase matching condition [150]:

$$\lambda_{TFG} = (n_{core} \pm n_{clad(m)})\Lambda = (n_{core} \pm n_{clad(m)})\frac{\Lambda_g}{cos(\theta)}, \tag{2.4}$$

where θ is the grating's tilt angle, Λ is the grating period along the fibre axis, and the "+"and "-" signs describe the cases in which the coupling occurs to the backward and forward propagating modes, respectively. A TFG can couple light in the same way as FBGs or LPGs depending on the tilt angle of the grating structure (θ) [150], as shown in Fig. 2.13. If $\theta < 45°$, the core mode will be coupled to the

backward propagating direction. If $\theta > 45°$, the core will be coupled to the forward propagating direction. For the special case where $\theta = 45°$, all the phase matched light will be completely radiated out of the fibre. The phase matching condition implies that the linewidth of attenuation bands is smaller than that of an LPG and the separation between them much smaller [151]. As a consequence, a number of attenuation bands can be monitored simultaneously and compared using a spectral range of less than 100 nm [151]. Another advantage of TFGs compared with LPGs is the negligible thermal cross-talk effect [149]. The fabrication of TFG biosensors for biochemical applications such urinary protein variations [152], virus [149], and cancer biomarker detection [153] has been reported. However, SPR platforms can be integrated with TFG-based sensors in order to improve their sensitivity, which means that the cladding of the optical fibre should be coated with a thin metal layer which complicates the manufacturing process. The performance of TFG-based biosensors remains unsatisfactory since the limits of detection achieved do not match the values achieved by other sensing platforms [149]. The main disadvantage of the TFG-based sensors is the fabrication process, which is more complex since the grating planes are sloped by an angle in relation to the longitudinal fibre axis [154, 155].

LPGs (explained in more detail in section 2.3.1), on the other hand, have a period within the range of 100 μm to 1 mm and the grating acts to couple the propagating core mode and the co-propagating cladding modes [137]. The typical length of an LPG is in the range from 10 to 50 mm [134, 156]. In Fig 2.14, the operation of the LPG is illustrated. LPGs are highly sensitive to changes in refractive index of the surrounding medium. For this reason, LPGs have been used as biochemical sensors in direct and label-free approaches [146, 135] for the detection of bacteria such as *E. coli* [157, 158, 159] and methicillin-resistant *Staphylococci aureus* (MRSA) [160].

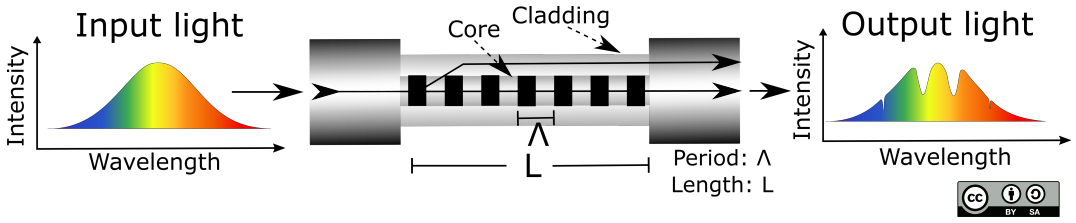

Figure 2.14: Schematic of the operation of an LPG.

Previously, some advantages of optical fibre-based sensors, among them compact size, lightweight, immunity to electromagnetic interference, self-referenced, high sensitivity and rapidity were mentioned. Another advantage of LPGs over other optical platforms such as SPR is the price and the portability of the sensor that could allow it to be used in various analytical situations [161]. In spite of the multiple advantages, LPG-based sensors present some drawbacks such as the required access to both ends of the fibre. Although an LPG can work in reflection mode, the cost of the setup is increased since a fibre optic coupler is required [162]. The reflection mode is achieved if one end of the optical fibre is coated with a reflecting layer, usually silver, that acts as a mirror to provide high reflectivity [163, 164]. A brief summary of the main distinguishing features of the most widely-used bacterial detection methods reviewed in Secs. 2.2.1, 2.2.2, 2.2.3, 2.2.4 is given in Table 2.2.

Table 2.2: Comparison of widely-used bacterial detection methods.

Abreviations used: Advantage (+), (−) Disadvantage.

Method	Notes
Traditional methods (Culturing, etc.) [36, 37]	(+) Sensitivity and selectivity (−) Time consuming (up to 1 week) (−) Need of skilled personal
ELISA [58, 50, 59, 56, 55]	(+) Sensitive and relatively fast (+) Easy to perform (−) Still time consuming (up to 3 days)
PCR [63, 57, 67, 65, 66]	(+) Highly sensitive and specific (+) Relatively fast (−) High cost of equipment (−) Generation of false-positive results
Flow cytometry [82, 83, 61, 84]	(+) Sensitive and fast (2 h) (−) Requires suspensions of single cells (minimum of clumps and debris)
ATP bioluminescence [85, 165, 87, 88, 89]	(+) Sensitive and relatively fast (+) Simplicity of the equipment required (+) High detectability (−) Light signal inestable over time (−) Cell-dependant light signal (−) Still time consuming (up to 2 days)
SPR [111, 166, 118, 116]	(+) Sensitive and fast (results within hours) (+) Commercially available equipment (−) Complicated detection of cells due to short penetration of evanescent wave ($\approx$ 100 nm) (−) Bulky and expensive equipment
FBG [109, 145]	(+) Compact size and sensitive (+) Easy to fabricate (−) Not sensitive to surrounding refractive index
LPG [146, 135, 158, 161, 159]	(+) Compact size, fast and highly sensitive (+) Easy to fabricate (+) Simple set up and minimum equipment (−) Need to access to both ends of the fibre

The advantages of LPGs as biosensors make them a good platform candidate for this project. A brief comparison of some of the achievements of the different methods for the detection of *Campylobacter jejuni* is given in Table 2.3.

Table 2.3: Detection of *Campylobacter jejuni*.

* Unless otherwise stated

Detection method	Type of assay	Time of analysis	Detection limit* (CFU/mL)	Ref.
Enumeration	Direct	5 days	500-600 CFU	[45]
ELISA	Sandwich	24 h	10^5	[56]
ELISA	Competitive direct	2.5 h	$2.1\text{x}10^4$	[58]
ELISA	Competitive indirect	6 h	10^4-10^6	[59]
PCR	–	7 h	10^2-10^3	[66]
Flow cytometry	–	–	10^7-10^8	[83]
ATP luminescence	–	–	10^4-10^5	[89]
SPR	Direct	40 min	$8\text{x}10^6$	[118]
SPR	Sandwich	1 h	$4\text{x}10^4$	[118]

2.3 Review of Long Period Gratings

In this section, a general overview of long period gratings will be presented. The main fabrication techniques, including amplitude mask, point-by-point, CO_2 laser exposure and electric arc will be discussed.

2.3.1 Long Period Gratings

An LPG is a periodic perturbation of the refractive index in the core, the cladding, or both in a section along the optical fibre. Such perturbation supports the coupling of light between the modes of the cladding and core [133].

Typically, the period of the LPG lies within the range of 100-1000 μm [167]. The LPG couples the core mode to a set of cladding modes at wavelengths that satisfy the phase matching condition [168]:

$$\lambda_{(x)} = (n_{core} - n_{clad(x)})\Lambda, \tag{2.5}$$

where $\lambda_{(x)}$ represents the wavelength at which coupling occurs to the linear polarized ($LP_{0,x}$) mode, n_{core} is the effective refractive index of the mode propagating in the core, $n_{clad(x)}$ is the effective refractive index of the $LP_{0,x}$ cladding mode, and Λ is the period of the grating. The cladding support a large number of cladding modes due to the larger radius compared to that the core (up to 25 times larger for a single-mode fibre (See Fig. **??**)). However, theoretical studies have shown that the coupling happens only to a subset of cladding modes that has similar electric field profiles [169, 170, 171]. This is, the coupling occurs to cladding modes with the appropriate symmetry to ensure a good overlap of their electric field profiles with that of the core mode. The high attenuation of the cladding modes results in the transmission spectrum of the fibre containing a series of attenuation bands centred at discrete wavelengths that satisfy equation 2.5, as shown in Fig. 2.15, each attenuation band corresponding to the coupling to a different cladding mode [137].

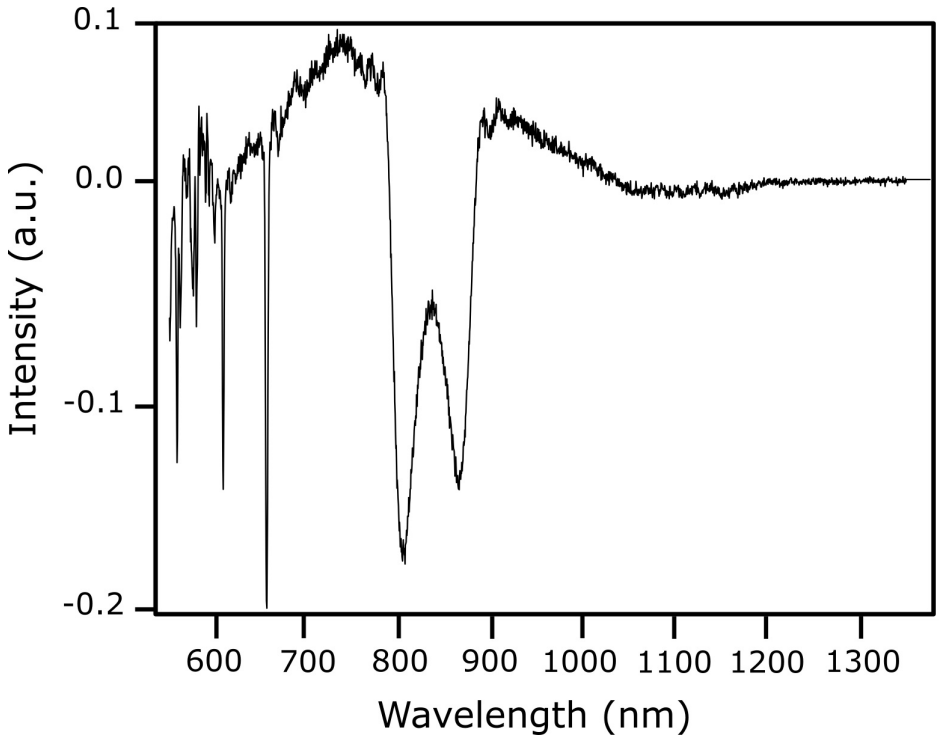

Figure 2.15: The transmission spectrum of an LPG, of length 4 cm and of period 113 μm fabricated in a single mode boron-germanium co-doped optical fibre, cut-off wavelength 635 nm, model PS750, Fibercore.

From the dependence of the phase matching condition on the effective refractive index of the cladding modes, the refractive index sensitivity of LPGs can be explained. The effective refractive indices of the cladding modes are dependent on the refractive index of the medium surrounding the cladding and thus the coupling and the transmission spectrum are sensitive to changes in the refractive index of the surrounding medium [137]. Such sensitivity is exhibited as a shift in the central wavelengths of the attenuation bands and in their value of the transmission. The relationship between the grating period, Λ, and the wavelength at which coupling occurs for a set of cladding modes is shown in Fig. 2.16.

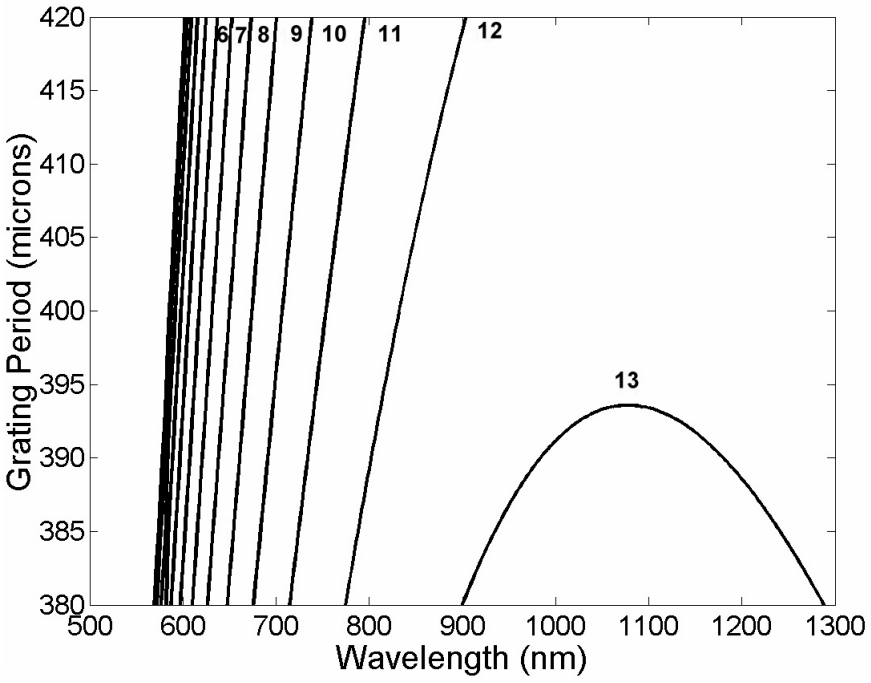

Figure 2.16: Phase matching curves for 2^{nd} order modes LP_{01} to LP_{013}. Plot from [172].

The transmission spectrum is sensitive to the period of the grating, the length of the LPG and to changes in the parameters of the environment that surrounds the LPG such as refractive index, temperature, strain and bend radius [173]. Changes in these parameters can modify the effective refractive index of the core and cladding modes and/or the period of the grating. As a consequence, the phase matching condition for coupling to the cladding modes is modified, resulting in a shift in wavelength of the attenuation bands [137]. Furthermore, it is widely known that sensitivity to perturbation of the surrounding environment of an LPG depends on the order of the cladding modes and that it exhibits a maximum, the so named turning point [174, 175] or phase matching turning point (PMTP). The PMTP is a point where the slope of the phase matching curve changes its sign and can be described based on Fig. 2.17. In Figure 2.17(a) the LPG period is chosen such that is possible to couple the 18th cladding mode, however the phase matching to the 19th cladding mode is not achieved, obtaining a transmission spectra shown in Figure 2.17(b). If an increase in the effective refractive index is caused, for example due to changes in the surrounding refractive index, the phase matching curves change, "moving upwards", as in Figure 2.17(c), with the subsequent appearance of a resonant band corresponding to coupling to the 19th cladding mode and a slight blue-shift in the central wavelength of the 18th cladding mode resonant band. Additional increases in the effective refractive index result in the further enlargement of the LP_{019} resonance band, which thereafter splits into two bands, the so called dual resonance [176].

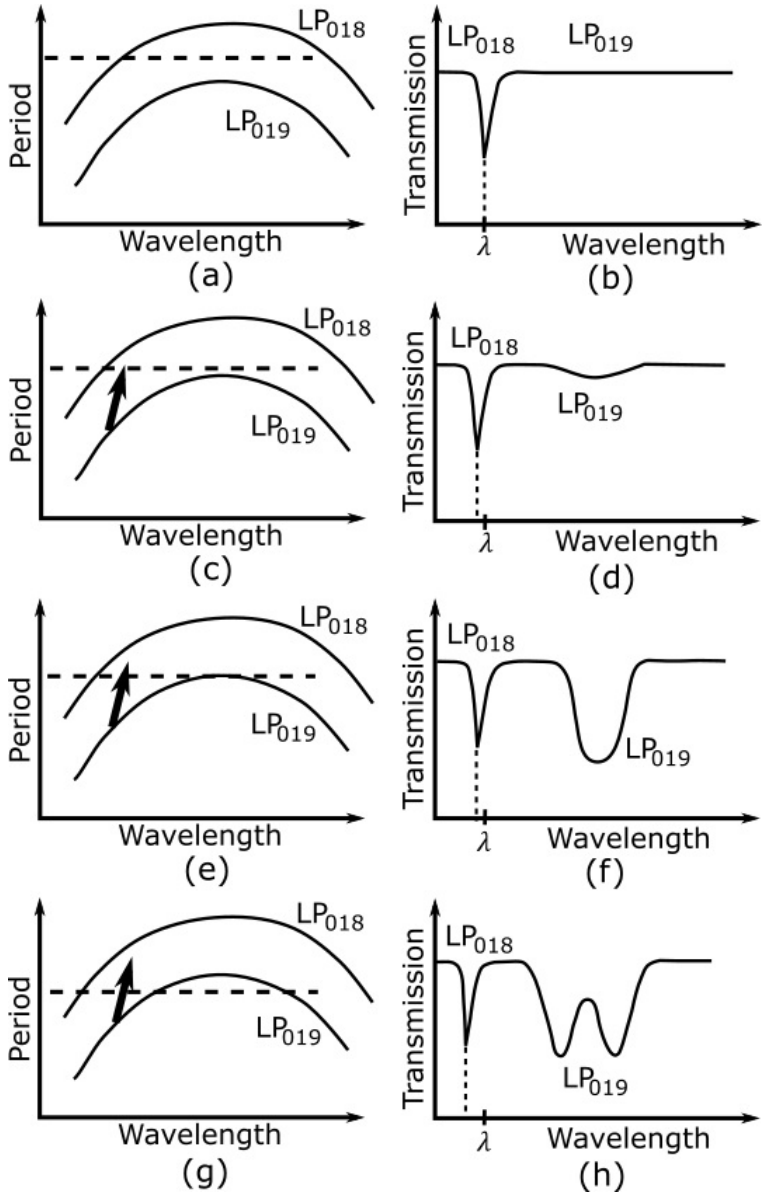

Figure 2.17: Schematic of an LPG near the PMTP. Modified figure from [176].

2.3.2 Long Period Grating fabrication techniques

In this section, the main techniques for LPG fabrication, summarized in Table 2.4, will be discussed. There are two main phenomena that are used to produce LPGs in optical fibres: UV photosensitivity and residual thermal stress [177, 178]. The former technique is the most widely employed [137], and involves the modification of the refractive index of the core of Germanium-doped silica fibres by exposure to light at wavelengths between 193 and 266 nm. The residual thermal stress technique involves the heating and rapid cooling of the core and cladding of a fibre, altering its viscosity, which modifies the refractive index [178]. This is used to induce a periodic index modulation along the length of the fibre. Within this technique, the two heating methods that are most commonly used are CO_2 laser exposure [179] and electric arcs [180]. Other techniques, such as femtosecond laser exposure [181], mechanical

microbends [182, 183], etched corrugations [184] and ion beam implantation [185], have been used to fabricate LPGs. However, the discussion presented in this review is limited to the most often used approaches. In addition, the described approaches could be performed with the available equipment at Cranfield University in the years in which this project was developed without need for additional purchase of expensive devices, such as femtosecond lasers.

Table 2.4: Main LPG fabrication techniques.

Phenomenon	Technique
UV Photosensitivity	Amplitude mask
	Point-by-point
Residual Thermal Stress	CO_2 laser exposure
	Electric arc

UV photosensitivity

The grating structure is created by exposing the fibre through an amplitude mask of appropriate period [133, 186], or by building the grating in a point by point fashion [187, 188, 168]. Schematics of these techniques are shown in Fig. 2.18.

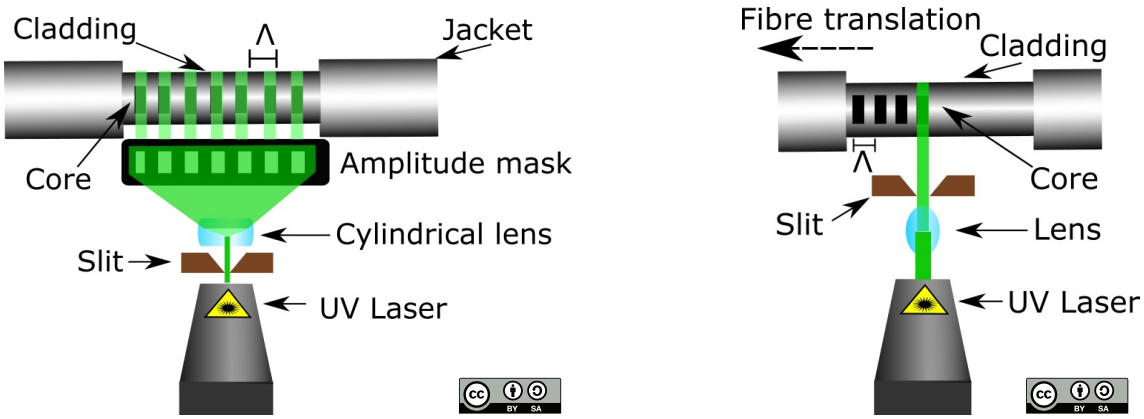

(a) (b)

Figure 2.18: Schematic of LPG inscription in a UV photosensitive optical fibre by (a) the amplitude mask, and (b) the point-by-point technique.

Amplitude mask

The amplitude mask (AM) contains an array of transparent windows that form a "bright-dark" periodical pattern with a period Λ. The optical fibre is exposed to the output of the UV laser through the mask, illustrated in Fig. 2.18a. This technique is suitable for repetitive use to produce LPGs of identical period with little requirement for precision during the laser exposure [189]. The commonly used amplitude masks are formed by chrome-plated silica [133], dielectric patterned [189], or lithography [190]. The disadvantages of this technique are that the period and length are restricted by the dimensions of the amplitude mask [191] and the fibre must be photosensitive. In addition, chrome on silica and dielectric masks are expensive, while metal masks suffer from oxidation and deformation [190].

Point-by-point technique

In the point by point method, the grating is created by translating the fibre relative to the laser beam, as shown in Fig. 2.18b. A UV laser is used to irradiate the fibre optic through a thin slit, while the fibre moves with a period Λ along a perpendicular axis to the laser beam. The fibre dwells at each point while is exposed for a duration such that a suitable refractive index is induced. The most notable advantages are the flexibility and the opportunity for complete customization because the grating structure and length are fully configurable [192]. This method allows the fabrication of LPGs of a number of grating configurations, including uniform grating period [188], where the period is constant along the fibre, chirped gratings [193], where the grating period varies, for example, linearly along the length of the fibre, tilted gratings [194], where the grating has a certain angle to the optical axis, not equal to 90° as in the case of regular gratings and π phase shifted gratings. The main disadvantage of this technique is the time taken to fabricate the LPG [191].

Both techniques, amplitude mask and point-by-point, are easy to put into practice. Nevertheless, the AM basis is more attractive for mass production, even though the point to point method is more flexible [178]. The main limitation of using UV laser exposure is that it is only possible to fabricate LPGs in UV photosensitive fibres. Additionally, the changes in the refractive index induced by the UV photosensitivity technique can only remain at temperatures <250°C, above which they are thermally annealed. As a consequence, LPGs fabricated by UV exposure are not suitable for high temperature applications [195].

Residual thermal stress

The residual thermal stress technique can be carried out using two heating methods: CO_2 laser exposure and electric arc. Both methods can be implemented in any kind of fibre and are suitable for high temperature applications (up to 1100 °C) [178]. The fabrication of the grating is carried out using the point by point technique [191].

CO_2 laser exposure

The CO_2 laser exposure approach for writing gratings in an optical fibre is a typical point-by-point technique. The optical fibre is periodically translated along

its longitudinal direction while it is irradiated with a CO_2 laser beam (wavelength 10 μm, mid-infrared) through a controlled slit. Silica is not transparent at this wavelength and as a result absorbs the energy from the CO_2 laser, whereby the fibre is heated [178]. Compared with the UV irradiation techniques, CO_2 laser exposure is less expensive and easier to apply since there is no requirement for the fibre to be photosensitive and CO_2 lasers are typically less expensive than UV lasers [196]. However, the major drawback of this approach is the minimum period of the grating that can be achieved due to heat transfer along the fibre axis [197] ($\Lambda > 180$ μm [198]). As discussed in Sec. 2.3.1, the sensitivity of attenuation bands depends on the order of the cladding modes, i.e. the higher the order of the cladding modes, the higher the sensitivity offered by the LPG [172, 199]. This is, of course, the most desired characteristic for sensing purposes. The higher orders are obtained by decreasing the grating period. Because of the minimum period achievable by this fabrication technique, the coupling with higher-order cladding modes is compromised, potentially limiting the sensitivity that can be achieved when the LPG is used as a sensor.

Electric arc

In the electric arc discharge method, the fibre is heated by an electric arc generated commonly by a fusion splicer. The electric arc is created between two fusion splicer electrodes for a time period of approximately one second (electrodes gap $\approx$ 1 mm) [180]. The point-by-point aproach is used by translating the fibre along an axis perpendicular to the arc by a distance. The main advantages of arc electric to inscribe LPGs are that it is easy-to-use, fast and relatively inexpensive [200]. However, the drawbacks are low repeatability of both physical and optical characteristics of the inscribed gratings [195], physical deformation of the fibre resulting in high level of losses compared to other techniques as UV photosensitivity, and the inability to inscribe gratings shorter than 221 μm because of the width of the electric arc [201].

Table 2.5 summarizes the main attributes of each technique, showing that the point-by-point technique provides advantages such as the complete customization of the grating structure and length that allows the tailoring of the sensor platform to the requirements of the application.

Table 2.5: Comparative between the main LPG fabrication techniques.

Abbreviations used: Advantage (+), (−) Disadvantage.

Technique	Notes
Amplitude mask	(+) Fast (+) Suitable for mass production (+) Easy to implement (+) Period of the grating Λ>100μm (+) Suitable for low temperature applications (< 250°C) (−) High cost of the chrome on silica and dielectric masks (−) Metal mask suffer from oxidation and deformation (−) UV irradiation only works with photosensitive fibres
Point-by-point	(+) Highly customized (+) Easy to implement (+) Period of the grating Λ>100μm (+) Suitable for low temperature applications (< 250°C) (+) Cheaper than amplitude mask (−) UV irradiation only works with photosensitive fibres (−) Time consuming
CO_2 laser exposure	(+) High temperature applications (< 1100°C) (+) To use in any kind of fibre (+) Easy to implement (+) Cheaper than UV photosensitive techniques (−) Period of the grating $\Lambda > 180$ μm (−) Low reproducibility
Electric arc	(+) Easy to implement (+) To use in any kind of fibre (+) High temperature applications (< 1100°C) (+) Cheaper than CO_2 exposure (−) Period of the grating $\Lambda > 221$ μm (−) Low reproducibility

2.4 Review of recognition elements

The recognition element (RE) is a vital component of a biological sensor. It is responsible for the specific recognition of the target analyte to generate a physicochemical signal which is monitored on the transducer [202]. The recognition element can be a sensitive biological element, such as an enzyme, antibody, nucleic acid, cell, bacteriophage, aptamer or a molecularly imprinted polymer, that binds the analyte (e.g. enzyme substrate, antigen, complementary nucleic acid, to mention a few) [203]. Recognition elements can be divided in two main groups: catalytic and affinitive (also called irreversible recognition elements or non-catalytic) [204].

2.4.1 Catalytic recognition elements

The catalytic group of recognition elements includes enzymes, microorganisms and tissues.

Tissues and whole cells

Tissue and whole cell (bacteria, algae, fungi) based sensors permit a complex sequence of reactions because co-enzymes and other cofactors are present in the more natural environment, which leads to the advantage of the detection of a species rather than a specific analyte. However, for some applications the lack of specificity is a major drawback [202]. In addition, whole cell sensors are mostly used for environmental applications (by measuring their metabolic status) such as the detection of pesticides and heavy metals, rather than for bacterial detection [205], i.e. the bacteria is used as recognition element rather than the target analyte.

Enzymes

Within the catalytic group, enzymes are the most widely used recognition element, due to their high level of selectivity and better performance when compared with non-biological catalysts. Enzymes are macromolecules (most of them are proteins and few are catalytic RNA molecules) that accelerate chemical reactions. Enzymes act upon molecules that are called substrates and convert the substrates into different molecules known as products. In an enzymatic sensor, the enzyme reacts selectively with its substrate (target analyte). An enzymatic sensor can measure the catalysis (produced species) or the inhibition (consumed species) of enzymes by the substrate. In other words, the enzyme can metabolize the substrate, so the concentration of the substrate is determined through measuring the catalytic transformation of the substrate by the enzyme; or, the enzyme can be inhibited by the substrate, so the concentration of the analyte is associated with a decrease in formation of enzymatic products [206].

Several enzymes, such as alkaline phosphatase, oxidase, gamma-glutamyl aminopeptidase and catalase have been employed in enzymatic tests for the detection of *Helicobacter pylori*, previously known as *Campylobacter pylori*, and *Campylobacter* spp. [207, 208]. Briefly, commercial tablet tests containing specific chromogenic substrates were used for the detection of enzymes produced by bacteria. Pre-enriched bacterial

samples were placed in a tube and the tablet containing a known substrate was added to the tube. The tube was hand shaken for about 15 seconds. The mixtures were incubated for 4 h at 37 °C. For the detection of urease, additionally to the detection with the tablet, a swab stick was dipped in urea broth and suspect colonies were touched. The positive detection of *H. pylori* was indicated by a pink colour on the swab that appeared in less than 30 seconds. On the other hand, *Campylobacter jejuni* was observed to be positive for oxidase, catalase and gamma-glutamyl aminopeptidase. A positive bacterial detection with oxidase was indicated by deep purple colour that appeared within 10 seconds after smearing a wooden stick on filter paper impregnated with 1 % tetramethyl-p-phenylenediamine dihydrochloride. For catalase, bacterial strains were touched with a capillary tube containing 10 volumes of hydrogen peroxide. The detection was indicated by effervescence in the tube. Finally, for the positive detection with the gamma-glutamyl aminopeptidase, an overnight incubation and a UV light were required.

Despite having high specificity and being easy-to-employ [209], the limitations of using enzymes as recognition elements are their instability via thermal denaturation, expensive and time consuming purification, and the fact that they are efficient only at optimum pH and temperature [206].

2.4.2 Affinity recognition elements

The affinity or non-catalytic group of recognition elements comprises nucleic acids, antibodies and the more recently introduced recognition elements such as bacteriophages (phages), molecularly-imprinted polymers (MIPs) and aptamers. In the field of affinity-base sensors, optical devices have a clear advantage over electrochemical devices due to their ability to monitor binding reactions directly [210]. Unlike optical sensors, electrochemical sensors detect the target analyte by relying on the use of label compounds such as enzymes, gold nanoparticles, fluorescence markers, etc. to create a signal. For this reason, the present review is focused on the used of RE integrated with optical transducers.

Nucleic acids

Deoxyribonucleic acid (DNA) is a molecule composed of two chains of nucleotides that form a double helix with the function of carrying and passing genetic information. DNA has been used as the RE for *Campylobacter* detection [211, 212, 213]. In nucleic acid-based sensors (also called genosensors), the DNA or RNA of the RE recognizes and binds (hybridizes) the DNA or RNA of the RE [206]. The high specificity between the single stranded DNA from the RE with the complementary strand from the analyte through the hybridization makes the detection of specific genes (such as bacterial genes) possible [214]. The advantages of using nucleic acids as REs for sensing applications are the high sensitivity, high specificity and stability. In addition, the sensor can be regenerated repeatedly and compared with antibody-based sensors, genosensors can be stored for longer periods [215]. Despite being mostly employed by electrochemical sensors and PCR [216], DNA has also been used as the RE in optical transducers. SPR has been applied to the detection of DNA using 17 mer (a single-stranded short DNA molecule with 17 bases) attached by adsorption

to the surface of glass prism. The hybridization to the target analyte (a 97 mer) was detected by angle modulation [217]. However, the major limitations of such genosensors are the long and labour intensive sample preparation, as hybridization occurs at specific conditions of temperature [217].

Antibodies

Immunoglobulins (Igs), or antibodies, have been the most popular affinity-RE used in sensors [214]. As was mentioned in Sec. 2.2.2, antibodies are glycoproteins produced by plasma cells of the immune system and have the ability to specifically bind an almost limitless variety of target molecules, which enables them to neutralize toxins and pathogens like bacteria or viruses [202]. Antibodies can be polyclonal if they are produced from different B cells or monoclonal if they are produced from a single B cell. Polyclonal antibodies can recognize multiple epitopes (target regions or locations on the antigen) on the same antigen. By contrast, a monoclonal antibody recognizes a unique epitope on the antigen [206]. Antibodies are commonly represented as a Y-shaped structure, as shown in the schematic in Fig. 2.19. The typical structure of an antibody contains two identical Fab (or F_{ab}, fragment antibody) sections attached to two identical Fc (or F_c, fragment crystallizable) sections. A binding site for the antigen is located in the variable region of the Fab sections (domains). The Fc region does not interact with the antigen, but contains functional groups (carboxylic groups) that allow the attachment to solid supports [202]. Equivalently, the antibody structure contains two identical heavy chain polypeptides and two identical light chains connected by disulfide bonds (also called SS-bonds) [218]. Each heavy chain contains two regions: the constant region and the variable region. The constant region is identical in all antibodies of the same isotype, but different in antibodies from different isotype. The variable region of the heavy chain is the same in antibodies produced by the same B cell. Igs of mammals are divided into isotypes according to the structure of the constant region of the heavy chains in IgA, IgG, IgD, IgE, and IgM [219]. These isotypes or classes differ in their biological properties, functional locations, number of constant domains, and ability to deal with different antigens. The composition of the total Ig pool, for example in human serum, is IgG (70-75%), IgA (15%), IgM (10%), IgE (less than 1%) and IgD (less than 1%) [219]. The dimensions of an antibody are 14 x 10 x 4 nm^3 and 7 x 5 x 4 nm^3 for the Fab fragments [220].

The main advantages of the use of antibodies as RE are the high sensitivity and selectivity. In addition, the integration with sensing platforms is easy to perform [214]. Another advantage is that various antibodies are commercially available [221].

Due to the multiple advantages, immunosensors (sensors using antibodies as the RE) have been explored in a wide variety of transducers such as electrochemical (amperometric [222], potentiometric [223], impedimetric [224], conductometric [225]), gravimetric or mass-sensitive (quartz crystal microbalance (QCM) [226], piezoelectric [227]), and optical (SPR [118], optical fibres [49], fluorescence [228]) for the detection of bacteria, microbial toxins and contaminants. Some examples of immunosensors were given in Sec. 2.2.4.

Despite the advantages, antibodies present some limitations. Antibodies lose their binding properties under hostile conditions of pH and temperature. In addition,

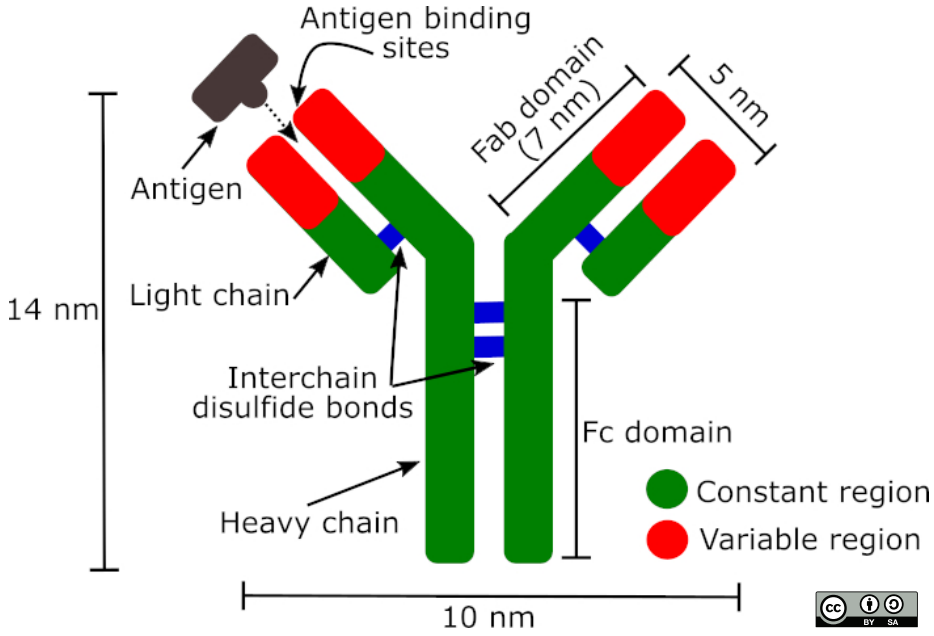

Figure 2.19: Schematic of an antibody.

the production of antibodies for toxic targets or compounds that cannot generate an immune response is complicated. Polyclonal antibodies are cheap and fast to produce (4-8 weeks) [229], but in order to obtain them, animals have to be immunized [221]. Another disadvantage of polyclonal antibodies is the low specificity compared with monoclonal antibodies [39]. On the other hand, monoclonal antibodies are highly specific but their production (by hybridoma technology) is expensive and time-consuming (3-6 months) [229, 214]. A general disadvantage of sensors with immobilized bio-material is that they have a limited shelf life and that they degrade over time. For instance, in the case of antibodies, they have to be maintained refrigerated at 2-8°C for up to 6 months [230]. For a longer shelf life of 18 months from date of despatch, they must be kept at -20°C or -80°C and repeated freezing and thrawing must be avoided as this may denature the antibody [231, 232].

Bacteriophages

Bacteriophages, or phages, are viruses that infect bacteria, use the host bacteria cell as an incubator for their own reproduction, and have the ability to display peptides or proteins in their surface (phage display) [214]. Phage display is an *in vitro* technique in which a gene encoding a peptide or protein is inserted into a bacteriophage, causing the phage to display the peptide or protein on its exterior [233]. A schematic of the phage display technique is shown in Fig. 2.20. Briefly, different sets of genes are inserted into bacteriophages to create a phage library. The library is exposed to the target analytes to promote the binding. The unbound phages are washed away and the bound pages are eluted from the analytes by changing the pH or incubating with detergents [234]. The eluted phages are then amplified and the cycle is repeated 3-5 times

Phages have been employed as RE for bacterial detection (mainly for *E. coli* [235])

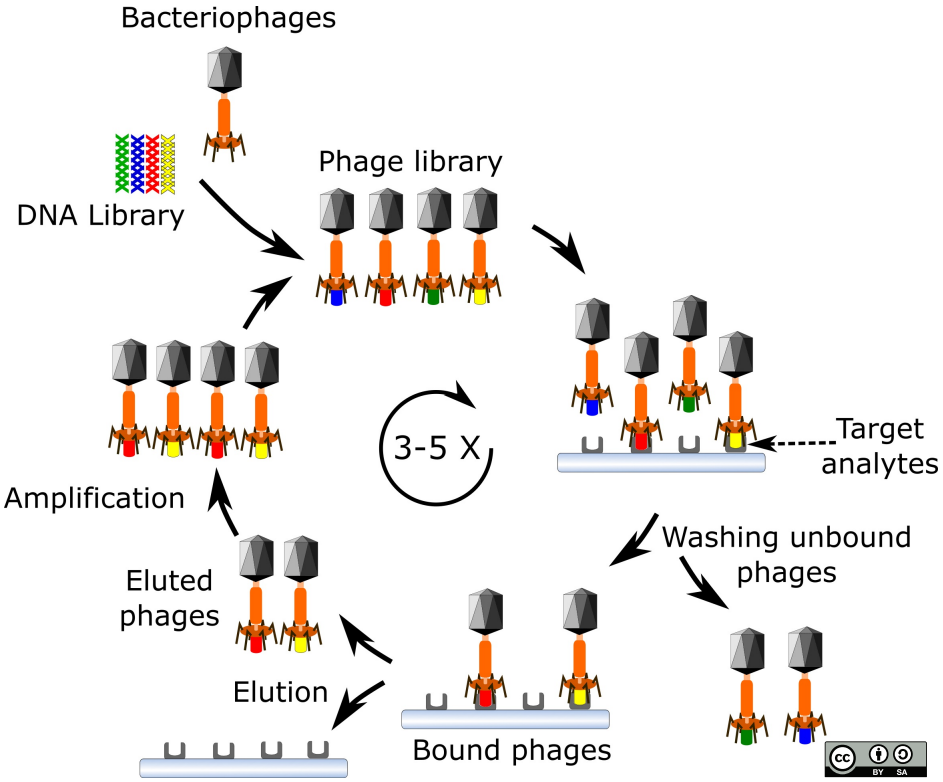

Figure 2.20: Schematic of the phage display technique.

due to their high sensitivity and specificity [235]. In addition, phage-based sensors are environmentally more robust than immunosensors. For instance, phages can be stored for longer times than antibodies with minimal loss in affinity [206], can be used in a range of pH from 3 to 11 [236, 237], and they maintain their binding ability at high temperatures (six weeks at 63 °C, and three days at 76 °C) [214]. Furthermore, bacteriophages are stable when they are exposed to organic solvents [234]. For example, phages retain their infectivity in 99% acetronile, 80% methanol and 50% ethanol [214]. Another advantage is that phages can be produced quickly and at low cost. In addition, bacteriophages are produced *in vitro*, avoiding the use of animals, which allows the production of phages for toxic targets. Phages have been used as RE for a number of optical transducers such as SPR [238], bioluminescence assays [239], and optical fibres [159]. For instance, Balasubramanian *et al.* reported an SPR sensor for the detection of *Staphylococcus aureus* using a phage as RE. Briefly, phages were immobilized by adsorption (5 min) onto the gold surface of the sensor and the non-specific sites were blocked with BSA (1 mg/mL in PBS). Later, the sensor was incubated in *S. aureus* solutions from 10^1 to 10^8 CFU/mL. The reported limit of detection was 10^4 CFU/mL. The previously described assay was repeated, incubating the sensor in the phage solution for 12 h. Despite the fact that the coverage of the surface by the phages was increased by 16%, there was no improvement in the sensitivity of the sensor. This may be due the random orientation of the phages and the self-interaction of the phages in the long term incubation. As with SPR, phages have been employed for the detection of *E. coli* using an LPG sensor. Briefly, a T4 phage solution at concentration of 10^{10} PFU/mL (plaque forming unit (PFU), a

measure of the number of viruses that are capable of lysing host cells and forming a plaque) in PBS was physically adsorbed onto the surface of an optical fibre containing an LPG for 4 hours. The sensor was washed several times to remove the unbound phages and incubated in BSA solution (1 mg/mL) for 30 minutes. Finally, the sensor was incubated in *E.coli* solution (10^8 CFU/mL) for 20 minutes and washed to remove the unbound bacteria. Brzozowska *et al.* reported an LPG sensor using a recombinant adhesive phage protein as recognition element [157]. Briefly, an LPG of 4 cm in length and period of 226.8 μm fabricated with an amplitude mask (see Sec. 2.3.2) was coated with a bacteriophage adhesin for the detection of bacteria (*Escherichia coli*). The adhesin (cell-surface component that facilitate adhesion or adherence to other cells or to surfaces) binds the bacteria (*E. coli*) by recognizing its bacterial lipopolysaccharide (LPS). LPS is the major component of the outer membrane of Gram-negative bacteria, contributing to its structural integrity and protecting the bacteria. LPS is also implicated in non-pathogenic aspects of bacterial ecology, including surface adhesion, bacteriophage sensitivity, and interactions with predators [240]. The response of the sensor was reported for a concentration of *E. coli* LPS of 5 μg.

Despite the promising advantages, bacteriophages present some drawbacks. The first disadvantage is that the field of immobilization of phages onto a sensor's surface is still underdeveloped and the orientated immobilization of phages is still a challenge [234]. A second disadvantage for integration with sensing platforms is their large size. The typical size of phages ranges from 24-200 nm in length, with T4 being one of the largest phages, being 200 nm long and 80-100 wide [241]. As, for example, SPR-based sensors detect the attachment of the target analyte within 100 nm [119], any bacterial interaction with the phage falls beyond the detection range. Finally, another disadvantage is that phages tend to lyse the captured bacteria, resulting in a loss of sensor signal when incubated for longer time periods [234].

Aptamers

Aptamers are nucleic acid (RNA or single-stranded DNA) or peptide (short chains of amino acid monomers) molecules obtained by a synthetic process *in vitro* based on the systematic evolution of ligands by exponential enrichment (SELEX). SELEX is an integrated chemistry technique that incorporates combinatorial chemistry, PCR and gene sequencing [221]. A schematic of the SELEX technique is shown in Fig. 2.21. Briefly, a random nucleic acid library (library of sequences, usually $\approx 10^{15}$) is incubated with the target analyte and the unbond sequences are washed away. Then, the bound nucleic acids are eluted, amplified by PCR and serve as an enriched library for the next cycle. The cycle is repeated up to 15 times [242]. Because of this artificial process, aptamers are also called "chemical antibodies" or "synthetic antibodies" [243], being approximately ten times smaller than antibodies ($\approx$ 2 nm [242]). Aptamers have been used as RE for the detection of a large number of target analytes [206], among them bacteria [244, 245], food contaminants [243] and cancer cells [246]. Sensors using aptamers as RE are referred to as aptasensors and possess a number of advantages over sensors using natural RE such as antibodies and enzymes. For example, aptamers are processed *in vitro*, which allows the customisation of the structure to select the specificity for the target analyte [242]. In addition, aptamers

are reproducible and suitable for toxic targets that are limited for antibodies that require the use of animals, avoiding furthermore batch-to-batch variations [247]. Additionally, aptamers are thermally stable and reusable [206].

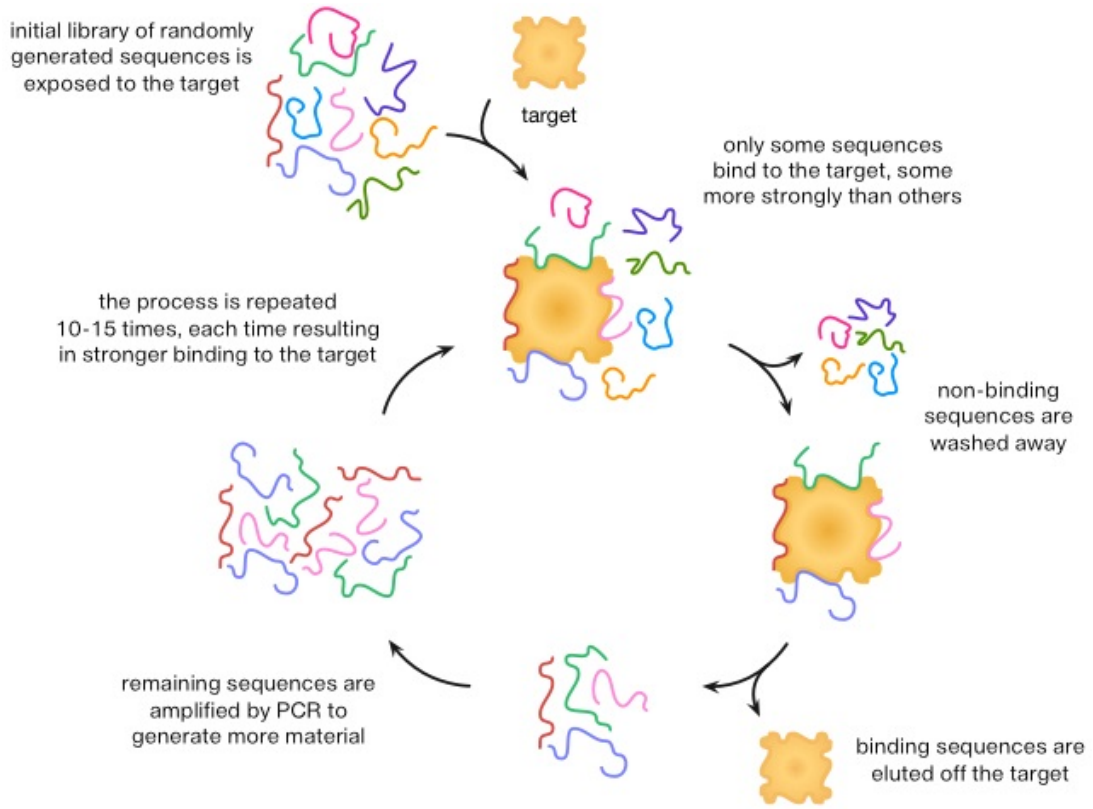

Figure 2.21: Schematic of the systematic evolution of ligands by exponential enrichment (SELEX) technique. Illustration from [248].

A fibre-optic sensor functionalized with an antibody in a sandwich assay with an aptamer for bacterial detection was reported by Ohk *et al.* [245]. Briefly, a polyclonal antibody specific to *Listeria monocytogenes* was immobilized onto the surface of an optical fibre. The antibody coated optical fibre was immersed in bacterial suspensions at 4°C for 2 h. After a washing to remove unbound bacteria, the optical fibre was immersed in a solution containing an aptamer labelled with a fluorescent dye (Alexa Fluor 647). Fluorescence intensity was recorded with the use of Analyte 2000 Fiber Optic Fluorometer. The reported limit of detection was $1x10^3$ CFU/mL. In different work, DNA aptamers were selected and characterized for the specific binding with *Campylobacter jejuni* using SELEX [244]. The binding of the 10-cycle aptamers with a solution contaning 10^8-10^9 cells was evaluated by flow cytometry analysis. Regarding the use of peptide aptamers as RE for sensing applications, an SPR-based sensor for the detection of bacterial toxins was reported by Dudak *et al.* [249]. In their work, a peptide from a library was selected for the detection of staphylococcal enterotoxin B. The peptide was immobilized covalently onto the gold-coated surface of the SPR chip. The limit of detection reported for the toxin was 20 μg/mL. Despite the promising advantages of aptamers as RE, the major drawbacks are the limited availability of aptamer types and the poor knowledge

of surface-immobilization technologies [242]. The main focus for aptasensors in the literature currently available is as the interaction aptamer-target in fluorescent transducers [247].

Molecularly imprinted polymers

Molecularly imprinted polymers (MIPs) are artificial recognition elements based on the "molecular key and lock" principle for enzyme-substrate interaction [250]. Some of them can be produced in size comparable with antibodies ($\approx$ 17 nm [251]). In the first stage, called complexation, the template or "key molecules" are mixed with functional monomers. Functional monomers have moieties that bind with functional moieties of the template. In the second stage, also referred as polymerization, the templates are fixed in the polymer matrix with crosslinkers, which act, metaphorically, like a "molecular glue". Finally, in the third stage, the template molecule is removed from the polymer matrix by washing with solvent [252], by washing with pressurized hot water [253], or by photo degradation [254]. A schematic of the molecular imprinting procedure is shown in Fig. 2.22. The advantages of MIPs as RE are that they posses a specificity comparable with antibodies or higher; MIPs are more stable than antibodies in extreme environmental conditions (up to 150 °C); MIPs have a long shelf life (8 years) without loss in affinity [214]; production of MIPs is carried out *in vitro*, being more reproducible and avoiding the use of animals and batch-to-batch variations; MIPs can be reusable, which reduces the cost of the assay [221]. A number of works have reported the use of MIPs for antibiotic detection [255, 256, 257]. Particularly, Korposh *et al.* reported an LPG sensor functionalized with MIPs for the detection of vancomycin [255]. Briefly, the synthesis and polymerization of the nanoMIPs specific for vancomycin was performed with the aid of an automated reactor (HEL Ltd., Borehamwood, UK). Vancomycin was immobilized on glass beads as a solid support. Later, the attached affinity nanoparticles were collected using hot washing. Finally, the nanoMIPS were concentrated by filtration and attached to the functionalized surface of an LPG. The sensor was tested for 10 nM, 100nM, 10 μM and 700 μM of vancomycin and the selecetivity was tested with solutions of amoxicillin, bleomycin and gentamicin. MIP is a promising approach for use as RE [250]. However, the major limitation of MIPs is that are not commercially available [221]. Another drawback is the time-consuming fabrication process and the complex protocols for integration with sensors [206]. To the best of my knowledge, the application of MIPs for *Campylobacter jejuni* detection has not been reported yet.

Table 2.6 summarizes the features of the main RE for bacterial detection.

Table 2.6: Comparative between the main recognition elements for bacterial detection.

Abbreviations used: Advantage (+), (−) Disadvantage.

Recognition element	Notes
Enzymes	(+) Specificity (+) Simple procedures (−) Costly and time consuming purification (−) Poor stability (−) Efficient only at optimum pH and temperature
Antibodies	(+) Specificity (+) Commercially available (+) Easy integration with sensors (−) Production requires use of animals (−) Lack of stability (−) Laborious production
Nucleic acids	(+) Stability (+) Very sensitive and selective (−) Limited target analyte (complementary nucleic acid) (−) Complicated sample preparation
Bacteriophages	(+) Sensitivity and Selectivity (+) Stability (−) Not commercially available (−) Large size
Aptamers	(+) Custom structure for high selectivity (+) Reproducible, reusable and cost effective (+) Thermally stable (−) Few commercially available (−) Poor knowledge of surface-immobilization
MIPs	(+) Specificity comparable with antibodies (or higher) (+) High stability (+) Reusable and low cost (+) Long shelf life (8 years) (−) Not commercially available (−) Complex fabrication procedures (−) Complex protocols for integration with sensors

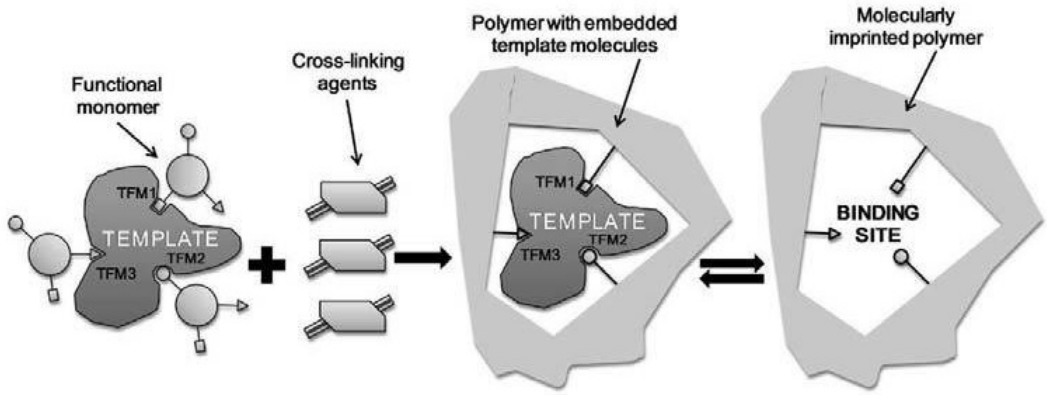

Figure 2.22: Schematic of the molecular imprinting process. Illustration from [250].

2.5 Review of immobilization techniques

Immobilization is the technique of binding the recognition element to a solid support (optical fibre, well-plate, SPR chip, etc.) as a means of increasing their activity and stability, improving the technological application of the reaction [258]. The immobilization aims to restrict the freedom of movement of the recognition element in a certain defined region or space with retention of its biochemical activity. Immobilization of the RE often stabilizes its structure, allowing its application even under harsh conditions of pH, temperature, and organic solvents and enables its use in the fabrication of biosensor probes [35].

There are a number of requirements that the immobilization technique must satisfy [202]:

1. The RE must be strongly attached to the sensing surface.
2. The RE must maintain its activity when immobilized on the sensing surface.
3. The RE must be stable and durable.
4. The RE must be highly specific to the target analyte.

Possible means of immobilization are entrapment, adsorption, covalent binding and affinity [221]. Schematics of these methods are shown in Fig. 2.23.

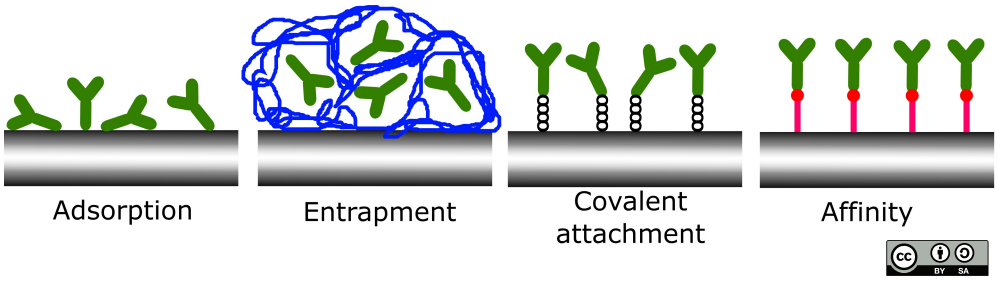

Figure 2.23: Schematic of the main immobilization techniques.

2.5.1 Entrapment

Entrapment consists of the encapsulation or caging of the RE by covalent or non-covalent bonds within matrices such as gels and polymers [203]. Entrapment has been mostly employed for the immobilization of cells and enzymes [259, 260, 261]. This method is fast, cheap and easy to perform, usually in mild conditions at room temperature. Furthermore, entrapment does not denature the RE, so they maintain their biochemical activity [202]. In addition, multiple types of REs can be immobilized within the same matrix [203]. Another advantage is that matrices are optically transparent, which makes entrapment an attractive immobilization method for biosensing applications [260]. However, the method presents some limitations. First, the leakage of the RE from the matrix can restrict the performance of the sensor [202]. Second, the matrix can block the active sites of the RE, compromising the sensitivity [221]. Finally, in terms of reproducibility, this method is poor as the entrapment of the RE within the matrix is not controlled [262].

2.5.2 Adsorption

In adsorption, the recognition element is bound to the carrier material via reversible surface interactions. The forces involved are electrostatic, van der Waal forces, ionic, H-bonding interactions, and possibly hydrophobic forces [35]. The forces are generally weak, but they are sufficiently large to allow reasonable binding. Adsorption utilizes existing surface interactions between the recognition element and the solid support and does not require chemical activation or modification. Although binding forces between the recognition element and the support are often very strong, they may be weakened by inappropriate changes in pH or ionic strength.

Adsorption is a simple method and the support can be easily recovered after use by promoting desorption of the recognition element with no noxious reagents involved. The main drawback is that the recognition element can be easily desorbed from the support by subtle changes in the reaction medium in the case of aqueous systems. In addition, the RE are randomly orientated on the surface of the sensor [202].

Smietana *et al.* [159] reported the detection of *E. coli* bacteria by physically immobilized bacteriophages over an LPG of 5 cm in length and 169.7 μm of period fabricated with an amplitude mask. Briefly, the LPG was cleaned with methanol and rinsed with deionized water and PBS. Then, the sensor was incubated for 4 hours in a T4 bacteriophage solution at a concentration of 10^{10} PFU/mL in PBS. The unattached phages were removed by rinsing the sensor with PBS. Next, the unbound sites of the surface were blocked with a BSA solution at a concentration of 1 mg/mL for 30 minutes. Then, the sensor was rinsed with PBS. Finally, the sensor was immersed in a bacterial solution of *E. coli* for 20 minutes and rinsed with PBS to remove unbound cells. A detected concentration of 10^8 CFU/mL was reported.

2.5.3 Covalent attachment

In covalent attachment, the bond occurs between the functional groups in the recognition element and the solid support. For the covalent binding, the surface of

the solid support must be derivatized (chemically modified to provide the functional groups) for the attachment with the recognition element [263]. The bond between the functional groups of the RE and the functional groups of the solid support may also be established with the use of a crosslinking reagent, also known as crosslinker [264]. The steps usually involved in the covalent attachment of a RE onto the surface of the solid support are: i) derivatization strategy, ii) crosslinker deposition and, iii) RE deposition. Depending on the solid support material, different derivatized strategies can be applied. For example, thiol-based chemistry is usually performed on gold surfaces and silane-based chemistry on silica surfaces [265]. The covalent attachment is the most widely employed method for the immobilization of enzymes and antibodies [35, 266, 267, 268].

One of the most studied surfaces for covalent attachment is silicon dioxide (SiO_2), also known as silica [263] (See Fig. 2.24). All silica-based materials such as glass, fused silica and quartz, can be derivatized through the same coupling strategy. Silanization is by far the most used derivation approach [263]. The goal of silanization is to form bonds across the interface between mineral components and organic components [269]. Silanization is the covering of a surface through self-assembly with organofunctional alkoxysilane molecules [270]. Silica-based surfaces can be silanized because they contain hydroxyl groups (-OH) which attack and displace the alkoxy groups (R-O, where R stand for carbon substituents or hydrogen atoms) on the silane, thus forming a covalent -Si-O-Si- bond [269]. In addition, silanization is used in glassware to increase its hydrophobicity and to reduce adherence of solutes such as cells, proteins and single-stranded nucleic acids to flask walls [271]. The silanization strategy requires a surface pre-activation step, which is carried out with acids, usually strong acids such as sulphuric acid (H_2SO_4) and hydrochloric acid (HCl), or other acid solutions such as piranha. Following the acid treatment, the activation procedure involves a treatment with strong bases, such as sodium hydroxide (NaOH) [263]. This pre-activation step generates the silanol groups (Si-OH) at the surface of the solid support for the later reaction with the silane [272].

Depending on the functional group to be introduced (e.g. amino group or thiol group), different silanes can be used [274, 269]. For example, 3-Aminopropyl-triethoxysilane (APTES) or 3-Aminopropyl-trimethoxysilane (APTMS) are usually employed for an amino-terminated surface [275, 276, 270, 277, 272, 278, 279], while for a thiol-terminated surface, 3-Mercaptopropyl-trimethoxysilane (MPTMS) is commonly used [267, 280, 264]. In the case of an amino-terminated surface, both APTES and APTMS generate silane layers of similar characteristics [281]. These silanes are a good starting point for the modification of the solid support [273]. They contain three alkoxy groups which make the silane molecules form polymeric films with a maximum coverage of the surface [273]. However, one advantage of APTES over APTMS is the reduced thickness of the layer for the silanes prepared in anhydrous toluene for 24 h and after exposure to water (8±2 Å for APTES vs 10±4 Å for APTMS) [281]. On the other hand, one advantage of APTMS, mainly used in optical applications [282, 277, 283], is the tensile strength, which is higher than that of APTES by more than 10% [284]. In addition, another drawback of APTES is that its three ethoxy groups polymerize in presence of water and can generate a low silane density layer and/or result in weakly attached silane molecules [281].

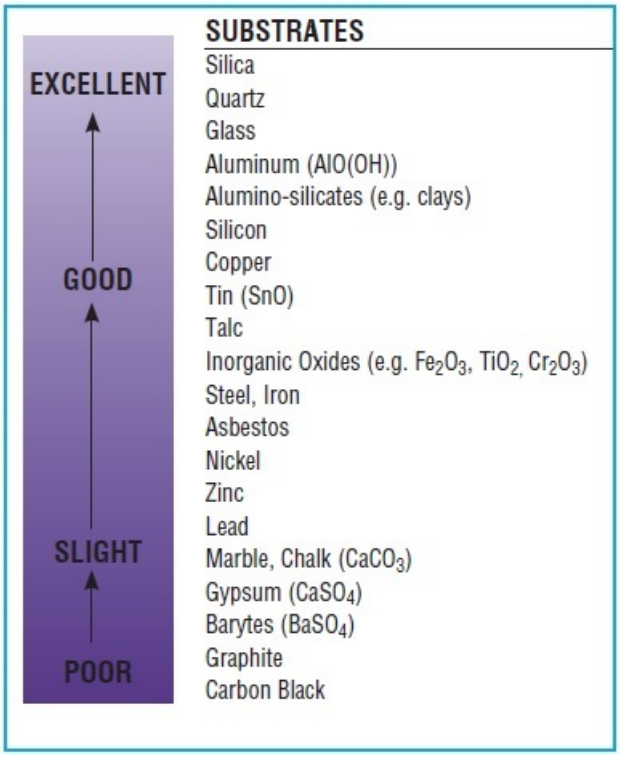

Figure 2.24: Silane effectiveness on inorganic substrates. Image from [273].

A crosslinker is a reagent that reacts with functional groups on two or more molecules to form a covalent linkage between the molecules [285]. Crosslinkers have a part called spacer arm which is the molecular span or "bridge" incorporated between the reactive groups of the molecule. The length of these chemical bridges ranges from zero to > 100 Å [285]. Depending whether the reagent has the same or different reactive groups at either end, crosslinkers can be classified as homobifunctional and heterobifunctional. Homobifunctional crosslinkers, such as formaldehyde and glutaraldehyde, have identical reactive groups at either end of the spacer arm. These types of crosslinkers are employed in one-step reaction procedures to attach molecules that contain like functional groups [286]. On the other hand, heterobifunctional crosslinkers such as N-(3-dimethylaminodipropyl)-N'-ethylcarbodiimide (EDC), N-hydroxy-succinimide (NHS) and N-hydroxy-sulfosuccinimide (NHSS), have different reactive groups at either end. These types of crosslinkers are used in one-step procedures, but they are also applied in two-step procedures (sequential conjugations) [285]. Formaldehyde is one of the most used crosslinkers but it is mainly employed for the fixation of cells and tissues [285, 287]. For the covalent attachment of antibodies on solid supports, crosslinkers such as EDC, NHS, NHSS, and glutaraldehyde are commonly employed since amino groups on the antibody surface can be easily attached to a variety of reactive moieties [265]. EDC and NHS are usually used together [288, 289, 290, 228]. EDC couples carboxyl groups (-COOH) to primary amines ($-NH_2$). EDC reacts with a carboxyl group to form an ester group. One advantage of the use of EDC as a crosslinker is that it is soluble in water, which avoids the use of organic solvents [291]. However, one drawback is that the formed ester group is very unstable in aqueous solution [291]. NHS or NHSS are used to increase

the stability of the reactive ester and quickly react with amino groups, forming a stable bond [291]. Glutaraldehyde is the most popular homobifunctional crosslinker in use in recent years [292]. Glutaraldehyde is used to couple amino-terminated surfaces and amino-terminated REs [286]. One advantage is that these glutaraldehyde conjugates are easy to make [285]. Another advantage of using glutaraldehyde over EDC/NHS coupling is that it allows the reduction of the procedure by one processing step [265]. Glutaraldehyde is used for other purposes, including as a detergent and as a fixative for cell and tissues [293, 287].

Bandara *et al.* reported the covalent attachment of antibodies on the surface of an LPG for the detection of methicillin-resistant *Staphylococci aureus* (MRSA) [160]. Concisely, the surface of the LPG sensor, with a period of 116 μm, was functionalized to create a layer containing the functional groups for the later covalent attachment of antibody. The antibody (mouse monoclonal antibody to penicillin-binding protein for detection of methicillin-resistant staphylococci) was chemically prepared for attachment onto the surface of the sensor by mixing equal volumes (0.5 mL) of N-hydroxy-sulfosuccinimide (NHSS) and N-(3-dimethylaminodipropyl)-N'-ethylcarbodiimide (EDC). The prepared antibody (100 μg/mL) was added to the sensor and incubated for 1 hour. Subsequently, the free sites on the surface of the sensor were blocked to avoid non-specific adsorption with 1 % of dry milk for 10 min. The sensor was washed and exposed to dilutions of bacterial suspensions, achieving a limit of detection of 10^2 CFU/mL. Then, the specificity of the sensor was tested against a methicillin-sensitive *S. aureus* (MSSA). For bacterial concentration of 1 x 10^6 CFU/mL of the target analyte (MRSA), the light transmission was reduced by 50.3%. In contrast, when exposed to a different bacterial strain (MSSA) at the same concentration, the light transmission was reduced by 1.8%.

The immobilization of the RE by covalent binding to a solid support has multiple advantages that have led to it becoming the most employed immobilization method [266]. First, the immobilized RE is highly stable [221, 203] due to the covalent network formed between the surface and the silane molecules [269]. Second, the strength of the attachment is very strong [35], minimizing the RE loss through desorption from the solid support [294]. Finally, as a result of the strong bond of the RE to the solid support, the binding is irreversible [295].

Despite covalent attachment being more controlled than adsorption, in which the immobilization is randomly orientated and poorly controlled, the binding occurs through one of several functional groups on the surface of the RE [202], and as a consequence there are still a set of possible orientations [296]. Another disadvantage is the possible denaturation (activity loss) of the RE due to use of toxic chemicals [221, 203, 295].

2.5.4 Affinity

Affinity allows the control of the RE's orientation with the aim of avoiding the blocking of their binding sites. The oriented and site-specific immobilization is achieved by creating affinity bonds between the solid support (for example with avidin, lectin) and specific groups in the RE (for example biotin, carbohydrate residue) [203]. In many cases, REs need to be labelled with an affinity tag (for

example biotin).

The most notable advantage of affinity is that all REs have the same orientation [221]. This uniform and oriented immobilization results in a higher sensitivity compared with random binding methods [297]. In addition, REs are highly stable [203].

This immobilization method presents some limitations. First, the procedure is long and complicated. Second, the need for the presence of specific groups on the RE, for example, biotin [203]. Third, the RE can suffer from denaturation (loss in activity) due to the labelling process [221]. Finally, streptavidin exhibits a peptide that presents high affinity for the transmembrane receptors displayed on the cell surface, which promotes the binding of non-specific bacteria [298].

An SPR sensor for monitoring antigen recognition using the avidin-biotin method was reported by Mu *et al.* [299]. Briefly, a gold coated (50 nm) prism was cleaned and exposed to 5 mmol/L of ethanolic solution of 3,3′-dithiodiglycolig acid (DDA) for 1 hour to form a charged self-assembled monolayer on the gold surface. After rinsing in water, the prism was immersed in a crosslinker mix solution of 50%-50% of 0.25 mL of 100 mg/mL EDC and 0.25 mL of 100 mg/mL NHS for 1 hour to activate carboxyl groups and to conjugate to amino groups. After rinsing in water, the activated sensor was exposed to 0.2 mg/mL of avidin solution for 1 hour and blocked against nonspecific binding in 5% BSA in PBS. Finally, the sensor was exposed to 2 μg/mL of biotinlated antibody (antibody with a covalently attached biotin) (anti-rabbit IgG) for 40 mins. The detection assay was performed by exposing the sensor to the target antigen, rabbit anti-human factor B, at concentrations in the range of 0.5-100 μg/mL for 30 min.

An LPG-based sensor functionalized with bacteriophage adhesin for bacterial detection was published by Koba *et al.* [158]. In essence, an LPG of period 226.8 μm and 4 cm in length was fabricated with an amplitude mask. The surface was functionalized and the adhesin was attached. Following several washing steps with phosphate buffered saline (PBS), the sensor was immersed in bacterial dry weights of *E. coli* B at concentrations of 10^7 CFU/mL. In order to evaluate the selectivity of the sensor, it was tested with *E. coli* K12 and *Salmonella enterica*, resulting in responses of approximately of 50% and 20% relative to that achieved from the target bacteria (*E. coli* B). The high response of the sensor to the non-target bacteria may be due to non-specific adsorption onto the surface of the sensor.

Each immobilization technique offers advantages and disadvantages, summarized in Table 2.7. Since there is not a perfect method, the selection of the most suitable technique depends on the nature of the recognition element and the desired performance of the sensor. This implies that it is important to consider the sensitivity, stability, reproducibility, difficulty of implementation and cost [300, 268].

Table 2.7: Comparison between the main immobilization techniques for recognition elements.

Abbreviations used: Advantage (+), Disadvantage (−), Recognition element (RE).

Immobilization technique	Notes
Adsorption	(+) Very simple procedures (+) No denaturation of the RE (+) Solid support easily recovered after use (−) Instability (desorption) (−) Random orientation
Covalent attachment	(+) High stability (+) Mainly used for antibodies and enzymes (+) Minimum RE loss through desorption (+) Strong strength of the bond (−) Laborious procedure (−) Possible denaturation of RE due to toxic substances (−) Not-fully controlled orientation
Entrapment	(+) Fast, cheap and easy to perform (+) Multiple RE can be immobilized (+) Matrices optically transparent (−) Mainly used for cells and enzymes (−) Matrix can block the active sites of RE (−) Possible RE leakage from the matrix (−) Poor reproducibility
Affinity	(+) Stability (+) Uniform and orientated immobilization (+) Sensitivity (−) Long and complicated procedure (−) Need of specific groups on the RE (e.g. biotin) (−) Possible denaturation of RE due to labelling (−) Binding of non-specific bacteria

2.6 Review of cell staining

Bacteria are single-cell (prokaryotic) organisms which can have either a coccus, rod or spiral shape, ranging in size from 0.25 x 1.2 μm to 40 μm, with the most common size being between 1 and 5 μm [301]. The correct identification of bacteria is important in many areas such as agriculture, clinical microbiology and food industry [302]. One way to identify pathogens is with the use of an optical microscope [303]. However, most bacteria are colourless and have a refractive index similar to the solution where they are suspended [302]. Bacterial staining (or cell staining) is a technique used in light microscopy that facilitates the identification and characterization of bacteria by enhancing the visualization of the cell or specific elements due to the physical or chemical union between the dye and the cell component [303]. Cell staining is employed to increase the contrast between the bacteria and the background to differentiate among morphological types, to study internal elements, to observe metabolic processes or to differentiate between live and dead cells [304]. There are two types of bacterial staining, depending on how the stain interact with the bacterial cell: negative staining and positive staining. In the negative staining technique, the dye is used to colour the background, leaving the cell uncoloured. On the other hand, in the positive staining technique, the dye is attached to the bacterial cell, giving it a colour. Positive staining can be divided in simple and differential. Simple staining employs only one dye, but the information obtained is limited to the shape and size of the bacterial cells. On the other hand, differential staining methods are more complex as they employ different dyes to distinguish different groups of bacterial cells or their different parts. An overview of the main methods for bacterial cell staining is shown in Table 2.8.

2.6.1 Simple staining

Simple staining is the process of using a single dye to colour bacterial cells [303]. The dyes are positively charged, contain at least one chromophore (colour-bearing group), and are soluble in water and/or organic solvents [305]. Dyes bind well on bacteria suspended in pH solutions close to 7 (neutral) because under this condition bacteria are negatively charged [302]. The staining times are usually short, from 30 seconds to 2 minutes. The most used stains are crystal violet, carbon fuchsin and methylene blue [306]. This method is generally applied for morphological studies of heat-fixed bacteria smears [303]. The advantages of simple staining are that it is a fast, simple and cheap method. However, the main drawback is that since heat is applied for the fixing with the solid support (usually a glass slide), there is shrinkage of the cell, so the size determination of the cell is not accurate.

2.6.2 Negative staining

Negative or background staining is an easy and rapid method to examine the morphological structure and size of bacteria that are difficult to stain or that are too delicate to be heat-fixed [307]. In this method, bacterial cells are mixed in a drop of a pigment, usually indian ink, nigrosine, methylamine tungstate, ammonium molybdate, or uranyl acetate, and dispersed over a glass slide [306]. Actually, these

Table 2.8: Overview of the main methods for bacterial cell staining

Negative staining	For size, shape and arrangement of cells			
Positive staining	Simple staining	For size, shape and arrangement of cells		
	Differential staining	Group separation	Gram staining	Gram positive
				Gram negative
			Ziehl-Neelsen	Acid-fast
				Nonacid-fast
		Structure visualization	Flagella	Leifson staining
			Capsule	India ink staining
				Anthony staining
			Endospore	Dorner staining
				Schaeffer-Fulton staining

pigments are not bacterial stains since they do not penetrate the cell because these pigments are positively charged and are rejected by the negatively charged bacteria; rather, the pigments colour the glass slide, increasing the background contrast and leaving the cells transparent [302]. The advantages of negative staining are that it is a simple, fast and cheap method. In addition, this method is suitable for bacterial cells such as spirochaetes that are challenging to stain. Another advantage of negative staining is that it can be applied to bacterial cells that are too delicate to be heat-fixed. However, one limitation of this method is that it does not allow the high resolution examination of the cells since there is no stain within the cell to enhance the visualization. In other words, the visualization of anatomical parts of the cell such as granule, endospore and flagella is complicated [302].

2.6.3 Differential staining

Differential staining is used to identify a culture with more than one type of bacteria and also to investigate their physical characteristics. Usually more than one dye is used and the procedures are longer than simple staining and negative staining.

Typically, differential stains are used for general identification of bacterial cells, rather than identifying the species. Some of the most used differential staining methods for bacterial identification are endospore staining, Ziehl Neelsen staining and Gram staining. The selection of the differential staining method depends on the type of characteristic that need to be distinguished. For example, the endospore staining method is used to identify bacteria that can produce endospores, and analogously for other structural stainings (flagella, capsule, etc.). The Ziehl Neelsen staining method is used to identify bacteria that have fatty acids in their cell walls. The Gram staining method is employed to classify bacteria in two groups based on the characteristics of their cell wall. The differential staining methods from Table 2.8 will be described below.

Ziehl-Neelsen staining

The Ziehl-Neelsen staining method is the result of independent contributions from Koch, Ehrlich, Ziehl, Rindfleisch and Neelsen [308]. These contributions, made during the same period (1882-1883), were improvements to the Koch's original method for the staining of the tubercle bacillus. However, it was referred as the Ziehl-Neelsen method for the first time in 1893 [308]. The Ziehl Neelsen staining, also known as acid fast staining, is used to identify bacteria that posses fatty acids (mycolic acids) such as the ones that belong to the genera *Mycobacterium* or *Nocardia*. The cell wall of these kinds of bacteria contains a high concentration of lipids that make it waxy, hydrophobic, and impermeable to routine stains. The staining classifies bacteria in two groups: acid-fast bacteria and nonacid-fast bacteria. Acid-fast bacteria are those which are able to maintain the primary stain when treated with acid or ethanol-based substances during the decolorization process. A phenolic compound used as a primary stain is carbol-fuchsin due to its ability to penetrate the lipid cell wall. Carbol-fuchsin is a mixture that includes phenol, water, and basic fuchsin. When carbol-fuchsin penetrates into a cell, the phenol and basic fuchsin are distributed within the cell due to phenol's solubility in lipids [309]. Following the decolorization process with acid, the smear is counterstained with methylene blue or malachite green which stains the decolorized bacteria to increase the contrast with the red stained acid-fast bacteria. Acid fast cells stain red while non-acid fast bacteria, such as *Campylobacter*, stain blue. The main advantage of this method is that allows the staining of bacteria difficult to stain with simple staining methods. However, one limitation of this method is the laborious protocol, involving heat and solvent-based stains [302]. Furthermore, its major drawback is the low sensitivity ranging from 20% to 43% [310]. Non-acid bacteria (e.g. *Campylobacter jejuni, Escherichia coli, Listeria monocytogenes*) can be stained with simpler and faster methods such as Gram's staining.

Gram staining

The Gram stain is the most widely employed differential staining method in microbiology [307]. It was developed by Gram in 1884. Gram staining is a simple, fast, cheap and effective method employed for the initial classification of unknown isolates,

for morphological identification and to determinate the number of bacteria in clinical samples [311].

Most bacteria are encapsulated by a cell wall. The cell wall is formed mainly by a negatively charged polymer matrix that consists of cross-linked chains of amino sugars (*N*-acetylglucosamine and *N*-acetylmuramic acid) called peptidoglycan [235]. Depending on the structure and thickness of the cell wall, bacteria can be classified in Gram positive or Gram negative (see Fig. 2.25). Both types of bacteria possess an inner cell membrane which contains several proteins and both may have flagella. Gram positive bacteria possess a single layered (as they lack of outer membrane) cell wall that consists of a thick layer of peptidoglycan, which also contains proteins and lipids [302]. The cell wall is straight, even and rigid. The rigidity is due to the high amount of peptidoglycan (about 80% of the cell wall). The typical thickness of the cell wall is 15-80 nm, with a low content of lipids (1-4%) and a very narrow or absent periplasmic section. Gram positive bacteria have a proteinaceous membrane channel to allow the exchange of substances across the membrane, opening one end at the time, the intracellular or the extracellular gate. Gram positive bacteria do not present lipopolysaccharides (LPS). On the other hand, Gram negative bacteria possess a thinner peptidoglycan layer located between two cell membranes. The cell wall is bilayered, wavy, uneven and elastic, with a typical thickness of 8-12 nm. The elasticity of the cell wall is due to the low amount of peptidoglycan (2-12% of the cell wall). The lipid content is about 11-22%. The outer membrane contains lipopolysaccharides (LPS) and proteins known as porins that cross the membrane and act as channels to allow diffusion [235]. Unlike the proteinaceous membrane channel in Gram positive bacteria, porins open simultaneously both the intracellular and extracellular gates. Gram negative bacteria present periplasm, an aqueous environment containing a high concentration of proteins and the peptidoglycan, which may form a hydrated gel [312].

Gram staining is based on the ability of bacteria cell wall to retain the primary dye during solvent treatment. In the Gram's method, the primary stain is crystal violet. Once the cell walls are stained, iodine is added as mordant [302]. A mordant is a dye that increases the attachment of the primary stain to the cell wall. The iodine and the crystal violet form a complex that is difficult to remove from the cell wall. However, the solvent treatment (acetone and ethanol mixture) with a decolorizer dissolves the lipids from the Gram negative bacteria. The removal of the lipids allows the leaching of the primary stain, leaving the bacteria colourless. On the other hand, the cell wall of the Gram positive bacteria is dehydrated by the solvent treatment, shrinking the cell and closing the pores. As a consequence, the stain is locked inside the bacteria. The final step in Gram's method is the counterstain with the aim to give the decolorized Gram negative bacteria a colour.

The overall protocol takes less than 10 minutes. At the end of the process, Gram positive bacteria display a bluish purple colour and Gram negative bacteria display a pinkish red colour [313]. The main advantage of Gram's method is that it stains *Campylobacter* stronger than other methods [314, 315]. However, the duration of decolorization is critical since a prolonged exposure of bacteria to the decolorizing solution will remove the stain from both Gram positive and Gram negative bacteria [316].

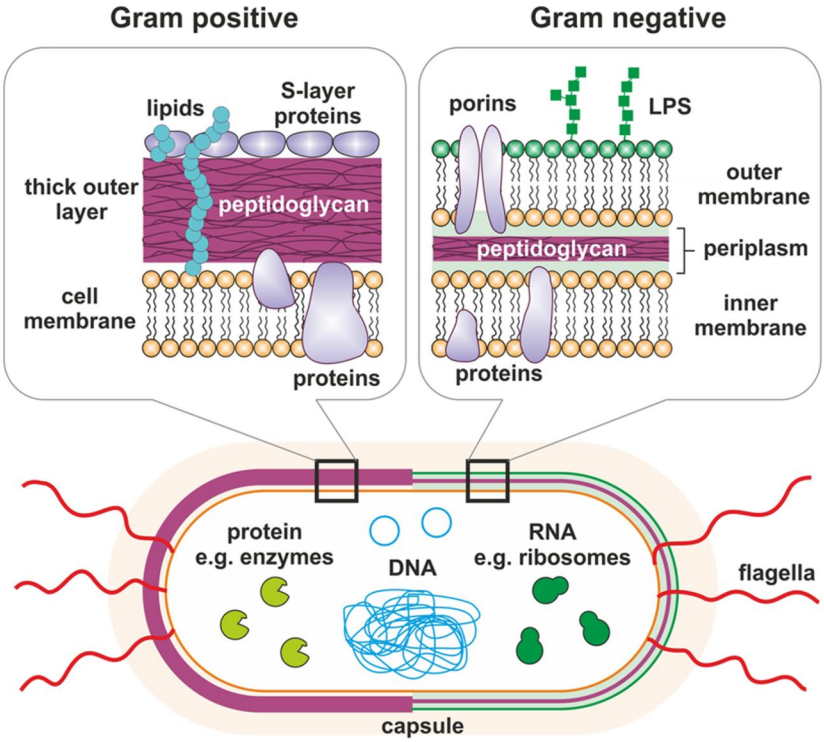

Figure 2.25: Schematic of the structure of the cell wall of Gram positive and Gram negative bacteria. Image from [235].

Flagella staining

Flagella are helical filaments that protrude out from the cell surface. The main function of flagella is motility, in liquid and on solid surfaces [317]. This allows the bacteria to betake to nutrients and favourable conditions, a process known as chemotaxis [318]. The diameter of flagella is typically about 20 nm [319], which lies below the resolution of an optical microscope ($\approx$ 400 nm) [35]. In order to visualize flagella, a staining is applied to make them appear thicker. One way commonly used to achieve this is the Leifson's method.

Leifson staining was first reported in 1930 [320]. The Liefson stain consists on a mixture of ammonium or potassium alum, tannic acid, and basic fuchsin in an ethyl alcohol [320]. In this method, the tannic acid of the stain produces a colloidal precipitate which is later colourized with the basic fuchsin and visible with microscopy. After staining, flagella display a red colour. The overall time for the staining takes around 15 minutes [321]. However, an inconvenient of this method is the short shelf life of the stain of only few days at room temperature [322].

Endospore staining

The endospore staining method is used to identify bacteria that can produce endospores, such the ones that belong to the genera *Bacillus* and *Clostridium* [35]. Endospores are cell structures that allow some bacteria to survive under critical environmental conditions of pH, temperature or starvation [323]. These structures posses a resistant cover which made them tolerant to heat and chemicals [306]. For

this reason, some stains based on water such as the Gram stain are not suitable for this staining [324]. Two of the most used methods to stain endospore bacteria are the Dorner method and the Schaeffer and Fulton method [35].

Dorner staining was proposed by Dorner in 1922 [324]. The stain produces a red spore surrounded by a transparent region. The contrast is provided by the application of nigrosine for a negative staining. The overall procedure takes around 15-20 minutes [307]. However, a limitation of this method is the use of heating as a mordant and solvent-based stains [302].

Schaeffer and Fulton staining also known as the malachite green method, was proposed as an optimized version of the Dorner staining in terms of effectiveness and rapidity [325]. This method utilizes malachite green to stain the endospore and safranin to stain the vegetative section of the cell [303]. At the end of the stain, endospore will show a green colour surrounded by a pink region. The overall procedure takes around 10 minutes [303]. However, like in the Dorner staining, a limitation of this method is the the use of heat as a mordant and the use of solvent-based stains that can destroy non-endospore bacteria [302].

Capsule staining

A capsule is a polysaccharide structure that covers the outer layer of the cell. In most bacteria, the capsule is composed of monosaccharides linked together via glycosidic bonds. However, some bacteria present capsules composed of peptide and protein-carbohydrate [318]. Capsule is synthesized in the cytoplasm and secreted to the outside of the cell, surrounding the bacterium. Capsules are produced in response to environmental conditions, such as an environment with a temperature of 37 °C and high glucose concentrations. Capsules are responsible for the protection of bacteria from host immune responses and for the prevention of bacterial desiccation [318]. The purpose of capsule staining is to distinguish capsular material from the bacterial cell. However, capsules are non-ionic structures, which means that dyes do not bind them. In order to observe capsules using microscopy, two commonly used methods are the India ink method and Anthony's method.

India ink method. In this method, the background is stained with India ink. Then, the bacterial cell is stained with crystal violet and later washed with water. The cell wall remains stained but the colour of the capsule is removed [35]. Capsules are fragile and can be damaged with heat. In the washing stages of the protocol, the rinse with water must be done very gently since water can remove the capsule from the cell wall. At the end of the stain, capsules can be observed as clear transparent halos placed between the stained bacteria and the stained background.

Anthony's stain. This method was proposed in 1931 by Anthony for the staining of cell capsules [326]. In this method, bacterial cells are stained with crystal violet as the primary dye. Although the dye is adhered to the capsule, it is not absorbed. By using cooper sulphate as decolorizer reagent, the colour is taken out from the capsule. Moreover, the cooper sulphate acts as a counterstain, staining the decolorized capsule with a light blue colour. Then, the stained bacteria can be observed as a dark purple zone surrounded by a light blue zone. Like in the india ink method, the smear should not be heated, washed or blotted dry. The heat can destroy the capsule, the blot drying can distort the capsule or remove the bacteria

from the glass slide, and the water washing can remove the capsule from the cell wall since the capsule is water soluble.

The protocols of the staining methods described above can be found in Appendix A. Table 2.9 summarizes the characteristics of the main methods for bacterial staining.

From Table 2.9, the most suitable staining method for this project is Gram's staining.

From the literature review and for the best of our knowledge, the novelty of this project includes an LPG-based immunosensor for *Campylobacter jejuni* detection and further enhancements of the sensitivity by staining approaches.

Table 2.9: Comparative between the main methods for bacterial staining.

Abbreviations used: Advantage (+), Disadvantage (−).

Staining method	Notes
Negative staining	(+) Easy and rapid (+) Suitable for cells that are difficult to stain (+) Suitable for cells that are delicate to be heat fixed (−) Not suitable for structure visualization (−) Cell is not stained (not suitable for this project)
Positive staining:	
Simple staining	(+) Fast and simple (30 seconds to 2 minutes) (+) Suitable for morphological studies of heat fixed cells (−) Shrinkage of the cell due to heat applied for fixing
Gram staining	(+) Simple, cost-effective and fast (less than 10 min) (+) Suitable for size and shape determination of bacteria (+) Strong stain for *C. jejuni* (−) Decolorization step is critical
Ziehl Neelsen staining	(+) Suitable for bacteria with high lipid concentration in the cell wall (−) Laborious procedure (50-60 min) (−) Too arduous for non-acid fast bacteria
Leifson staining	(+) Relatively fast procedure (15 minutes) (+) Suitable for flagella visualization (−) Short shelf life of stain (only few days)
India ink staining	(+) Suitable for capsule visualization (+) Relatively fast procedure (15-20 minutes) (−) Washing step is critical
Anthony staining	(+) Suitable for capsule visualization (+) Relatively fast procedure (15-20 minutes) (−) Delicate procedure
Dorner staining	(+) Suitable for endospore visualization (+) Relatively fast procedure (15-20 minutes) (−) Use of heat and solvent-based chemicals
Schaeffer and Fulton staining	(+) Suitable for endospore visualization (+) Fast procedure (around 10 minutes) (−) Use of heat and solvent-based chemicals

2.7 Summary

In this chapter, reviews of the literature pertinent for the development of this thesis were performed. First, a review focused on the detection, identification and quantification aspects of the established methods for bacterial detection, especially the detection of *Campylobacter jejuni*, was presented in Sec. 2.2. A comparison of the widely-used bacterial detection methods was presented in Table 2.2. Achievements of the different methods for the detection of *C. jejuni* were shown in Table 2.3. The advantages of LPGs as biosensors made them a promising platform candidate for this project, including compact size, lightweight, immunity to electromagnetic interference, ease of fabrication and high sensitivity. Another advantage of LPGs over other optical platforms such as SPR is the price and the portability of the instrumentation that could allow it to be used in various analytical situations. An overview of LPGs, including the main fabrication techniques, was presented in Sec. 2.3. A comparative between the main LPG fabrication techniques was presented in Table 2.5. The point-by-point technique provides advantages such as the complete customization of the grating structure and length that allows the tailoring of the sensor platform to the requirements of the application.

As mentioned in Sec. 2.4, the RE is a vital component of a biological sensor. It is responsible for the specific recognition of the analyte to generate the signal which is monitored on the transducer. A comparative between the main RE for bacterial detection, including enzymes, antibodies, nucleic acids, bacteriophages, aptamers and MIPS, was presented in Table 2.6. Unfortunately, there is no universal or all-purpose RE, and a number of attributes should be considered in its selection for the desired application, such as specificity, stability, availability, cost and ease to integrate with the sensing platform. Polyclonal antibodies were selected as RE due to its advantages such as high sensitivity and selectivity. In addition, the integration with sensing platforms has shown to be easy to perform. Another advantage of polyclonal antibodies over other REs, such as MIPs or aptamers, is their commercial availability. A comparative between the main immobilization techniques for REs, including adsorption, covalent binding, entrapment and affinity, was depicted in Table 2.7. Finally, as a means to enhance the sensitivity of the sensor, an overview of the main cell staining methods was provided in Sec. 2.6. Table 2.9 presented a comparative between the main methods for bacterial detection. Gram's staining seems to be the best candidate method to enhance the sensitivity of the sensor developed in this project due to its advantages such as the simple, fast, cost-effective and strong stain for *C. jejuni* cells.

Chapter 3

Long Period Gratings Fabrication and Software Development

In this chapter, the method used to fabricate the long period gratings (LPGs) used in this research will be presented. Also, the development of software for data analysis will be described.

3.1 Long period gratings fabrication

In this section, the experimental setup and procedure used to fabricate the LPGs used in this research will be described.

3.1.1 Experimental setup

LPGs were fabricated using the point-by-point technique, exploiting the UV sensitivity of Ge-doped optical fibres. Advantages of this method, as described previously in Sec. 2.3.2, are its flexibility and the ability to fully customize the grating. LPGs were fabricated by exposing the fibre to the output from a frequency-quadrupled neodymium-doped yttrium aluminium garnet (Nd:YAG) laser (TRLi-450, max output: 600 mJ, pulse duration: 8-10 ns, rep. rate: 10 Hz, from Litron Lasers Ltd) as shown in Fig. 3.1. The output from the laser was focussed into the fibre by a UV silica bi-convex lens (diameter 25.4 mm, focal distance 100.0 mm). In order to define the length of the section of the fibre to be irradiated, a slit was placed between the lens and the fibre. This practical approach simplifies the setup, avoiding the use of more complicated methods to change the period of the grating, such as using different focal length lenses to change the beam waist [168]. The width of the slit was adjusted by a motorized translation stage which was controlled by computer (M-110.1DG, travel range 5 mm, minimum incremental motion 50 nm, from Physik Instrumente (PI)). The optical fibre was mounted in a customized V-grooved fibre holder, shown in Fig. 3.2. The V-grooved fibre holder was fixed on a translation stage (M-150.11, precision linear stepper stage, minimum incremental motion 0.02 μm, from Physik Instrumente (PI)). The period of the grating is determined by the distance that the fibre is moved between exposures, while the ratio of the slit width

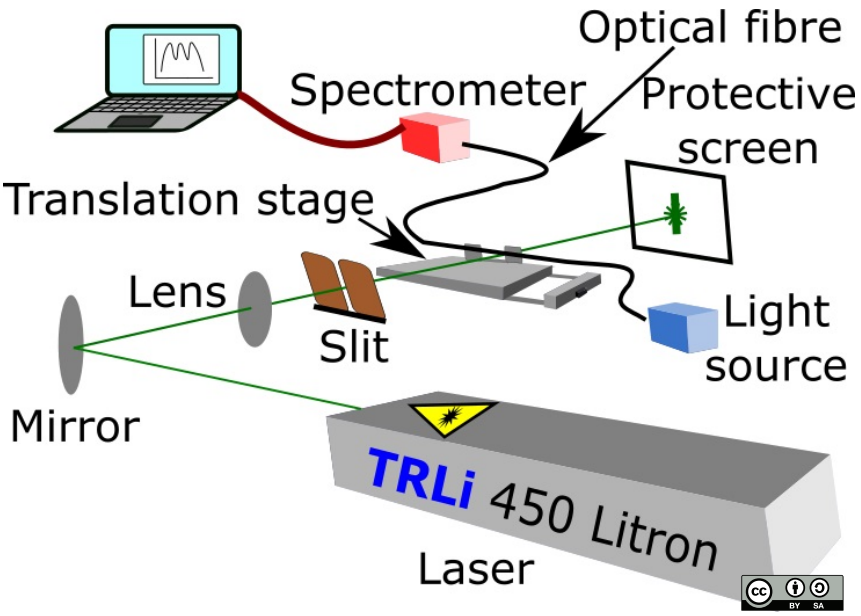

(a)

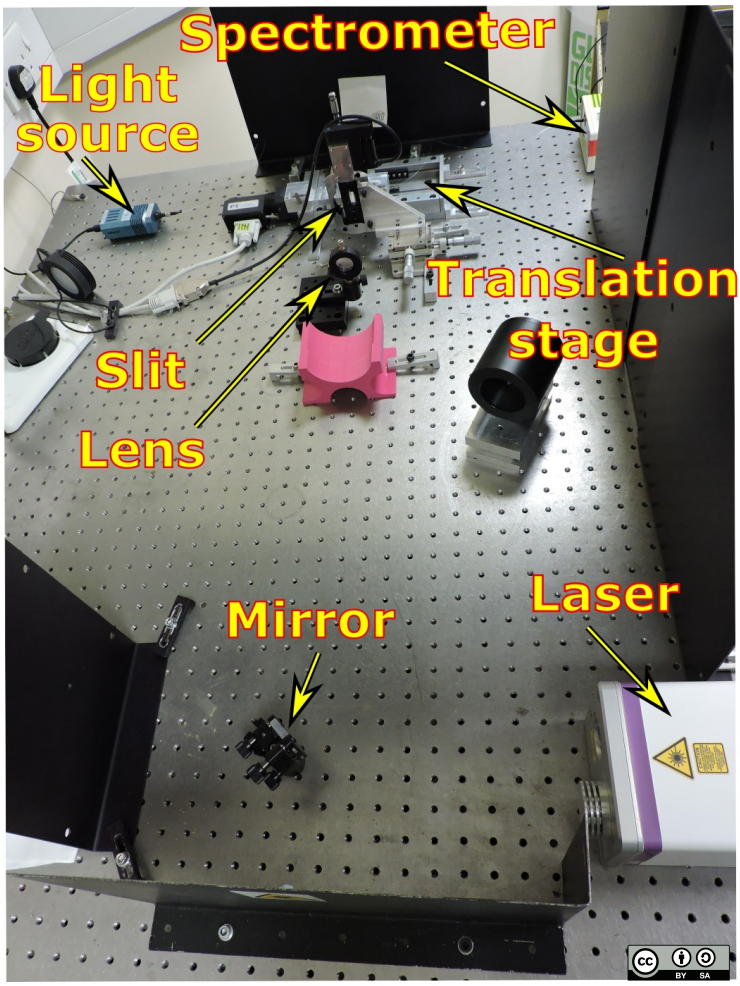

(b)

Figure 3.1: The (a) schematic and (b) image of the experimental setup for the fabrication of LPGs.

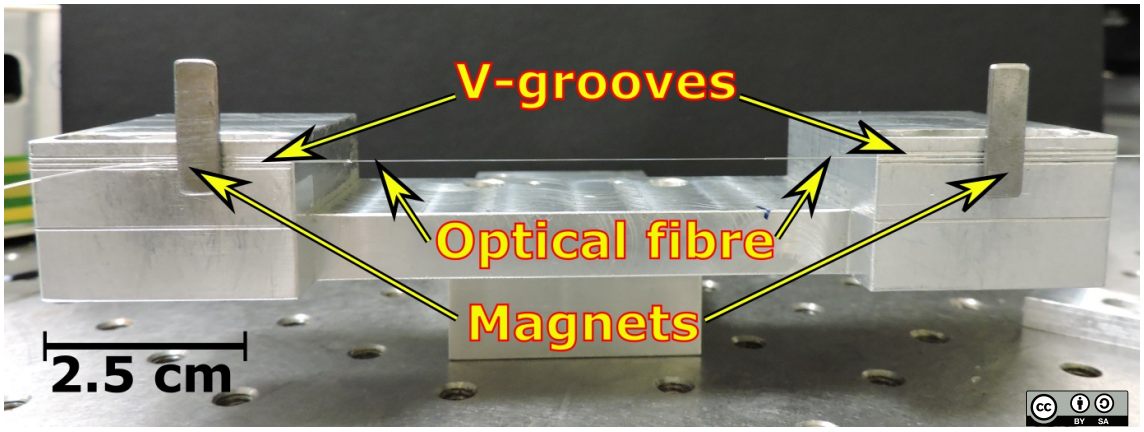

Figure 3.2: Image of the V-grooved holder.

to the period defines the duty cycle, which can also have an influence on the form of the LPG's transmission spectrum [327].

An image of the assembly of the slit, the translational stages and the V-grooved optical fibre holder is shown in Fig. 3.3. In Fig. 3.4, the opening and closure of the slit can be observed indirectly by the presence and absence, respectively, of light from the UV laser incident over the protective screen's surface. In Fig. 3.4a, the optical fibre was irradiated according with the chosen dwell time, which is determined by the LabVIEW program that controls the translation stage. The exposure time had been studied previously by Partridge *et al.* [328]. Briefly, the fabrication of LPGs by the repeated exposure of the fibre, also known as the overwrite method, allows the fabrication of LPGs with low sensor to sensor variability by enabling tracking of the resonance bands during fabrication. The exposure of the optical fibre to the laser irradiation can be stopped during the fabrication process when the central position of the attenuation bands match the desire specification. It was demonstrated that the resonant bands were visible using an exposure time of 5 seconds, with a total cycle time of 30 minutes. In Fig. 3.4b, the slit is closed while the translational stage moves the fibre to its next position, depending on the chosen period, because any exposure of the region between the grating planes had been shown to influence the transmission spectrum and affect the reproducibility of grating fabrication.

The transmission spectrum was monitored by coupling the output from a tungsten halogen white-light source (model LS-1, optimized for use in the VIS-Shortwave NIR range (360-2000 nm), from Ocean Optics) into one end of the optical fibre and coupling the other end to a spectrometer (model SD2000 from Ocean Optics). The spectrometer was connected, via the USB port, to a desktop computer, where the transmission spectrum was visualized using a customized LabVIEW program. The LabVIEW program was also used to control the translational stages that were used to move the fibre and to open and close the slit, allowing the user to choose the period and length of the grating, number of cycles, dwell time and duty cycle. An example of the interface of the LabVIEW program used to input the settings to fabricate the LPGs and to visualize the transmission spectrum is shown in Fig. 3.5.

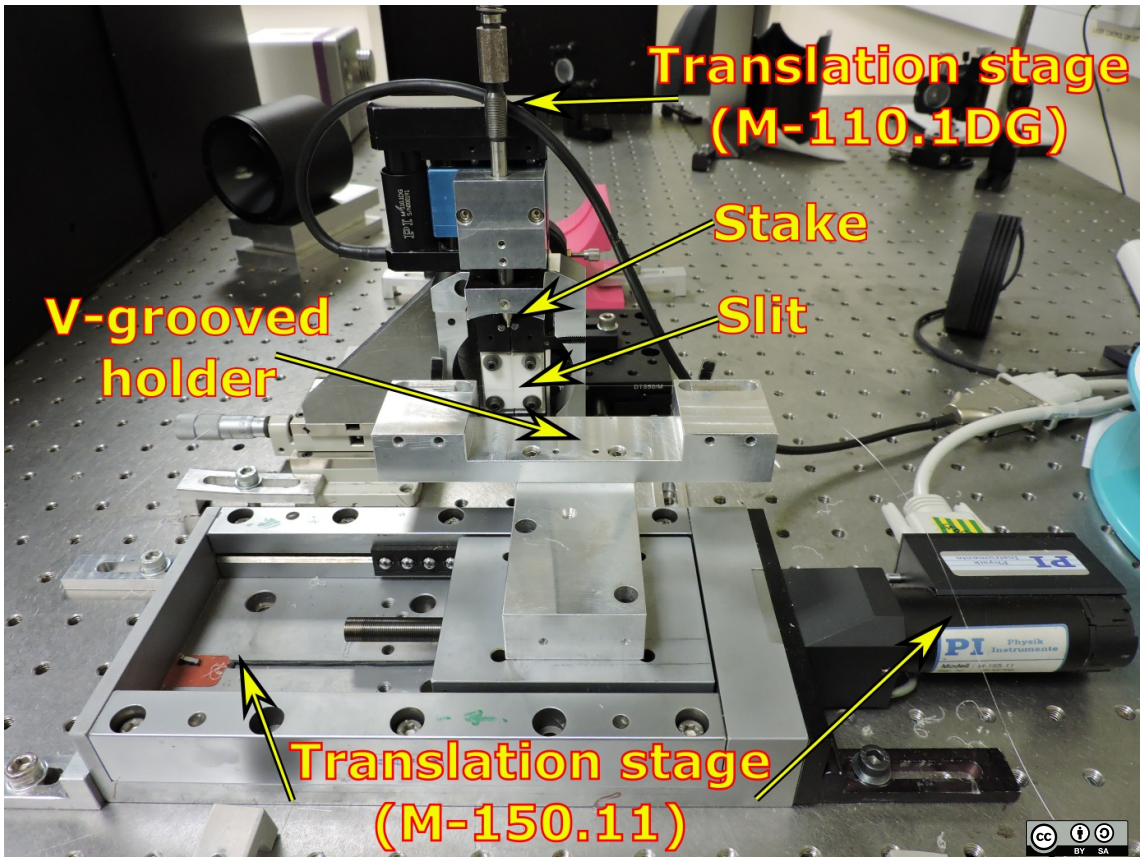

Figure 3.3: Image of the assembly of the V-grooved holder, the slit and the translational stages. The metallic stake attached to its translation stage opens the slit when it is moved downwards.

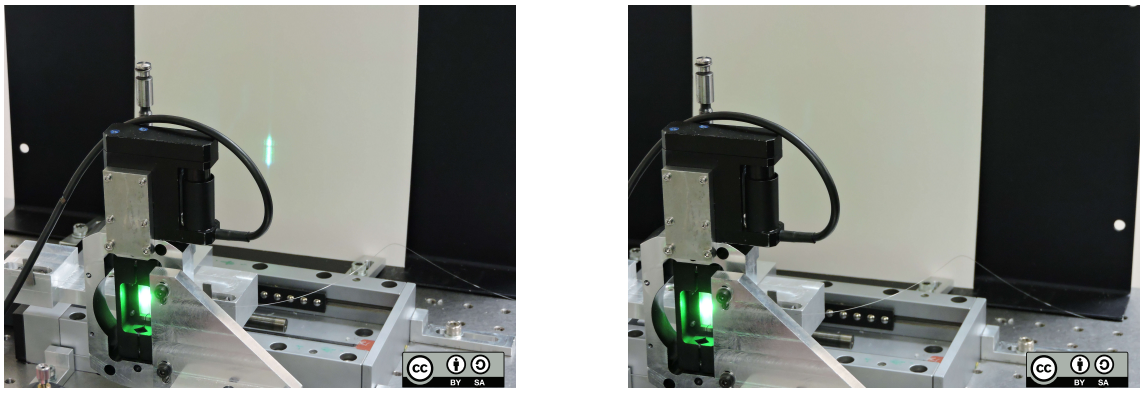

(a) (b)

Figure 3.4: The (a) presence and (b) absence of light from the UV laser over the protective screen's surface show the opening and closure, respectively, of the slit.

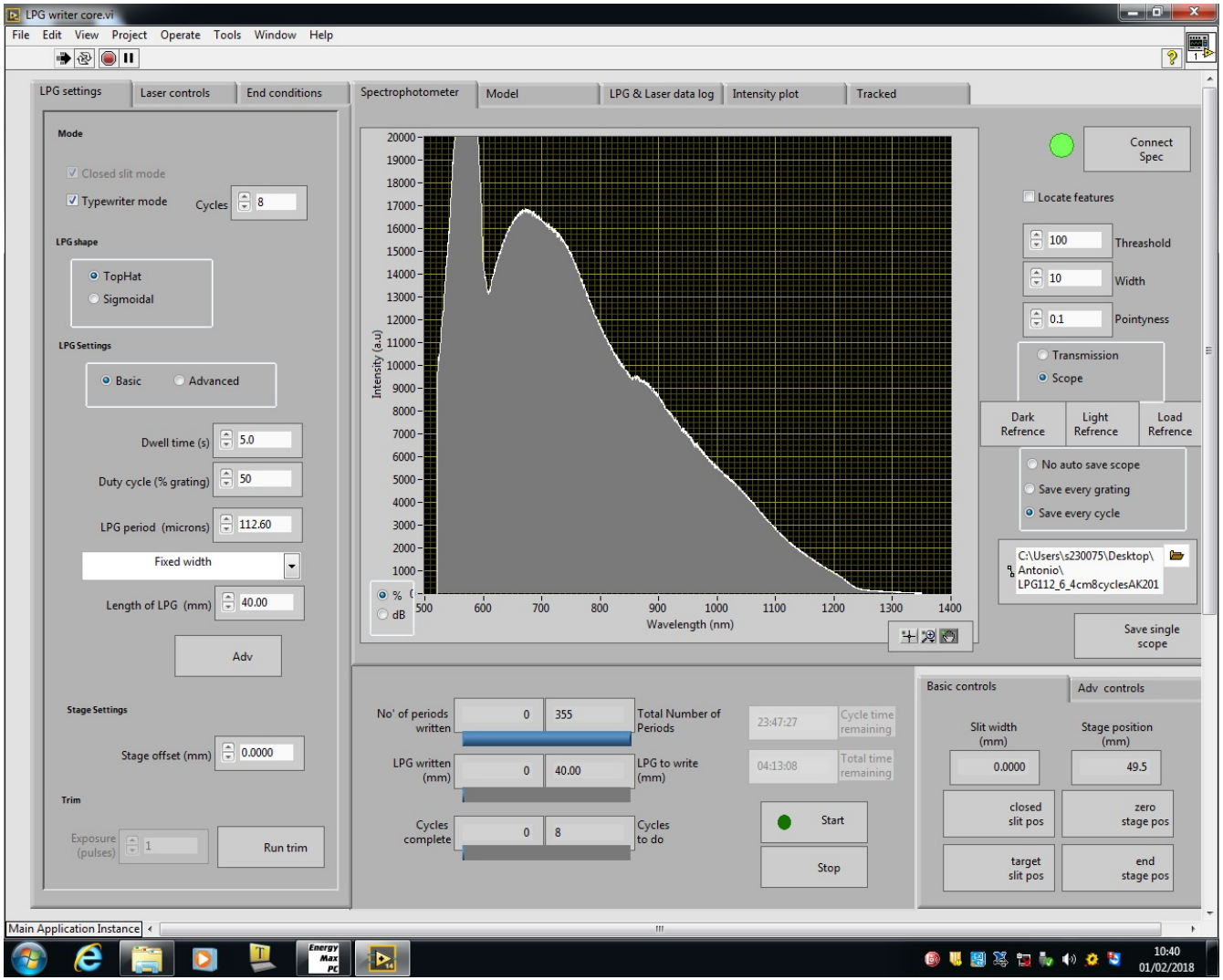

Figure 3.5: Screenshot of the interface of the LabVIEW program used to introduce the LPG fabrication settings and to visualize the transmission spectrum.

3.1.2 Long period gratings fabrication procedure

LPGs were fabricated in a photosensitive single mode boron-germanium co-doped optical fibre (PS750, cut-off wavelength 635 nm, core diameter 4.8 μm, cladding diameter 125±1 μm, coating diameter 241 μm, from Fibercore). The short cut-off wavelength of this fibre allows that the LPG resonance bands to be observed using a low cost system comprising a tungsten halogen light source and a CCD spectrometer. Prior to fixing the fibre on the V-grooved holder, a length of approximately 4 cm of the jacket (acrylate) was removed from the central part of the optical fibre using a mechanical fibre stripper (model JIC-375 from Jonard Tools). The jacket was removed because it is absorbing the UV and its presence would impede the fabrication of the grating. The exposed cladding was wiped with optical tissue moistened with isopropyl alcohol (IPA) to remove the plastic residuals, shown in Fig. 3.6. Then the fibre was fixed on the V-grooved holder with magnets, ensuring that it was straight and taut. The beginning of the exposed cladding was aligned with the gap of the slit.

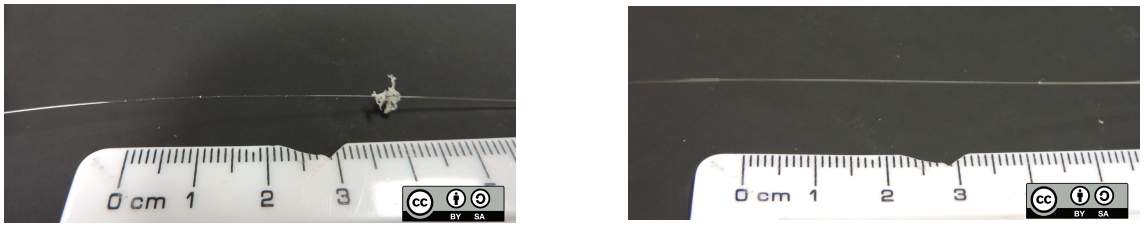

(a) (b)

Figure 3.6: Optical fibre with approx. 4 cm of the plastic jacket removed using a mechanical stripper. In (a), jacket residuals can be observed on the surface of the cladding. In (b), the cleansed cladding after wiping the jacket residuals with optical tissue moistened with IPA, can be seen.

The coupling of the fibre with the light source and the spectrometer was achieved via SMA bare fibre adapters (from Newport Corporation), also known as bullet connectors. Since the internal diameter of the hole in the ferrule in the SMA adapters is 125 μm (cladding diameter), a section of the jacket (approx. 4 cm) was removed from both ends of the optical fibre and cleaned with IPA. Then, both ends of the optical fibre were cleaved with a precision fibre cleaver (model VF-15H from INNO Instrument Inc.). Optical fibre cleaving is a controlled process that is used to break the fibre in order to obtain a flat end face, perpendicular to the longitudinal axis of the optical fibre (<0.5°). Defective ends downgrade the coupling efficiency [329].

To test the fabrication system and verify that it was configured to fabricate LPGs with the required period and duty cycle, an optical fibre with its buffer jacket intact was irradiated. The fibre was observed under an optical microscope (Olympus BX51). An optical image of the irradiated fibre jacket is shown in Fig. 3.7. The repeatability of the fabrication system was tested by fabricating LPGs of the same period. Fig. 3.8 shows the transmission spectra of LPGs of period 112.3 μm. Four attenuation bands were identified and their central wavelengths were determined for each transmission spectrum. The identification of the attenuation bands' central

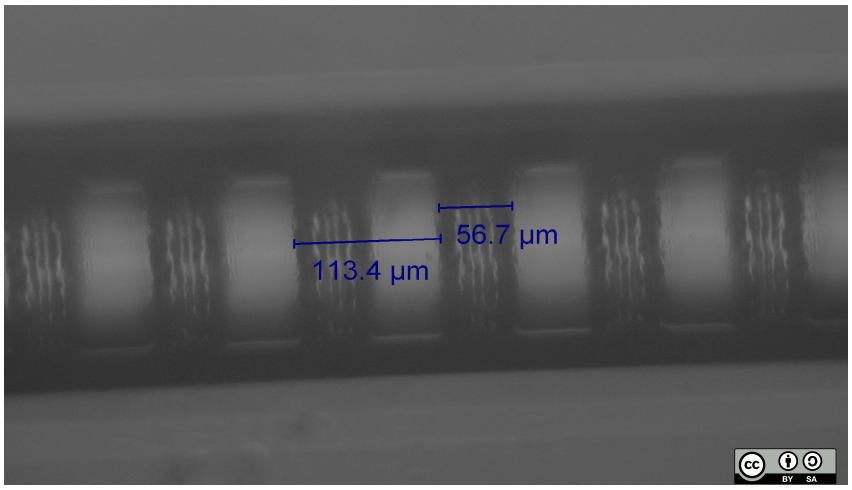

Figure 3.7: Periodic structure with a period of 113.4 μm inscribed on the plastic jacket of a single mode optical fibre. The darker areas are those parts exposed to the UV laser irradiation.

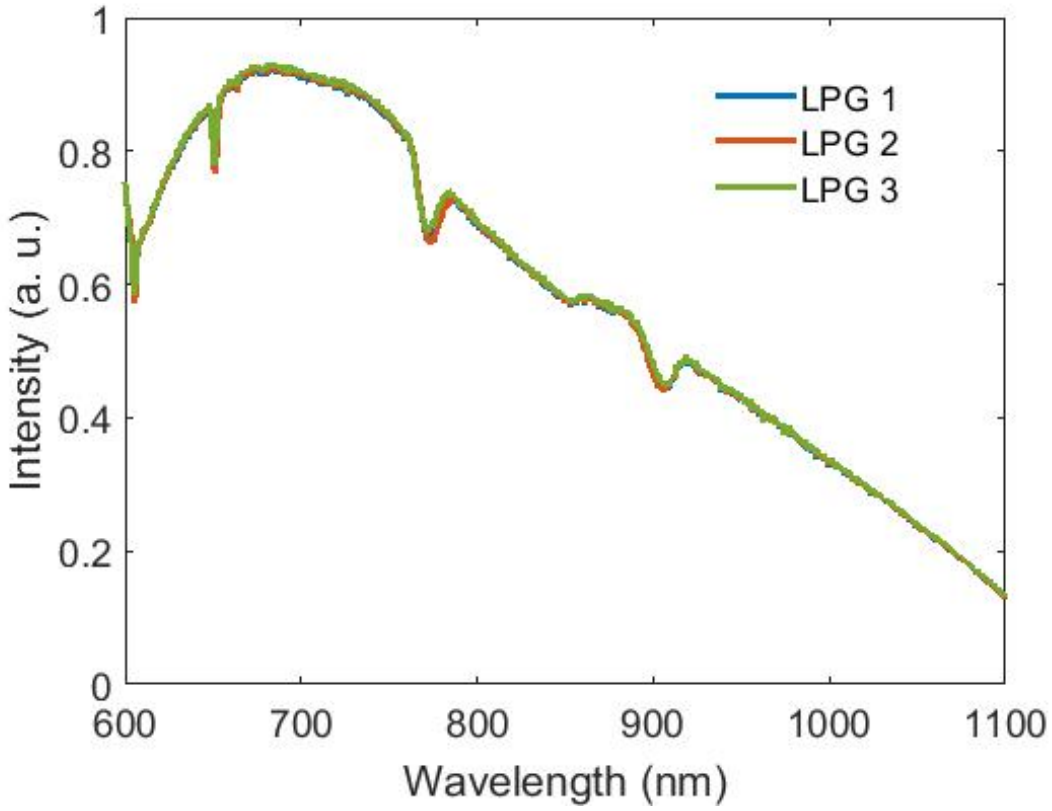

Figure 3.8: Transmission spectra of LPGs of period 112.3 μm, showing the repeatability of the fabrication system.

Table 3.1: Attenuation bands' central wavelengths for the LPGs of period 112.3 μm fabricated using the point-by-point technique.

LPG 1		LPG 2		LPG 3	
Wavelength (nm)	Intensity (a.u.)	Wavelength (nm)	Intensity (a.u.)	Wavelength (nm)	Intensity (a.u.)
603.88	0.2104	603.88	0.1390	603.50	0.2230
649.99	0.0571	649.99	0.0627	649.99	0.0748
769.22	0.0877	770.01	0.0932	769.22	0.0836
901.99	0.0528	901.18	0.0548	901.99	0.0495

wavelengths is described in Sec. 3.2.2. The results are shown in Table 3.1. It can be observed that the second attenuation band of the three LPGs is centred at the same wavelength. The first, third and fourth attenuation bands are slightly shifted between them with a difference of 0.38, 0.79 and 0.81 nm, respectively. The intensity values of the attenuation bands' central wavelengths were different in the three LPGs possibly due to changes in the coupling conditions or could also have been a result of a change in the power from the laser, which gives a different index modulation amplitude and thus central wavelengths would be different. The sensitivity of the bands' central wavelengths to the index modulation amplitude is higher for higher order modes. The intensity values of the attenuation bands from Table 3.1 do not correspond to the intensity values of the attenuation bands in Fig. 3.8 due to the method used for the calculation (see Sec. 3.2.2). This is adequate for the investigations that will be carried out in this thesis and these small variations in the transmission spectrum will not influence the sensitivity to the target analyte.

3.2 Development of software for data analysis

In this section, the development of software for data analysis is described.

3.2.1 Introduction

In general, data analysis is a key step for biosensor development since information, for example regarding the analyte concentration or binding kinetics, is extracted from the sensor's signal [109]. Particularly in this thesis, most of the generated data concerned the transmission spectrum of optical fibres that contained LPGs. As was mentioned in Sec. 2.3.1, the transmission spectrum presents a series of attenuation bands centred at discrete wavelengths that are dependent on the period of the LPG and on the properties of the surrounding environment, such as the optical thickness of the coating deposited on the cladding. In order to find the wavelengths of the attenuation bands, the transmission spectra had to be smoothed to reduce the influence of noise arising from fluctuations in the light source and optical cavities formed between optical surfaces. An example of a noisy transmission spectrum is shown in Fig. 3.9.

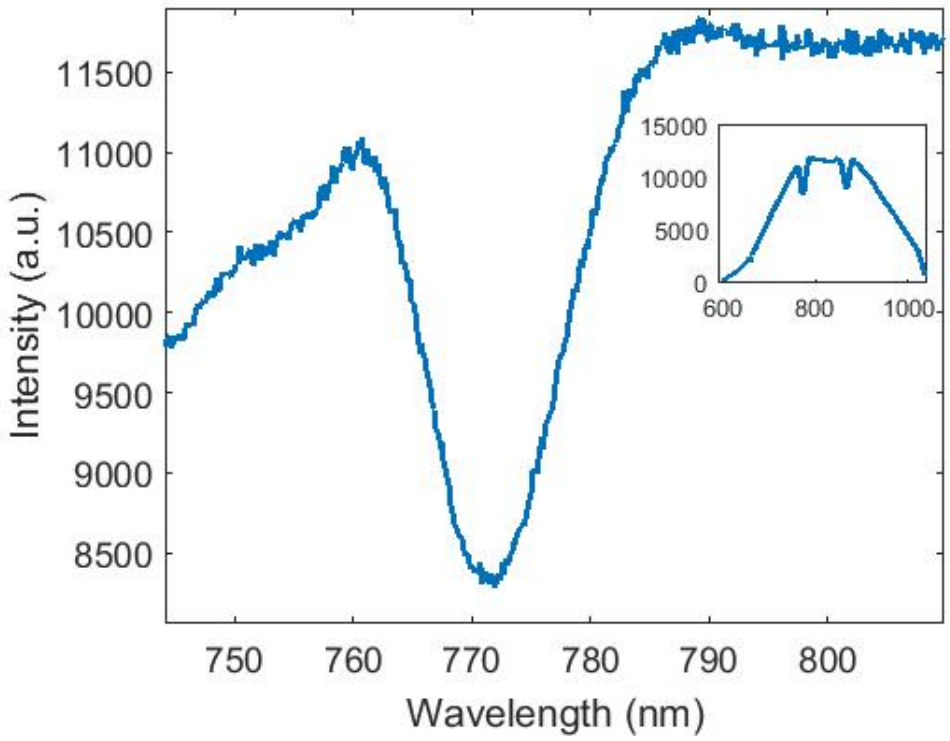

Figure 3.9: Example of a noisy transmission spectrum.

With the aim of carrying out a data analysis process customized for this project, a number of programs were developed in Matlab (Matrix Laboratory, MathWorks®). The approaches to determining the attenuation bands' central wavelengths are described in the following section.

3.2.2 Identification of the central wavelengths of the attenuation bands

From the identification of the central wavelengths of the attenuation bands of the LPG's transmission spectrum, information such as antibody attachment on the surface of the cladding or bacterial binding could be extracted. However, two main challenges need to be overcome in order to properly identify the central wavelengths. First, locating the attenuation bands within the overall transmission spectrum, especially those that are shallow, represents a challenge. In addition, the presence of noise in the transmission spectrum complicates the identification of the attenuation bands' central wavelengths since noise causes the appearance of false minima. With the aim of identifying the central wavelengths of the attenuation bands of the LPG's transmission spectrum, a number of approaches were assessed.

The first challenge can be solved by normalising the LPG's transmission spectrum to a baseline spectrum. To avoid misunderstandings, this normalization will be referred in this thesis as the difference spectrum. The term normalization will be used for the linear transformation of the maximum value of the intensity to 1. A simple solution could be to obtain the difference spectrum from the baseline spectrum

of the fibre without the LPG, as shown in Fig. 3.10. However, changes in coupling conditions are encountered experimentally when connecting and disconnecting the fibres (see Sec. 4.4.1), as shown in Fig. 3.10a and Fig. 3.10c, where the same LPG and the baseline from the fibre without the LPG are plotted. As can be seen in Fig. 3.10b and Fig. 3.10d, the difference spectrum differs significantly due to the change in the transmission spectrum of the baseline. In Fig. 3.10e, the normalized transmission spectra from the LPG and baseline from Fig. 3.10c are shown. The normalization, in this case, allowed the baseline to appear as an envelope of the LPG transmission spectrum. The difference of the normalized data made it easier to identify the attenuation bands, as illustrated in Fig. 3.10f. However, the presence of noise complicates the localization of the attenuation bands' central wavelengths, as can be observed in Fig. 3.10d. As can be inferred, selecting a suitable baseline that matches the LPG's transmission spectrum, i. e. an envelope (transmission spectrum in the absence of LPG), can be time-consuming.

To avoid the problems with variations in the coupling conditions encountered experimentally when connecting and disconnecting the fibres, the aim was for the baseline to be determined directly from each recorded LPG's transmission spectrum.

To achieve this, a program was designed to determine the local maxima from the filtered LPG transmission spectrum to construct the envelope and to obtain the difference spectrum, from which the attenuation bands' central wavelengths were identified. The local maxima (peaks) were calculated using a built-in function in Matlab which compares the difference in intensity values. The filtering of the data was an important step in the determination of the envelope spectrum. For example, if the filtering was insufficient, then the calculation of the envelope spectrum would fail, as shown by the yellow line on Fig. 3.11(top), where the calculated envelope spectrum includes the attenuation band at a wavelength of 887 nm, which was not represented in the difference spectrum (Fig. 3.11(bottom)). Similarly, in Fig. 3.12, insufficient filtering caused the failure calculation of the envelope, and thus the failure of the calculation of the difference spectrum, where no attenuation band was represented.

In the development of this program, two filtering approaches were assessed. The first approach utilized two types of filters (mean and median filters) to smooth the experimental data. The mean filter, or convolution filter, replaces the central value in a window (kernel) with the mean of the values in the window. The mean filter is easy to implement. However, its weakness is presented at the borders if the window is larger than the available data points for the filtering. This problem was solved by removing data points at the borders of the data. The median filter replaces the central value in a window with the median of the values in the window. The median filter, unlike the mean filter, tends to preserve the sharp edges of the transmission spectrum [330]. The LPG's transmission spectrum (experimental data) was filtered using the mean filter, the median filter, or a combination of both. The filtered data was used to identify the local maxima (peaks) with the aim to determine the envelope of the transmission spectrum. A peak, in this case, was an intensity value that was larger than its two adjacent values. The envelope was calculated by adjusting with splines the local maxima. Subsequently, transmission spectrum of the LPG was subtracted from the envelope and the difference was plotted. Since the difference

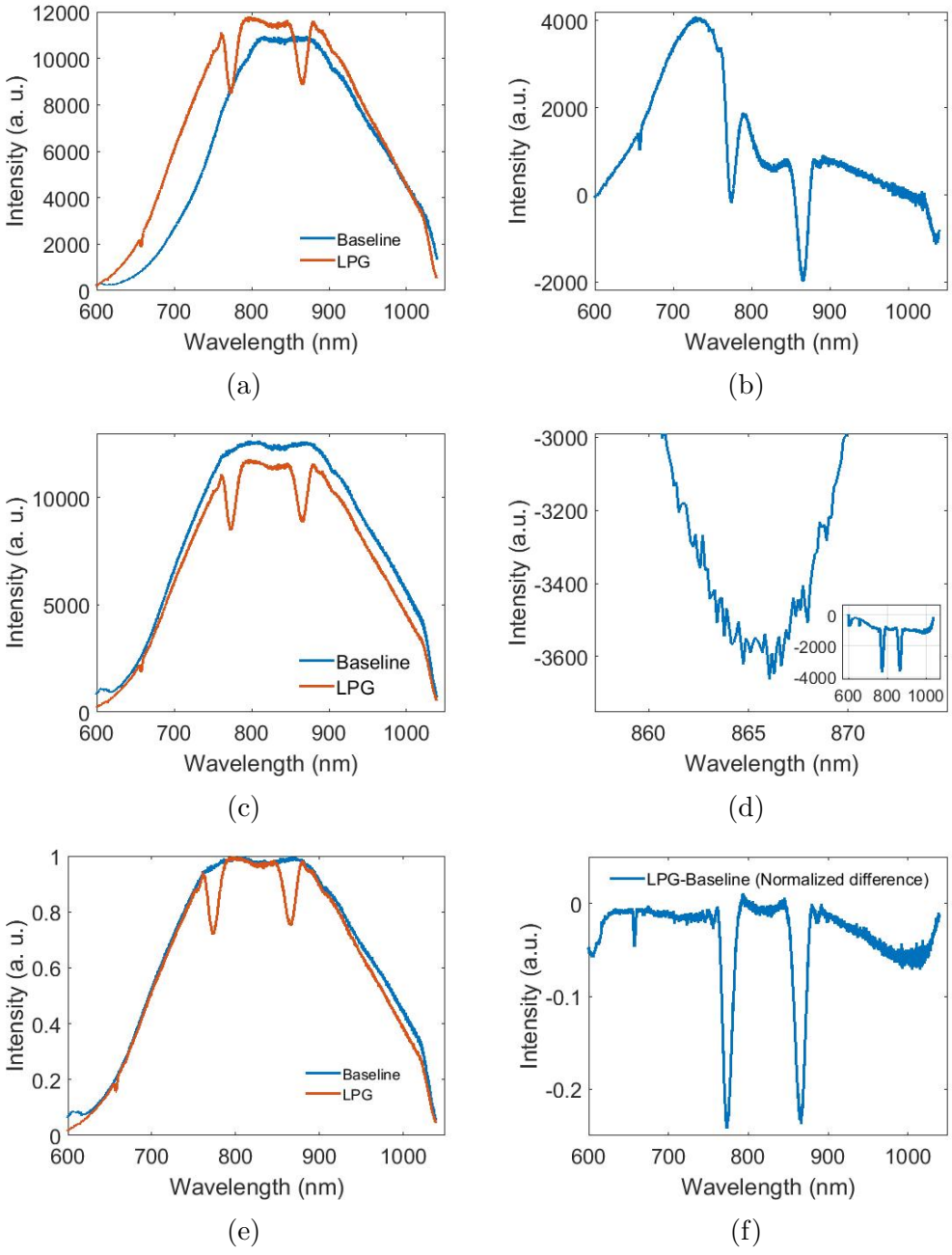

Figure 3.10: In (a) and (c), the LPG transmission spectrum and the baseline of the fibre without the LPG for different coupling conditions due to connection and disconnection of the fibre is shown. In (e), the normalized spectrum from (c) is shown. The normalization in this case, causes the baseline to appear as an envelope for the LPG. In (b), (d) and (f), the difference spectrum from (a), (c) and (e), respectively, is plotted.

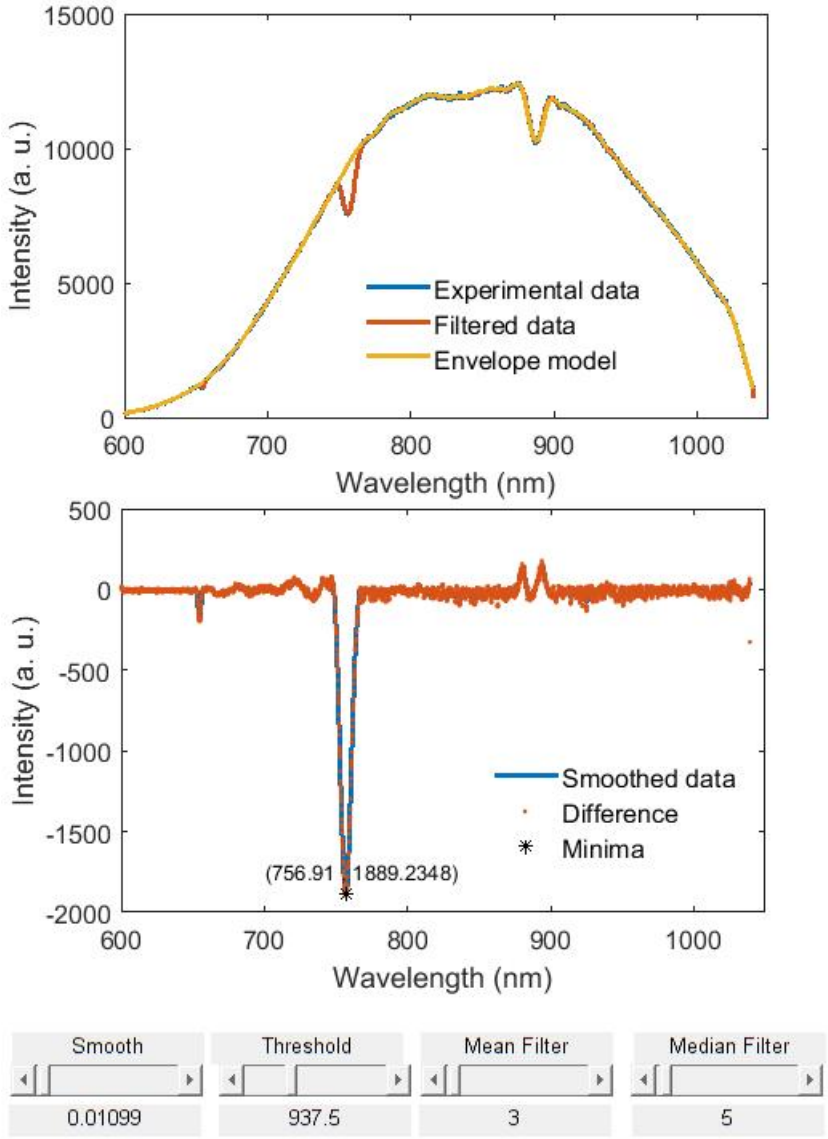

Figure 3.11: Example of an output figure from the Matlab program. The experimental data was filtered using a median filter 1 x 5. Insufficient filtering resulted in a failed calculation of the envelope, and thus a failed calculation of the difference spectrum.

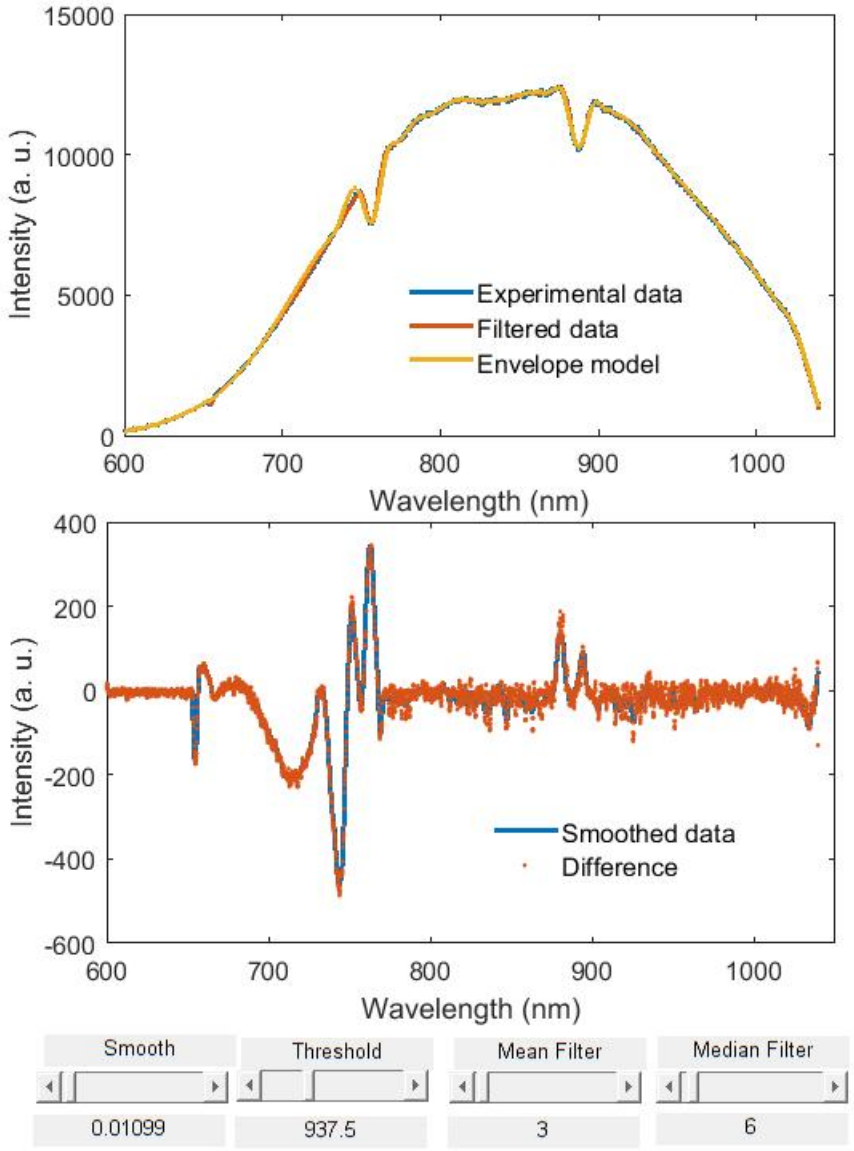

Figure 3.12: Example of an output figure from the Matlab program. The experimental data was filtered using a median filter with a 1 x 6 kernel. Insufficient filtering resulted in a failed calculation of the envelope, and thus a failed calculation of the difference spectrum where none attenuation band was represented.

spectrum still presents a certain level of noise after filtering, it is possible that the signal would have to be filtered again. In order to avoid an excessive shift of the attenuation band of the filtered data caused by the repetitive use of a convolution filter (moving average) and/or the use of a large kernel, the difference spectrum was smoothed using splines. Finally, the minima of the attenuation bands of the difference spectrum were calculated by comparing the difference in intensity values. In this case, a local minimum was an intensity value that was lower than its two adjacent values. The figure generated by the software included a graphic interface that allowed the user to adjust the smoothing parameter for the difference spectrum, the threshold to ignore the undesired values (mostly noise-generated local minima), and the kernel for the mean and median filters. Following the example from Fig. 3.11, if the median filter kernel is increased by two points (kernel = 7), as shown in Fig. 3.13, the envelope omitted the attenuation band centred around 900 nm. However, the filtering removed peaks from the transmission spectra in the region around 700 nm and in wavelengths larger than 1000 nm, which caused a deficient fitting over the filtered data, generating round features on the difference plot. Nonetheless, in both cases, the calculated central wavelengths of the attenuation band were the same (756.91 nm) but the depth of the band differed.

The second approach assessed used a fast Fourier transform (FFT) to filter the data. Unlike the previous approach, the program only used one filter. The FFT, in this case, converts the transmission spectrum from its wavelength domain to the frequency domain, and vice versa. The FFT used in this program was the standard built-in function from Matlab. The program generated an output figure containing four subplots. The first subplot was generated with the raw experimental data. In the second subplot, the transmission spectrum in the frequency domain was plotted. The third subplot contained the reconstructed (filtered) spectrum and the envelope function. The reconstructed spectrum was generated with the frequencies selected using the Fourier filter slider, located on the bottom of the figure. The program calculated the local maxima (peaks) from the filtered data using a Matlab built-in function which compared the difference in intensity values. Then, the envelope function was generated using splines to fit the peaks found in the filtered data. Finally, the fourth subplot was generated by subtracting the filtered spectrum from the envelope. The difference was normalized and the peaks were found, according to the threshold value set by the slider located on the bottom of the figure. An example of an output figure is shown in Fig. 3.14. It can be observed that this program calculated the same wavelength value for the minimum of the attenuation band centred in 756.91 nm as the preliminary approach that used the mean and median filters. This program was more efficient in the sense that only one filter is used, compared with the three filters required in the preliminary approaches. An additional example is shown in Fig. 3.15. Finally, the minima could be saved in a text file (.txt) created by the program in the same folder by clicking the save minima button located at the right-hand side of the threshold slider. In addition, the program was able to load a single or multiple files in text format (.txt) containing the transmission spectrum recorded by the Ocean Optics spectrometer. The text file could contain, or not, text or description of the data. In addition, the figures generated include a graphic interface that allows the user to modify the available

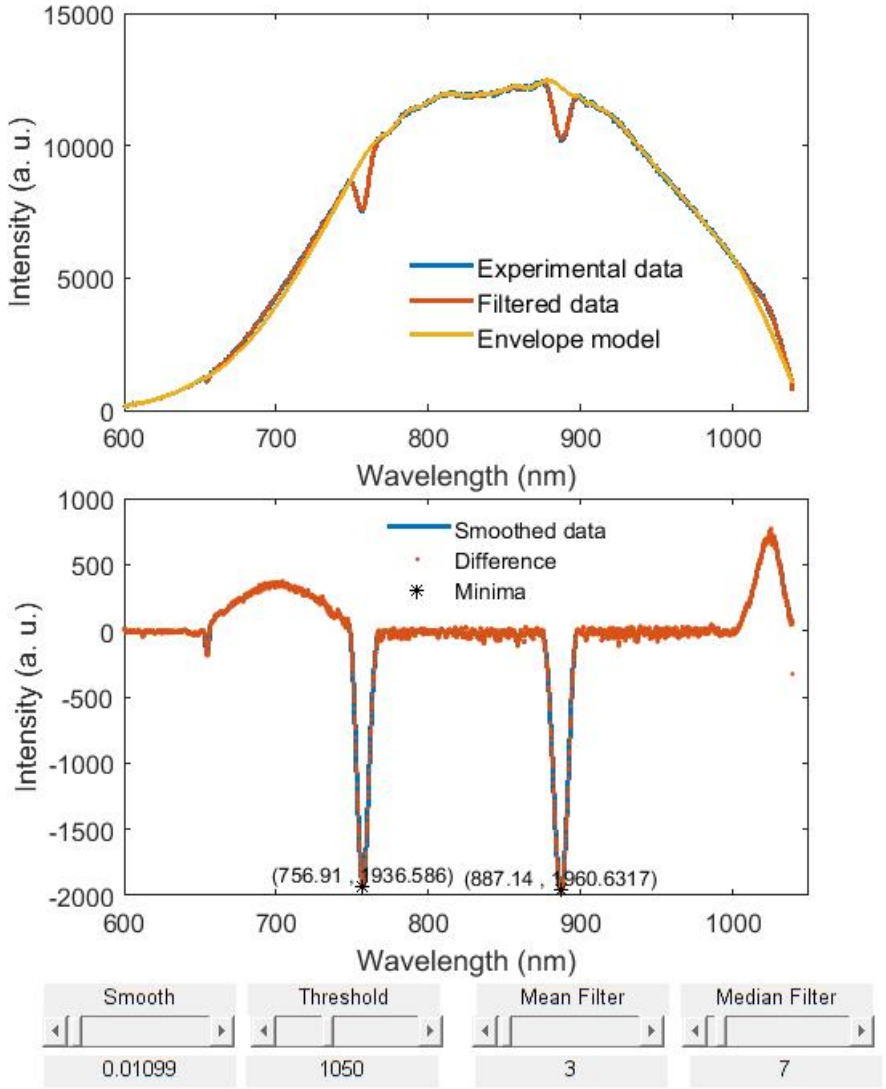

Figure 3.13: Example of an output figure from the customized Matlab program for mean and median filters of kernel size 1 x 3 and 1 x 7, respectively. A change in the filtering parameters resulted in the identification of the attenuation band centred at 887 nm. However, the increase in the filter parameters resulted in a failed calculation of the envelope at wavelengths such as 700 and 1050 nm, and thus a failed calculation of the difference spectrum.

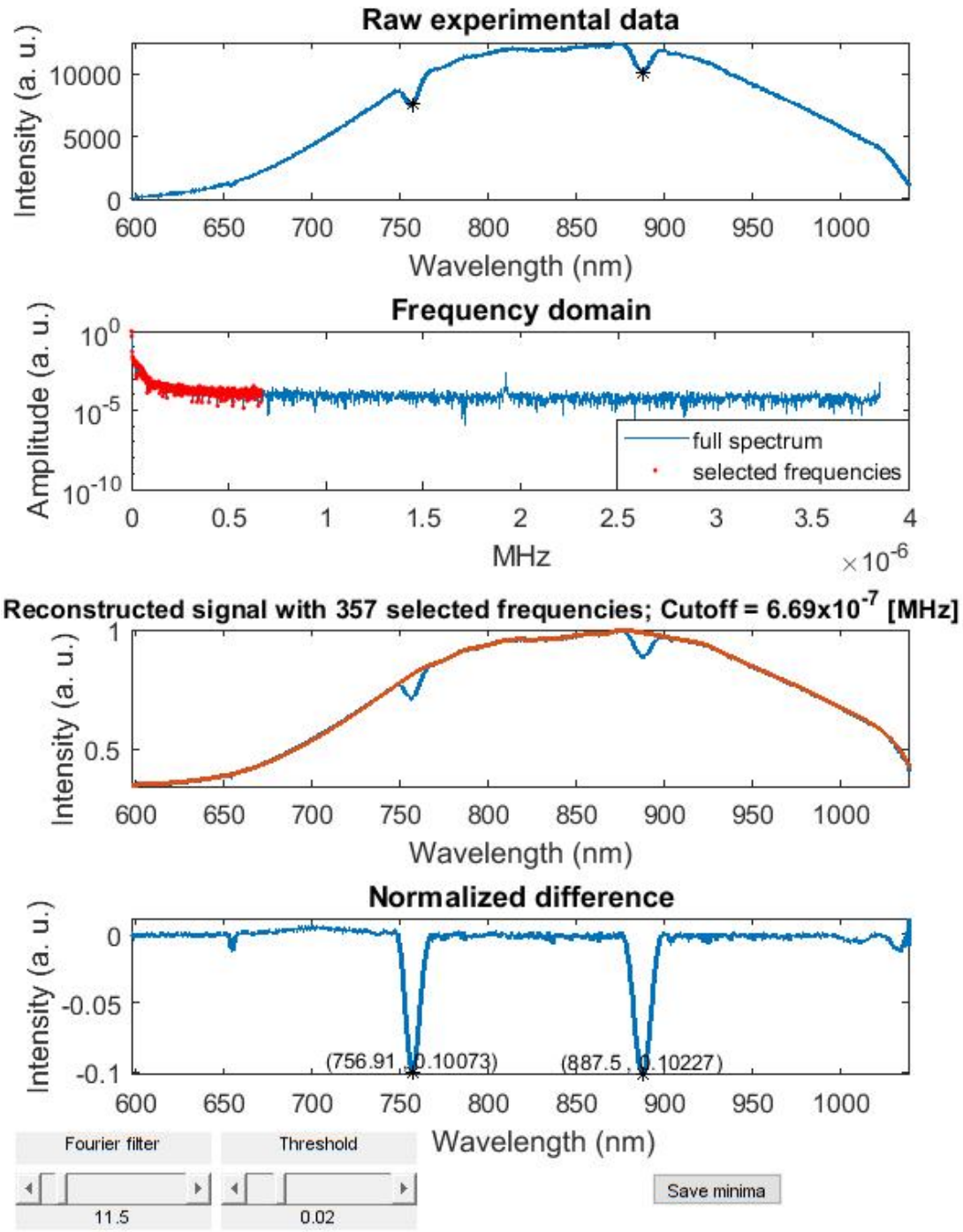

Figure 3.14: Example of an output figure from the Matlab program. The subplots show (top to bottom): the raw experimental data, the transmission spectrum in the frequency domain, the filtered spectrum and the envelope function, and the normalized difference spectrum, respectively. The minima values, the Fourier filter and the threshold parameters are saved in a .txt file by clicking the save minima button.

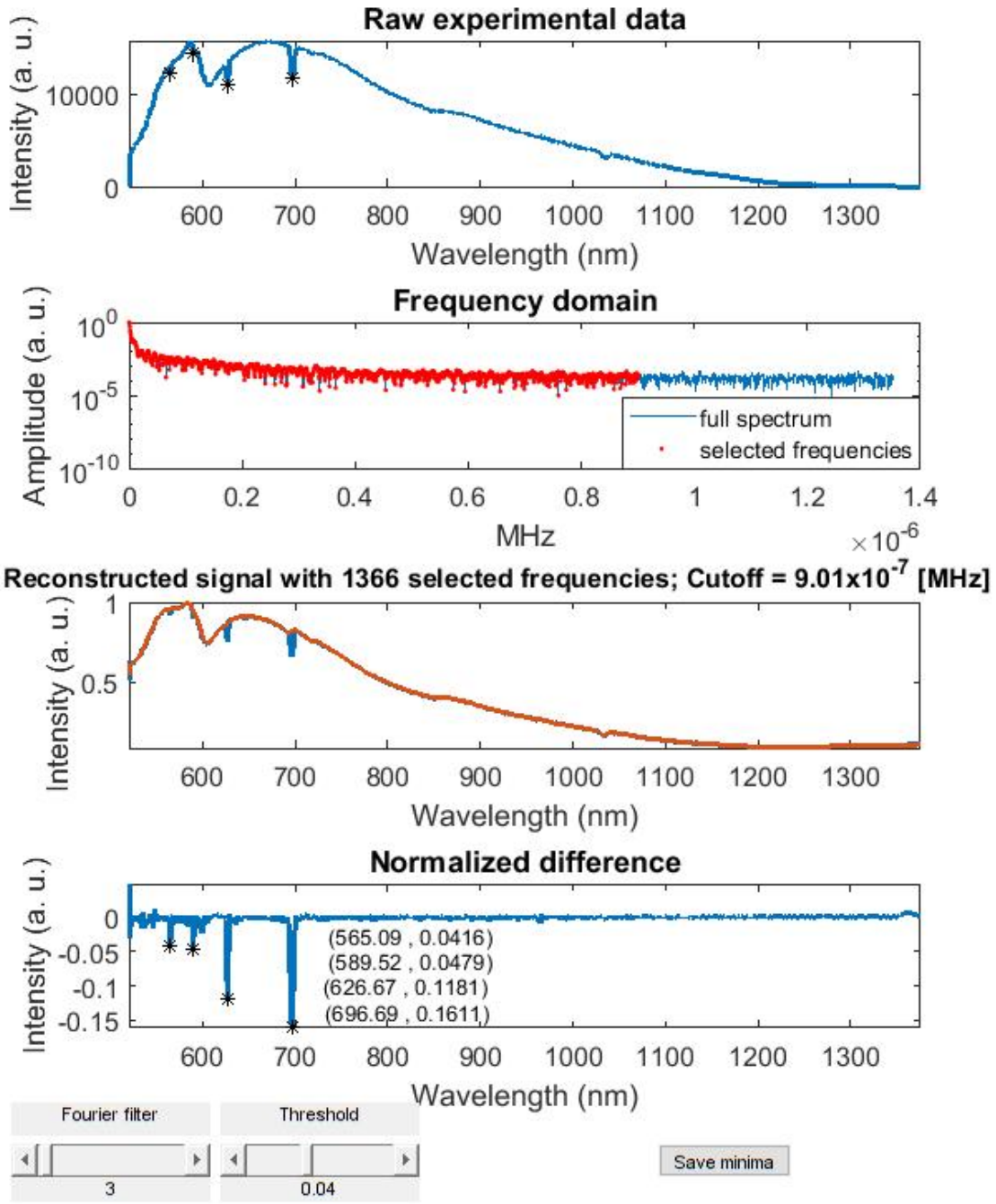

Figure 3.15: Example of an output figure from the customized Matlab program for a Fourier filter parameter of 3 and a threshold of 0.04. The subplots show (top to bottom): the raw experimental data, the transmission spectrum in the frequency domain, the filtered spectrum and the envelope function, and the normalized difference spectrum, respectively. Once the minima were calculated, their location is indicated in the raw spectrum as a reference.

parameters, such as Fourier filter parameter and threshold, directly in the figure with the use of sliders. This is an advantage that facilitates the visualization and comparison of different files and the observation of how the transmission spectrum was affected by a change in the parameters.

One of the most frequent reasons to use a filter is to eliminate or reduce the noise from a signal. Amongst the most widely used tools to filter signals are the median, mean and Fourier based filters. The mean and median filters are easy to understand and implement due to the use of a discrete window (kernel) to carry out the filtering of the signal. However, these types of filters present some limitations, particularly little flexibility due to the discrete nature of the window. To illustrate this, a comparison between Fig. 3.11, Fig. 3.12 and Fig. 3.13 is useful. Insufficient filtering resulted in the failure of the calculation of the envelope spectrum, as shown by the yellow line on Fig. 3.11(top), which was not represented in the difference spectrum (Fig. 3.11(bottom)). A single change of one step in the median filter window (kernel size from 5 to 6) resulted in a complete failure in the calculation of the envelope spectrum, and thus a complete failure in the calculation of the difference spectrum, where none of the attenuation bands were represented, as shown in Fig. 3.12. An additional single change in the window size of the median filter (kernel size from 6 to 7) resulted in an proper calculation of the envelope spectrum, and thus in a proper calculation of the difference spectrum where the identification of the attenuation bands was acceptable, as shown in Fig. 3.13. As can be noticed, the smallest change in the median filter parameter resulted in extreme cases, where the attenuation bands were not properly identified. On the other hand, the Fourier filter possesses the advantage of being more flexible than median/mean based filters in the sense that it is possible to establish a sharper cut-off frequency. Also, the Fourier filter has a grounded and well-studied theory and the literature available is abundant. A further advantage of the Fourier filter is that it allows the quantification of the noise, which is challenging in the case of filtering using mean/median filters. For the particular case of the sensing system described in this thesis, the aim was to calculate the minima of the central wavelengths of the attenuation bands of the LPG's transmission spectrum. One way in which this problem could be addressed is to design an algorithm to automatically eliminate the noise from the transmission spectrum, to smooth the signal and to calculate the minima of the central wavelengths of the attenuation bands. However, the challenge is that the attenuation bands of the transmission spectra may vary in number, width and depth. To design such an algorithm, the number of attenuation bands as well as their width and depth should be known in advance in order to establish a criteria for the proper selection of the frequencies to be used in the Fourier filter. However, the LPG should be fabricated and the sensor tested in order to know the profile of the transmission spectrum, which is a similar to the chicken-and-egg situation. In this case, it was easier to visually inspect the transmission spectrum and select manually (with the use of the slider for the Fourier filter parameter) a cut-off frequency that would allow to filter the signal and to localize the minima of the central wavelenghts of the attenuation bands of the LPG's transmission spectrum. It is worth mentioning that, despite the presentation of only a couple of examples in this thesis, hundreds of files containing the transmission spectra of LPGs of different periods within the range from 108.5

to 113.7 μm were analysed using the approaches described above. It was observed that when using the approach that employs the Fourier filter, with an appropriate selection of the number of frequencies, the reconstruction of the signal was accurate and reproducible (according to the author's criteria) and, as a consequence, so was the calculation of the normalized difference.

The source of noise in the sensing system may arise from fluctuations in the light source and optical cavities formed between optical surfaces, and from noise related with the CCD-based spectrophotometer [331]. Even though it is challenging to quantify the noise from each source, it is possible to quantify the overall noise in the system using the Fourier filter. For example, in Fig. 3.14, the signal was reconstructed with 357 selected frequencies, using a cut-off frequency of 6.69x10^{-}7MHz. The frequencies above the cut-off frquency were considered noise.

3.3 Summary

In this chapter, the experimental setup and the procedure used to fabricate the LPGs, using the point by point method, used in this research were described. As mentioned in Sec. 2.3.2, this technique allows the tailoring of the grating to the requirements of the application. The fabrication system was tested and verified that it was configured to fabricate LPGs with the required period and duty cycle. The repeatability of the fabrication system was also tested.

In Sec. 3.2, the development of software for data analysis was described. Information such as bacterial attachment on the surface of the cladding could be extracted from the identification of the central wavelengths of the attenuation bands. The presence of noise and the localization of shallow attenuation bands within the overall transmission spectrum complicates the identification of the attenuation bands' central wavelengths. A number of approaches to overcome these challenges were assessed. The approach that used a FFT to filter the experimental data and to reconstruct the transmission spectrum demonstrated to overcome the challenges and allowed a proper identification of the attenuation bands' central wavelengths. This program was more efficient in the sense that only one filter is used, compared with the three filters required in the preliminary approaches.

Chapter 4

Cleaning Methods and Surface Coating

4.1 Cleaning methods

The cleaning of the surface of the section of the optical fibre containing the long period grating (LPG) is a crucial step in the development of the sensor. The sensor must be physically and chemically clean because contaminant films can mask effective rinsing, cause poor adhesion of deposited layers and lead to harmful decomposition products [332]. Moreover, the choice of an unsuitable cleaning method may cause a deficient or null attachment of the recognition elements onto the surface of the fibre. For this reason, the surface of the fibre, and the glassware used during the coating deposition, must be free of contaminants [333]. In the literature, a variety of cleaning methods have been reported, generally using a combination of acids, bases and organic solvents at different temperatures. Unfortunately, there is no cleaning substance nor method that is universally accepted [267]. Procedures for the cleaning of solid supports have to be tailored for the desired application, considering the degree of surface cleanliness required and the contaminants involved [334].

In this section, some of the basic surface cleaning methods are discussed. Subsequently, the most widely used cleaning methods in the development of biochemical sensors will be compared, including solvent treatment, the use of piranha solution and a two-acids based method.

4.1.1 Basic surface cleaning methods

Basic surface cleaning methods such as rubbing, immersion, ultrasonic cleaning, electrical discharge, heating, spray cleaning and vapour degreasing, to mention a few, are simple and rapid procedures that achieve a good level of cleanliness.

Rubbing the surface of a glass substrate with a solvent-wet cotton wool or lens tissue is one of the simplest cleaning methods [335]. This method is suitable for the removal of particles smaller than 5 μm. For larger particles, it is recommended to blow them off with a rubber bulb or an air can or to rinse them off in a liquid stream [334]. Rubbing cleaning is specially recommended for surfaces that are clean apart from dust that cannot be removed by blowing [334]. The surfaces cleaned using

this approach possess a high level of cleanliness. However, the resulting cleanliness depends on the contaminants presents in the cotton wool or lens tissue that is used. Recontamination can be avoided by using a new tissue/cotton wool after each pass over the surface [335]. For some contaminants, such as grease and fingerprints, it is difficult to establish when the surface is clean. For this reason, the rubbing cleaning method is used mainly as a pre-cleaning step.

Immersion cleaning, also known as dip cleaning, is a simple and very often used method. The solid support (substrate) is submerged in a open tank of plastic, stainless steel or glass, filled with a cleaning liquid, with the use of tweezers or a dipping basket. The cleaning liquid may or may not be agitated. The wet substrate is then removed and dried with a tissue or nitrogen gas [335, 336]. When acids are employed as the cleaning fluid, rinsing with de-ionized (DI) water prior to the drying step is required [332]. One drawback of this method is the number of repetitions that need to be performed (in the same or in another cleaning fluid). In addition, the immersion time and the type of cleaning fluid need to be tailored for the potential contaminants present on the surface [336].

Ultrasonic cleaning is a method mainly employed to remove strongly adhered contaminants by cavitation. This process is performed in a stainless steel tank equipped with transducers that generate a mechanical vibration that perturbs a cleaning fluid such as DI water or isopropyl alcohol (IPA). The action of the sound waves generates imploding bubbles, which can produce an instantaneous pressure of up to 1000 atm [335]. Glass is usually cleaned at frequencies between 20 and 40 kHz. Ultrasonic cleaning has been demonstrated to be a rapid method. For instance, glass slides, contaminated with fingerprints and ordinary lubricating oil, were immersed in IPA for two minutes, showing no cleaning. However, ultrasonic cleaning in IPA removed the fingerprints in 30 seconds and the oil in 2 minutes [336]. One drawback of this procedure is the frequent breakage of glass substrates [332].

Cleaning procedures such as electrical discharge, heating, spray cleaning, and vapour degreasing accomplish a high level of cleanliness. However, they present drawbacks that make them unsuitable for the aim of this project. Both the electrical discharge and the cleaning by heating procedures can induce changes in the refractive index of the core and/or cladding of the fibre, modifying the transmission spectrum of the LPG, as was discussed in Sec. 2.3.2. Cleaning by heating, for example, can reach temperatures of up to 350 °C [335]. Spray cleaning is suitable for removal of particles larger than 5 μm [335] with an efficiency between 97 and 99.95% [337], but it lacks effectiveness for the removal of thin films of contaminants [334]. In addition, the use of solvents in spray cleaning can cause an unevenly clean surface [335]. Vapour degreasing is usually employed as the final step in a cleaning procedure to remove oils and grease from glass surfaces. Besides being time consuming, as the surface has to be immersed in the vapour several times [336], the major drawback is the fact that surfaces cleaned by this procedure present static electrification. This may influence not only the deposition of the recognition element when is immobilized, for example, by adsorption (as discussed in Sec. 2.5.2), but it can also attract dust particles from the atmosphere, recontaminating the surface [335]. In addition, vapour degreasing shows a low efficiency (11-28%) in removing large particles ($> 5\mu$m) from optically polished glass, compared with ultrasonic cleaning (69-92%) [337].

None of these basic procedures meets all the criteria required of a high level of cleanliness method [338, 337]:

1. Rapid procedure,
2. High degree of homogeneity of the surface cleanliness,
3. Negligible damage/alteration of the substrate material,
4. Environmentally friendly or easy and cheap to dispose residual products,
5. Minimum recontamination.

However, when combined, basic surface cleaning methods can accomplish a high level of cleanliness [267].

In this study, some of the basic surface cleaning methods such as rubbing, immersion, and ultrasonic cleaning were tested. Despite being simple and rapid procedures, they turned out to be inappropriate for this study. For example, the rubbing method was tested on an LPG of period 109.6 μm. After the fabrication of the LPG, the surface of the cladding of the optical fibre was cleaned by rubbing with optical tissue moistened with isopropyl alcohol (IPA). The fibre was immersed in DI water at 20°C and its transmission spectrum was recorded (see Section 4.4 for details about the interrogation of the optical fibre and the experimental setup). Then, the fibre was immersed in 10% of bovine serum albumin (BSA) for 2 hours. After the protein deposition, the surface of the cladding was cleaned by rubbing with optical tissue moistened in IPA, as described above. Then the fibre was interrogated when immersed in DI water at 20°C and its transmission spectrum was recorded. The process was repeated one more time. The blue curve in Fig. 4.1 represents the transmission spectra of the cleaned LPG, which was bare of all coating protein and represents a baseline for the sensor. The red curve, red-shifted around 3 nm from the baseline, represents the transmission spectrum of the LPG cleaned by rubbing after being coated with protein (BSA). The green curve, further shifted by around 1 nm from the red curve, represents the transmission spectrum of the LPG cleaned by rubbing after being coated with BSA. As can be observed, the rubbing cleaning method failed in the removal of the coating protein, shown as a shift in the central wavelength of the attenuation band. Similar results were obtained from the immersion cleaning method in which the optical fibre was immersed for 10 minutes in a stainless steel tank filled with IPA. The tailoring of this method such as the selection of the cleaning liquid and the incubation times would be challenging and possibly resulting in a long procedure. On the other hand, ultrasonic cleaning method proved to be impractical as the breakage of the fibre resulted in less than 5 minutes.

4.1.2 Standard surface cleaning methods

The standard surface cleaning methods are multi-step procedures used to remove contaminants with the purpose of improving the attributes of the surface for the further deposition of films and/or coatings (including recognition elements). These

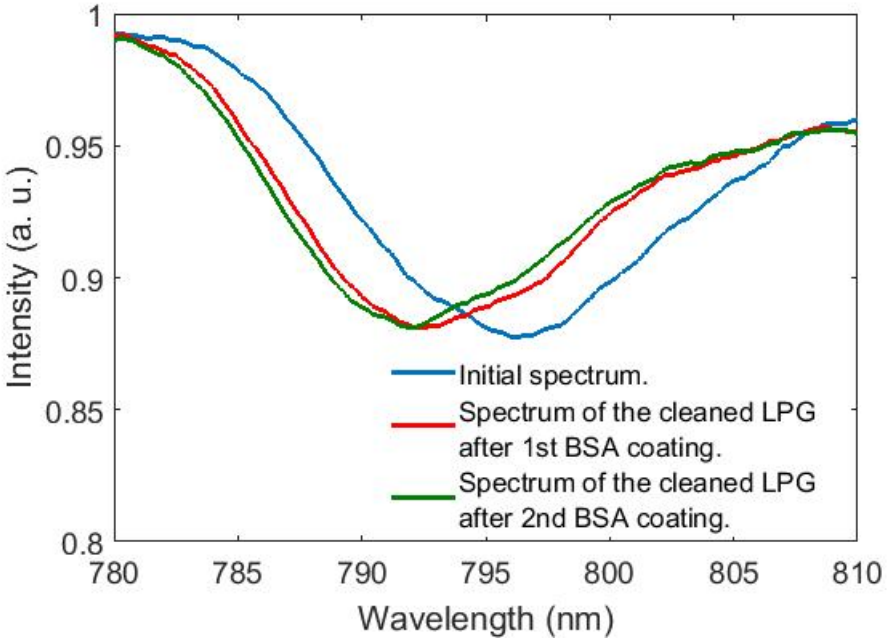

Figure 4.1: Transmission spectra of an LPG of period 109.6 μm, immersed in DI water at 20°C, cleaned by rubbing after being coated by adsorption with BSA at concentration of 10% for 2 hours. The cleaning method fails in removing the BSA from the surface of the cladding of the optical fibre, shown as a shift in the central wavelength of the attenuation band.

procedures are generally a sequence of basic methods. In addition to providing a high level of cleanliness, these methods, depending on the method and reagents involved, can promote the functionalization of the surface (as a pre-activation step in a silanization process, as discussed in Sec. 2.5.3) for the further deposition of a coating [267].

Solvent treatment is one of the simplest standard cleaning methods [335]. In this method, a solvent (e.g. isopropyl alcohol, methanol or ethanol) is used to remove organic and biological material through dissolution. The following protocol was adapted from [339]. Briefly, the cladding-exposed section of the optical fibre was rubbed three times with an IPA-wet tissue (2-ply medical wipes, 66x80 sheets, Kimberly Clark). The rubbing was done in only one direction, along the longitudinal axis of the fibre, using a new tissue in each pass (in the subsequent descriptions, unless otherwise stated, the rubbing cleaning is performed in this way). Then, the optical fibre was immersed in an ultrasonic tank containing IPA(Pure, 99.5+%, from Acros Organics) for 15 minutes. The fibre was removed from the tank and rinsed several times with DI-water (Ultrapure water, resistivity: 18.2 MΩcm, Barnstead^{TM}Smart2Pure^{TM}water purification system from Thermo Scientific). Finally, the fibre was dried using nitrogen gas.

Piranha solution, also know as piranha etch, is a mixture of a strong acid (concentrated sulphuric acid (H_2SO_4)) or base (ammonium hydroxide (NH_4OH)) with hydrogen peroxide (H_2O_2), and is mainly employed to remove organic contaminants from surfaces. The most common mixture is 3:1 (H_2SO_4:H_2O_2), i. e. three parts of

sulphuric acid and one part of hydrogen peroxide, although there are protocols that use mixtures in the range from 4:1 to 7:1 [340, 341]. These solutions, at different ratios made with sulphuric acid, are known as acid piranha. One of the advantages of acid piranha solution over other cleaning solutions such as base piranha (a mix of ammonium hydroxide (NH_4OH) with hydrogen peroxide) is that the reaction in the acid piranha is self-starting, so that the solution does not have to be heated to initiate the reaction [342, 343]. Piranha solution is extremely hazardous and may result in explosion if not handled with care. For the preparation of piranha solution, see Appendix B. The method presented in this work was adapted from [340, 344, 289, 118]. Briefly, a buffer coating removed section of an optical fibre was cleaned by rubbing. Then, the fibre was immersed in piranha solution (3:1) for 10 minutes. The optical fibre was carefully removed from the beaker to avoid any splash. Finally, the sensor was rinsed with DI water, followed by drying with nitrogen gas. Due to the corrosive nature of piranha solution, it was observed that the plastic jacket of the optical fibre, when in contact with the solution, was burned. Other piranha-based methods, such as that presented in [345], were tested. However, these methods, involving ultrasonic rinsing after the immersion in piranha (up to 1 hour immersion time), were found to result in the breakage of the fibre in less than 5 minutes.

Another standard cleaning method based on the use of two different acids was tested. This method was reported by Dressick *et al.* for the cleaning of fused silica slides [346] and by Cras *et al.* for the cleaning of microscope glass slides [267]. This method will be referred as "the two-acids-based cleaning method". The reagents involved are methanol, hydrochloric acid and sulphuric acid. The methanol (HPLC grade, purity $\geq 99.9\%$) was purchased from Fisher Scientific, while hydrochloric acid (ACS reagent, 37%) and sulphuric acid (ACS reagent, 95.0 - 98.0%) were purchased from Sigma-Aldrich. For this study, the method consisted of soaking the LPG sensor in 1:1 (Methanol:Hydrochloric acid) for at least 30 minutes, rinsing with DI water, and soaking in concentrated sulphuric acid for at least 30 minutes. The optical fibre was then removed from the acid and rinsed thoroughly with DI water, followed by immersion in boiling DI water for 30 minutes. This approach removes surface contaminants effectively and allows for uniform silanization of the glass surface [267].

A summary of the cleaning methods tested in this study is presented in Table 4.1.

4.1.3 Comparison of cleaning methods

Atomic force microscopy (AFM) supplies images of surface roughness by mechanically moving a tip across the surface to detect contours of the topography [347]. The surface roughness may be estimated based on a number of statistical parameters [348]. The most important amplitude parameters that characterize the surface topography are the average roughness (R_a), the root mean square (RMS) roughness average (R_q), and the maximum vertical distance between the highest and lowest data points in the image (R_{max}) [348, 349]. The average roughness is defined as the arithmetic average of the absolute values of the surface height deviations measured from the

Table 4.1: Cleaning methods tested in this study.

Abbreviations used: isopropanol (IPA), de-ionized (DI).

Method	Steps
Solvent-based	Rub the sensor with an IPA-wet tissue (3 times). Sonicate the sensor in IPA for 15 minutes. Rinse with DI water. Dry with nitrogen gas.
Piranha solution	Rub the sensor with an IPA-wet tissue (3 times). Immerse the sensor in 3:1 (sulphuric acid:hydrogen peroxide) for 10 minutes. Rinse with DI water. Dry with nitrogen gas.
Two-acids-based	Rub the sensor with an IPA-wet tissue (3 times). Immerse the sensor in 1:1 Methanol:Hydrochloric acid for 30 minutes. Rinse with DI water. 30 minutes in concentrated sulphuric acid. Rinse with DI water. 30 minutes in 100°C DI water. Dry with nitrogen gas.

mean plane [350]:

$$R_a = \frac{1}{N}\sum_{i=1}^{N} |z_i - \overline{z}|\,, \tag{4.1}$$

where z_i represents the surface height at each data point on the surface profile and $\overline{z}$ is the average height of the surface profile, defined as:

$$\overline{z} = \frac{1}{N}\sum_{i=1}^{N} z_i. \tag{4.2}$$

The average roughness is the most widely used roughness parameter for general control quality, since it is easy to calculate and gives a general description of amplitude variations [348]. However, from equation 4.1, it can be noticed that it does not distinguish between peaks and valleys.

The RMS roughness is defined as [350]:

$$R_q = \sqrt{\frac{1}{N}\sum_{i=1}^{N} (z_i - \overline{z})^2}. \tag{4.3}$$

The RMS roughness represents the standard deviation of the distribution of surface heights and is more sensitive to large deviations from the mean plane than the average roughness (R_a) [348]. The RMS roughness is easy to calculate and summarizes the surface roughness in a single value [350].

Three optical fibre probes, each one cleaned with each one of the methods described in Table 4.1, were scanned in an atomic force microscope, model Dimension 3100, from Veeco Digital Instruments by Bruker, equipped with a Nanoscope V controller, software Nanoscope version v7.30r1sr3. The size of the scanned area was 5 μm by 5 μm. The AFM images of the optical fibres cleaned using the IPA-based, piranha-based, and two-acids-based methods are shown in Fig. 4.2a, Fig. 4.2b, and Fig. 4.2c, respectively.

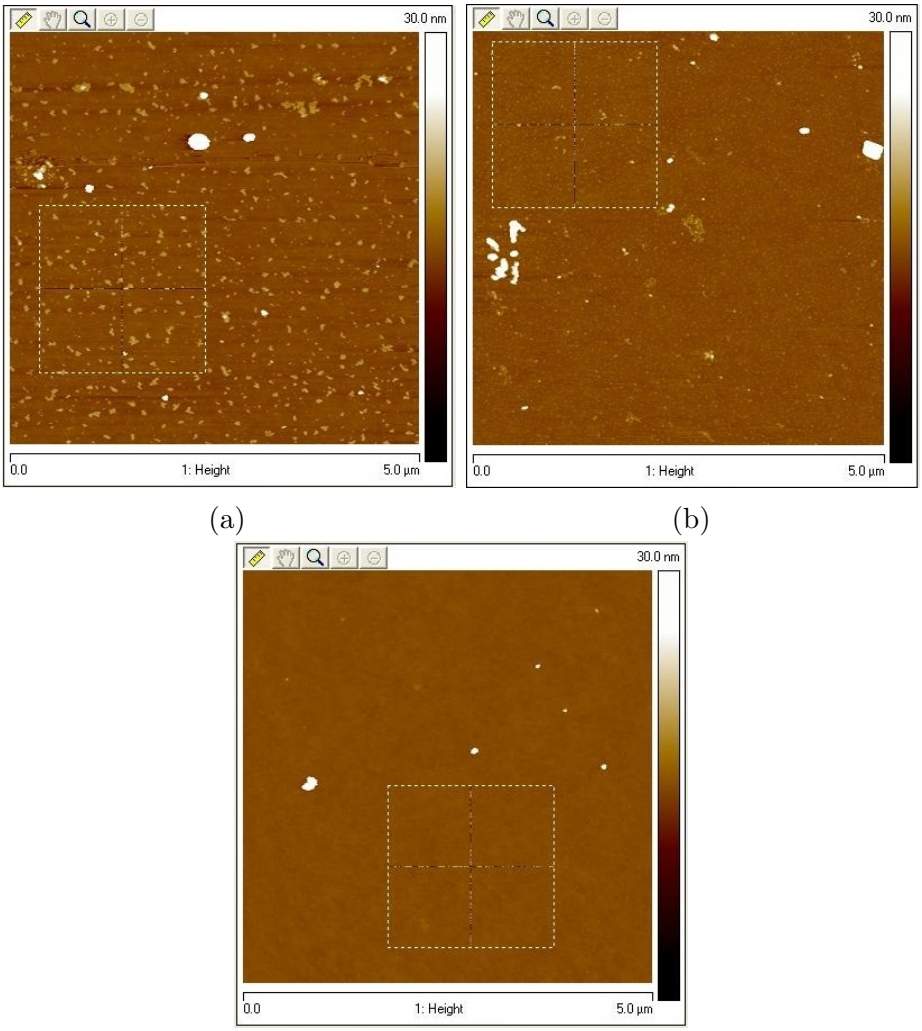

Figure 4.2: AFM images of optical fibres cleaned using the: (a) solvent-based, (b) piranha-based, and (c) two-acids-based cleaning method.

The parameters R_a, R_q, and R_{max} were calculated for the 5 μm by 5 μm image projected surface area and for a 2 μm by 2 μm box. This small, or cursor, box, in each image, was chosen to avoid the high peaks, seen as white dots in Fig. 4.2. A summary of the surface roughness amplitude parameters from the AFM study of the optical fibres cleaned by the different methods is presented in Table 4.2.

The topographies of three optical fibres cleaned using the three different methods, generated from the data obtained from the AFM, are shown in Fig. 4.3.

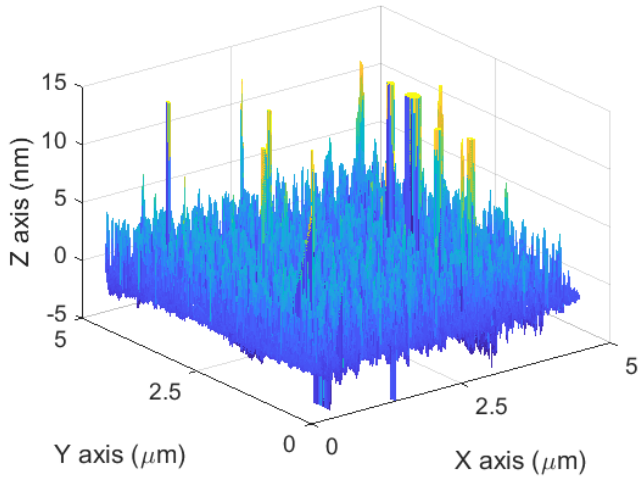

(a)

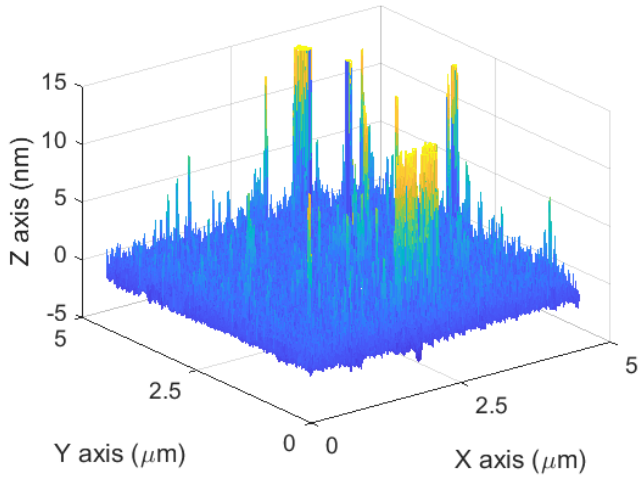

(b)

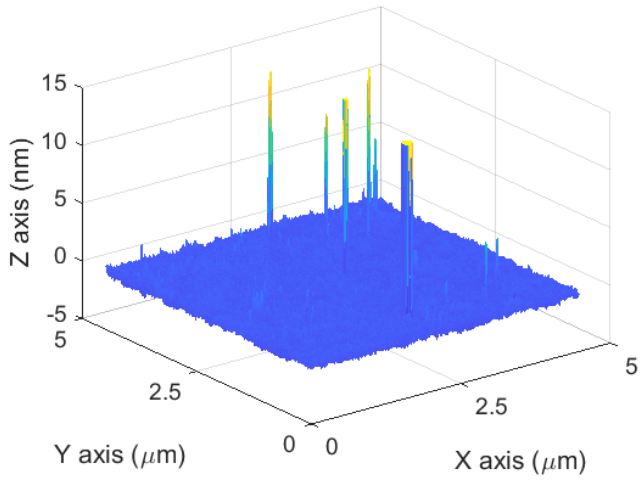

(c)

Figure 4.3: Topography of three optical fibres cleaned using: (a) alcohol solution, (b) piranha solution, and (c) the two-acids based method.

Table 4.2: Surface roughness statistical parameters from the AFM images corresponding to optical fibres cleaned by different methods. Parameters obtained from the entire image ((5 μm)^2) and the box defined by the cursor box ((2 μm)^2).

Units in [nm], unless otherwise stated. Abbreviations used: Root mean square (RMS)

Parameter	Image surface area	IPA	Piranha	Two-acids
Average roughness (R_a)	(5 μm)^2	0.863	0.582	0.209
	(2 μm)^2	0.517	0.318	0.157
RMS roughness (R_q)	(5 μm)^2	4.74	2.70	1.63
	(2 μm)^2	0.965	0.526	0.200
R_{max}	(5 μm)^2	147	100	91.3
	(2 μm)^2	20.8	8.81	3.08

The optical fibre cleaned by the IPA-based method presented the highest level of roughness between the three tested methods (see Fig. 4.3a). The average roughnesses for the entire image and the cursor box were calculated as 0.863 nm and 0.517 nm, respectively. The RMS roughnesses were calculated as 4.74 nm and 0.965 nm for the entire image and the cursor box, respectively. The maximum vertical distances between the highest and lowest data points in the image were measured as 147 nm and 20.8 nm for the entire image and the cursor box, respectively. The solvent-based method is effective in removing large particles, but the removal of contaminants within the micrometer range requires additional steps. On the other hand, the optical fibre cleaned with the two-acids-based method resulted in a "smoother" surface, as can be appreciated in Fig. 4.3c. The average roughnesses calculated were 0.209 nm and 0.157 nm for the entire image and the cursor box, respectively. Similarly, the RMS roughnesses were calculated as 1.63 nm and 0.200 nm for the entire image and the cursor box, respectively. Finally, the maximum vertical distances between the highest and lowest data points in the image and cursor box were measured as 91.3 nm and 3.08 nm, respectively. The optical fibre cleaned using the piranha-based method presented a roughness level that lays between the fibre cleaned with the solvent-based method and the one cleaned with the two-acids-based method. Despite being a more commonly used surface cleaning method [351, 345], piranha-based cleaning can result in fragility of the fibre, compromising its practical application.

The two-acids-based cleaning method was chosen for the further cleaning stages in the development of the sensor, based on the results obtained from this study.

4.1.4 3D-printed device for sensor cleaning

The cleaning methods presented in Sec. 4.1.2 are relatively fast and easy to perform. However, one issue faced during the implementation of the protocols was the placing of the optical fibre inside the beaker for the immersion in the cleaning reagent. The proper fixation of the fibre can be laborious and time consuming. In contact with the sulphuric acid or the piranha solution, the jacket of the fibre is burned (the

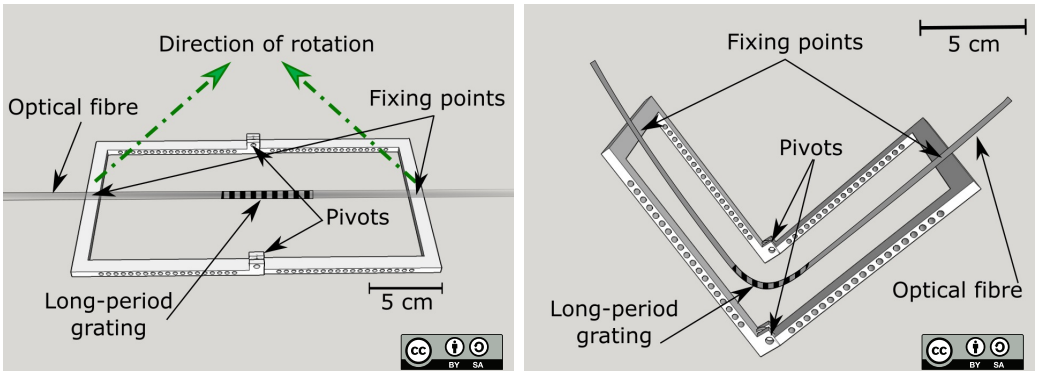

(a) Cleaning holder initial position. (b) Cleaning holder final position.

Figure 4.4: Schematic of the cleaning holder design.

plastic became black and then detached from the the fibre). An inadequate fixation of the optical fibre may result in the contamination of the cleaning reagent due to the detachment of the plastic jacket of the fibre and the possible deposition of the plastic residue onto the sensing region. This may result in a considerable increment in the cleaning time, as well as in the amount of chemical waste generation. In addition, the removal of the jacket may increase the fragility of the fibre. Finally, the uncontrolled detachment of the jacket makes it difficult to know the exact location of the LPG.

In order to avoid these problems and to have a controlled immersion of the optical fibre in the cleaning reagent, a cleaning holder was designed. The holder consisted of a 2-part rectangular frame, joined in the middle of one of its symmetry axes by a small 3D-printed post. These two sites acted as pivots. The idea is similar to a fully open book that is being closed. Parallel to the same symmetry axis, i. e. to the pivots, small holes were made to attach the 3D-printed supports, allowing the use of different heights and angles. A schematic of the cleaning holder frame design is shown in Fig. 4.4.

The design was fabricated using a 3D printer, model Ultimaker 2 Extended+, from Ultimaker. The filament system of the printer is optimized for a number of filament materials, including polylactic acid (PLA). The PLA filament, available in a wide range of colours, is safe and easy to print with, provides a good quality surface, and is compatible with high print speeds [352]. PLA is a biodegradable polymer which has been applied for a variety of applications, such as a drug carrier in drug delivery systems, in tissue engineering and as a packaging material [353]. The PLA melting temperature is 145-160°C, though it is only suitable for use in applications below 60°C [352]. PLA is soluble in chloroform, and exhibits solubility in pyridine, acetone, water, methanol and ethanol [354]. Other PLA properties, synthesis and applications, out of the scope of this project, can be found in [354, 353]. Despite its solubility in solvents, the cleaning device was printed using a PLA filament since the 3D-printed parts are not in direct contact with the cleaning substances. In addition, in the course of this project, it was observed that the cleaning device showed adequate resistance to splashing of acids and solvents. The black colour of the PLA filament used to build the frame was chosen to facilitate the visualization of the fixed fibre.

With the aim to reduce the chemical waste, a 3D-printed beaker base was modelled

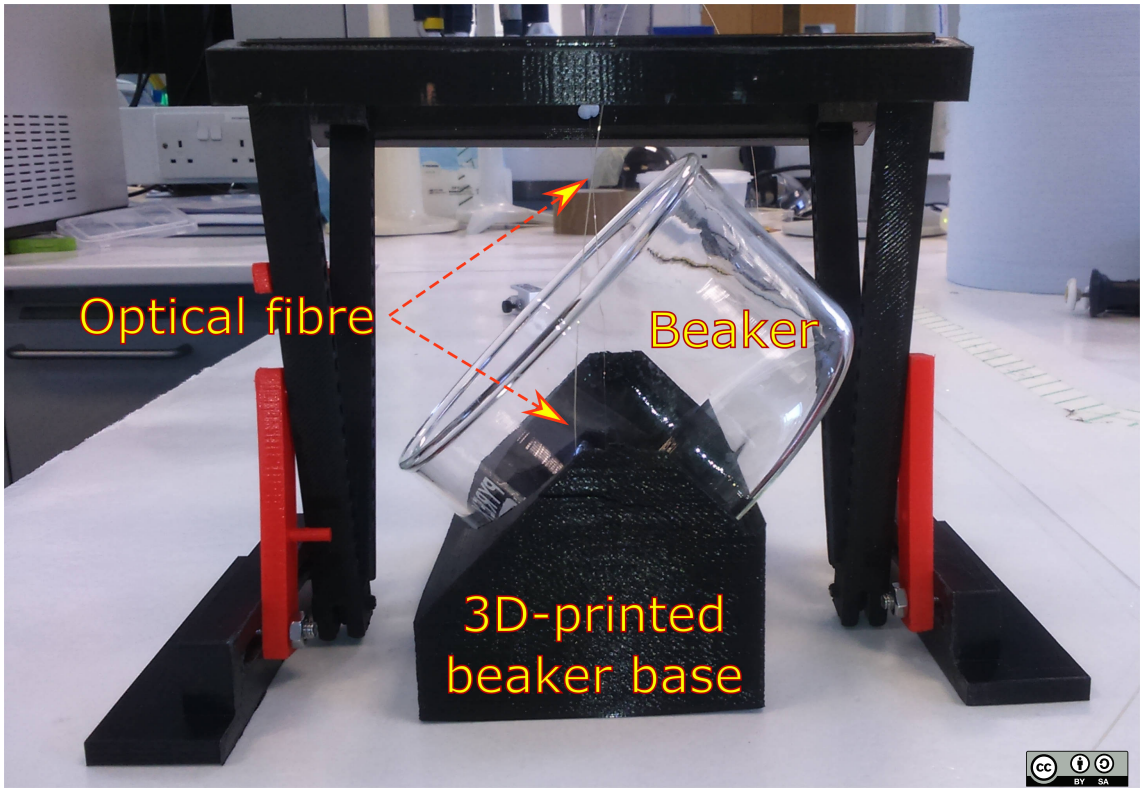

Figure 4.5: Optical fibre cleaning setup using the 3D-printed holder and the 3D-printed beaker base.

and fabricated. The base was designed to hold a low form glass beaker at an angle of 45 degrees. In this way, the cleaning holder ensured that the optical fibre followed the contour of the base of the beaker, without getting in direct contact, and minimized the amount of the chemicals involved. An image of the cleaning setup for an optical fibre held by the 3D printed device and the 3D-printed beaker base holding a beaker is shown in Fig. 4.5.

The main feature of the 3D-printed holder is that the fixing of the fibre is rapid and simple. The fibre can be fixed on the holder with adhesive tape or a reusable adhesive such as blu tack. In addition, another advantage of the holder is that it allows the simultaneous cleaning of a number of fibres, with the fibres remaining separate from one another when immersed in liquid, as shown in Fig. 4.6. This cleaning device was used in the further experiments to clean the surfaces of the LPG sensors.

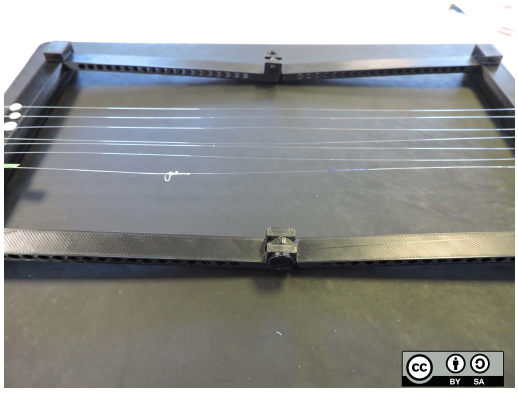

(a) Multiple optical fibres fixed on the 3D-printed cleaning holder frame.

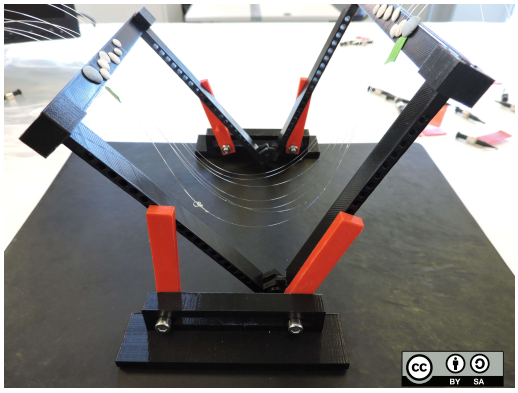

(b) 3D-printed cleaning device holding a number of optical fibres.

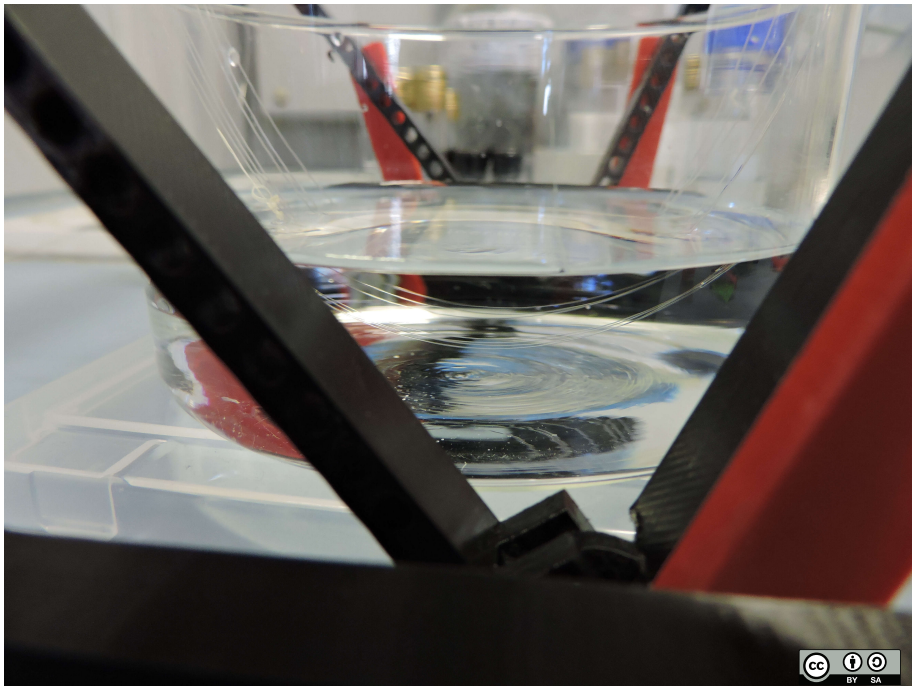

(c) 3D-printed device holding a number of optical fibres immersed in liquid, with the fibres remaining separate from one another.

Figure 4.6: Cleaning device holding a number of optical fibres.

4.2 Design of the sample container

In this section, the design and optimization of the container that was used to accommodate the LPG sensor for incubation will be described.

There are a number of desirable requirements to be met by the material from which the container was fabricated, for example, it should be resistant to the corrosive substances involved in the different cleaning protocols, it should be chemically inert to avoid undesirable reactions with the biological materials employed in the experiments, and it should be stable under temperature changes.

Polytetrafluorethylene (PTFE), better known by its commercially brand name Teflon®, is a synthetic thermoplastic polymer, white at room temperature, with chemical, mechanical and electrical properties that make it attractive for use in this project. The main chemical, mechanical and electrical properties of PTFE are listed in Table 4.3.

PTFE is essentially chemically inert [355]. Only few chemicals, such as molten alkali metals and some fluorochemicals as chlorine trifluoride, are known to react with the PTFE up to its upper-use temperature (260°C) [356]. In addition, the chemical structure of PTFE produces other useful properties, such as low-surface adherability, low friction and insolubility. PTFE mantains its mechanical properties from -268 to 260°C and exhibits practically zero water absorption (<0.01% in 24 h). More details about these and other properties of PTFE can be found in the report of DuPont® [356].

PTFE containers were designed with the aim of producing an LPG immersion chamber for the functionalization and coating of the fibre for the bacterial assays. The design aimed to minimize the amount of reagents and solutions required in the experiments. For design purposes, only the volume of the internal cavity was considered. It should be noted that the capacity of each container is higher than the volume of the internal cavity because of the meniscus formation due to the material hydrophobicity, as shown in Fig. 4.7. The fabrication of all of the containers was carried out by Staines from the Centre for Engineering Photonics, Cranfield University. In order to facilitate the visualization of the position of the sensor within the container in Fig. 4.8 - 4.11, a section of optical fibre was dyed in crystal violet for 15 minutes.

Four containers, shown in Fig. 4.8, with different internal volumes were fabricated. All containers had a "V"-shaped channel at each end to hold the optical fibre in the central region of the internal cavity, except for one container, shown in Fig. 4.8d, in which the "V"-shaped channels were biased to one side, so that the sensor was placed closer to one of the walls of the internal cavity.

The first container, referred as container 1 for identification purposes and shown in Fig. 4.8a, had internal dimensions of 50 x 10 x 2 mm (length x width x depth), equivalent to 1000 μL, and a capacity of 2000 μL of DI water. This initial model was employed in the very first experiments of this project, in which disposable plastic pipettes with a 3 mm external diameter tip were used to pour in and to remove the testing solutions (pumping system).

Container 2, shown in Fig. 4.8b, had internal cavity dimensions of 40 x 4 x 2 mm (equivalent to 320 μL) and a capacity of 800 μl. As the distance between inner

Table 4.3: Main polytetrafluorethylene (PTFE) properties.

Chemical	Chemical resistance to corrosive substances
	Nonsolubility
	Nonadhesivenes
	Nonflammability
	Long-term weatherability
Mechanical	Flexibility at low temperatures
	Low coefficient of friction
	Stability at high temperatures
Electrical	Low dielectric constant
	Low dissipation factor
	High arc-resistance
	High surface resistivity
	High volume resistivity

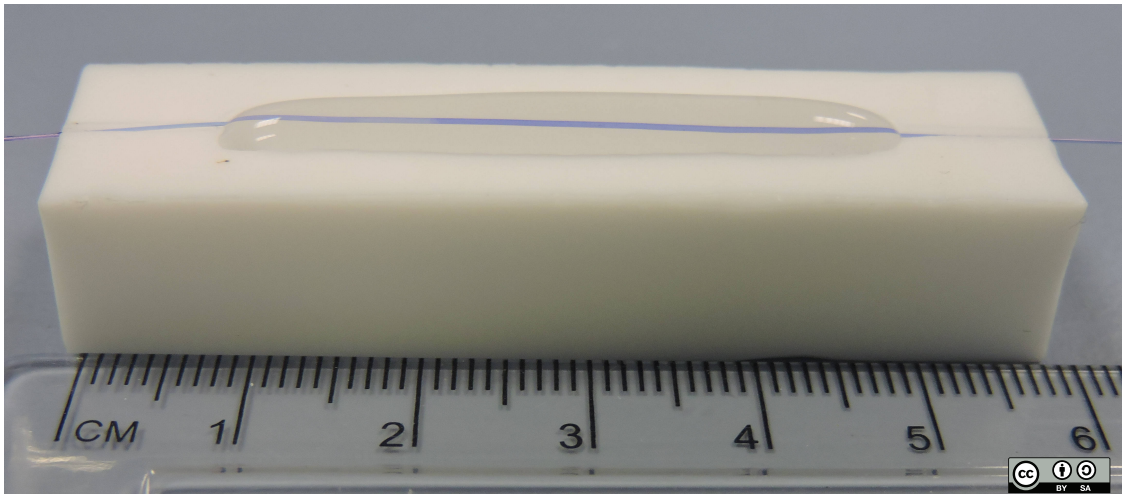

Figure 4.7: Image of a PTFE container filled with DI water. A convex meniscus formation due to the PTFE hydrophobicity can be observed.

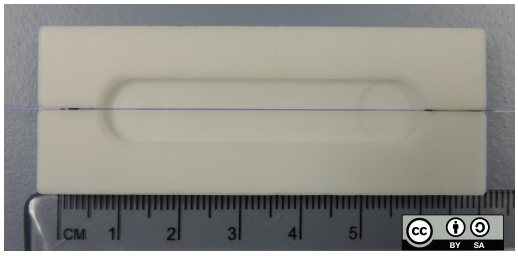

(a) Container 1, internal cavity dimensions: 50 x 10 x 2 mm, capacity: 2000 μL.

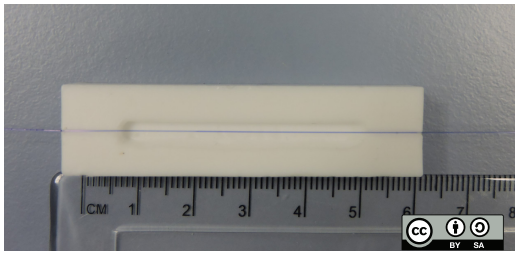

(b) Container 2, internal cavity dimensions: 40 x 4 x 2 mm, capacity: 800 μL.

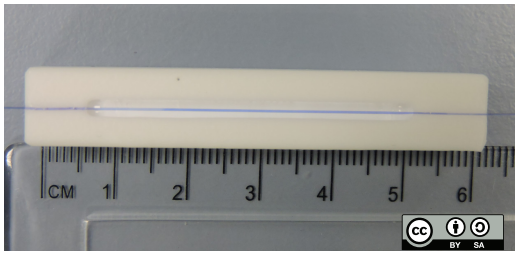

(c) Container 3, internal cavity dimensions: 40 x 2 x 2 mm, capacity: 250 μL.

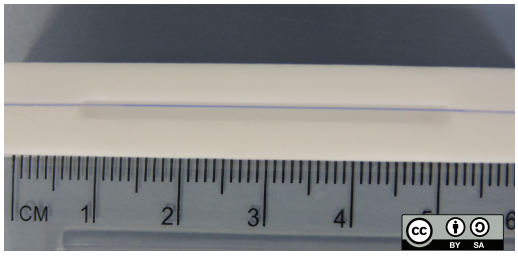

(d) Container 4, internal cavity dimensions: 40 x 2 x 2 mm, capacity: 250 μL.

Figure 4.8: PTFE containers with different internal cavity dimensions.

walls and the sensor was approximately 2 mm, the use of the disposable plastic pipette to remove the solution without removing the fibre from its position was compromised. In this case, a syringe (10 mL BD Plastipak^{TM}) with a sterile needle (Terumo, cannula 0.8 mm, length 38 mm) was used.

With the aim to reduce the volume of container 2, container 3, shown in Fig. 4.8c, was fabricated by reducing the width of container 2 by half, i. e. 40 x 2 x 2 mm, (equivalent to 160 μL). The capacity of this container was estimated to be 250 μL of DI water. For practical purposes, this is the minimum volume for the internal cavity, considering the length of the LPG, the superficial tension of the liquid, and the manual handling of the pumping system. However, due to the reduced space between the LPG sensor and the internal walls of the cavity ($<$ 1 mm), the needle could touch the LPG, modifying its tension or, breaking it, as shown in Fig. 4.9a.

Container 4 was fabricated with the "V"-shaped channels biased to one side while maintaining the same internal volume (40 x 2 x 2 mm), as shown in Fig. 4.8d.

This model had more space in which to manipulate the needle inside the cavity, as shown in Fig. 4.9b, avoiding the issues associated with container 3. Fig. 4.9 shows a visual comparison of the space available in containers 3 and 4 to manipulate the needle to remove the liquid solution.

However, one drawback of this configuration is that the liquid solution is not completely removed from the container. A remnant of the solution stays between the LPG sensor and the closest inner wall of the cavity, as shown in Fig. 4.10. This may result in deficient rinsing of the fibre in the washing steps of the corresponding protocols for functionalization, active coating, and bacterial assays.

The container chosen to hold the LPG sensor for the active coating and the bacterial assays was container 3, i. e. the one with internal volume of 40 x 2 x 2 mm

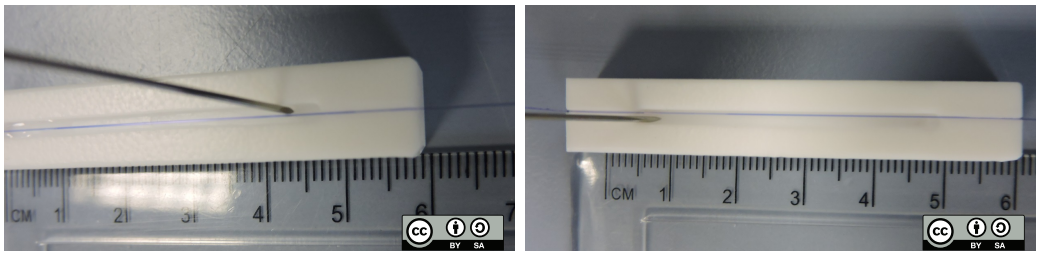

(a) Container 3. (b) Container 4.

Figure 4.9: Visual comparison of the space available in containers 3 and 4 to manipulate the needle.

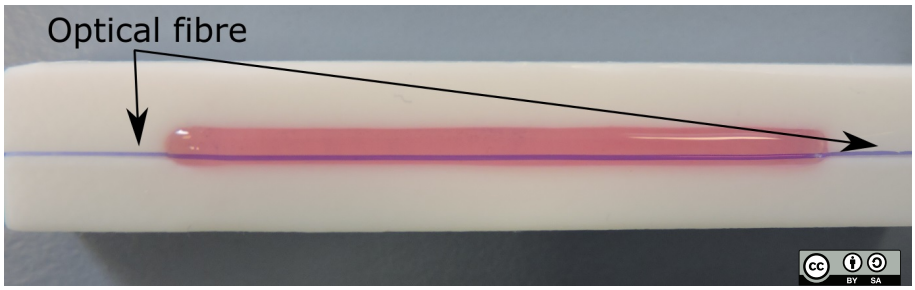

(a) PTFE container holding a blue dyed optical fibre probe incubated in pink dyed solution.

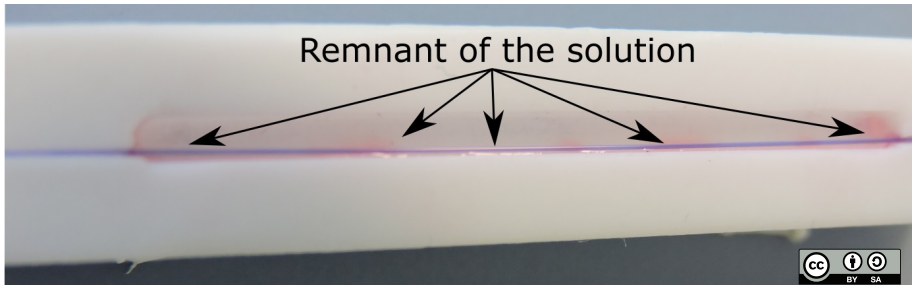

(b) Remnant of the pink dyed solution between the blue dyed optical fibre probe and the inner wall of the container.

Figure 4.10: PTFE container with the optical fibre holder channels placed next to the edge of an inner wall.

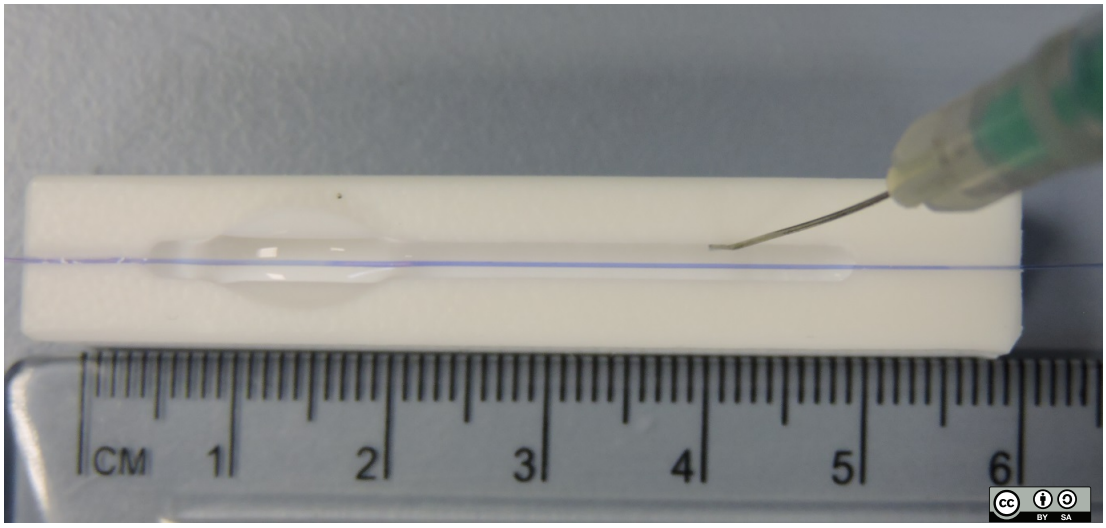

Figure 4.11: Optical fibre placed in the centre of container 3 with an insulin needle for liquid extraction.

with the centred "V"-shaped channel, shown in Fig. 4.8c. For the manual ejection system, a 1 mL insulin syringe (Terumo) with a needle (BD Micro-Fine+, gauge 0.33 mm, length 12.7 mm) was selected. The distance between the LPG placed in the central region of the container and the internal walls of the cavity (< 1 mm) left enough space to manipulate the thin needle for the removal of the liquid solution, as shown in Fig. 4.11.

4.3 Surface activation and coating proteins

In this section, the process used for the silanization of the surface of the cladding of an optical fibre and the proteins used for the coating, i. e. the antibody and the blocking protein against non-specific binding, are described.

4.3.1 Silanization

Silanization is the most commonly used way to introduce a variety of functional groups onto a glass surface [357]. Silanized surfaces provide a reliable substrate for the immobilization of recognition elements [358]. APTMS is one of the most commonly used reagents to prepare an active amine-terminated layer on oxides such as silica and quartz [359]. The main advantage of an aminosilane monalayer on the surface of the oxide is the rapid formation of covalent bonds between the oxide surface and the anchoring groups, thus stabilizing the monolayer and facilitating further modifications [360]. In this section, the functionalization of the surface of optical fibres by silanization, using both an amine and a thiol silanes, is investigated.

Reagents

Methanol (HPLC grade) from Fisher Scientific, 3-Aminopropyl-trimethoxysilane (APTMS) (95%) from Acros Organics, 2,4,6-Trinitrobenzene sulfonic acid (TNBS)

(5% w/v Methanol solution) from Thermo Scientific, 3-Mercaptopropyltrimethoxysilane (MPTMS), toluene (anhydrous, 99.8%) from Sigma-Aldrich, acetone (HPLC ≥99.8%) from Sigma-Aldrich, sodium hydroxide (≥98%, pellets (anhydrous)) from Sigma-Aldrich.

Methods

The surfaces of two optical fibres (one for the test and one as control) were cleaned following the protocol of the two-acids-based method (see Sec. 4.1.2). This cleaning method acts as a pre-activation procedure for a silanization strategy, generating the silanol groups (Si-OH) at the surface of the fibre required for the later reaction with the silane. The silanization method described in this study was modified from the procedure outlined by Canfarotta *et al.* [361]. Briefly, the surface of one optical fibre was activated by boiling the fibre in 150 mL of sodium hydroxide (NaOH, 1 M) for 5 minutes to obtain the hydroxyl groups (-OH). The fibre was removed from the beaker and rinsed thoroughly with DI water. The fibre was then washed with acetone and dried for 2 h under the fume hood. The fibre was incubated overnight in 20 mL of a freshly prepared solution of 2% (vol/vol) of APTMS in toluene at room temperature in a closed container. The fibre was removed from the toluene and washed 3 times with methanol and 3 times with acetone. The fibre was dried under the fume hood for at least 2 h. After the APTMS treatment, amino groups (which have positive electric charge) were formed on the surface of the optical fibre [283]. In order to verify the presence of amino groups on the surface of the optical fibre, a solution of TNBS was used. TNBS is a rapid and sensitive reagent for the quantification of free amino groups [362]. TNBS reacts with primary amines to form a reddish yellow-coloured derivative. The chemical reaction is shown in Fig. 4.12. The two

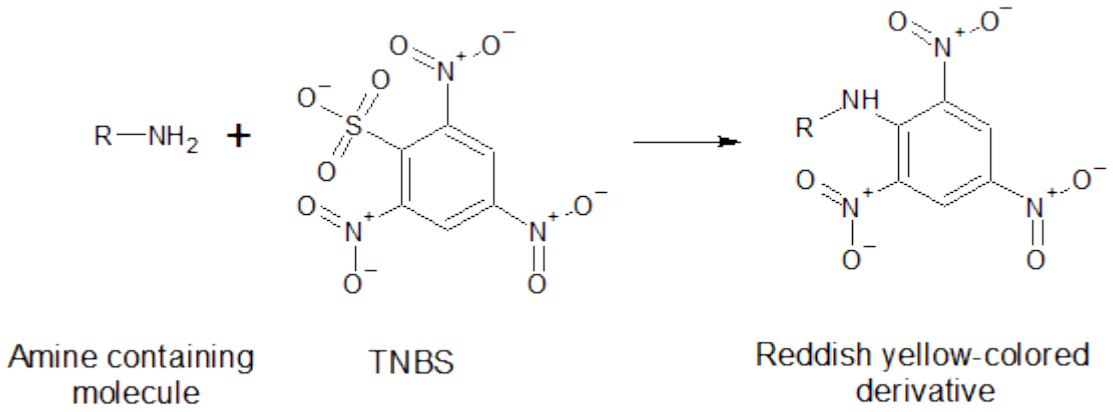

Figure 4.12: Reaction of amino groups with TNBS and the reddish yellow-coloured derivative.

fibres were incubated in 5 mL of a 2% solution of TNBS in PBS for 10 minutes at 40°C (the solution tends to form crystals at room temperature) in a bain-marie [363]. The reddish yellow colour on the surface of the silanized optical fibre, shown in Fig. 4.13, indicates the presence of amino groups. The control fibre did not present a change in colour. Another optical fibre was functionalized by silanization using

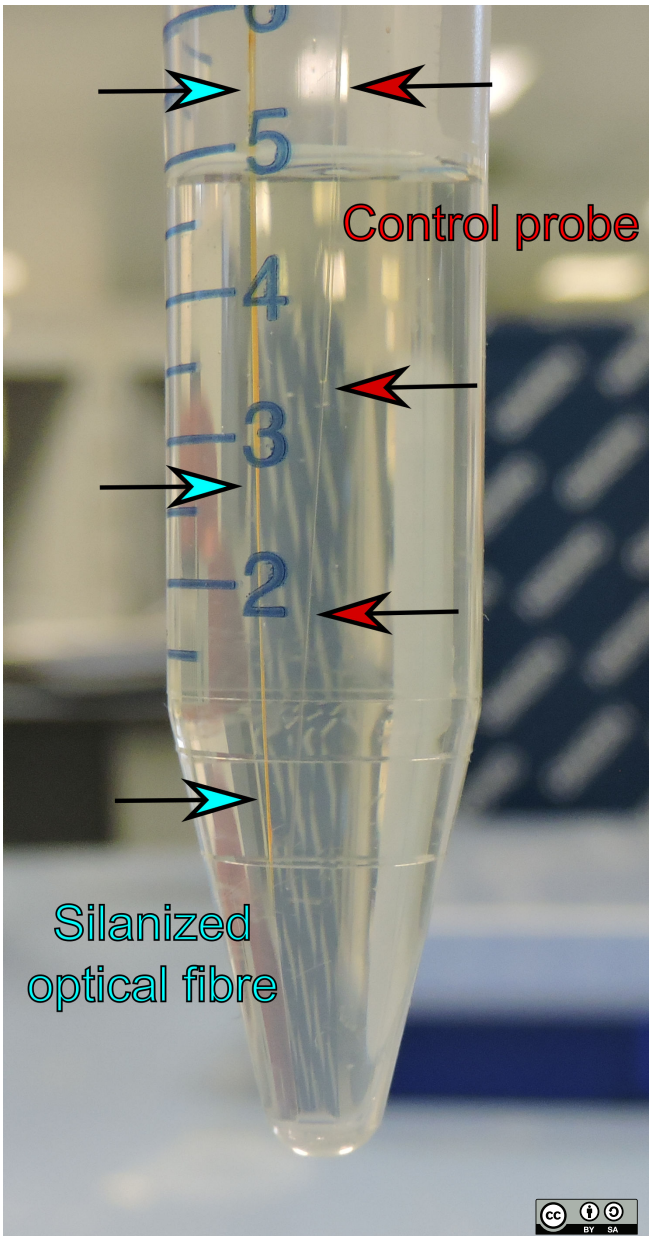

Figure 4.13: Silanization test on two optical fibres. The reddish yellow colour in the silanized probe indicates the presence of amino groups.

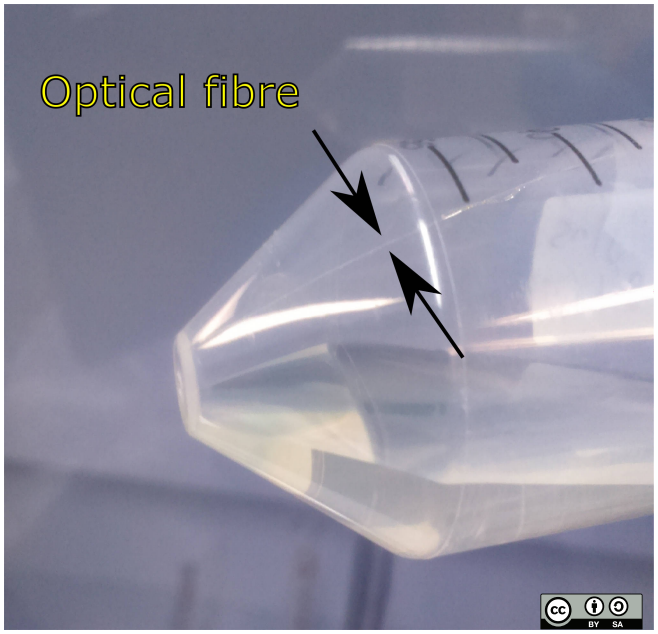

Figure 4.14: Optical fibre silanized using a thiol silane (MPTMS) and tested for the presence of amino groups (-NH_2). Since MPTMS generates sulphydril groups (-HS) on the surface of the fibre instead amino groups, no coloured derivative was expected.

a thiol (sulphydril group -HS) silane (MPTMS). The functionalization of a solid substrate using a thiol silane can follow the same protocol as the functionalization using an amine silane [364]. The silanization using MPTMS generates a layer of sulphydril groups. In this case, when tested for the presence of amino groups using the TNBS solution, no yellow colour was displayed on the surface of the fibre, as shown in Fig. 4.14. It was observed that the location of the optical fibre within the beaker containing the silane solution in toluene is important. When in contact, the toluene removed the plastic jacket from the fibre, as shown in Fig. 4.15, which may compromise the resistance of the fibre. In addition, the uncontrolled removal of the plastic jacket can compromise the identification of the exact location of the LPG in the fibre. For example, Fig. 4.16 shows the transmission spectra of an uncoated LPG of period 112.6 μm and 4 cm of length, when sections of length 1 cm, 2 cm, 3 cm, and 4 cm were immersed in DI water at 20°C, acting as a liquid-level sensor, as described by Khaliq *et al.* [365]. This would be a problem because the position of the central wavelength of the attenuation bands would change and the wavelength shifts due to the functional coating and bacterial binding would be misunderstood. For these reasons, two preventive measures were considered. First, after the LPG fabrication, pieces of coloured tape were stuck to the plastic jacket at known distances from each end of the LPG, writing the distance (in cm) from the beginning and end of the LPG respectively on both tapes. This simple solution prevents the loss of knowledge of the location of the grating, even if a random section of plastic jacket is removed by the toluene. Second, the use of the 3D-printed device facilitates the placing of the optical fibre inside the beaker in a way that ensures that only the LPG region is immersed in the solution of silane in toluene. This allows the length of plastic jacket

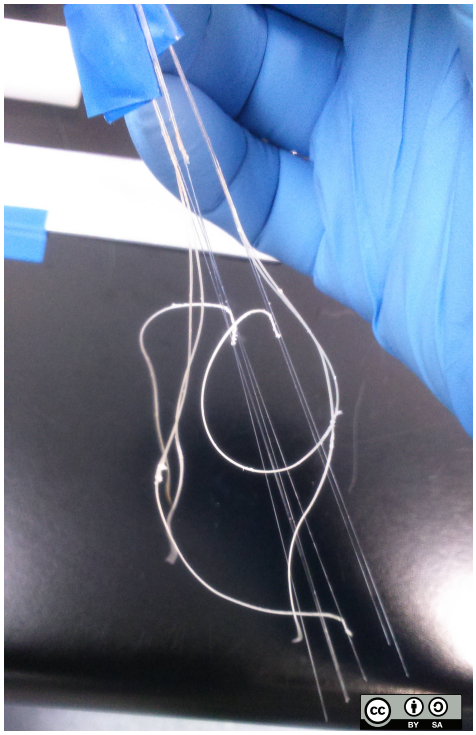

Figure 4.15: Image of optical fibres incubated in a solution of amine silane (APTMS) in toluene. The toluene solution removes the plastic jacket from the fibre.

that needs to be removed to be minimized, also minimizing the fragility of the fibre.

4.3.2 Polyclonal antibody specific to *Campylobacter jejuni*

The first use of antibodies as an analytical tool goes back to 1945, when Coombs *et al.* presented a method to amplify the effect of weak antibodies, with particular reference to Rh antibodies [366]. The first antibody immobilization on to a solid support was reported later in 1967 by Catt and co-workers [367, 368]. The use of antibodies as recognition elements, as was mentioned in Sec. 2.4.2, has the advantages of being easy to integrate into different measurement platforms and their high specificity [234]. Polyclonal antibodies, unlike monoclonal antibodies, recognize more than one epitope on the target analyte. This allows multiple antibodies to bind through the antigen, amplifying the signal in a number of immunoassays [231]. In addition, polyclonal antibodies with high specificity produce a stronger signal than monoclonal antibodies [231]. The production of polyclonal antibodies against the target analyte is stimulated by the immunization of a variety of animals including rats, hamsters, rabbits, guinea pigs, chickens, pigs, goats, sheep, bovines, donkeys and horses [369]. The choice of the proper animal species depends on several factors such as: i) the amount of antigen available for immunization, ii) the amount of antibody required, iii) the time required to obtain the antibody response, and iv) the cost [369]. For polyclonal antibody production, the most widely employed animal has been the rabbit, due to its ability to respond to a wide variety of antigens, its production of highly specific antibodies in a relatively short time (77 days), convenient size to

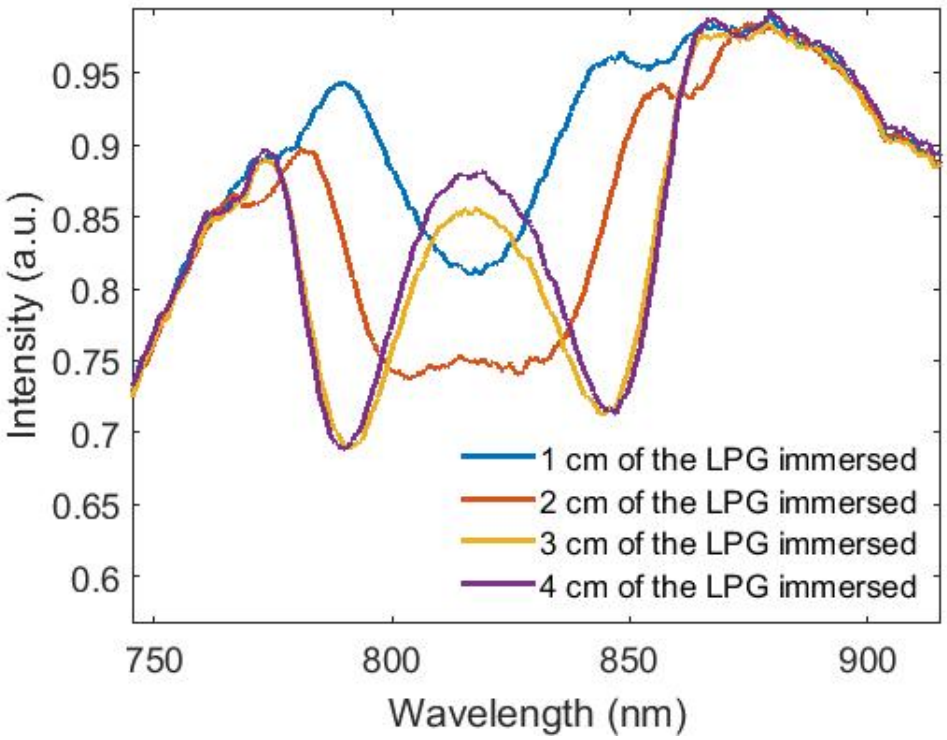

Figure 4.16: Transmission spectra of an uncoated LPG of period 112.6 μm, 4 cm of length, when different lengths of the grating (1, 2, 3 and 4 cm, respectively) were immersed in DI water at 20°C.

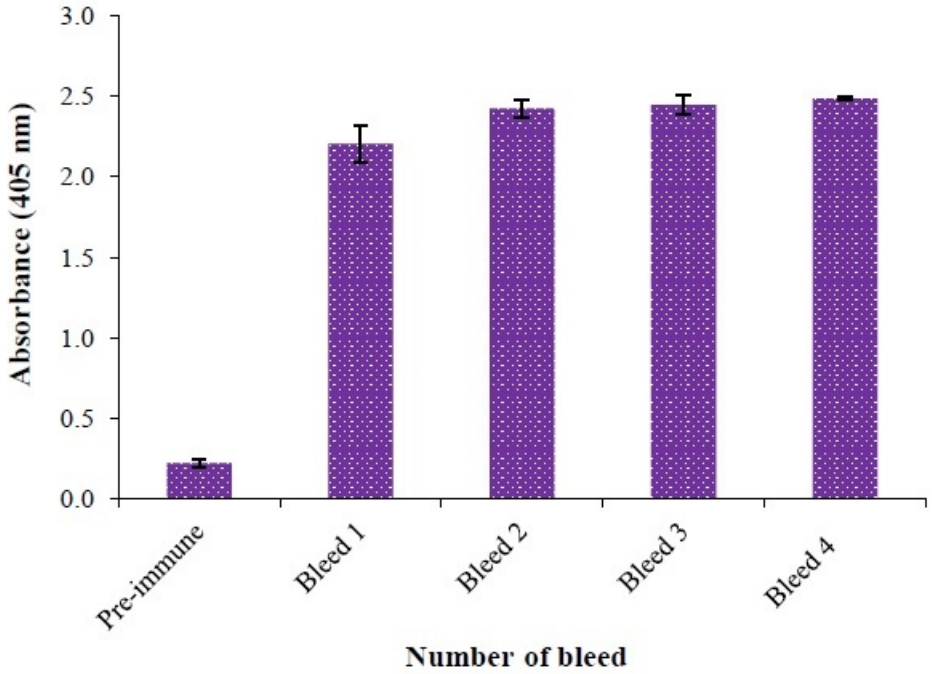

Figure 4.17: Antiserum determination over the course of the rabbit immunisations using an indirect ELISA assay. Graph from [372].

handle and bleed, long life span (5-8 years) and adequate volumes of antisera (blood serum that contains antibodies) (<100 mL) [370, 231]. In addition, rabbit polyclonal antibodies are more specific than goat, chicken or sheep antibodies [371]. For a detailed description of the production of antibodies, including procedures, critical steps, evaluations and suggestions, the reading of [370, 229, 231] is recommended.

The rabbit polyclonal antibody specific to *C. jejuni* used in this work was obtained from the Malaysian Agricultural Research and Development Institute (MARDI) by Masdor and Tothill (School of Aerospace, Transport and Manufacturing, Cranfield University). The detailed description of the production of the polyclonal antibodies, out of the scope of this project, can be found in Masdor's PhD thesis [372]. Briefly, *C. jejuni* cell suspensions (500 μL) at concentration of 1 x 10^9CFU/mL and 500 μL of adjuvant (a substance that enhances the body's immune response to an antigen) were injected subcutaneously to two 5-6 months-old New Zealand white rabbits. A booster injection was applied weekly after the initial immunisation (+ three booster injections). The bleeding of the rabbits for antibody determination was carried out two weeks after each booster injection. A fifth bleeding was carried out one week after the fourth one, without immunisation in between. The development of polyclonal antibody specific to *C. jejuni* over the course of the immunisations was assessed using an indirect ELISA assay. The immune response produced by the described method occurs in two stages. The first injection induces the primary stage of the response, producing only a small amount of antibodies. Subsequent injections or booster injections induce the second stage of the immune response, producing a large amount of highly specific antibodies [373], as shown in Fig. 4.17.

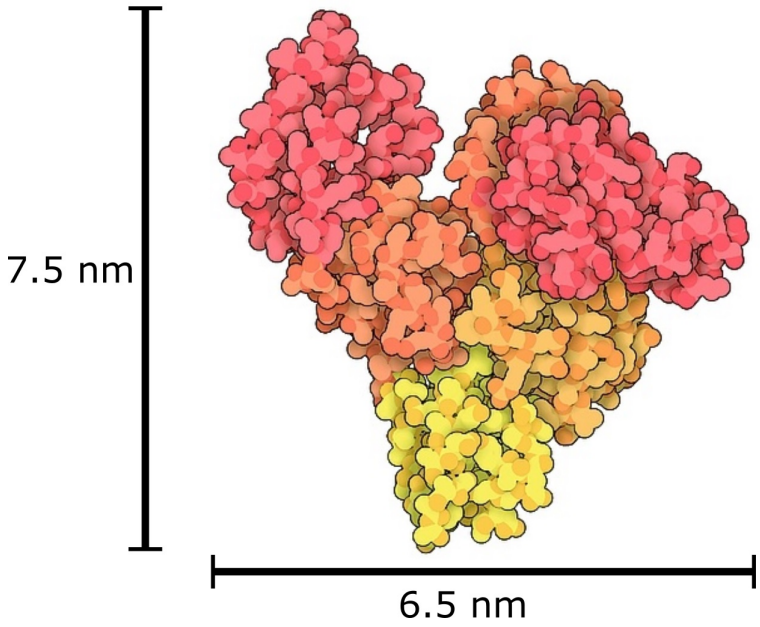

Figure 4.18: Schematic of BSA with the heart-shape. Modified from [377].

4.3.3 Protein coating against non-specific binding

In the development of a biochemical sensor, preventive measures have to be taken to avoid, or at least to minimize, the non-specific adsorption of biomolecules on the surface of the solid support. The non-specific adsorption can take place in any site not covered by the recognition element. There are two ways to prevent such binding. One is the addition of high concentrations of immunologically inert substances to the antigen solution, promoting competition for the available sites on the support [47]. The other way is to add a blocking agent in a separate step between the coating with the recognition element and the assay with the target analyte solution. This last method has the advantage of increasing the competing ability of the blocker. The most commonly used blocking agents are non-fat dried milk, detergents such as tween-20, triton X-100, and proteins such as normal rabbit serum, normal horse serum, bovine serum albumin, casein and gelatin [47]. However, when using detergents as blocking agents or adding to a washing solution, care has to be taken with the denaturation of the recognition element and the formation of bubbles. Compared with Tween-20 and casein, bovine serum albumin has been shown to have the best capability as a blocking agent on the surface of magnetic beads for the detection of *Campylobacter jejuni*, assessed with a competitive ELISA test [58]. Bovine serum albumin (BSA) is a heart-shaped protein which is presumed to occur in milk as a result of leakage from the blood in the mammary gland during milk production [374]. The average dimension of BSA are 7.5 x 6.5 x 4.0 nm^3 [375]. The isoelectric point of BSA calculated from its amino acid sequence is pH 5.4 [376]. The isoelectric point is the pH at which the overall charge of the protein is zero (neutral charge). A schematic of BSA is shown in Fig. 4.18. The main uses of BSA are as: i) a stabilizer for other proteins and enzymes [378], i. e. increasing the shelf-life of proteins and enzymes during storage, protecting them from environmental stresses,

ii) a carrier protein [379], and iii) a blocking protein against non-specific binding [135, 268, 380, 381, 162, 357, 382]. The BSA used in this work (protease free, fatty acid free, essentially globulin free, pH 7, ≥98%) was purchased from Sigma-Aldrich and it was used as blocking reagent against non-specific binding. BSA is soluble in water. However, in biochemical applications, the pH of solution needs to be controlled because changes in this variable may denature the biochemical material or change its properties [35]. The most often employed buffers for biochemical interactions are phosphate buffered saline (pH 7.4), Tris-HCl (pH 8.5), and 50-mm carbonate (pH 9.6). In order to promote the adhesion to the solid support, it is recommended to use a buffer with a pH value one or two units higher than the isoelectric point of the blocking protein [47]. For instance, at pH higher than the isoelectric point of BSA, the electrostatic interactions between the solid support and the blocking protein are increased as a result of the decrease of the repulsive energy and the zeta potential of BSA (ζ_{BSA}) due to the increase in the pH value [376].

PBS is the most widely used solvent to make a BSA solution to reduce non-specific binding [135, 383, 380, 162]. PBS is a water-based buffer solution containing sodium phosphate, sodium chloride, and in some formulations, potassium chloride and potassium phosphate. One of the advantages of phosphate buffered saline (PBS) is that is suitable for a large number of antigens [47]. The PBS used in this work was purchased from Sigma-Aldrich in the form of tablets. One tablet dissolved in 200 mL of DI water yields 0.01 M phosphate buffer, 0.0027 M potassium chloride and 0.137 M sodium chloride, pH 7.4, at 25 °C. Then, the PBS was filtered to remove the non-dissolved salts using a vacuum Buchner filter flask with funnel, commonly known as a vacuum flask, and a Whatman^{TM}membrane filter (cellulose nitrate) with pore size of 0.2 μm, from GE Healthcare Life Sciences UK Limited. In the subsequent descriptions, unless otherwise stated, the PBS was prepared as described here.

4.4 Sensor surface active coating

In this section, the experimental setup for the deposition of an antibody coating and the blocking coating for the non-specific binding of the target bacteria will be described.

4.4.1 Experimental setup

The transmission spectrum of an LPG is sensitive to changes in parameters such as refractive index, strain, bend radius, and temperature, as mentioned in section 2.3.1. The experimental setup was designed to keep the strain, bend radius, and temperature constant during the experiment. Briefly, the LPG was mounted inside a temperature chamber (IKA® KS 4000i control) in the central part of a PTFE container, fixing the fibre at both ends of the sensing section in a customized frame to keep the tension constant during the experiment. The optical fibre was interrogated by coupling the output from a broad band light source (HL-2000-FHSA, wavelength range: 360-2400 nm, Ocean Optics) into one end and connecting the other end to a CCD spectrometer (HR4000, wavelength range: 200-1100 nm, optical resolution: 0.12 nm, Ocean Optics). Both the light source and spectrometer were kept outside

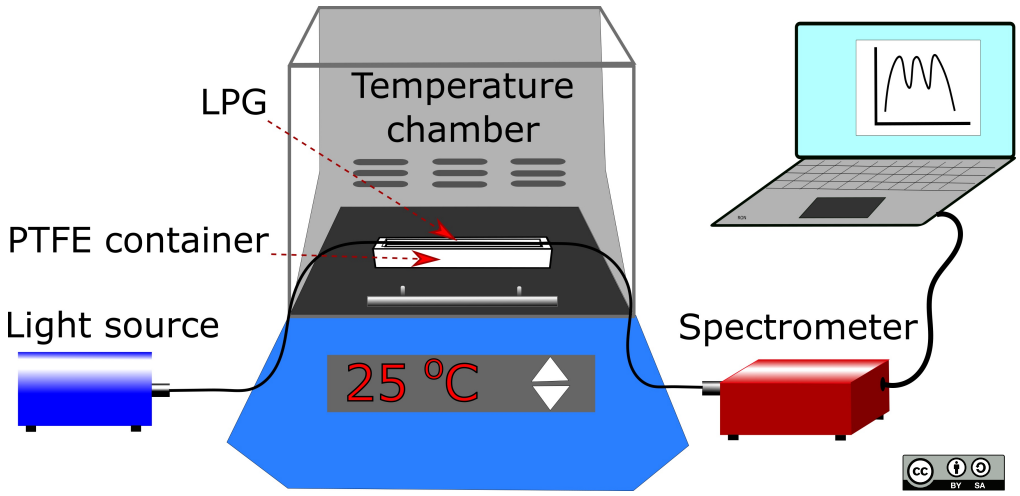

Figure 4.19: Schematic of the experimental setup.

the chamber, as shown in Fig. 4.19. The spectrometer was connected, via the USB port, to a computer, where the transmission spectrum was visualized using the software SpectraSuite®, from Ocean Optics, Inc. The temperature chamber was set at 25°C. Room temperature has been widely used for the coating of a number of solid substrates, including optical fibres, with antibodies due to their high stability in this range of temperatures [280, 384, 385, 386, 387, 388]. For example, humanized monoclonal antibody has demonstrated stability for 8 weeks when stored at 25°C, and 1 week at 37°C [389]. However, temperatures of incubation such as 4°C, 21°C, 25°C, 35°C and 37°C are commonly used for stationary conditions, although the incubation time may vary [390, 391]. For example, at 4°C a longer incubation should be given (overnight). In general, for stationary assays involving the reaction of antigen and antibodies the incubation time is 1-3 h at 37°C [47].

Temperature stabilization

The temperature range for the temperature chamber, according to the manufacturer, is RT+5°C to 80°C [392]. If the experiment inside the temperature chamber is required to be performed at 25°C, the maximum temperature of the laboratory has to be 20°C. The temperature of the laboratory was set at 19°C and monitored over three days to determine the temperature fluctuations in the lab. The temperature at different hours over the course of three days is shown in Fig. 4.20. The maximum temperature reached was 19.4°. Therefore, the temperature of the lab was kept at 19°C and the temperature chamber was set up at 25°C.

The response of an LPG of period 112.6 μm and of length 4 cm to temperature changes, in the range of 24 to 38°C, was investigated. The temperature dependence of the central wavelength, in air, of the left-hand-side attenuation band of the dual resonance band of the LPG is shown in Fig. 4.21. The band showed a linear response induced by temperature changes in the range from 24 to 38°C. The temperature sensitivity of that particular attenuation band was 1.1 nm/°C. This demonstrates the importance of maintaining the temperature constant during the experiments.

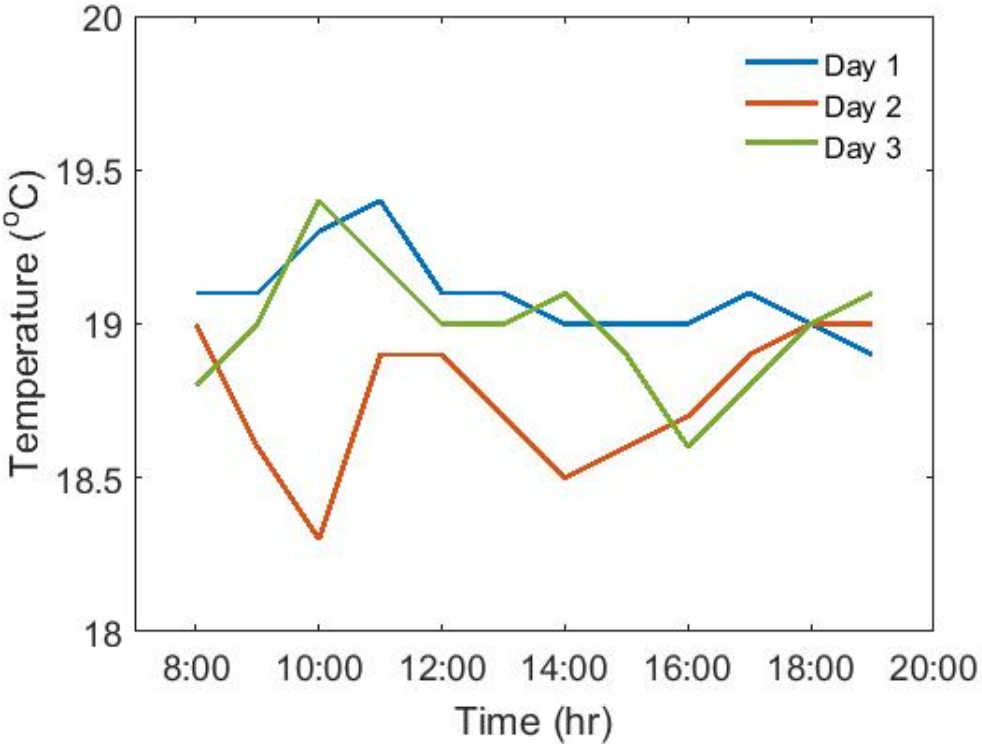

Figure 4.20: Lab temperature fluctuations over three days when lab temperature was setup at 19°C.

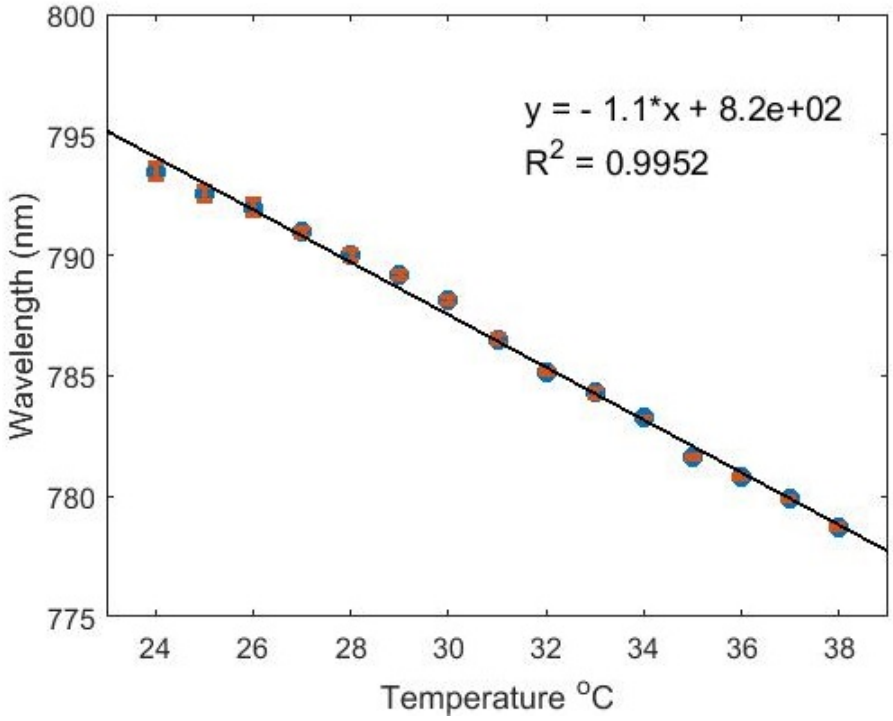

Figure 4.21: Temperature dependence of the central position of an attenuation band of an LPG in air, with period 112.6 μm and 4 cm of length.

Invariance of the attenuation band

Changes in the location of the central wavelengths of the attenuation bands in the transmission spectrum of an LPG due to the action of connecting and disconnecting both ends of the fibre to and from the light source and the spectrometer, respectively, were investigated.

An LPG of period 112 μm and of length 4 cm was interrogated as described earlier in this section. A section of the jacket (approx. 4 cm) was removed from both ends of the fibre with a mechanical stripper. The exposed cladding was rubbed with an optical tissue moistened with IPA to remove the jacket residuals. Then, both ends of the fibre were cleaved with a precision fibre cleaver. The cleaved ends of the fibre were coupled via SMA bare fibre adapters to the light source and the spectrometer, respectively. This action will be referred as connecting or connection. The action of decoupling the bare fibre adaptors from the light source and the spectrometer, and the unmounting of the fibre from the adaptor will be referred as disconnecting or disconnection. The central part of the fibre containing the LPG was mounted inside the temperature chamber and fixed in a customized frame to keep the temperature and strain constant during the experiment. The connecting and disconnecting actions were repeated 9 times. The duration of each connection was 10 seconds, during which the transmission spectra were saved every 1.25 seconds for a total of 8 files per connection. The transmission spectra of the 9 fibre connections are shown in Fig. 4.22. Then, the minima of each transmission spectrum were calculated using the

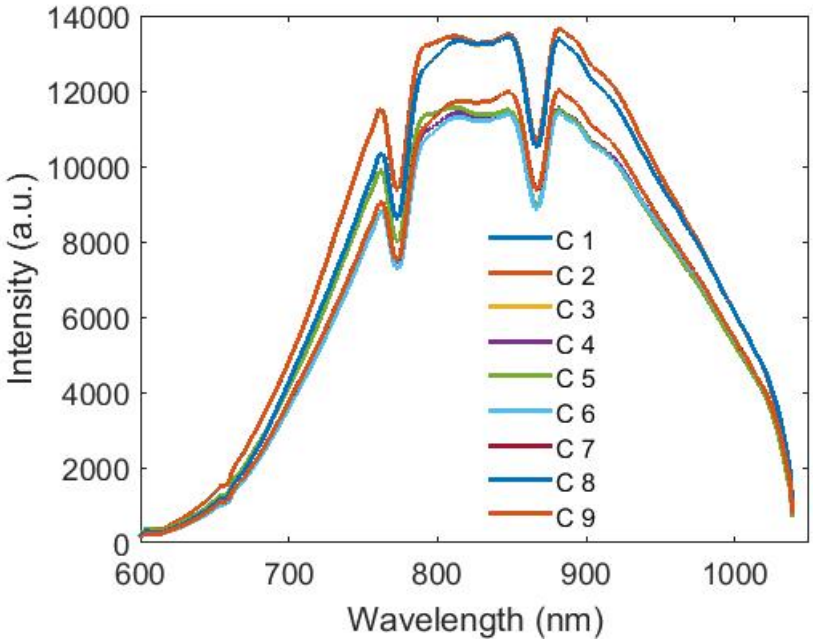

Figure 4.22: Transmission spectra of an LPG of period 112 μm and 4 cm of length after 9 connection-disconnection processes, obtained whilst interrogated to a light source and a spectrometer.

customized Matlab program. Statistical data were obtained using the Data Analysis Tool, from Microsoft Excel. The mode was 772.67 nm, representing the 86% of the

data. The mean value was calculated as 772.69 ± 0.03 nm, with a confidence level of 95%. The different connecting processes produced variations in the fibre coupling efficiency, resulting in different intensities for each transmission spectrum. However, the central wavelength of the attenuation band, according with the statistical results, remained invariant under constant conditions of temperature, strain and refractive index.

4.4.2 Enhanced physical adsorption

In this section, the physical adsorption of antibodies and proteins onto the surface of an LPG, enhanced by a silanization strategy, will be presented.

Methods

An LPG of length 40 mm and period 113.2 μm, selected to provide high sensitivity, was fabricated in a single mode boron-germanium co-doped optical fibre using the point-by-point method described in Sec. 2.3.2. The fibre was cleaned using the two-acids-based method and silanized as described in Sec. 4.3.1. Then, the silanized section of the fibre was mounted on a customised frame and the sensing zone positioned in the middle of the reaction container. The sensor was interrogated as mentioned in Sec. 4.4.1. The fibre was initially incubated in PBS in order to record a baseline spectrum prior to coating. The incubation was carried out for 40 minutes due to the high hydrophobicity of the surface after silanization [393]. Following this, the fibre was rinsed three times with DI water. Rabbit polyclonal antibody specific for *Campylobacter jejuni* (10 μg/mL, in sodium acetate buffer, pH 5.0) was added to the container and the fibre was incubated for 4 hours. The antibody solution was removed from the container and the fibre was washed with DI water. PBS was added to the container and the transmission spectrum of the LPG was recorded. A solution of 500 μg/mL of BSA in PBS was then added to the container and the fibre was incubated for 30 minutes. The fibre was again rinsed with DI water and incubated in PBS before a final spectrum was recorded. The recorded spectra are shown in Fig. 4.23.

Results

The blue curve (starting spectrum) in Fig. 4.23 represents the transmission spectrum of the silanized surface of the LPG, which was bare of all coating materials and represents a baseline for the sensor. The red curve, red-shifted around 3 nm from the baseline, represents the transmission spectrum of the sensor coated with antibody. The yellow curve, further shifted by around 5 nm from the red curve, represents the transmission spectrum of the sensor coated with the blocking protein against non-specific binding. The measurable shifts of transmission spectra indicate that both the antibody and protein coating had occurred.

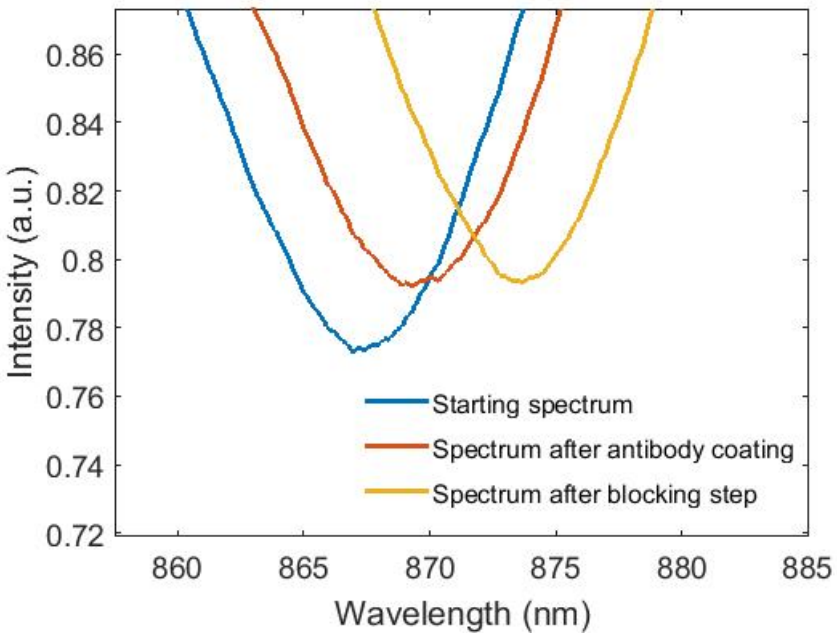

Figure 4.23: LPG period 113.2 μm, 4 cm, 6 cycles, 25°C. Transmission spectra of an attenuation band initially centred at 837nm (blue) and after antibody coating (red) and blocking coating (yellow).

4.4.3 Covalent attachment

Glutaraldehyde (GA) was used for first time in 1963 for the fixation of tissues. Since then, GA has found other applications including the crosslinking of proteins [394]. GA, as mentioned in Sec 2.5.3, is an homobifunctional crosslinker. GA converts the amine-terminated surface to an aldehyde-terminated one [295], which is able to bind with the amino (N-terminus) groups of antibody [395]. Amino and carboxyl (C-terminus) groups are ubiquitous throughout the antibody structure [296]. The thickness of the glutaraldehyde layer is $\approx$ 0.7 nm [396]. The GA solution (Grade I, purified, 25% in H_2O) used in this study was purchased from Sigma-Aldrich. GA is highly toxic if inhaled (corrosive to the respiratory tract) or absorbed through skin, and also may cause sensitization by inhalation and skin contact. The personal protective equipment required to handle GA includes faceshields, gloves, goggles, lab coat and manipulation should always take place under the fume hood. Typical concentrations of GA as a crosslinker for the development of biochemical sensors range from 1% to 12.5% in water or PBS and incubation times from 30 minutes to 2 hours [395, 276, 135, 397, 398, 295, 399]. In alkaline solutions ($\geq$ pH 7.5), the activity of GA is increased, but the stability of the solution is compromised due to polymerization [400]. A pH in the range of 7.0 to 7.4 is recommended because of the high reactivity toward proteins at around neutral pH values due to the molecular forms of GA in aqueous solutions and the functional groups, such as amine, thiol and phenol, present in the surface of the proteins [401, 394].

Methods

An LPG of length 40 mm and period 112.6 μm, selected to provide high sensitivity, was fabricated in a single mode boron-germanium co-doped optical fibre with the point-by-point method. The fibre was cleaned using the two-acids-based method and silanized as described in Sec. 4.3.1. The silanized (APTMS-modified) surface of the LPG was allowed to react with 5% (v/v) of GA in PBS for 30 minutes at room temperature under the fume hood. The crosslinking of amino groups with GA carried out in neutral and basic conditions was faster as compared to acidic conditions. The slow reaction kinetics in acidic conditions is mainly used to create hydrogels of various shapes and sizes [402]. The fibre then was thoroughly washed with DI water, a final rinse with PBS and fixed in a customised frame and mounted inside the temperature chamber as described in Sec. 4.4.1. Rabbit polyclonal antibody specific for *Campylobacter jejuni* (50 μg/mL in sodium acetate buffer, pH 5.0) was added to the container and the fibre was incubated for 4 hours.

A schematic of the successive stages occurring on the surface of the LPG during the antibody coating process is shown in Fig. 4.24. The physical thickness of an APTMS monolayer is 0.8±0.1 nm [281], and the thickness of the APTMS + glutaraldehyde layer is 1.5±0.1 nm [396].

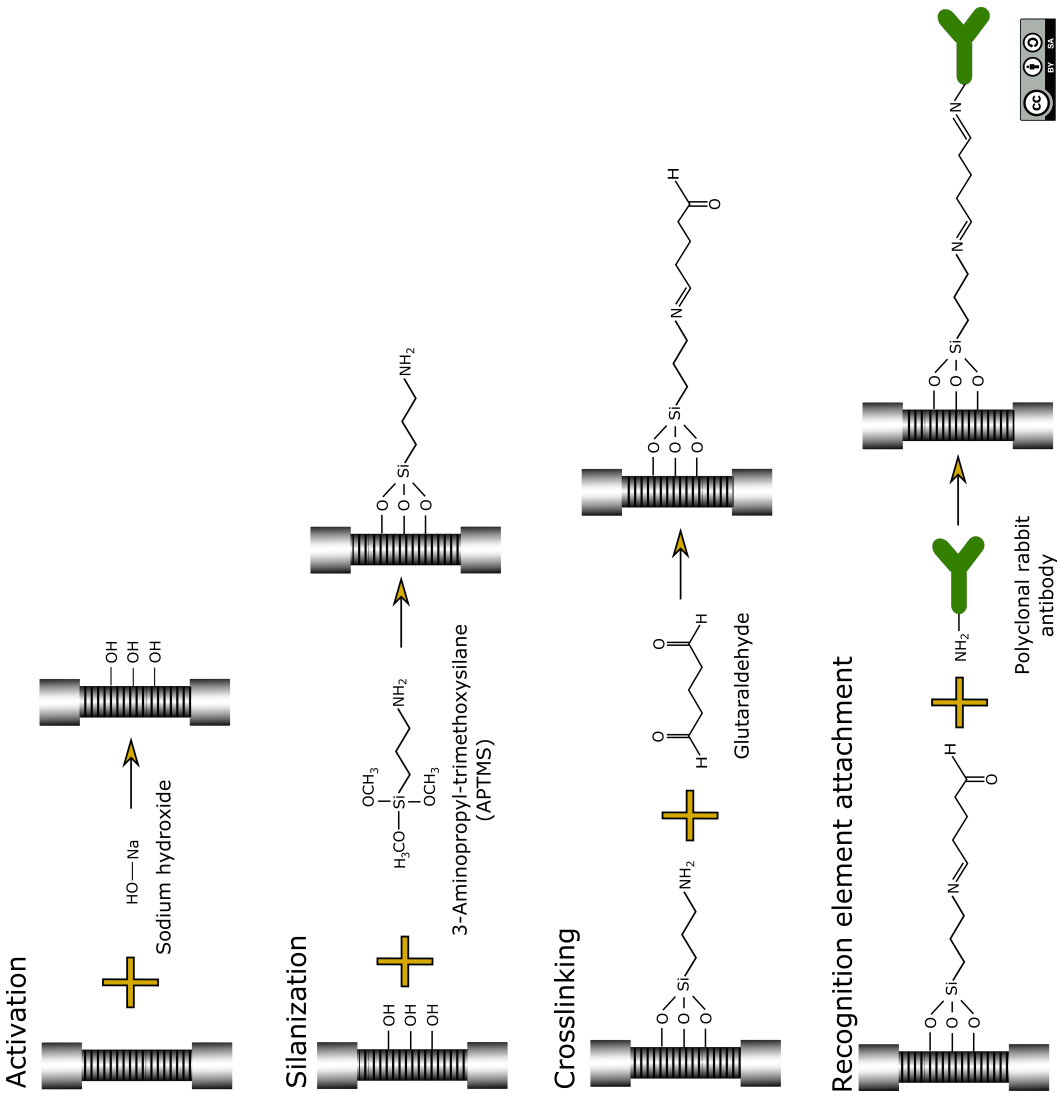

Figure 4.24: Schematic of the successive stages occurring on the surface of the LPG during the antibody coating process.

In an earlier experiment, a different GA solution (grade II, 25%, not specially purified) from Sigma-Aldrich was used as crosslinker. A 5% (v/v) of GA in PBS was prepared to incubate the fibre for 30 minutes, i. e. having the same conditions as with the purified GA. The creation of a reddish yellow layer on the surface of the sensor was observed. This can be explained by the polymerization effect of GA. The polymerization rate of GA depends on temperature, pH and purity [403]. The degree of polymerization of GA stored at temperatures between -14° and 60° has been demonstrated to be higher for solutions stored at the highest temperatures. In the same way, the rate of polymerization has been shown to be higher at higher pH values at the same temperature. At values above pH 8.5, the polymerization takes place quickly, even at temperatures as low as 4° [403]. In addition, non-purified GA has been demonstrated stronger denaturing effects, even at low concentrations, on antigens than is exhibited by purified GA [401].

Optimization of the antibody concentration

The optimal antibody concentration was investigated. An LPG of period 112.6 μm and 4 cm of length was cleaned using the two-acids-based method, mounted inside the temperature chamber at 25° and interrogated as described in Sec. 4.4.1. The transmission spectrum was recorded, with the LPG surrounded by air, as a first baseline. This baseline served as a reference for the cleaning method. The fibre was then unmounted from the fixed frame, silanized as described in Sec. 4.3.1 and mounted again inside the temperature chamber at 25° as described in Sec. 4.4.1. A PBS solution was added to the sample container and the transmission spectrum was recorded as a second baseline. This baseline served as a reference for the antibody coating. Rabbit polyclonal antibody specific to *Campylobacter jejuni* was prepared in sodium acetate buffer (0.1 M, pH 5.0) at concentrations of 0 (control), 10, 30, 50 and 70 μg/mL, respectively. The first antibody solution was added to the sample container for 4 hours. The antibody solution was removed from the sample container and the fibre was washed 3 times with PBS to remove the unattached antibodies. Then, PBS was added to the sample container and the transmission spectrum was recorded for comparison with the second baseline. The sensor was coated with 500 μg/mL of BSA in PBS for 30 minutes to block any site not covered by the antibodies and to avoid the non specific binding of bacteria onto the surface of the sensor. The BSA solution was removed from the sample container and the sensor was washed 3 times with PBS to remove the unbound proteins. A solution of a fixed concentration of *Campylobacter jejuni* in PBS (10^6 CFU/mL) was added to the sample container and the sensor was incubated for 1 hour. The bacterial solution was removed from the sample container and the sensor was washed 3 times with PBS to remove the unbound bacteria. Finally, PBS was added to the sample container and the transmission spectrum was recorded. Then, the fibre was removed from the fixed frame located inside the temperature chamber and cleaned using the two-acids-based method and the process was repeated using an increased antibody concentration. Once the fibre was coated with all the different antibody concentrations, the experiment was repeated two more times. Results presented in Fig. 4.25 show the response of the sensor coated with different antibody concentrations to *Campylobacter jejuni* cells at a concentration of 10^6 CFU/mL. From Fig. 4.25, the rabbit polyclonal antibody

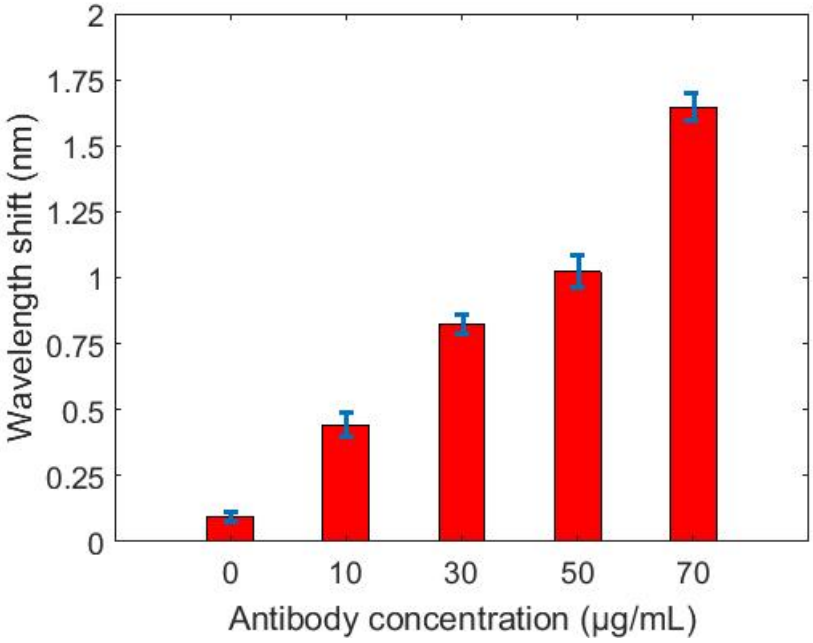

Figure 4.25: Response of the sensor coated with different antibody concentrations to *C. jejuni* (10^6 CFU/mL).

at concentration of 70 μg/mL offered the best performance, generating a shift of the central wavelength of an attenuation band of ≈1.65 nm. The antibody coating at concentration of 50, 30, 10, and 0 μg/mL generated a wavelength shifts in the same attenuation band of 1.02, 0.82, 0.44 and 0.09 nm respectively.

Despite the observation that the antibody concentration of 70 μg/mL promoted the greatest response of the sensor to bacterial cells, the antibody concentration chosen for the majority of the experiments done during the development of this work was 50μg/mL, unless otherwise stated. The main reason for this choice this was the large amount of antibody required for each coating, since the volume of the sample even in the optimized container was large (250 μL) compared with other sensing platforms such as SPR, in which the sample volume can be as low as 10 μL [404]. Another reason is the limited amount of antibody available from this batch. The use of polyclonal antibodies as RE presents a drawback that is the batch-to-batch variations [405]. With the aim to avoid this issue and guarantee the realization of all experiments with antibodies from the same batch, a lower antibody concentration (50 μg/mL) was chosen for the realization of the majority of experiments.

Optimization of the protein concentration against non-specific binding

The blocking step is an important stage in order to obtain a good response from the sensor to the specific target cell. Inadequate blocking may generate a signal caused by non-specific binding, while excessive blocking can mask the antibodies from binding the target cells. Therefore, the optimal concentration of the protein used to block the sites not covered by the antibody was investigated. An LPG of period 112.6 μm and 4 cm of length was cleaned using the two-acids-based method and

silanized as described in Sec. 4.3.1. The optical fibre was fixed in a customized frame inside the temperature chamber and interrogated as described in Sec. 4.4.1. The temperature chamber was set up at 25°C. A PBS solution was added to the sample container soaking the silanized region surrounding the LPG and the transmission spectrum recorded as a baseline. The PBS was removed from the sample container. Rabbit polyclonal antibody specific to *C. jejuni* at a concentration of 50 μg/mL was added to the sample container for 4 hours. The antibody solution was removed from the container and the LPG was washed with PBS to remove the unbound antibody. A second incubation with PBS was carried out and the transmission spectrum was recorded. The PBS was removed from the container. Solutions of bovine serum albumin (BSA) at concentrations from 0 to 700 μg/mL in PBS were freshly prepared in incremental steps of 100 μg/mL. The BSA blocking solution at concentration of 100 μg/mL was added to the sample container for 30 minutes. The BSA solution was then removed and the LPG sensor was washed with PBS to remove the unbound proteins. PBS was added to the sample container and the transmission spectrum was recorded. The PBS was removed from the sample container and *C. jejuni* at a concentration of 10^6 CFU/mL was added to the sample container for 1 hour. The bacterial solution was removed from the container and the sensor was washed with PBS to removed the unbound cells. PBS was added to the sample container and the transmission spectrum was recorded. The optical fibre was then removed from the temperature chamber, cleaned, the process repeated for the next BSA concentration (200 μg/mL) and similarly for the rest of BSA concentrations (300-700 μg/mL). The response of the sensor coated with rabbit polyclonal antibody at a concentration of 50 μg/mL and blocked with different BSA concentrations to *C. jejuni* (10^6 CFU/mL) is shown in Fig. 4.26. The sensor showed the greatest response

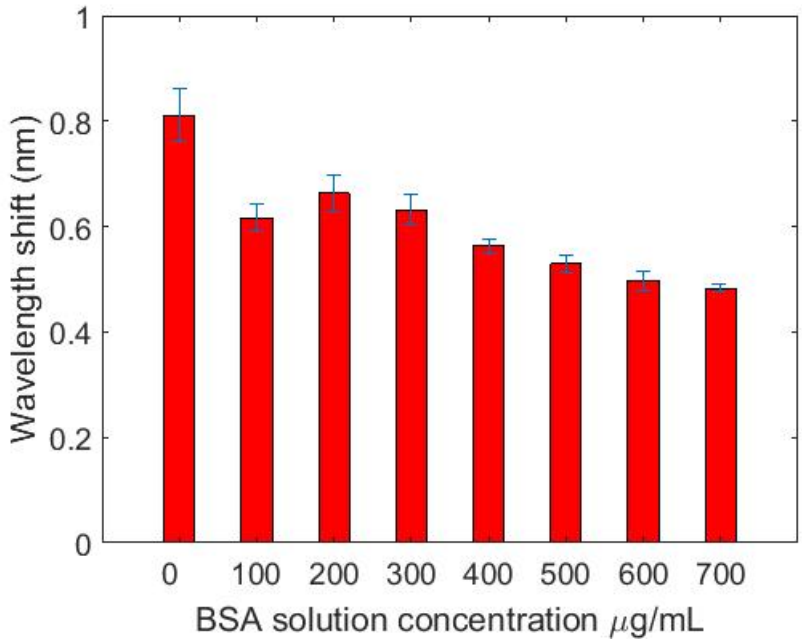

Figure 4.26: Response of the sensor blocked with different BSA concentrations to *C. jejuni* (10^6 CFU/mL).

to *C. jejuni* at a fixed concentration of 10^6 CFU/mL for the blocking concentration of 200 μg/mL of BSA in PBS ($\approx$ 0.66 nm). However, the response of the sensor could have been generated by a combination of specific and non-specific binding, as in the case of the control concentration of BSA (0 μg/mL) ($\approx$ 0.81 nm). For this reason, an additional control was considered in order to investigate the adequacy of the blocking layer. The process was repeated, testing the response of the sensor to a fixed concentration of a different bacteria. The target bacteria for this control experiment was *Escherichia coli*, a gram-negative enterobacterium, usually present in the gastrointestinal tract of humans and animals, contaminated food and drinking water supplies. The sensor was cleaned, silanized, coated with the same type of antibody and coated with different concentrations of blocking protein as described above. The response of the sensor coated with rabbit polyclonal antibody at a concentration of 50 μg/mL and blocked with different BSA concentrations to *E. coli* (10^6 CFU/mL) is shown in Fig. 4.27. From Fig. 4.27, the sensor coated only

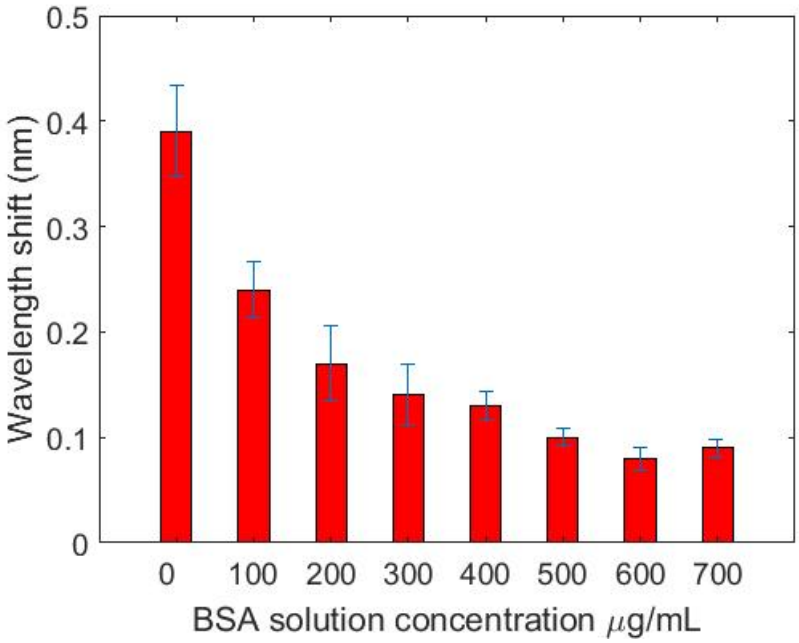

Figure 4.27: Response of the sensor blocked with different BSA concentrations to *E. coli* (10^6 CFU/mL).

with the antibody layer, i. e. with a control concentration of the blocking protein (BSA at a concentration of 0 μg/mL in PBS) showed the highest response to *E. coli*. The measurable shift ($\approx$ 0.39 nm) generated by the non-specific binding of *E. coli* on the surface of the sensor represents 48% of the response generated by the combination of specific and non-specific binding of *C. jejuni*, which is an indicator of the specificity of the antibody employed in this assay. The specificity of the sensor is evaluated in Sec. 5.2.4. For BSA concentrations of 500 μg/mL and higher, it can be noticed that the wavelength shift falls within the resolution of the spectrometer (0.12 nm). Hence, it was considered that the surface of the sensor was saturated with the blocking protein. Therefore, the optimal concentration of the blocking protein was 500 μg/mL. In Fig. 4.26, the higher response of the sensor for BSA concentrations

less than 500 μg/mL suggests that part of the response was generated by non-specific adsorption of the bacterial cells (*C. jejuni*) on the surface of the sensor. The decrease in sensor response for concentrations greater than 500 μg/mL, suggests a saturation of the blocking protein and a possible masking of the antibodies. In the subsequent experimental descriptions, unless otherwise stated, this is the concentration used for the coating against non-specific binding.

4.5 Summary

The different stages of the fabrication of the immunosensor were covered in this chapter. In Sec. 4.1, different cleaning methods, as a crucial first step in the development of a biosensor, were discussed. A number of cleaning methods were evaluated, including solvent-based, piranha solution-based and two acids-based methods. The two acids-based method resulted in a smoother surface, without a visible damage of the optical fibre. In Sec. 4.1.4, the design and fabrication of a 3D-printed device for LPGs cleaning was presented. The 3D-printed device allowed the simultaneous cleaning of a number of fibres. In addition, it helped in the reduction of chemical waste production. In Sec. 4.2 the design and optimization of the sample container used to accommodate the LPG sensor for the stationary incubation steps were presented. The final design had a capacity of 250 μL.

Methodologies for reliable and repeatable functionalization and coating of the optical fibre sensing platform were developed. In Sec. 4.3, the process used for the silanization of the surface of the cladding of the optical fibre and the proteins used for the coating were discussed. In Sec. 4.4, the experimental setup for the deposition of the antibody coating and the blocking coating for the non-specific binding of the target bacteria were described. Changes in the location of the central wavelengths of the attenuation bands in the transmission spectrum of an LPG due to the action of connecting and disconnecting both ends of the fibre to and from the light source and the spectrometer, respectively, were investigated. The results showed an invariance in the location of the attenuation bands' central wavelengths due to the action of connecting and disconnecting under constant conditions of temperature, strain and refractive index. Finally, the optimization of the concentration of the polyclonal antibody and the blocking protein was performed.

Chapter 5

Bacterial Assay and Cell Staining

5.1 *Campylobacter jejuni* cells

The *Campylobacter jejuni* cells used in this work were provided by Masdor and Tothill (School of Aerospace, Transport and Manufacturing, Cranfield University). The detailed description of the preparation of the bacterial cells can be found in Masdor's PhD thesis [372]. Briefly, a commercially available specialized media recommended for the selective isolation of *C. jejuni* (Campy Cefex Agar, from Acumedia®, Neogen® Corporation) was prepared, according to the the manufacturer's instructions [406], for the further cultivation of *C. jejuni*. The Campy Cefex Agar was prepared by mixing 44.4 g of agar in one litre of DI water, heated with agitation and boiled for 1 min to dissolve the agar. The agar solution was autoclaved at 121°C for 20 min and cooled down to 50°C. One vial (5 mL) of *Campylobacter* supplement (16 mg of cefoperazone, from Acumedia®, Neogen® Corporation) and 500 μL of sterile laked horse blood (from Fisher Scientific) were added to the agar solution. The solution was well mixed and poured into petri dishes. The *Campylobacter* supplement acted as a selective agent to inhibit enteric flora and the horse blood provided the nutrients for *Campylobacter* spp. [407]. Ready-to-use, disposable inoculating loops containing stabilized, preserved and viable *C. jejuni* quality control microorganisms (Culti-Loops® of *C. jejuni* subsp. *jejuni* ATCC® 33291™from Remel, part of Thermo Fisher Scientific) were cultivated according to the manufacturer's instructions. The Culti-loops®were striped directly on the petri dishes containing the agar. The petri dishes were incubated at 42°C for 48 h inside a 2.5 L atmosphere generation system (Oxoid™AnaeroJar™, from Thermo Fisher Scientific), shown in Fig. 5.1, containing a gas generation sachet to produce a suitable gaseous atmosphere (85% N_2, 10% CO_2 and 5% O_2) for the growth of *C. jejuni* (CampyGen™2.5L sachet, from Fisher Scientific). After the 48 h incubation, a plate was cultured in 10 mL of Bolton broth (from Fisher Scientific), a medium for the selective pre-enrichment of *Campylobacter* organisms, and incubated at 42°C for 48 h. The Bolton broth contains nutrients to aid resuscitation of sublethally injured cells and it is formulated to avoid the need for a microaerobic atmosphere. Bolton broth was prepared by mixing 13.8 g in 500 mL of DI water, heated with agitation and boiled. The broth was sterilized by autoclaving at 121°C for 20 min. The broth then was cooled to 50°C and 25 mL of laked horse blood and 1 vial of Bolton broth selective supplement (from

Figure 5.1: Oxoid^{TM}AnaeroJar^{TM}2.5 L atmosphere generation system. Image from [408].

Fisher Scientific) were added to the broth. The Bolton broth selective supplement contains 10 mg of cefoperazone, 10 mg of vancomycin, 10 mg of trimethoprim and 25 mg of cycloheximide per vial and each vial is sufficient for 500 mL of medium. These antibiotics optimize the selectivity for *Campylobacter* spp. acting against Gram-positive bacteria (vancomycin), Gram-negative bacteria (cefoperzaone), a wide variety of Gram-positive and Gram-negative bacteria (trimethoprim) and yeasts (cycloheximide) [409]. After the 48 h of incubation, 10 mL of the bacterial inoculum were transferred to a Duran bottle containing 90 mL of Bolton broth for an additional 48 h incubation under microaerophilic conditions. Bacterial cells were obtained by centrifugation at 10,000 g for 15 minutes at 4°C on a benchtop centrifuge (Sorvall^{TM}Legend^{TM}X1, Thermo Fisher Scientific). The pelleted bacterial cells were washed with PBS and suspended in PBS. In order to obtain a bacterial concentration of 1 x 10^8CFU/mL, the bacterial suspensions were adjusted to optical densities of 1.6 at 600 nm, on a UV/Vis spectrophotometer (Perkin-Elmer Lambda 20 GenTech Scientific, Inc.) [372]. The bacterial concentrations were confirmed by a traditional method (spread plate method). Finally, the bacterial cells were heat-killed (inactivated) at 70°C for 30 minutes. The pathogen components of bacteria were destroyed, but cells maintain some of their integrity to be recognized by the immune system and provoke a response.

5.2 Direct assay for bacterial detection

The LPG-based sensors coated with rabbit polyclonal antibody specific to *C. jejuni* and blocked against non-specific binding, using the methods described in Chapter 4, were tested in a direct assay with *C. jejuni* cells at different concentrations. The

binding between the antibody and the antigen depends completely on non-covalent interactions including coulombic interactions, hydrogens bonds, van der Waals forces and hydrophobic interactions [218]. Bacterial solutions at a concentration of 10^8 CFU/mL were diluted to concentrations ranging from 10^7 to 10^1 CFU/mL. Briefly, in order to obtain a concentration of 10^7 CFU/mL, 100 mL of the original bacterial solution was extracted, poured into 900 mL of PBS and mixed in a vortex. To obtain a bacterial concentration of 10^6 CFU/mL, 100 mL was extracted from the bacterial solution at 10^7 CFU/mL and poured into 900 mL of PBS and mixed in a vortex, and so on.

5.2.1 Evaluation of the immunosensor fabricated by the enhanced physical adsorption coating method

In this section, the evaluation of the immunosensor coated using the physical adsorption of antibodies and proteins method, enhanced by a silanization strategy, described in Sec. 4.4.2, is presented.

Briefly, the immunosensor was set up and interrogated, as described in Sec. 4.4.1. Then, it was incubated in PBS in order to record a baseline spectrum prior the bacterial assay. The PBS was removed from the sample container and the first bacterial solution was added to the sample container for 1 hour, which is a standard incubation time for antibody-antigen reactions at stationary conditions [47]. The bacterial solution was then removed from the container and the sensor was rinsed three times with PBS to remove the unattached cells. Then, PBS was then added to the sample container and the transmission spectrum was recorded for comparison with the first baseline spectrum. The fibre was removed from the fixed frame located inside the temperature chamber and cleaned using the two-acids-based method and the process was repeated using an increased bacterial concentration. Once the sensor was tested with all the different bacterial concentrations, the experiment was repeated two more times. To avoid repetition in the description of the subsequent experiments, unless other stated, the bacterial assays were performed as described. Results presented in Fig. 5.2 show the response of the immunosensor to *C. jejuni* cells at different concentrations. Fig. 5.2a shows the response of the sensor to *C. jejuni* bacteria at concentrations from 10^1 to 10^7 CFU/mL and the corresponding standard curve. As can be observed, the sensor exhibited a low response to the low bacterial concentrations and a high response for the higher concentrations. However, the variation in the mean values at high bacterial concentrations (error bars) were larger as at low concentrations. This can be explained by the fact that the LPG was coated with antibodies using an adsorption method. Although the surface of the LPG was functionalized by a silanization strategy, which in theory offers a stronger attachment due to the creation of functional groups as a simple adsorption, the antibodies could still exhibit a random immobilization and desorption, as mentioned in Sec. 2.5.2. This affected the reproducibility of the assay and generated large variations in the sensor's response at a fixed bacterial concentration. At high concentrations, competition to occupy the available binding sites was promoted. However, at low concentrations, the response of the sensor could be affected by desorption. The noise floor of the system could be suggested as another limiting factor for the response of

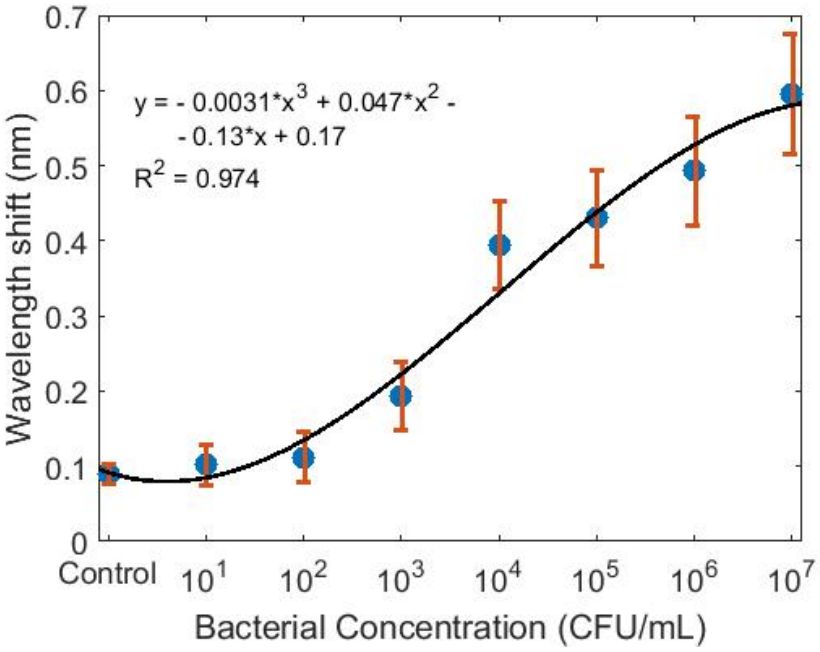

(a)

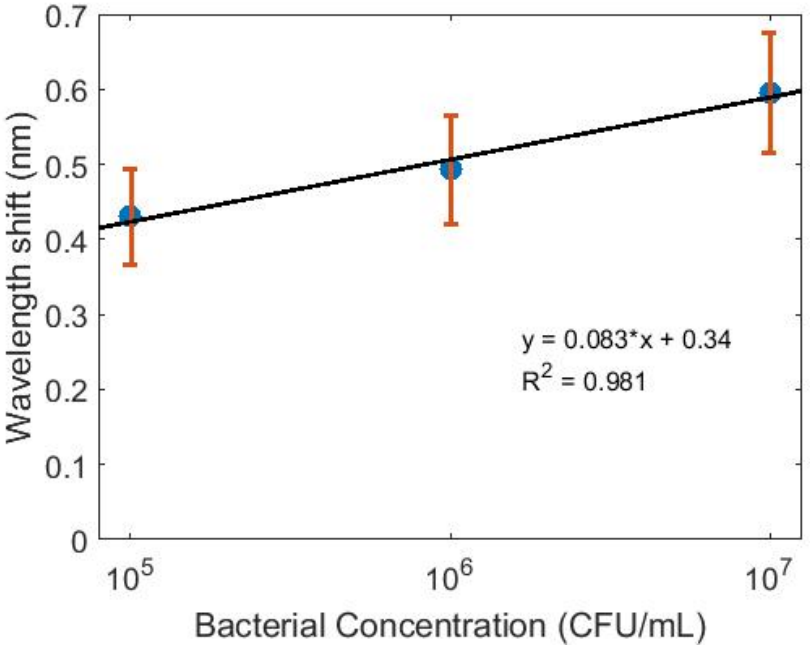

(b)

Figure 5.2: In (a), response of the sensor to *C. jejuni* bacteria at concentrations from 10^1 to 10^7 CFU/mL and the corresponding standard curve. In (b), the dynamic range of the sensor. The error bars represent the standard deviation of triplicates.

the sensor at low concentrations. However, the transmission spectra generated by the sensor were filtered using a Fourier filter, which eliminates noise from the signal as described in Chapter 3. A more detailed noise analysis of the sensing system used in this thesis is suggested as future work. The dynamic range of the immunosensor, i. e. the concentration range where the sensor exhibited a linear relationship between the bacterial concentration and the measured response (also know as analytical signal), was 10^5-10^7 CFU/mL, as shown in Fig. 5.2b.

5.2.2 Evaluation of the immunosensor fabricated by the covalent attachment coating method

In this section, the evaluation of the immunosensor coated using the covalent attachment of antibodies method, as described in Sec. 4.4.3, is presented.

Briefly, the immunosensor was set up and interrogated as described in Sec. 4.4.1. The sensor was incubated in PBS to record a baseline spectrum prior the bacterial assay. The PBS was removed from the sample container and the direct assay for bacterial detection in the range from 10^1 to 10^7 CFU/mL was performed. The response of the immunosensor to *C. jejuni* is shown in results presented in Fig. 5.3. In Fig. 5.3a, the calibration curve, also known as standard curve, for the detection of *C. jejuni* at concentrations from 10^1 to 10^7 CFU/mL in a direct assay is shown. As can be observed, the highest value of the sensor's response was obtained for a bacterial concentration of 10^7 CFU/mL and the lowest for a concentration of 10^1 CFU/mL. However, the mean of the sensor's response for a bacterial concentration of 10^1 and 10^2 CFU/mL is lower than the spectrometer's resolution. Hence, the limit of quantification, i. e. the lowest bacterial concentration considered as detected by the sensor was 10^3 CFU/mL. The dynamic range of the immunosensor was estimated to be from 10^3 to 10^6 CFU/mL, as shown in Fig. 5.3b. Compared with the immunosensor coated with antibodies by the enhanced physical adsorption method described in 5.2.1, this immunosensor exhibited a longer dynamic range by an order of magnitude. However, the limits of linearity are different. This can be explained by the fact that in this case, the antibodies are strongly attached to the cladding of the fibre. This avoids desorption during the multiple rinsing of the fibre and the incubation steps. In addition, if not fully uniform, the crosslinker (GA) promotes a more controlled orientation of the antibodies as the physical adsorption. This contributes to the high antibody-antigen interaction and the reproducibility of the assay, shown by the high response of the sensor and the small variation in the analytical signal for the different bacterial concentrations (error bars), respectively. The high antibody-antigen interaction allows a saturation of the available binding sites at lower bacterial concentrations, seen as a flattening of the standard curve at concentrations greater than 10^6 CFU/mL.

As mentioned in Chapter 1, a mean concentration of 9 x 10^4 CFU/mL has been determined to be the dose of *C. jejuni* required for a human to develop campylobacteriosis [16]. However, a human experimental study revealed that doses as low as 800 CFU can cause the illness in young healthy adults [17]. Taking into consideration the high contamination level of *Campylobacter jejuni* in poultry products (approximately 10^3 CFU/g [18, 19], 10^3-10^4 CFU/plate [20], 5x10^8 CFU/mL

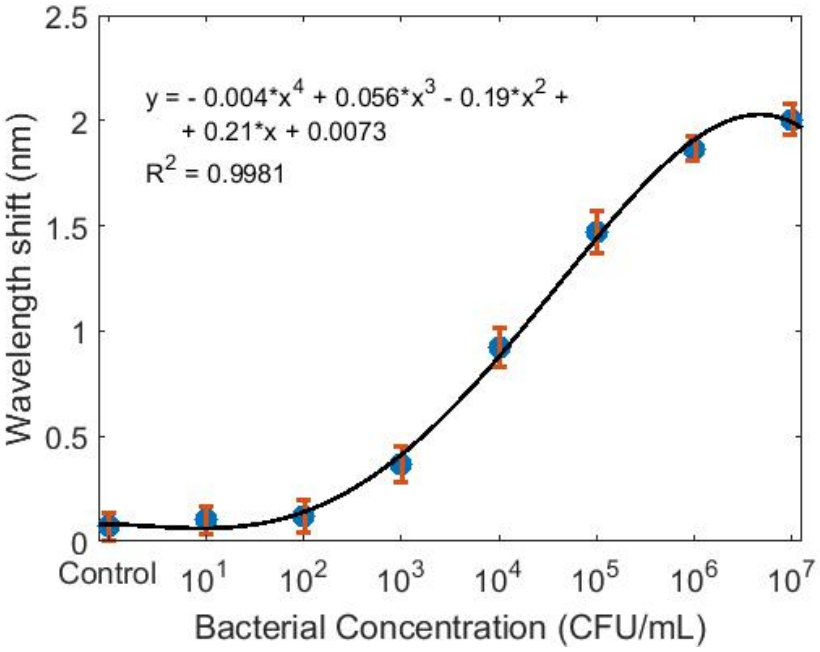

(a)

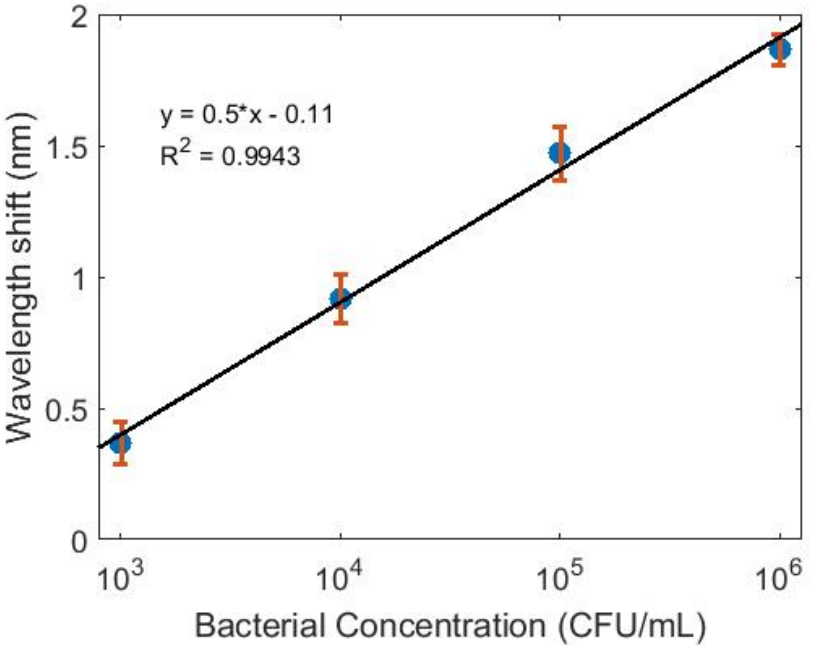

(b)

Figure 5.3: In (a), response of the sensor to *C. jejuni* bacteria at concentrations from 10^1 to 10^7 CFU/mL and the corresponding standard curve. In (b), dynamic range of the sensor. The error bars represent the standard deviation of triplicates.

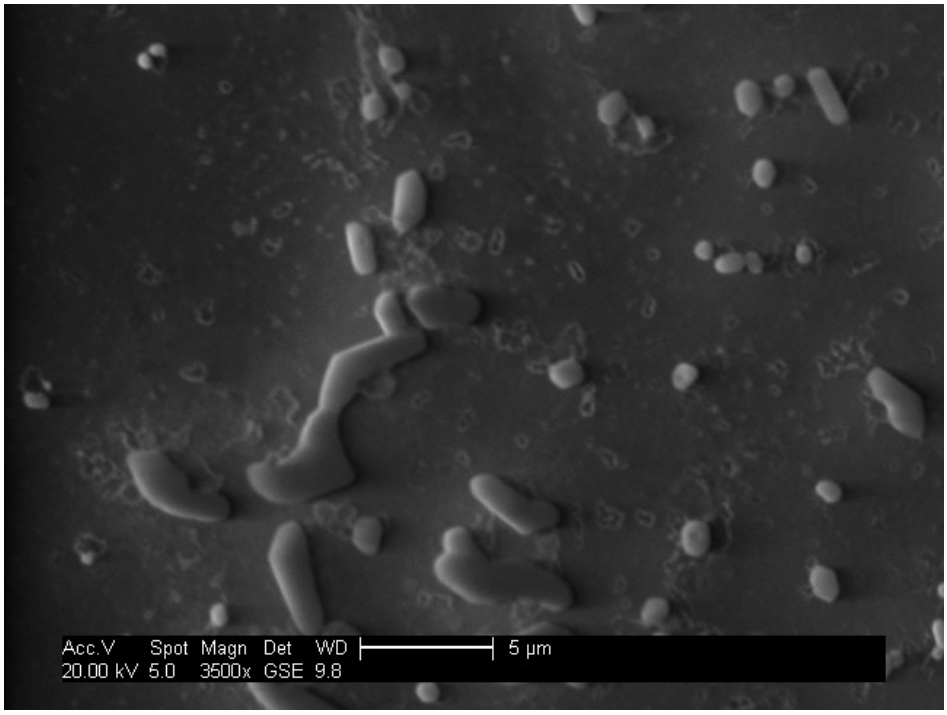

Figure 5.4: *Campylobacter jejuni* cells at concentration of 10^6 CFU/mL attached on the surface of a LPG-based immunosensor.

[21]), unpasteurized milk (6.4x10^7 CFU/mL [21]) and water (10^3-3.2x10^8 CFU/mL [22]), contaminated food can provide the necessary doses to develop the disease in humans.

The bacterial attachment on the surface of the immunosensor was confirmed with an image obtained from an environmental scanning electron microscope (ESEM) (XL30, resolution: 3.5nm@30kV, PHILIPS) for a concentration of 10^6 CFU/mL. In Fig. 5.4 bacteria attached on the surface of the fibre can be observed. The different sizes indicate different bacterial growth and illustrate a morphological change from spiral to spherical shape.

5.2.3 Evaluation of the stability of the immunosensor

The stability of the immunosensor was assessed by evaluating its response to *C. jejuni* (10^6 CFU/mL) after 24, 48 and 72 hours of storage at 4°C, 25°C and 35°C. A freshly prepared immunosensor was considered as zero hours of storage. Briefly, the immunosensor was incubated in PBS at 35°C and the transmission spectrum was saved as a baseline. The response of the freshly prepared immunosensor was considered to exhibit a performance of 100%. All bacterial assays were performed at 35°C for comparison. The results are presented in Fig. 5.5. As can be observed, the storage temperature and the storage time influence of the performance of the sensor. The immunosensor stored at 4°C exhibited a similar performance in the days following its preparation as the freshly prepared sensor. On the other hand, the response of the immunosensor stored at 35°C was degraded by the temperature, losing its binding ability by nearly 74% in the first 24 hours and 98% in 48 hours.

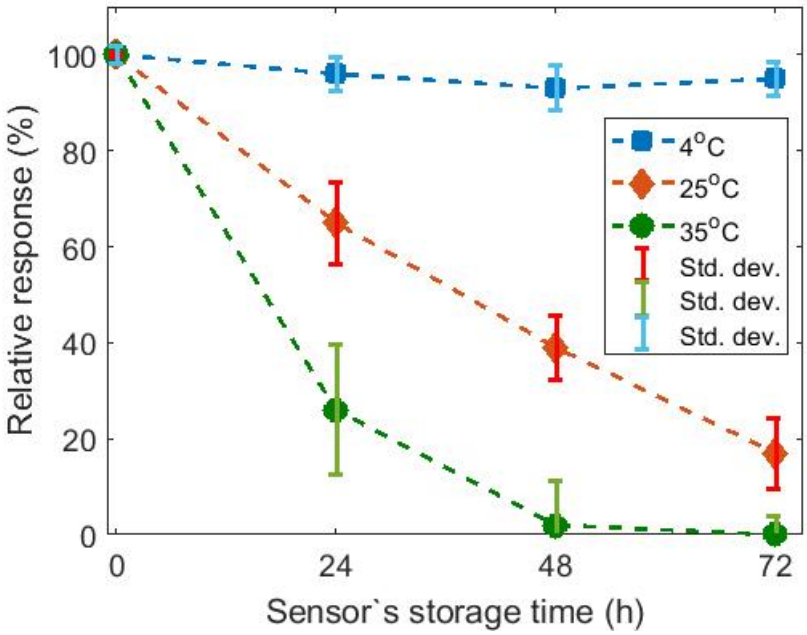

Figure 5.5: Response of the sensor to the target bacteria (10^6 CFU/mL) after 0 (freshly prepared), 24, 48, and 72 hours of storage at 4°C, 25°C and 35°C. Error bars are the standard deviation of triplicates.

The storage temperature of 25°C denatures the antibody coating more gradually than storing at 35°C. For example, the immunosensor stored at 25°C lost 35% of its binding capacity in the first 24 hours after its preparation, 61% in 48 hours and 83% in 72 hours.

The evaluation of the effect of the temperature on the stability of antibodies has been widely studied [410, 411, 412, 413, 414]. For example, mouse monoclonal antibodies have exhibited total degradation above 70°C in two hours [414]. Human monoclonal antibody have exhibited more degradation at 37°C (6.5%) than at 8°C (0.9%) when stored at pH 4 for 14 days [413]. Antibody fragments have retained their biochemical activity for at least a year when stored at 4°C in PBS buffer (40 mM, pH 7.2) [415]. Rabbit polyclonal antibodies and papain (an enzyme present in papaya) soluble complexes have been shown to lose 75% of their biochemical activity after 2 hours at 75°C. However, when stored at 4°C, the antibody-enzyme complex retained 82% of its activity after 15 days of storage [416] in a phosphate buffer (pH 8.6). The thermal stability of monoclonal antibody specific for β-galactosidase (enzyme typically assayed from *E.coli*) was monitored using an ELISA direct assay for different incubation days and different temperatures [410]. The antibody fixed in 96-well plates retained its activity for more than 6 months when stored at 25°C in humidify boxes and lost all its detectable binding activity after 30 weeks at 37°C and in 3 days at 76°C.

From the studies of the literature, monoclonal antibodies have exhibited a higher non-reversible thermal stability than polyclonal antibodies. In addition, the thermal stability depends on other parameters of the storage, such as humidity and pH. The high stability exhibited by the LPG immunosensor stored at 4° developed in this

thesis could be related not only with the temperature but also with the humidity present in the fridge where it was stored. In order to increase the shelf life of the immunosensor developed in this thesis, storage in different conditions of pH and temperature could be further investigated.

5.2.4 Evaluation of the specificity of the sensor

The specificity of the sensor was evaluated by testing its performance against other common foodborne bacteria. Bacterial solutions of *Listeria monocytogenes*, *Salmonella typhimurium* and *Escherichia coli* were obtained by Masdor and Tothill (School of Aerospace, Transport and Manufacturing, Cranfield University) from the culture collection of the MARDI, Malaysia.

Listeria monocytogenes are rod-shaped Gram-positive bacteria that have an approximate size of 0.4 to 0.5 by 0.5 to 2 μm^2. *L. monocytogenes* is the cause of listeriosis, a foodborne illness with a moderate number of infections (23,150 cases worlwide in 2010 [417]) but a high mortality rate (20-30%) despite adequate treatment [418]. The main food vehicles implicated in listeriosis are crustaceans, shellfish, cheese, meat, meat products, mixed salad, caramel apples and ice cream [419]. Concentrations of *L. monocytogenes* as low as 10^2CFU/mL have been reported to cause outbreaks of listeriosis [420].

Salmonella typhimurium are cylindrical rod-shaped Gram-negative bacteria that have an approximate size of 0.7 to 1.5 by 2 to 5 μm^2. *Salmonella* is a common cause of gastroenteritis worldwide, causing 93.8 million of reported infections and 155,000 deaths per year [421]. The major route of transmission is contaminated water and food, such as fresh vegetables and fruit, poultry, dairy products and eggs [421]. A mean concentration of $>10^4$CFU has been calculated to be the dose of *Salmonella* to be ingested by an adult human to cause infection [422].

Escherichia coli are rod-shaped Gram-negative bacteria that have an approximate size of 1.1 to 1.5 by 2 to 6 μm^2 [423]. Strains of *E. coli*, such as *E. coli* O157, that produce Shiga toxin can cause severe illness, characterized by diarrhea, vomiting and stomach cramps, and death [424]. The main routes of transmission are contaminated water and food, person to person and contact with animals [424]. Doses as low as 140 CFU of *E. coli* O157:H7 and 10^6 CFU of other pathogenic strains have been reported to cause infection in humans [425].

An LPG of period 112.6 μm and length 40 mm was cleaned, silanized, coated with rabbit polyclonal antibody specific to *C. jejuni* by covalent attachment and blocked against non specific binding, as described in Sec. 4.1.2, Sec. 4.3.1, Sec. 4.4.3 and Sec. 4.4.3 respectively. The experimental setup was prepared as described in Sec. 4.4.1. Bacterial solutions of *E. coli*, *Salmonella*, *Listeria* and *C. jejuni* at a concentration of 10^6 CFU/mL were prepared in PBS. The sensor was incubated in PBS for 30 minutes to allow the temperature chamber to stabilize. The transmission spectrum was recorded as a baseline and the PBS was removed from the container. The first bacterial solution was added to the sample container and the sensor was incubated for 1 hour. Then, the bacterial solution was removed from the container. The sensor was washed three times with PBS to remove the unattached bacteria. Finally, PBS was added to the container for 30 minutes and the transmission spectrum was recorded

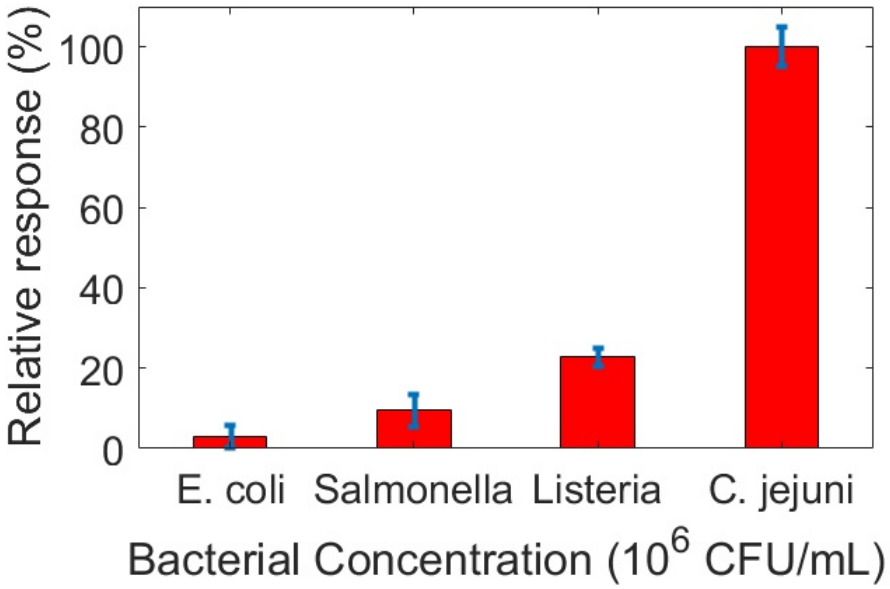

Figure 5.6: Response of the sensor to different species of bacteria: *Escherichia coli*, *Salmonella typhimurium*, *Listeria monocytogenes*, and *Campylobacter jejuni*.

as a second baseline. Then, the fibre was removed from the fixed frame located inside the temperature chamber and the process was repeated for the following bacterial solution. The response of the sensor to different bacteria is shown in Fig. 5.6. The sensor exhibited a relative response of 100% for *C. jejuni*, 22.77% for *Listeria*, 9.47% for *Salmonella* and 3.01% for *E. coli*. A comparative of the average dimensions of the bacteria used to evaluate the specificity of the sensor is presented in Table 5.1.

Table 5.1: Comparative of the average size of the bacteria used to evaluate the specificity of the sensor.

Bacteria	Gram type	Dimensions (μm)
Listeria monocytogenes	Positive	0.4-0.5 by 0.5-2
Salmonella typhimurium	Negative	0.7-1.5 by 2-5
Escherichia coli	Negative	1.1-1.5 by 2-6
Campylobacter jejuni	Negative	0.2-0.8 by 0.5-5

The results indicated that selectivity may be related with the size of the bacteria. The relatively high response of the sensor for *Listeria monocytogenes* (22.77%) could be associated to the small size of the bacteria which probably is filling the gaps uncovered by the blocking protein, generating a non-specific response. This could suggest that the blocking coating against non-specific binding can be improved, especially for the further testing of the sensor with real samples. On the other hand, the origin of the response exhibited by the sensor against *Listeria* may be due to polyclonal nature of the antibodies employed, which are able to recognize different

epitopes. In studies from the literature that evaluated cross-reactivity of sensors involving antibodies and similar bacteria to those used in this work, the relationship between the bacterial size and cross-reactivity level was not mentioned [380, 289, 118]. In those studies, the optimization of the blocking protein concentration was not mentioned either. However, the cross-reactivity levels (in percentage) reported in the literature were in the same range of values as that presented in this thesis. For example, Kaushik *et al.* reported a fibre optic biosensor for the detection of *Salmonella typhimurium*, based on multimode interference, functionalized with monoclonal antibodies and blocked against non-specific binding with BSA [380]. They reported the sensor's response against non-target bacteria of ≈29% for *E. coli* and ≈17% for *Staphylococcus aureus*. Masdor *et al.* reported a cross-reactivity level of 10% for *Salmonella typhimurium*, 6.6% for *Listeria monocytogenes* and 5.3% for *Escherichia coli* in a SPR-based sensor for the detection of *C. jejuni* [118].

The optimization of the selectivity of the sensor and a further investigation of the validity of the relation between the size of bacteria and the selectivity exhibited by the immunosensor is proposed in Sec. 6.2.2.

5.3 Bacterial staining

Gram staining is the most important procedure in microbiology for bacterial identification since it classifies the eubacteria, single-celled prokaryotic microorganisms also called just bacteria, into two fundamental groups according to their stainability as Gram positive and Gram negative. As mentioned in Sec. 2.6, Gram positive bacteria retain the primary dye (crystal violet) during solvent treatment, whereas Gram negative bacteria do not retain the primary dye and are decolourized by the solvent, having to be counterstained in order to give the decolorized bacteria a colour. Despite its long history, of more than a century, the exact mechanism of the Gram reaction was not clearly understood [426, 427]. For many years, there were mainly two separate conceptions of the mechanism of Gram stain: that based on the idea that a specific cellular substance was responsible of the retention of the dye, and the one based on the permeability difference between cell types [426]. In recent years, a basic understanding of its mechanism has emerged [428]. It has been recognized that the retention of the stain relies on the cell wall characteristics and that it is independent of the cell surface isoelectric point (negatively charged for all bacteria) [428], as discussed in Section 2.6.3.

The stain generates a change in the refractive index of the cells [436] without altering the shape and form of bacteria [311]. The refractive index of bacteria and cells has been widely measured. The refractive index of bacteria has been estimated to be 1.38, considering a refractive index of 1.37 and 1.39 for cytoplasm and nucleus, respectively, based on data of the refractive index of the different components of mammalian cells [429]. The same values were reported elsewhere for spherical mammalian cells [430]. The average refractive indices for the cell wall and cytoplasm when cells are suspended in water were calculated to be 1.37 and 1.42 respectively [431]. The refractive index of $1x10^8$ cells/mL of *Serratia marcescens* and *E. coli* suspended in water was calculated from interference microscope measurements as 1.382 and 1.383, respectively [432]. In addition, the refractive index of bacterial layers

depends on the bacterial concentration. For example, for *E. coli* at concentrations of 10^3, 10^4, 10^5, 10^6, and 10^7, the refractive indices were calculated to be 1.3515, 1.3530, 1.3540, 1.3545 and 1.3548, respectively [434]. In this section, the enhancement of the sensitivity of the sensor using Gram's staining is explored.

5.3.1 Methodology

An LPG of period 112.6 μm and 4 cm of length was cleaned using the two-acids-based method and silanized. It was mounted inside the temperature chamber and fixed in a customized metal frame. The temperature chamber was set at 35° and the sensor was interrogated as described in Sec. 4.4.1. The fibre was incubated in PBS and the transmission spectrum was recorded as a baseline prior to coating. The LPG was coated with 50 μg/mL of rabbit polyclonal antibody specific to *C. jejuni* for 3 hours. An additional advantage of using polyclonal antibodies is that, in general, when cell staining is performed with this type of antibody, the signal is stronger [218]. The antibody solution was removed from the sample container and the surface of the LPG was washed 3 times with PBS to remove the unbound antibody. The fibre was incubated in PBS to record a baseline prior the blocking step. Then, the surface of the LPG was blocked against non-specific binding with 500 μg/mL of BSA in PBS for 30 minutes. The blocking solution was removed from the sample container and the LPG was washed 3 times to removed the unbound proteins. The LPG was incubated in PBS to record a baseline prior the bacterial assay. Bacterial dilutions of *C. jejuni* in the range from 10^1 to 10^6 CFU/mL were prepared as described in Sec. 5.2. A volume of 250 μL of the first concentration of the bacterial dilution was poured in the sample container for 1 hour. After that time, the bacterial solution was removed from the container and the surface of the fibre was washed 3 times with PBS to remove the unbound cells. The sensor was incubated in PBS to record a baseline prior the cell staining. The Gram staining kit, containing crystal violet solution, iodine solution, decolorizer solution and safranin solution, was purchased from Sigma-Aldrich. The Gram's staining protocol presented in Sec. 2.6.3 was adapted for the needs of this project. The bacterial cells, attached on the surface of the fibre were stained as follows. The surface of the sensor was flooded with Gram's crystal violet solution and left to stand for 1 minute. The stain was removed from the sample container and the surface of the sensor was gently washed with DI water. The sensor was flooded with iodine solution and allowed to remain for 1 minute. The iodine solution was removed from the sample container and the sensor was washed with DI water. The surface of the sensor was decolorized with Gram's decolorizer solution until no blue dye flowed from the container. Then, the sensor was washed with DI water. The bacterial cells were counterstained with safranin solution for 1 minute. Finally, red safranin solution was washed off with DI water and the sensor was let it dry. A schematic of the Gram staining procedure is shown in Fig. 5.7. The decolorizing step is important, as further delay will cause excess decolorization in the Gram-positive bacteria, and the purpose of staining will be defeated. After the staining, the fibre was incubated in PBS and the transmission spectrum was recorded as a baseline. The fibre was removed from the fixed frame located inside the temperature chamber, cleaned using the two acids-based method and the process

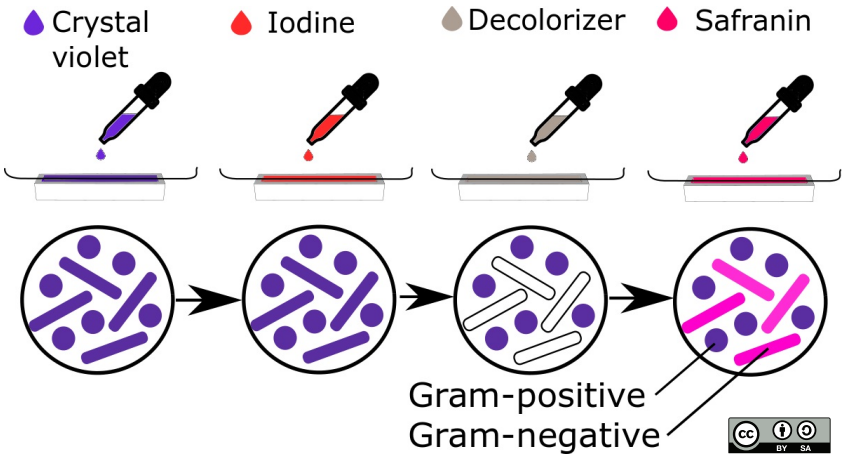

Figure 5.7: Schematic of the Gram stain procedure.

was repeated using an increased bacterial concentration. The response of the sensor to *C. jejuni* at concentrations from 10^1 to 10^7 CFU/mL is shown in the results presented in Fig. 5.8a. In Fig. 5.8a, the calibration curve, for the detection of stained *C. jejuni* at concentrations from 10^1 to 10^7 CFU/mL in a direct assay is shown. The highest value of the response was obtained for a bacterial concentration of 10^7 CFU/mL and the lowest for a concentration of 10^1 CFU/mL. However, the mean of the sensor's response for a bacterial concentration of 10^1 CFU/mL is lower than the spectrometer's resolution. Hence, the limit of detection was estimated to be 10^2 CFU/mL. The dynamic range of the immunosensor, determined from 10^2 to 10^6 CFU/mL, was enhanced by the bacterial staining by an order of magnitude compared with the dynamic range of the immunosensor tested with unstained bacteria. The limit of detection was estimated to be 10^2 CFU/mL The bacterial attachment was validated with images, shown in Fig. 5.9, obtained from an ESEM (XL30, PHILIPS) and an optical microscope (BX51, Olympus). Fig. 5.9a shows an image from the ESEM of the stained bacteria attached on the surface of the sensor. Fig. 5.9b shows an image from the ESEM of a single stained *C. jejuni* cell, attached on the surface of the sensor. Fig. 5.9c shows an optical image obtained at magnification 60×. Gram-negative cells, such as *C. jejuni*, display a pinkish red tone after being stained using the Gram's staining method. Fig. 5.9 shows that the surface coverage of the bacteria on the antibody coated LPG is not complete, with the bacteria arranged randomly and with evidence of some clumps of bacteria. Similar images have been shown for the attachment of bacteria to optical fibres, for example in [399] and [437]. This shows that the response of the LPG transmission spectrum to the attachment of bacteria is a measure of the surface coverage, which increases with increasing concentration of bacteria and, as the dimensions of the bacteria are much smaller than the period of the LPG and are randomly distributed, the effect appears as an average change in the coating's optical thickness [438], which influences the cladding mode effective index.

A t-test was performed to evaluate if the Gram's staining was significantly effective in the enhancement of the sensitivity of the immunosensor. A paired sample t-test was chosen since the response of the same type of immunosensor (antibody coating covalently attached on the surface of the LPG) was compared under different

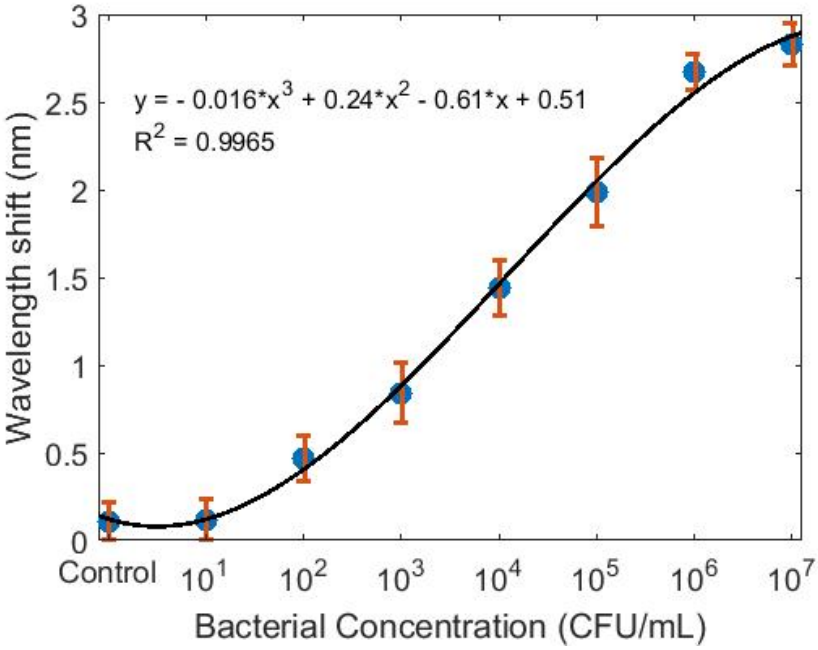

(a)

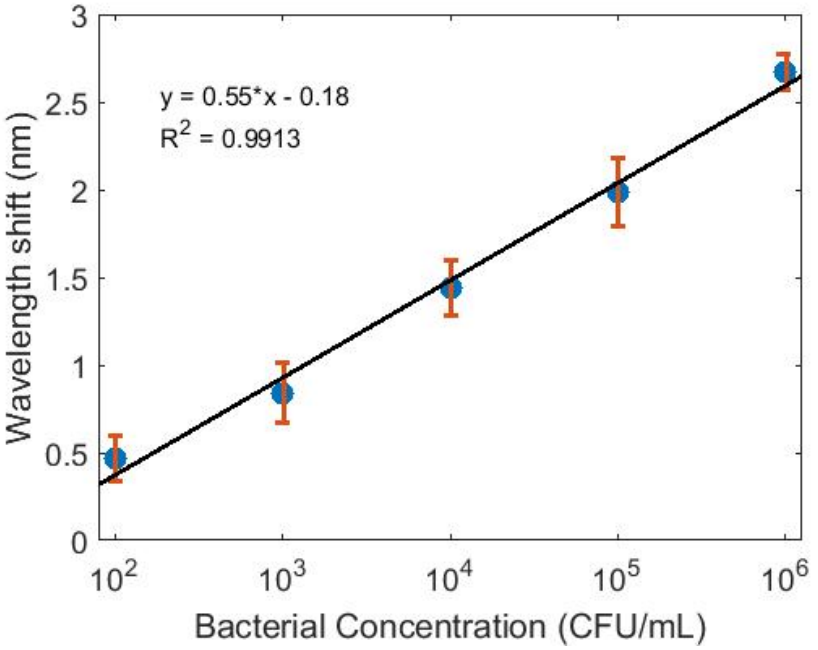

(b)

Figure 5.8: In (a), response of the sensor to stained *C. jejuni* bacteria at concentrations from 10^1 to 10^7 CFU/mL and the corresponding standard curve. In (b), dynamic range of the sensor. The error bars represent the standard deviation of triplicates.

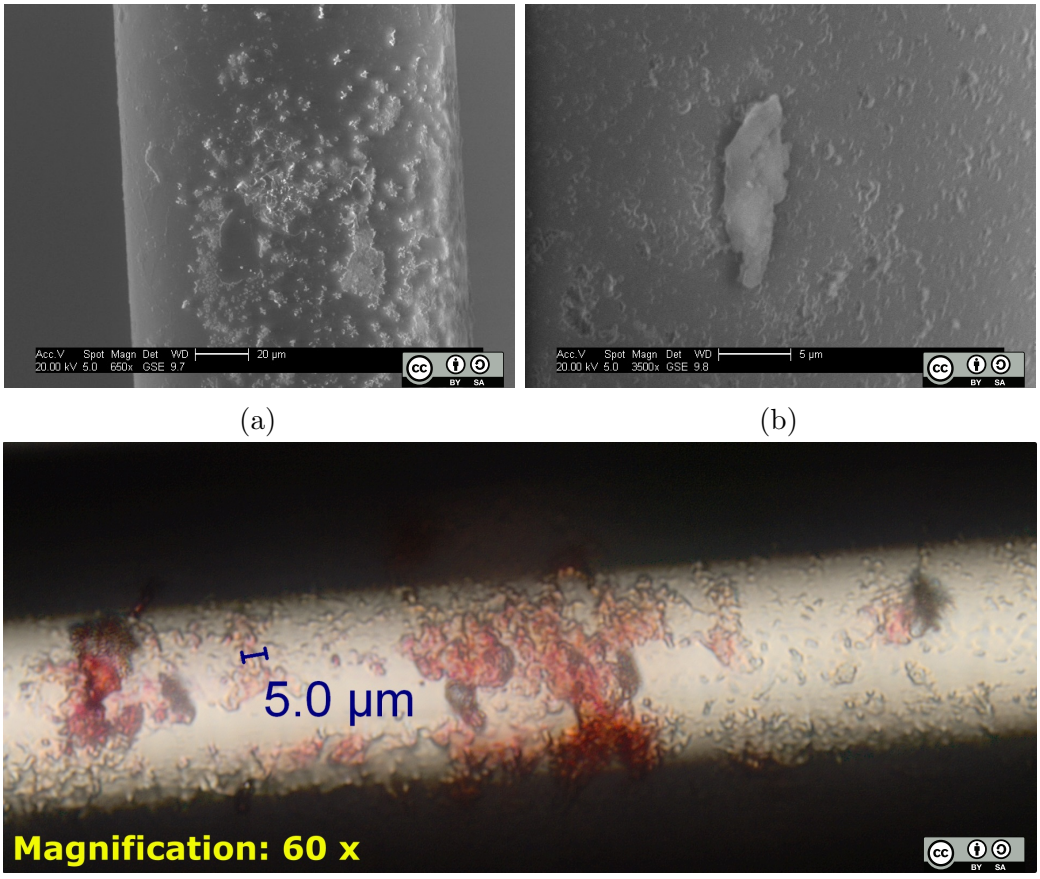

(a) (b)

(c)

Figure 5.9: Images of stained *Campylobacter jejuni* cells attached to the surface of the LPG immunosensor. (a) and (b) obtained with an ESEM. (c) obtained with an optical microscope at magnification 60×. Gram-negative organisms display a pinkish red tone.

conditions: unstained and stained bacteria. The t-test was performed using the Data Analysis Tools from Microsoft Excel, for a p-value of 0.05. The results obtained are shown in Table 5.2. The more relevant values from the t-test are highlighted in Table 5.2. The t Stat, or t-value indicates the size of the difference in mean values relative to the variation in the response of the sensor to different bacterial concentrations. In other words, the t value, in absolute value (4.1892), means that the unstained bacterial assay is around 4 times as different from the stained bacterial assay as they are within each other. In addition, the high value of the t Stat parameter indicates a high repeatability of the results. From the t-test results, it can be inferred that the Gram's staining was significantly effective in the enhancement of the sensitivity of the immunosensor developed in this thesis. In addition, this immunosensor matches the limits of detection achieved by other sensing platforms such as SPR for the detection of foodborne bacteria [439]. Taking into consideration the high contamination level of poultry products with *Campylobacter jejuni* (approximately 10^3 CFU/g [18, 19], 10^3-10^4 CFU/plate [20]), the performance of the sensor matches the concentrations that occur in real samples. However, the immunosensor presents some limitations.

Table 5.2: Results from the t-Test for a paired two sample for means.

	Unstained bacterial assay	Stained bacterial assay
Mean	0.8646	1.3053
Variance	0.6696	1.1901
Observations	8	8
Pearson correlation	0.9921	
Hypothesized mean diff.	0	
Degrees of freedom	7	
t Stat	-4.1893	
P(T≤t) one tail	0.0020	
t critical one tail	1.8946	
P(T≤t) two tail	0.0041	
t critical two-tail	2.3646	

First, the large volume of samples that are required for the assay (250 μL) compared to other platforms such as SPR-based sensors that uses sample volumes as low as 10 μL. This may be a limitation in the development of the sensor due to the high cost of antibodies. Another limitation is the long time for the assay (1-3 hours for stationary conditions) compared to faster sensing platforms such as SPR (20 minutes). Improvements and further work are proposed in the last chapter of this thesis.

5.4 Summary

The experimental results of the bacterial detection using a direct assay were presented in this chapter. In Sec. 5.1 the preparation of the bacterial cells was described. The responses of the immunosensor fabricated by the enhanced physical adsorption method to different concentrations of the target bacteria were shown in Sec. 5.2.1. This immunosensor showed a low response to low bacterial concentrations and the reproducibility was compromised due to the coating method employed for the antibody immobilization. The lowest bacterial concentration detected was 10^5 CFU/mL.

The evaluation of the immunosensor fabricated by the covalent attachment coating method was presented in Sec. 5.2.2. The GA promoted a more controlled orientation of the antibodies. This contributed to the high antibody-antigen interation and the reproducibility of the assay. As a result, the sensor exhibited a larger dynamic range and it was able to detect a concentration of 10^3 CFU/mL of *C. jejuni* cells. The stability of the immunosensor was assessed by evaluating its response to the target analyte after 24, 48 and 72 of storage at different temperatures. The results showed that the immunosensor exhibited a higher stability at 4°C. On the other hand, the immunosensor exhibited a low non-reversible stability at 35°C, losing its binding ability by nearly 98% in 48 hours. The specificity of the sensor was evaluated by testing its performance against other common foodborne bacteria such as *Listeria*

monocytogenes, *Salmonella typhimurium* and *Escherichia coli*. The results indicated that the sensor exhibited a relative response of 100% for *C. jejuni*, 22.77% for *Listeria*, 9.47% for *Salmonella* and 3.01% for *E. coli*.

The enhancement of the sensitivity of the sensor using Gram's staining was explored. Cell staining induced a change in the refractive index of the cell, enhancing the signal detected, improving the limit of detection by one order of magnitude to 10^2 CFU/mL. The bacterial attachment was validated with images obtained from an optical microscope and an ESEM. An statistical analysis was performed to evaluate if the staining was effective in the enhancement of the sensitivity of the sensor. From the results, it was inferred that the Gram's staining was significantly effective in the enhancement of the sensitivity of the immunosensor developed in this thesis. In addition, the statistical analysis indicated a high repeatability of the results. The performance of the sensor developed in this thesis matches the limits of detection achieved by other sensing platforms such as SPR. In addition, the performance of the sensor matches the bacterial concentrations that occur in real samples.

Chapter 6

Conclusions and Outlook

6.1 Summary and conclusions

In this thesis, the development of an optical immunosensor for *Campylobacter jejuni* detection using the fibre optic long period grating sensor platform, was presented. During the course of the research, a number of key aspects in the development of biosensors were considered, such as transduction signal generation, fluidics design, reduction of the sample consumption, surface immobilization chemistry, elimination of non-specific binding, detection format, sensitivity, selectivity, detection time and data analysis.

The fabrication of a long period grating with characteristics suitable for bacterial detection, using the point-by-point technique that involves the UV irradiation of photosensitive doped optical fibre, has been achieved. This technique allowed the tailoring of the sensor platform to the requirements of this project. In addition, software for the analysis of the experimental data generated in the course of this project was developed. The program was designed with the aim of identifying the central wavelengths of the attenuation bands of the LPG's transmission spectrum. A number of approaches to determining the attenuation bands' central wavelengths were assessed. The used approach calculates the minima of the attenuation bands using a Matlab built-in function which compares the difference in intensity values to find the peaks from the transmission spectrum, smoothed using a fast Fourier transform filter. The program contained an interactive graphical interface that allows the user to select the value of the parameter for the Fourier filter to re-construct the signal, to select the value of the threshold to ignore the undesired minima and the option to save the calculated minima.

A number of different surface cleaning methods were tested with the aim of ensuring effective and repeatable deposition of antibody coatings onto the cladding of the optical fibre. Piranha solution is a standard cleaning method that is widely used in the preparation of a variety of sensing platforms. However, it can result in fragility of the fibre, compromising its practical application. Other methods, such as solvent-based cleaning and that based on the use of hydrochloric acid + methanol and sulphuric acid, referred in this thesis as two-acids-based method, were tested. Of these three methods, the two-acids-based approach resulted in a smoother surface with no visible damage. The cleaning methods were evaluated using a surface

roughness scanning. As a result of the issues faced during the implementation of the cleaning protocols, such as the positioning of the optical fibre inside the beaker for immersion in the cleaning reagent, a 3D-printed device for fibre cleaning was designed and fabricated. The 3D-printed cleaning device allowed the rapid and simple fixing of the fibre for cleaning, reducing the cleaning time and waste generation. In addition, it allowed the simultaneous cleaning of a number of fibres. The selection of the material, design and optimization of the container that was used to accommodate the optical fibre for incubation was then carried out. PTFE was chosen due to its advantageous properties, such as chemical resistance to corrosive substances, non-solubility, non-adhesiveness and low coefficient of friction. The design of the sample container was optimized by reducing its capacity from 2000 μL to 250 μL.

The surface of the LPG was covered with an antibody coating using two methods: adsorption and covalent binding. In both cases, the surface was treated against non-specific binding with BSA. The optimal concentration of antibody solution was investigated, revealing that optimal concentration was 70 μg/mL. However, due to the large volume of the sample (250 μL) and the limited amount of antibody from the available batch, it was decided to use a lower concentration (50 μg/mL) to guarantee that all experiments were done with antibodies from the same batch. It is well known from the literature that antibodies from different batches can exhibit a distinct performance, which would affect the repeatability of the sensor. The concentration of the blocking protein for the chosen antibody concentration was investigated, revealing that the optimal concentration of BSA was 500 μg/mL. The sensitivity of the sensor was then evaluated in a direct assay. This type of assay is easy, rapid and cheap to perform, since only one type of antibody is necessary and labelling is not required. The sensor was tested against different bacterial concentrations (10^1 to 10^6 CFU/mL). The sensor created using covalent binding exhibited a lower limit of detection for *Campylobacter jejuni* cells (10^3CFU/mL) than that created via the adsorption coating method (10^4 CFU/mL). It was demonstrated in this thesis that the use of antibodies as recognition elements provided high sensitivity and selectivity. The selectivity, often called cross-reactivity, was evaluated in a direct assay against different bacteria. *Escherichia coli*, *Listeria monocytogenes* and *Salmonella typhimurium* were selected since they, like *C. jejuni*, are foodborne pathogens and usually are found together in real samples. The results showed that the sensor exhibited a high selectivity, generating a response of 100% for *Campylobacter jejuni* (target bacteria), 22.77% for *Listeria monocytogenes*, 9.47% for *Salmonella typhimurium* and 3.01% for *Escherichia coli*. The origin of the relatively high response of the sensor to *Listeria* (22.77%) can be due to two reasons. First, of these three non-target bacteria, *Listeria* have the smallest average size. The small size of the bacteria could allow them to fill the gaps in the antibody coating where the surface of the fibre is not covered by the blocking protein, generating a non-specific response. If this is the case, the blocking coating would be a key feature to improve before testing the sensor with real samples. On the other hand, the origin of the response exhibited by the sensor against *Listeria* may be due to the polyclonal nature of the antibodies used in this thesis, which are able to recognize different epitopes. This may be investigated in further work by blocking the surface with a smaller blocking agent. Finally, the enhancement of the sensitivity of the sensor using Gram's staining was explored. This staining method was selected

due to its simplicity, rapidity, and reports in the literature, which demonstrated that it stains *C. jejuni* cells stronger than other methods [314, 315]. Cell staining improved the limit of detection to 10^2 CFU/mL. Studies from the literature based on optical platforms such as surface plasmon resonance have reported limits of detection for *Campylobacter jejuni* within the range of 10^2-10^6 CFU/mL. Finally, bacterial attachment was confirmed with an environmental scanning microscopy and an optical microscope.

Table 6.1 summarizes the attributes of the immunosensor developed in this thesis.

Table 6.1: Summary of the features of the immunosensor for *Campylobacter jejuni* developed in this thesis.

Feature	**Notes**
Transduction signal generation:	Optical fibre long period grating
Biorecognition molecule:	Rabbit polyclonal antibody specific to *C. jejuni*
Detection format:	Direct assay
Fluidics design:	PTFE container, optimized capacity for stationary conditions
Sample volume:	250 μL
Surface cleaning:	Two-acids based method
Immobilization chemistry:	Covalent attachment
Non-specific binding:	Minimized by the optimization of the blocking protein concentration
Detection time:	1 hour
Limit of detection:	10^3 CFU/mL 10^2 CFU/mL (enhanced by Gram's staining)
Specificity:	Highly specific against *Escherichia coli*, *Listeria monocytogenes* and *Salmonella typhimurium*

The reliable, repeatable and fast sensor for *Campylobacter jejuni* that has been developed during this project has the potential for use in the detection of this harmful pathogen in water and food. The performance matches the measurement

requirements and the assay can be performed in 1 hour, as compared with 2-5 days for traditional methods. This could have a significant impact in the prevention of gastroenteritis. The sensor system, shown in Fig. 4.19, has the potential to be low-cost, portable and suitable for use in developing countries where the need is greater.

6.2 Outlook

The immunosensor developed in this PhD project has the potential to be low-cost, portable and suitable for use for the fast and sensitive detection of harmful bacteria. However, a number of features should be improved before it can be used in practice with real samples. First, the high sensitivity of LPG-based sensors to external parameters such as temperature, bending and refractive index changes in the surrounding environment is, paradoxically, its main limitation. While via suitable packaging, the effect of strain and bending can be mitigated, it is challenging to distinguish, from a conventional LPG, if a shift in the central wavelength of an attenuation band was promoted by a change in the temperature or refractive index of the surrounding region. For this reason, the use of a temperature chamber was required in the work presented here. However, it compromises the portability of the immunosensor. To overcome this challenge, improvements to the sensing platform could be considered. For example, the use of TFGs as sensing platforms, discussed in Section 2.2.4, has been shown to allow the creation of sensing systems that are sensitive to environmental refractive index changes but insensitive to temperature [148, 440].

Second, the current sensor system was tested with well-known bacterial concentrations in buffer exhibiting good sensitivity to the target. In order to reliably test the immunosensor with food or water samples, a number of improvements can be made. For example, contaminated food or contaminated water may contain not only the target bacteria but other analytes such as viruses, fungus and other interfering material. For example, raw chicken samples are amongst the most challenging matrices to analyse due to the high content of lipids, nucleic acids and proteinaceous materials [372]. Despite the optimisation of the concentration of the protein against non-specific binding for the immunosensor developed in this thesis, as discussed in Section 4.4.3, the blocking coating was not perfect. Non-target analytes may generate a false response from the sensor by binding in the sites not covered by the blocking protein. Alternatively, pre-treatment of the sample could be performed. For instance, a proven strategy to reduce the non-specific response from real samples is via the application of several dilutions and the addition of high concentrations of blocking agents to the sample or the running buffer [372, 441].

Third, the cost of rabbit polyclonal antibody specific for *Campylobacter jejuni* ($375 USD $\approx$ £300 for 1 mL) may be a limitation when considering the need for a low cost sensor, considering the large volume of the sample (250 μL). Another possibility could be to explore the use of different REs such as aptamers or MIPs. Although these REs are not commercially available, have complex fabrication protocols and the surface immobilization for the integration with sensors is not well developed [242, 206], these have the advantages of being stable, low-cost and reusable [206, 221].

Finally, the sensitivity of the immunosensor developed in this project could be enhanced by carrying out indirect, sandwich or competitive assays, which are, despite being more complex to perform, up to 5 times more sensitive than the direct assay [54].

Potential improvements and future research based on the work presented in this thesis is outlined.

6.2.1 Development of a microfluidic chamber and OCT

As it was mentioned in Sec. 4.2, the meniscus of the sample solution formed on the top of the teflon container increases the sample volume for no benefit. The influence of the meniscus can be reduced with the use of a microfluidic chamber. A microfluidic chamber was designed with the aim to minimize the sample volume, to facilitate the washing steps with the running buffer and to avoid evaporation during stationary incubation at higher temperatures.

In the development of the microfluidic chamber, three versions were designed, fabricated and tested. All consisted of three parts: i) the polytetrafluoroethylene (PTFE) container, described in Sec. 4.2, ii) a base to hold the PTFE container, and iii) a lid with an inlet and an outlet. The base was fabricated with the Ultimaker 3D-printer described in Sec. 4.1.4. The bases from the different designs are shown in Fig. 6.1. The lid was fabricated in a 3D-printer model Form 2 from FormLabs.

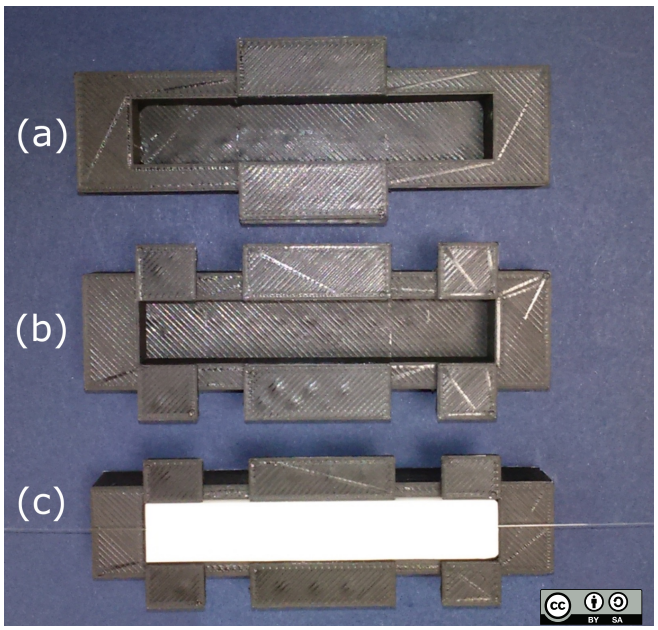

Figure 6.1: Sample container holder bases from the (a) initial, (b) second, and (c) final design.

Schematics of the top and bottom views of the lid design are shown in Fig. 6.2a and 6.2b, respectively. The bottom of the lid was in contact with the PTFE sample container and contained a groove to house a seal in order to keep the sample enclosed. The top of the lid contained two hollow cylinders that acted as the inlet and the outlet for the sample, respectively. In addition, it contained tabs that acted as pressure

zones to keep the lid firmly attached to the base holder using bulldog clips. Images of the different lid versions are shown in Fig. 6.2c. The final version of the flow cell had

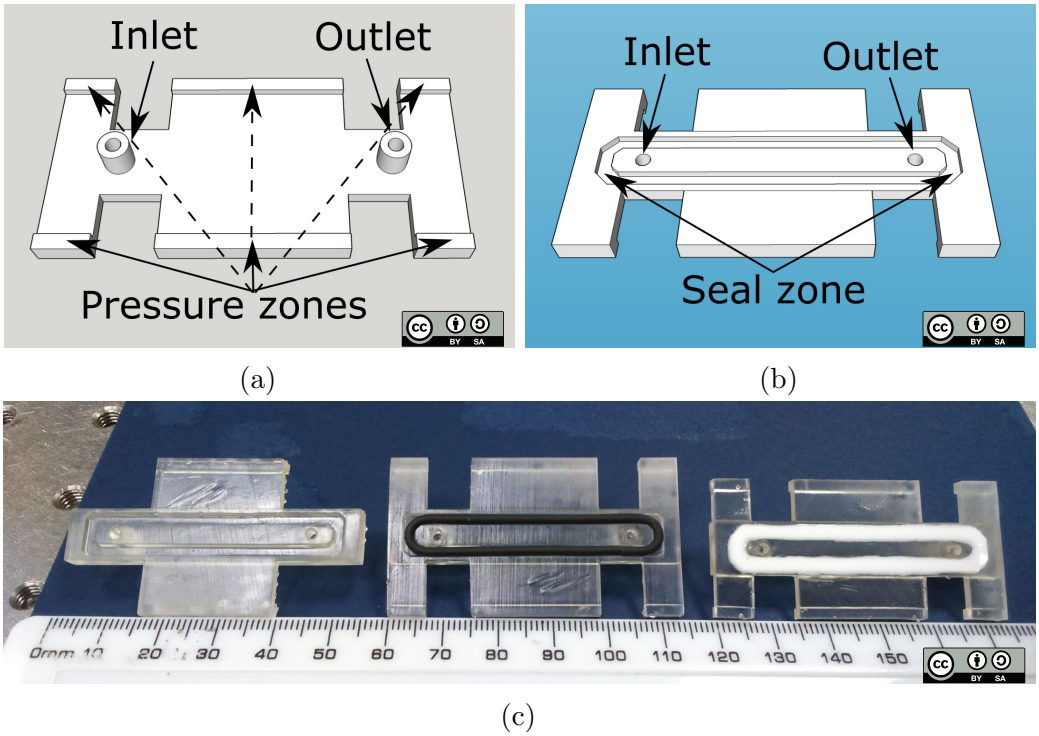

Figure 6.2: Schematic of the (a) top and (b) bottom views the microfluidic chamber lid. Image of the three different sample container lid designs in (c).

50% narrower tabs and it was sealed with silicone rubber (T28 silicon rubber RTV (room temperature vulcanised) + T6 catalyst, from Alec Tiranti Ltd, UK). This silicone rubber is suitable for working at temperatures between -20°C and 250°C. The silicone rubber, unlike the O-ring used in the previous versions of the device which presented leaks, is pourable and soft enough to adapt to the contour of the contact surface and seal any leaks. The device is shown in Fig. 6.3. The microfluidic chamber was tested using DI water as a sample test. The device exhibited sealed properly and showed no leaks. However, when tested with IPA (less dense than water) the device presented leaks. The microfluidic chamber developed in this thesis has the potential to be used as both a cleaning device and a sample container. This could reduce the sensor fabrication time and avoid damaging the fibre when manipulated. In addition, the materials involved in the fabrication of the device showed a high resistance to corrosive substances such as the acids employed for the cleaning of the fibre. However, the leaking exhibited when used with solvents represents a major problem. Alternative sealing solutions can be explored and the fabrication of the device in glass could be considered. On the other hand, the sample volume can be reduced by approximately 36% (160 μL final sample volume) or even more if the inner dimensions of the sample container are reduced. This could increase the sensitivity of the sensor by allowing the use of higher concentrations of antibodies and reducing the chemical waste. Additionally, the semitransparent lid of the microfluidic chamber may be used to study the bacterial flow using optical coherence tomography (OCT).

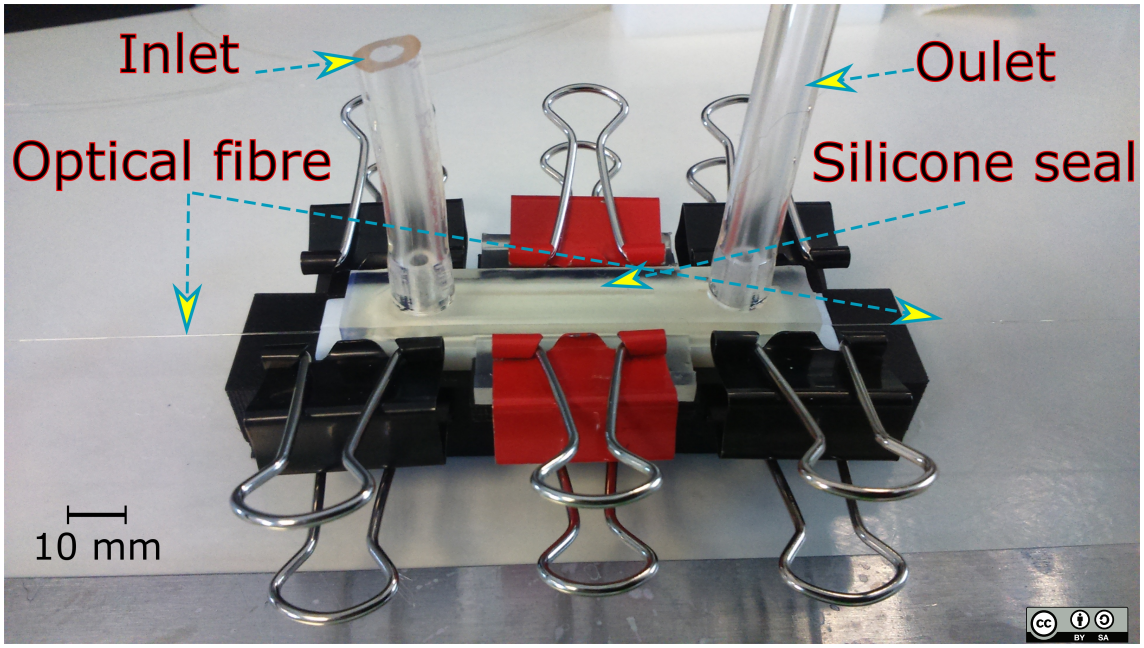

Figure 6.3: Image of the microfluidic chamber sealed with silicone.

OCT is an interferometric technique commonly employed to provide cross-sectional views of internal structures of biological materials by measuring the reflected light. Recently, OCT has been applied to identify latex particles through a high velocity flow in a microfluidic channel [442]. This technique may be applied to explore the bacterial flow through the microfluidic chamber and to investigate the precipitation times of the bacterial cells on the bottom of the container. The dimensions of the chamber should be adapted to match with the suitable dimensions used in OCT (lid width 175 μm and container deep 800 μm). This information could be useful to reduce the assay time by promoting the bacterial attachment by agitating the sample using syringes as pumps in the inlet and outlet. Under mixing conditions most antigen-antibody reactions are optimum after 30 min at 37°C, so the assays can be greatly sped up with no loss in sensitivity [47].

6.2.2 Optimization of the selectivity of the sensor

The immunosensor developed in this thesis was shown to be highly sensitive and selective. However, understanding the origin of the response exhibited by the sensor against non-target bacteria is a key element for further improvements. If the response was caused by non-specific adsorption, improvements in the blocking coating can be performed. The blocking against non-specific binding of the surface with an additional blocking agent to fill the surface not covered by the BSA is proposed. The selection of a suitable blocking agent also needs to be explored. Non-fat dried milk, gelatin or proteins, such as normal rabbit serum or normal horse serum, could be potential blocking agents.

The results obtained in this thesis indicated a relation between the size of bacteria and the cross-reactivity level. The investigation of the validity of this statement is proposed for future research. Briefly, a number of foodborne bacteria with different

average dimensions, such as *Clostridium perfringens* (0.3-2 by 1.5-20 μm) could be added to the bacterial test set. In addition, the use of monoclonal antibodies could also be explored.

6.2.3 Development of methods for distinguishing live and dead cells

The development of methods for distinguishing live and dead cells is proposed. ViaGram^{TM}Red^{+} Bacterial Gram Stain and Viability Kit, from Thermo Fisher Scientific, provides fluorescent staining protocols for fluorescence microscopy, which differentially stains Gram-positive and Gram-negative bacteria, and at the same time, discriminates live from dead cells based on plasma membrane integrity [443]. Fluorochromes are chemicals that absorb light of short wavelength and emit light of a longer wavelength and may be used as fluorescent dyes to stain bacteria [35]. 4',6-diamidino-2-phenylindole (DAPI) stains blue bacteria with intact cell membranes (live cells). On the other hand, SYTOX® stains green bacteria with damaged cell membranes (dead cells). The Texas Red®-X dye-labeled WGA (wheat germ agglutinin) selectively binds the surface of Gram-positive bacteria, staining them red [303]. Thus, the three fluorescent dyes cover the four possible combinations, as shown in Table 6.2. In this research line, the suitability of other fluorescent dyes commonly

Table 6.2: Summary of the staining pattern for the ViaGram^{TM}Red^{+} kit.

	Gram-positive	**Gram-negative**
Live cells	Blue interior Red surface	Blue interior
Dead cells	Green interior Red surface	Green interior

used for cell staining such as propidium iodide (PI) could be explored. Based on the results presented in Sec. 4.4.1 regarding the invariance of the attenuation band in a process of connection-disconnection in and out from the light source and spectrometer under constant conditions of strain, bend, refractive index of the surrounding medium and temperature, the characterization of the sensor may be performed in a shorter time frame. The experimental setup, shown in Fig. 6.4 is suggested. Briefly, eight PTFE sample containers can be placed inside a temperature chamber. Instead of the commonly used metal frame to fix the fibre, 3D-printed cubes of 1 cm^3 with an inner rectangular groove to insert a magnet could be used to act as fixing supports for the optical fibre. The cube contains a "V-grooved" line channel on the top face (deep approximately half of the diameter of the jacket of the optical fibre) to keep

the fibre aligned when it is fixed with a magnet. The cubes can be fixed to the tray with glue or double-faced tape and aligned with the sample container. Each of the sample containers could contain a known concentration of Gram-positive live cells, Gram-negative live cells, Gram-positive dead cells, Gram-negative dead cells and four controls (sample solutions without bacteria). In order to avoid cross-contamination of the samples and as an additional protection measure due to mutagenicity and toxicity of DAPI and SYTOX, the covering of the samples with customised 3D-printed lids is strongly recommended. This setup would allow the incubation of multiples fibres

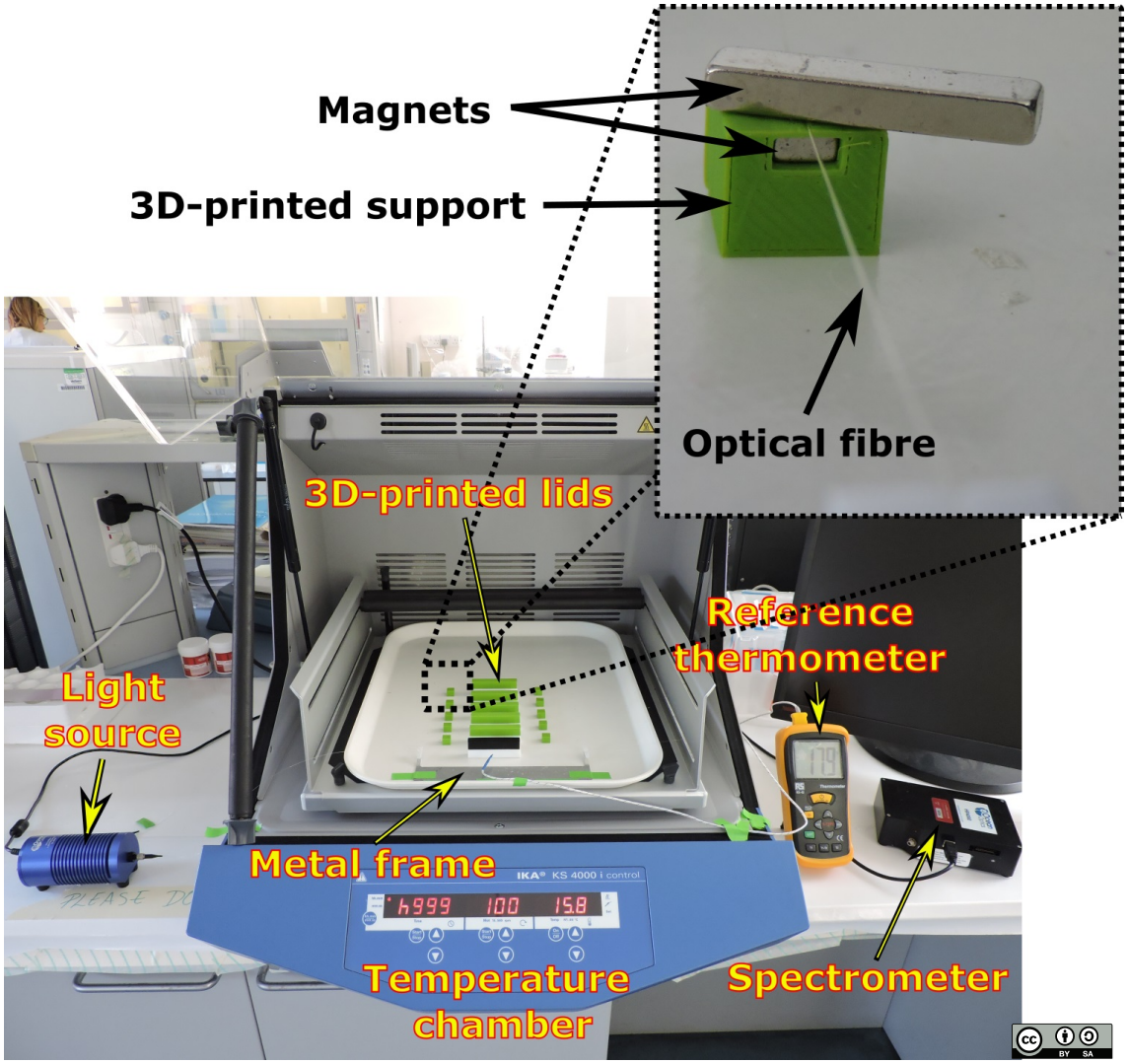

Figure 6.4: Image of the setup containing multiple sample containers and 3D-printed supporters.

at the same time, using only one light source and one spectrometer, by connecting and disconnecting the fibres to save the experimental data when required. The experimental data could be validated by fluorescence microscopy.

6.2.4 Improvements to the sensing platform

The performance of the immunosensor developed in this thesis could be enhanced further with the use of a high-resolution spectrometer, with an associated increase in the cost of the system. The sensitivity could be improved by coupling to a lower order mode (LP_{11}) at the PMTP. However, this could happen at a longer wavelength, outside the range of the CCD spectrometer with this fibre cut-off wavelength [199]. To overcome this, a shorter cut-off wavelength optical fibre could be used, but there can be challenges with coupling light into such fibre efficiently from a incoherent extended source like the tungsten halogen bulb used in this project. An alternative approach to enhance the resolution of the measurements would be to improve the performance of the sensing platform. This can be achieved with the use of different LPG configurations, such as cascaded LPGs [444, 445, 446, 447, 448]. A cascaded LPG consists of two or more LPGs inscribed in series along the same section of the fibre. The fabrication of two cascaded LPGs generates intrinsically a Mach-Zehnder interferometer (MZI) within the fibre, as shown in Fig. 6.5. The first LPG couples

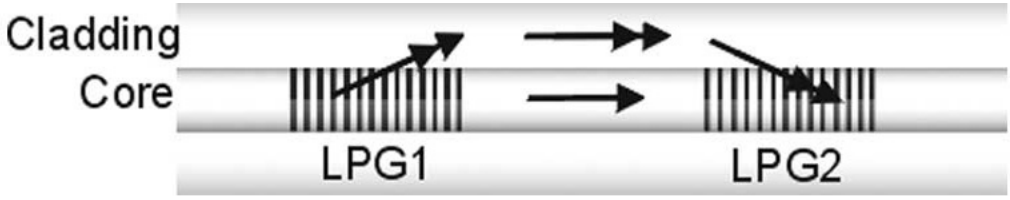

Figure 6.5: Schematic of a cascaded LPG's operation. Reproduced from [447].

the light to a cladding mode. Then, the light propagates via the cladding or the core. The second LPG couples the light back into the core. The light coupled into the core by the second LPG is phase shifted with respect to the light that travelled through the core, producing a sinusoidal channelled transmission spectrum within the attenuation bands, which looks like an interference fringe pattern [447], as shown in Fig. 6.6, due to the difference between the effective refractive indices of the core and cladding modes [447]. As the phase and the resonance wavelength are both dependent upon the difference between the core and cladding mode effective indices, both the phase of the channelled fringes and the resonance band central wavelength exhibit changes at the same rate when the cascaded LPG experiment an external perturbation [446]. The interference fringes within the attenuation bands can enhance the resolution and the sensitivity of the measurement [444]. While this configuration may increase the surface area to be coated by the biorecognition molecule, the fabrication of cascaded LPGs of length as short as 2 cm, separated by 3 cm, has been demonstrated and used for refractive index sensing and temperature monitoring [447]. In theory, this could enhance the sensitivity of the immunosensor developed in this thesis, keeping constant the area to be coated by the recognition element due to the features of the channelled spectrum are much narrower than the LPG resonance band. Previous work has shown that coating only the section of fibre separating the LPGs, the central wavelengths of the features of the channels spectrum shift in response to both temperature and the RI of the coating, while the resonance band envelop will respond only to temperature, which could allow the use

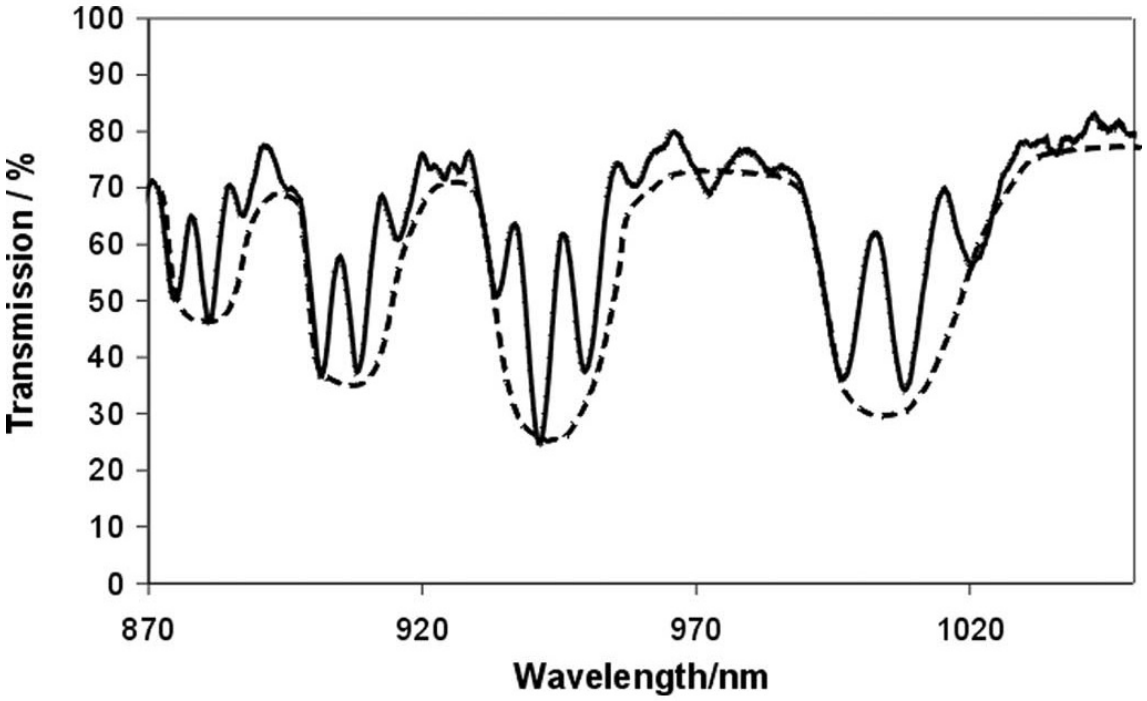

Figure 6.6: Transmission spectrum of a cascaded LPG. Interference fringes within the attenuation bands can be observed. Reproduced from [447].

of the sensor in an environment where the temperature is less closely controlled [445].

The physical modification of the optical fibre such as tapering the fibre [449, 450], or etching the cladding [451], has been demonstrated to improve the sensitivity of LPGs to the surrounding refractive index. Tapered optical fibres facilitates a strong interaction between the propagating modes and the coating, allowing the evanescent field to penetrate further into the surrounding medium. However, a careful handling of the optical fibre containing the LPG is required since these approaches compromises the mechanical integrity of the fibre. The use of the microfluidic chamber, described in Sec. 6.2.1 could help to overcome this challenge, providing a protected environment for the fibre.

List of publications

The following publications have resulted from the work presented in this thesis:

Peer-Reviewed Conference Papers

1. Romero, A. R., Partridge, M., Masdor, N. A., James, S. W., Tothill, I. E., & Tatam, R. P. A fibre optic long period grating immunosensor for *Campylobacter jejuni* with enhanced sensitivity by bacterial staining. In *26th International Conference on Optical Fiber Sensors (OFS-26)* (Lausanne, Switzerland, 2018), OSA Technical Digest (Optical Society of America), p. WF2. (Poster presentation).

2. Romero, A. R., Masdor, N. A., Partridge, M., James, S. W., Tothill, I. E., & Tatam, R. P. Fibre optic long period grating sensor for *Campylobacter jejuni* detection. In *2017 IEEE SENSORS* (Glasgow, Scotland, UK, 2017), vol. 1, IEEE, pp. 1-3. (Poster presentation).

Papers in preparation

1. Romero, A. R., Partridge, M., Masdor, N. A., James, S. W., Tothill, I. E., & Tatam, R. P. Working title: Long period grating immunosensor for *Campylobacter jejuni*.

2. Romero, A. R., Masdor, N. A., Partridge, M., James, S. W., Tothill, I. E., & Tatam, R. P. Working title: Long period grating immunosensor for bacterial detection with enhanced sensitivity by cell staining.

Appendix A. Staining methods

The procedures and protocols of the most widely used methods for cell staining, described in Section 2.6, are outlined.

Ziehl-Neelsen staining

The procedure of the Ziehl Neelsen staining involves three different reagents:

1. *Primary stain*−Carbol-fuchsin (0.3%): Dissolve 50g phenol in 100 mL ethanol (90%) or methanol (95%). Add 3 g of basic fuchsin in the mixture and add distilled water to complete 1 L.

2. *Decolorizing solution*−Acid alcohol (3% + 9.5% ethanol) or 25% sulphuric acid.

3. *Counterstain*−Methylene blue or malachite green.

The protocol of the Ziehl-Neelsen staining method is as follows:

1. Prepare a bacterial smear on the surface of a clean glass slide and let it dry for 30 minutes.

2. Heat fix the smear by passing the slide 3 or 4 times just above a Bunsen burner or place the slide on a slide warmer at 65-75°C.

3. Boil water ($\approx$ 2 cm) in a beaker to generate steam.

4. Place the glass slide on the top of the beaker and flood the bacterial smear with carbol-fuchsin.

5. Cover the glass slide and steam it for 5 minutes.

6. Uncover the glass slide and remove the stain with water.

7. Wash the glass slide with the decolorizing solution (either sulphuric acid or acid alcohol) for 2 minutes.

8. Wash the glass slide with water.

9. Flood the bacterial smear with the counterstain solution for 30-45 seconds.

10. Wash with water, blot dry and observe under microscope.

Gram staining

The protocol of the Gram staining method is as follows:

1. Prepare a bacterial smear on a glass slide.
2. Flood the smear with crystal violet and let it stand for 1 minute.
3. Pour off the stain and gently wash with water.
4. Flood the smear with iodine solution and let it stand for 1 minute.
5. Pour off the iodine and gently wash with water.
6. Wash with decolorize solution until no blue dye flows from the slide.
7. Wash the glass slide with water.
8. Flood the smear with safranin solution and let it stand for 1 minute.
9. Wash off the counterstain with water and let it dry.

Leifson staining

The protocol of the Leifson staining method is as follows:

1. Heat a glass slide in a Bunsen burner.
2. On the central section of the hot slide, mark a circle or oval with a pencil.
3. Once the slide gets cold, place several loopfuls at one end inside the oval.
4. Tilt the glass slide to allow bacteria to flow down over the surface of the glass slide.
5. Let the sample to air-dry. If heat is applied, flagella can be damaged.
6. Flood the sample with Liefson stain and let the alcohol to evaporate.
7. Remove the stain, let the glass slide to air-dry and examine under microscope.

Dorner staining

The protocol of the Dorner staining method is as follows:

1. In a small test tube, disperse several loopfuls in approx. 5 drops of water.
2. Add 5 drops of carbol fuchsin (same amount as water) to the bacterial solution.
3. Heat the bacterial solution in a beaker of boiling water (bain-marie) for 10 minutes.
4. On a glass slide, mix several loopfuls from the bacterial solution with a drop of nigrosine.

5. Spread the nigrosine-bacteria mixture on the slide.

6. Dry and examine under microscope.

Schaeffer and Fulton staining

The protocol of the Schaeffer and Fulton staining method is as follows :

1. Heat-fix a smear on a clean glass slide.

2. Boil water ($\approx$ 2 cm) in a baker to generate a steam.

3. Place the slide on the top of beaker.

4. Flood the slide with malachite green and steam for 5 minutes.

5. Remove the slide, let it cool and rinse with water for 30 seconds.

6. Flood with safranin for 30 seconds and wash with water for 30 seconds.

7. Dry and examine under microscope.

India ink method

The protocol of the India ink staining method is described as :

1. Add a loopful of bacterial cells on a glass slide.

2. Put a drop of India ink next to the bacterial loopful.

3. Drag the Indian ink and the bacterial loopful over the the surface of the glass slide with the aid of another slide.

4. Let it air dry for 5-7 minutes. Do not heat.

5. Flood the smear with crystal violet for 1 minute.

6. Wash off the crystal violet stain with water and tilting the slide at a 45°.

7. Let the slide air-dry and observe under microscope.

Notes: For the negative stain in step 2, the Indian ink can be replaced with Congo Red or Nigrosin. Capsules are fragile and can be damaged with heat (step 4). In the washing stage in step 6, the rinse with water must be done very gently since water can remove the capsule from the cell wall.

Anthony's stain

The protocol of the Anthony's staining method is as follows :

1. Place a drop of crystal violet near the edge of a clean glass slide.

2. Take a loopful of bacterial cells and mix it with the crystal violet placed on the slide.

3. Drag the mixture over the surface of the glass slide with the aid of another slide.

4. Allow the formed film to air dry, usually 5-7 minutes.

5. Rinse the glass slide with 20% of cooper sulfate solution.

6. Let the glass slide to air dry and observe under microscope.

Appendix B. Piranha solution

Piranha solution is a cleaning mixture of concentrated sulphuric acid (H_2SO_4) and hydrogen peroxide (H_2O_2). Piranha is a very hazardous substance that requires a careful handling. Special personal protection equipment must be worn, including safety goggles, lab coat and heavy duty rubber gloves (standard nitrile gloves do not provide enough protection). This protocol must be done under a fume hood at all time. Unless otherwise specified, all reagents to perform this protocol were purchased from Sigma-Aldrich.

Materials: Concentrated sulphuric acid (ACS reagent, 95.0-98.0%), hydrogen peroxide solution (35 wt % in H_2O, ACS specification), pipettes (Eppendorf Research® plus), Pasteur pipettes, pipette bulbs, two 150 mL low form Pyrex® borosilicate glass beakers, a 5 L beaker.

Notes: Sodium bicarbonate (ACS reagent, $\geq$ 99.7%) or baking soda, pH dip strips (Hydrion Brilliant) are also used for the neutralization of the piranha solution for a safe disposal.

To prepare 4 mL of piranha solution 3:1, first pour the sulphuric acid in a beaker (step 1). This is to avoid contaminating the main bottle as well as a safety manner as smaller volumes are involved. Pour 3 mL of sulphuric acid in a graduated beaker using the Pasteur pipettes and the pipette bulbs (step 2). Do not use other type of pipettes since they can be damaged by the acid. Then, pour hydrogen peroxide in a beaker (step 3). With a pipette, transfer 1 mL of hydrogen peroxide from the beaker to the graduated cylinder that contains 3 mL of sulphuric acid slowly (step 4). The solution will heat up and react violently if hydrogen peroxide is poured fast. A schematic of the piranha solution preparation is shown in Fig. B.1.

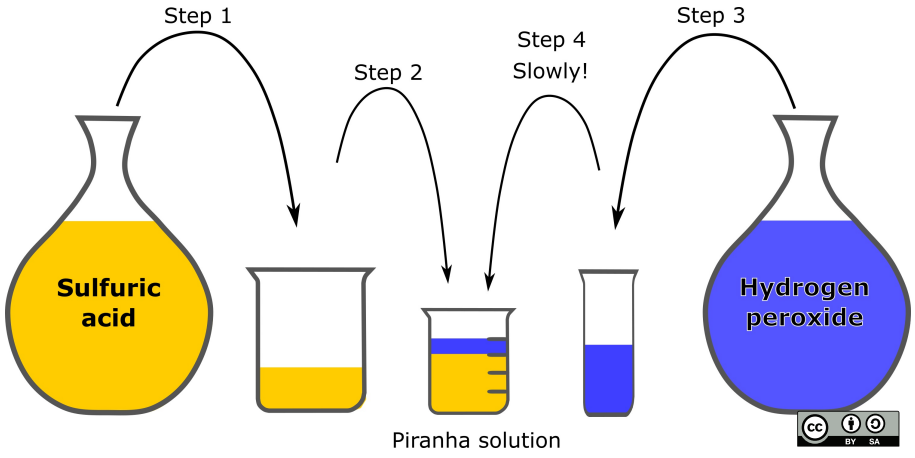

Figure B.1: Schematic of the piranha solution preparation.

For waste disposal, allow piranha solution to cool down for several hours. Pour the piranha solution in a large beaker containing a large volume of water (at least 10 times the amount of piranha solution). Then, neutralize with sodium bicarbonate. Verify the pH with the dip strips.

References

[1] D. Acheson and B. M. Allos, "Campylobacter jejuni infections: update on emerging issues and trends," *Clinical Infectious Diseases*, vol. 32, no. 8, pp. 1201–1206, 2001.

[2] European Food Safety Authority (EFSA), "The European Union summary report on antimicrobial resistance in zoonotic and indicator bacteria from humans, animals and food in 2014," Tech. Rep. 2, EFSA, 2016.

[3] B. Devleesschauwer, M. Bouwknegt, M.-J. J. Mangen, and A. H. Havelaar, "Health and economic burden of campylobacter," in *Campylobacter* (G. Klein, ed.), ch. 2, pp. 27–40, Elsevier, 2017.

[4] Food and Agriculture Organization of the United Nations/World Health Organization, "Salmonella and campylobacter in chicken meat: meeting report," tech. rep., FAO/WHO, Rome, Italy, 2009.

[5] World Health Organization, "The global view of campylobacteriosis," tech. rep., WHO, Utrecht, Netherlands, 2012.

[6] D. Werber, K. Hille, C. Franck, M. Dehnert, D. Altmann, J. Müller-Nordhorn, J. Koch, and K. Stark, "Years of potential life lost for six major enteric pathogens, Germany, 2004–2008," *Epidemiology and Infection*, vol. 141, no. 05, pp. 961–968, 2013.

[7] R. L. Scharff, "Economic burden from health losses due to foodborne illness in the United States," *Journal of Food Protection*, vol. 75, no. 1, pp. 123–131, 2012.

[8] I. Nachamkin, P. A. Barbosa, H. Ung, C. Lobato, A. G. Rivera, P. Rodriguez, A. G. Briseno, L. M. Cordero, L. G. Perea, J. C. Perez, M. Ribera, J. Veitch, C. Fitzgerald, D. Cornblath, M. R. Pinto, J. W. Griffin, H. J. Willison, A. K. Asbury, and G. M. McKhann, "Patterns of Guillain-Barré syndrome in children," *Neurology*, vol. 69, no. 17, pp. 1665 LP – 1671, 2007.

[9] J. E. Pope, A. Krizova, A. X. Garg, H. Thiessen-Philbrook, and J. M. Ouimet, "Campylobacter reactive arthritis: a systematic review," *Semin. Arthritis Rheum*, vol. 37, no. 1, pp. 48–55, 2010.

[10] J. P. Thornley, D. Jenkins, K. Neal, T. Wright, J. Brough, and R. C. Spiller, "Relationship of campylobacter toxigenicity in vitro to the development of

postinfectious irritable bowel syndrome.," *The Journal of infectious diseases*, vol. 184, no. 5, pp. 606–9, 2001.

[11] S. M. Man, "The clinical importance of emerging Campylobacter species," *Nature Reviews Gastroenterology and Hepatology*, vol. 8, no. 12, pp. 669–685, 2011.

[12] C. Schmutz, D. Mäusezahl, P. J. Bless, C. Hatz, M. Schwenkglenks, and D. Urbinello, "Estimating healthcare costs of acute gastroenteritis and human campylobacteriosis in Switzerland," *Epidemiology and Infection*, vol. 145, no. 4, pp. 627–641, 2017.

[13] C. C. Tam and S. J. O'Brien, "Economic cost of campylobacter, norovirus and rotavirus disease in the United Kingdom," *PLoS ONE*, vol. 11, no. 2, pp. 1–12, 2016.

[14] N. O. Kaakoush, N. Castaño-Rodríguez, H. M. Mitchell, and S. M. Man, "Global epidemiology of campylobacter infection," *Clinical Microbiology Reviews*, vol. 28, no. 3, pp. 687–720, 2015.

[15] S. Akhtar, M. R. Sarker, and A. Hossain, "Microbiological food safety: a dilemma of developing societies," *Critical Reviews in Microbiology*, vol. 40, no. 4, pp. 348–359, 2014.

[16] G. J. Medema, P. F. Teunis, A. H. Havelaar, and C. N. Haas, "Assessment of the dose-response relationship of Campylobacter jejuni," *International Journal of Food Microbiology*, vol. 30, no. 1-2, pp. 101–111, 1996.

[17] R. E. Black, M. M. Levine, M. L. Clements, T. P. Hughes, and M. J. Blaser, "Experimental Campylobacter jejuni infection in humans," *Journal of Infectious Diseases*, vol. 157, no. 3, pp. 472–479, 1988.

[18] J. Baré, M. Uyttendaele, I. Habib, O. Depraetere, K. Houf, and L. De Zutter, "Variation in campylobacter distribution on different sites of broiler carcasses," *Food Control*, vol. 32, no. 1, pp. 279–282, 2013.

[19] M. J. Nauta, M. Sanaa, and A. H. Havelaar, "Risk based microbiological criteria for campylobacter in broiler meat in the European Union," *International Journal of Food Microbiology*, vol. 158, no. 3, pp. 209–217, 2012.

[20] N. J. Stern and J. E. Line, "Comparison of three methods for recovery of Campylobacter spp. from broiler carcasses," *Journal of Food Protection*, vol. 55, no. 9, pp. 663–666, 1992.

[21] C. Yang, Y. Jiang, K. Huang, C. Zhu, and Y. Yin, "Application of real-time PCR for quantitative detection of Campylobacter jejuni in poultry, milk and environmental water," *FEMS Immunology and Medical Microbiology*, vol. 38, no. 3, pp. 265–271, 2003.

[22] A. D. Sails, F. J. Bolton, A. J. Fox, D. R. A. Wareing, and D. L. A. Greenway, "Detection of Campylobacter jejuni and Campylobacter coli in environmental waters by PCR enzyme-linked immunosorbent assay," *Applied and Environmental Microbiology*, vol. 68, no. 3, pp. 1319–1324, 2002.

[23] S. Wu, "Invasion," in *Molecular Medical Microbiology* (Y.-W. Tang, M. Sussman, D. Liu, I. Poxton, and J. Schwartzman, eds.), ch. 25, pp. 423–448, Academic Press, 2nd ed., 2015.

[24] A. C. Maue, K. L. Mohawk, D. K. Giles, F. Poly, C. P. Ewing, Y. Jiao, G. Lee, Z. Ma, M. A. Monteiro, C. L. Hill, J. S. Ferderber, C. K. Porter, M. S. Trent, and P. Guerry, "The polysaccharide capsule of Campylobacter jejuni modulates the host immune response," *Infection and Immunity*, vol. 81, no. 3, pp. 665–672, 2013.

[25] T. Humphrey, S. O'Brien, and M. Madsen, "Campylobacters as zoonotic pathogens: a food production perspective," *International Journal of Food Microbiology*, vol. 117, no. 3, pp. 237–257, 2007.

[26] T. Humphrey, M. Mason, and K. Martin, "The isolation of Campylobacter jejuni from contaminated surfaces and its survival in diluents," *International Journal of Food Microbiology*, vol. 26, no. 3, pp. 295–303, 1995.

[27] De Wood, Pooley, USDA, ARS, EMU (Public domain), via Wikimedia Commons, "Campylobacter jejuni." https://commons.wikimedia.org/w/index.php?title=File:ARS_Campylobacter_jejuni.jpg&oldid=258325816, Date Accessed: 29/10/2018.

[28] A. J. Levy, "A gastro-enteritis cutbreak probably due to a bovine strain of vibrio," *The Yale Journal of Biology and Medicine*, vol. 18, no. 1, pp. 243–258, 1946.

[29] M. Veron and R. Chatelain, "Taxonomic study of the genus Campylobacter Sebald and Veron and designation of the neotype strain for the type species, Campylobacter fetus (Smith and Taylor) Sebald and Veron," *International Journal of Systematic Bacteriology*, vol. 23, no. 2, pp. 122–134, 1973.

[30] F. S. Jones, M. Orcutt, and R. B. Little, "Vibrios (Vibrio jejuni, N.SP.) associated with intestinal disorders of cows and calves," *Journal of Experimental Medicine*, vol. 53, no. 6, pp. 853–863, 1931.

[31] E. Eltzov and R. S. Marks, "Fiber-optic based cell sensors," in *Whole Cell Sensing Systems I* (S. Belkin and B. M. Gu, eds.), ch. Fiber-Opti, pp. 131–154, Berlin, Heidelberg: Springer Berlin Heidelberg, 2009.

[32] P. J. Conroy, S. Hearty, P. Leonard, and R. J. O'Kennedy, "Antibody production, design and use for biosensor-based applications," *Seminars in Cell and Developmental Biology*, vol. 20, no. 1, pp. 10–26, 2009.

[33] J. A. Goode, J. V. Rushworth, and P. A. Millner, "Biosensor regeneration: a review of common techniques and outcomes," *Langmuir*, vol. 31, no. 23, pp. 6267–6276, 2015.

[34] T. Vo-Dinh and B. Cullum, "Biosensors and biochips: advances in biological and medical diagnostics," *Fresenius' Journal of Analytical Chemistry*, vol. 366, no. 6-7, pp. 540–551, 2000.

[35] P. S. Bisen, *Laboratory Protocols in Applied Life Sciences*. CRC Press, 2014.

[36] F. J. Bolton, D. Coates, P. M. Hinchliffe, and L. Robertson, "Comparison of selective media for isolation of Campylobacter jejuni/coli," *Journal of Clinical Pathology*, vol. 36, no. 1, pp. 78–83, 1983.

[37] P. Dekeyser, M. Gossuin-Detrain, J. P. Butzler, and J. Sternon, "Acute enteritis due to related vibrio: first positive stool cultures," *Journal of Infectious Diseases*, vol. 125, no. 4, pp. 390–392, 1972.

[38] F. J. Bolton, D. N. Hutchinson, and D. Coates, "Blood-free selective medium for isolation of Campylobacter jejuni from feces," *Journal of Clinical Microbiology*, vol. 19, no. 2, pp. 169–171, 1984.

[39] P. Leonard, S. Hearty, J. Brennan, L. Dunne, J. Quinn, T. Chakraborty, and R. O'Kennedy, "Advances in biosensors for detection of pathogens in food and water," *Enzyme and Microbial Technology*, vol. 32, no. 1, pp. 3–13, 2003.

[40] F. J. Merino, A. Agulla, P. A. Villasante, A. Diaz, J. V. Saz, and A. C. Velasco, "Comparative efficacy of 7 selective media for isolating Campylobacter jejuni," *Journal of Clinical Microbiology*, vol. 24, no. 3, pp. 451–452, 1986.

[41] C. A. Reddy, T. J. Beveridge, J. A. Breznak, G. A. Marzluf, T. M. Schmidt, and L. R. Snyder, *Methods for general and molecular microbiology*. American Society for Microbiology (ASM), 3rd ed., 2007.

[42] A. E. Yousef, "Detection of bacterial pathogens in different matrices: current practices and challenges," in *Principles of Bacterial Detection: Biosensors, Recognition Receptors and Microsystems* (M. Zourob, S. Elwary, and A. Turner, eds.), ch. 3, pp. 31–48, New York, NY: Springer New York, 2008.

[43] W. Rogers, "Steam and dry heat sterilization of biomaterials and medical devices," in *Sterilisation of Biomaterials and Medical Devices* (S. Lerouge and A. Simmons, eds.), ch. 2, pp. 20–55, Woodhead Publishing, 2012.

[44] C. L. Baylis, S. MacPhee, K. W. Martin, T. J. Humphrey, and R. P. Betts, "Comparison of three enrichment media for the isolation of Campylobacter spp. from foods.," *Journal of applied microbiology*, vol. 89, no. 5, pp. 884–91, 2000.

[45] F. Jorgensen, R. Bailey, S. Williams, P. Henderson, D. R. Wareing, F. J. Bolton, J. A. Frost, L. Ward, and T. J. Humphrey, "Prevalence and numbers of Salmonella and Campylobacter spp. on raw, whole chickens in relation to

sampling methods," *International Journal of Food Microbiology*, vol. 76, no. 1-2, pp. 151–164, 2002.

[46] P. Wood, *Understanding immunology*. Prentice Hall, 2001.

[47] J. R. Crowther, *ELISA*, vol. 42. New Jersey: Humana Press, 1995.

[48] P. Mandal, A. Biswas, K. Choi, and U. Pal, "Methods for rapid detection of foodborne pathogens: an overview," *American Journal of Food Technology*, vol. 6, no. 2, pp. 87–102, 2011.

[49] T. R. Holford, F. Davis, and S. P. Higson, "Recent trends in antibody based sensors," *Biosensors and Bioelectronics*, vol. 34, no. 1, pp. 12–24, 2012.

[50] E. Engvall and P. Perlmann, "Enzyme-linked immunosorbent assay (ELISA) quantitative assay of immunoglobulin G," *Immunochemistry*, vol. 8, no. 9, pp. 871–874, 1971.

[51] E. Engvall, "The ELISA, Enzyme-Linked Immunosorbent Assay," *Clinical Chemistry*, vol. 56, no. 2, pp. 319–320, 2010.

[52] S. Avrameas, "Enzyme markers: their linkage with proteins and use in immunohistochemistry," *The Histochemical Journal*, vol. 4, no. 4, pp. 321–330, 1972.

[53] J. Daintith, *Dictionary of Chemistry*. Oxford University Press, 6th ed., 2006.

[54] S. Aydin, "A short history, principles, and types of ELISA, and our laboratory experience with peptide/protein analyses using ELISA," *Peptides*, vol. 72, pp. 4–15, 2015.

[55] M. Magliulo, P. Simoni, M. Guardigli, E. Michelini, M. Luciani, R. Lelli, and A. Roda, "A rapid multiplexed chemiluminescent immunoassay for the detection of Escherichia coli O157:H7, Yersinia enterocolitica, Salmonella typhimurium, and Listeria monocytogenes pathogen bacteria," *Journal of Agricultural and Food Chemistry*, vol. 55, no. 13, pp. 4933–4939, 2007.

[56] L. Lilja and M. L. Hänninen, "Evaluation of a commercial automated ELISA and PCR-method for rapid detection and identification of Campylobacter jejuni and C. coli in poultry products," *Food Microbiology*, vol. 18, no. 2, pp. 205–209, 2001.

[57] V. Hinić, I. Brodard, A. Thomann, M. Holub, R. Miserez, and C. Abril, "IS711-based real-time PCR assay as a tool for detection of Brucella spp. in wild boars and comparison with bacterial isolation and serology," *BMC Veterinary Research*, vol. 5, pp. 1–8, 2009.

[58] Y. Che, Y. Li, and M. Slavik, "Detection of Campylobacter jejuni in poultry samples using an enzyme-linked immunoassay coupled with an enzyme electrode," *Biosensors and Bioelectronics*, vol. 16, no. 9-12, pp. 791–797, 2001.

[59] I. Hochel, D. Slavíčková, D. Viochna, J. Škvor, and I. Steinhauserová, "Detection of Campylobacter species in foods by indirect competitive ELISA using hen and rabbit antibodies," *Food and Agricultural Immunology*, vol. 18, no. 3-4, pp. 151–167, 2007.

[60] I. Hochel, D. Viochna, J. Skvor, and M. Musil, "Development of an indirect competitive ELISA for detection of Campylobacter jejuni subsp.jejuni O:23 in foods.," *Folia Microbiologica*, vol. 49, no. 5, pp. 579–86, 2004.

[61] J. Moldenhauer, "Overview of rapid microbiological methods," in *Principles of Bacterial Detection: Biosensors, Recognition Receptors and Microsystems* (M. Zourob, S. Elwary, and A. Turner, eds.), ch. 4, pp. 49–79, New York, NY: Springer New York, 2008.

[62] E. A. Mothershed and A. M. Whitney, "Nucleic acid-based methods for the detection of bacterial pathogens: present and future considerations for the clinical laboratory," *Clinica Chimica Acta*, vol. 363, no. 1-2, pp. 206–220, 2006.

[63] W. A. Day and I. A. N. L. Pepper, "Use of an arbitrarily primed PCR product in the development of a Campylobacter jejuni-specific PCR," *Applied and Environmental Microbiology*, vol. 63, no. 3, pp. 1019–1023, 1997.

[64] K. Mullis, F. Faloona, S. Scharf, R. Saiki, G. Horn, and H. Erlich, "Specific enzymatic amplification of DNA in vitro: the polymerase chain reaction," *Cold Spring Harbor Symposia on Quantitative Biology*, vol. 51, pp. 263–273, 1986.

[65] S. Toze, "PCR and the detection of microbial pathogens in water and wastewater," *Water Research*, vol. 33, no. 17, pp. 3545–3556, 1999.

[66] D. K. Winters, A. E. O'leary, and M. F. Slavik, "Polymerase chain reaction for rapid detection of Campylobacter jejuni in artificially contaminated foods," *Letters in Applied Microbiology*, vol. 27, no. 3, pp. 163–167, 1998.

[67] L. K. Ng, C. I. Bin Kingombe, W. Yan, D. E. Taylor, K. Hiratsuka, N. Malik, and M. M. Garcia, "Specific detection and confirmation of Campylobacter jejuni by DNA hybridization and PCR," *Applied and Environmental Microbiology*, vol. 63, no. 11, pp. 4558–4563, 1997.

[68] M. T. Herdman, D. Wyncoll, E. Halligan, P. R. Cliff, G. French, and J. D. Edgeworth, "Clinical application of real-time PCR to screening critically ill and emergency-care surgical patients for methicillin-resistant Staphylococcus aureus: a quantitative analytical study," *Journal of Clinical Microbiology*, vol. 47, no. 12, pp. 4102–4108, 2009.

[69] LabX, "Applied Biosystems QuantStudio 3 Real Time PCR." https://www.labx.com/item/applied-biosystems-quantstudio-3-real-time-pcr/4363374, Date Accessed: 28/10/2018.

[70] LabX, "Fluidigm high-throughput PCR system Biomark HD." https://www.labx.com/item/fluidigm-biomark-hd/LV37457873, Date Accessed: 28/10/2018.

[71] S. S. Iqbal, M. W. Mayo, J. G. Bruno, B. V. Bronk, C. A. Batt, and J. P. Chambers, "A review of molecular recognition technologies for detection of biological threat agents," *Biosensors and Bioelectronics*, vol. 15, no. 11-12, pp. 549–578, 2000.

[72] S. Arora, R. K. Agarwal, and B. Bist, "Comparison of ELISA and PCR vis-à-vis cultural methods for detecting Aeromonas spp. in foods of animal origin," *International Journal of Food Microbiology*, vol. 106, no. 2, pp. 177–183, 2006.

[73] L. Potucková, F. Franko, M. Bambousková, and P. Dráber, "Rapid and sensitive detection of cytokines using functionalized gold nanoparticle-based immuno-PCR, comparison with immuno-PCR and ELISA," *Journal of Immunological Methods*, vol. 371, no. 1-2, pp. 38–47, 2011.

[74] M. Madou and M. J. Tierney, "Required technology breakthroughs to assume widely accepted biosensors," *Applied Biochemistry and Biotechnology*, vol. 41, no. 1-2, pp. 109–128, 1993.

[75] B. Lee, "Review of the present status of optical fiber sensors," *Optical Fiber Technology*, vol. 9, no. 2, pp. 57–79, 2003.

[76] D. K. Soni, R. Ahmad, and S. K. Dubey, "Biosensor for the detection of Listeria monocytogenes: emerging trends," *Critical Reviews in Microbiology*, vol. 44, no. 5, pp. 590–608, 2018.

[77] A. Ramanavičius, A. Ramanavičiene, and A. Malinauskas, "Electrochemical sensors based on conducting polymer-polypyrrole," *Electrochimica Acta*, vol. 51, no. 27, pp. 6025–6037, 2006.

[78] O. S. Wolfbeis, "Analytical chemistry with optical sensors," *Fresenius' Zeitschrift für analytische Chemie*, vol. 325, no. 4, pp. 387–392, 1986.

[79] O. Pashchenko, T. Shelby, T. Banerjee, and S. Santra, "A Comparison of Optical, Electrochemical, Magnetic, and Colorimetric Point-of-Care Biosensors for Infectious Disease Diagnosis," *ACS Infectious Diseases*, vol. 4, no. 8, pp. 1162–1178, 2018.

[80] H. M. Shapiro, *Practical flow cytometry*. Hoboken, NJ, USA: John Wiley & Sons, Inc., 4th ed., 2003.

[81] H. M. Shapiro, "The evolution of cytometers," *Cytometry*, vol. 58A, no. 1, pp. 13–20, 2004.

[82] S. Ibrahim and G. van den Engh, "Flow cytometry and cell sorting," in *Cell Separation* (A. Kumar, I. Y. Galaev, and B. Mattiasson, eds.), vol. 106, pp. 19–39, Springer Berlin Heidelberg, 2007.

[83] P. F. Mixter, J. D. Klena, G. A. Flom, A. M. Siegesmund, and M. E. Konkel, "In vivo tracking of Campylobacter jejuni by using a novel recombinant expressing green fluorescent protein.," *Applied and environmental microbiology*, vol. 69, no. 5, pp. 2864–74, 2003.

[84] M. G. Ormerod, *Flow cytometry - a basic introduction.* De Novo Software, 2008.

[85] J. Chen and M. W. Griffiths, "Salmonella detection in eggs using LuX+ bacteriophages," *Journal of Food Protection*, vol. 59, no. 9, pp. 908–914, 1996.

[86] S. Fukuda, H. Tatsumi, S. Igimi, and S. Yamamoto, "Improved bioluminescent enzyme immunoassay for the rapid detection of salmonella in chicken meat samples," *Letters in Applied Microbiology*, vol. 41, no. 5, pp. 379–384, 2005.

[87] I. Kassem, Y. Sanad, D. Gangaiah, M. Lilburn, J. LeJeune, and G. Rajashekara, "Use of bioluminescence imaging to monitor campylobacter survival in chicken litter," *Journal of Applied Microbiology*, vol. 109, no. 6, pp. 1988–1997, 2010.

[88] F. P. Mathew, D. Alagesan, and E. C. Alocilja, "Chemiluminescence detection of Escherichia coli in fresh produce obtained from different sources," *Luminescence*, vol. 19, no. 4, pp. 193–198, 2004.

[89] L. K. Ng, D. E. Taylor, and M. E. Stiles, "Estimation of Campylobacter spp. in broth culture by bioluminescence assay of ATP," *Applied and Environmental Microbiology*, vol. 49, no. 3, pp. 730–731, 1985.

[90] E. Diesel, M. Schreiber, and J. R. Van Der Meer, "Development of bacteria-based bioassays for arsenic detection in natural waters," *Analytical and Bioanalytical Chemistry*, vol. 394, no. 3, pp. 687–693, 2009.

[91] S. Tauriainen, M. Karp, W. Chang, and M. Virta, "Luminescent bacterial sensor for cadmium and lead," *Biosensors and Bioelectronics*, vol. 13, no. 9, pp. 931–938, 1998.

[92] B. M. Willardson, J. F. Wilkins, T. A. Rand, J. M. Schupp, K. K. Hill, P. Keim, and P. J. Jackson, "Development and testing of a bacterial biosensor for toluene-based environmental contaminants," *Applied and Environmental Microbiology*, vol. 64, no. 3, pp. 1006–1012, 1998.

[93] G. Shama and D. J. Malik, "The uses and abuses of rapid bioluminescence-based ATP assays," *International Journal of Hygiene and Environmental Health*, vol. 216, no. 2, pp. 115–125, 2013.

[94] A. Roda, M. Mirasoli, E. Michelini, M. Di Fusco, M. Zangheri, L. Cevenini, B. Roda, and P. Simoni, "Progress in chemical luminescence-based biosensors: a critical review," *Biosensors and Bioelectronics*, vol. 76, pp. 164–179, 2016.

[95] T. Kahlke and K. D. Umbers, "Bioluminescence," *Current Biology*, vol. 26, no. 8, pp. R313–R314, 2016.

[96] J. Lee, "Bioluminescence: the first 3000 years (review)," *Journal of Siberian Federal University, Biology*, vol. 1, no. 2008 1, pp. 194–205, 2008.

[97] R. Boyle, "New experiments concerning the relation between light and air (in shining wood and fish)," *Philosophical Transactions (1665-1678) of The Royal Society*, vol. 2, pp. 581–600, 1667.

[98] L. Farris, M. Y. Habteselassie, L. Perry, Y. Chen, R. Turco, B. Reuhs, and B. Applegate, "Luminescence techniques for the detection of bacterial pathogens," in *Principles of Bacterial Detection: Biosensors, Recognition Receptors and Microsystems* (M. Zourob, S. Elwary, and A. P. F. Turner, eds.), ch. 10, pp. 213–230, New York, NY: Springer New York, 2008.

[99] E. Chappelle and G. Levin, "Use of the firefly bioluminescent reaction for rapid detection and counting of bacteria," *Biochemical Medicine*, vol. 2, no. 1, pp. 41–52, 1968.

[100] K. Wills, "ATP bioluminescence and its use in pharmaceutical microbiology," in *Rapid Microbiological Methods in the Pharmaceutical Industry* (M. C. Easter, ed.), ch. 6, p. 10, CRC Press, 1st ed., 2003.

[101] J. Li, G. L. Kolling, K. R. Matthews, and M. L. Chikindas, "Cold and carbon dioxide used as multi-hurdle preservation do not induce appearance of viable but non-culturable Listeria monocytogenes," *Journal of Applied Microbiology*, vol. 94, no. 1, pp. 48–53, 2003.

[102] B. J. Cheek, A. B. Steel, M. P. Torres, Y.-Y. Y. Yu, and H. Yang, "Chemiluminescence detection for hybridization assays on the flow-thru chip, a three-dimensional microchannel biochip.," *Analytical Chemistry*, vol. 73, no. 24, pp. 5777–5783, 2001.

[103] J. Homola and M. Piliarik, "Surface plasmon resonance (SPR) sensors," in *Surface Plasmon Resonance Based Sensors* (J. Homola, ed.), ch. 2, pp. 45–67, Springer-Verlag Berlin Heidelberg, 2006.

[104] J. Homola, *Surface plasmon resonance based sensors*, vol. 4 of *Springer Series on Chemical Sensors and Biosensors*. Springer Berlin Heidelberg, 2006.

[105] A. Sharma, R. Jha, and B. Gupta, "Fiber-optic sensors based on surface plasmon resonance: a comprehensive review," *Sensors Journal, IEEE*, vol. 7, no. 8, pp. 1118–1129, 2007.

[106] J. Zenneck, "Über die Fortpflanzung ebener elektromagnetischer Wellen längs einer ebenen Leiterfläche und ihre Beziehung zur drahtlosen Telegraphie," *Annalen der Physik*, vol. 328, no. 10, pp. 846–866, 1907.

[107] B. Liedberg, C. Nylander, and I. Lunström, "Surface plasmon resonance for gas detection and biosensing," *Sensors and Actuators*, vol. 4, no. C, pp. 299–304, 1983.

[108] J. Homola, "Electromagnetic theory of surface plasmons," in *Surface Plasmon Resonance Based Sensors* (J. Homola, ed.), ch. 1, pp. 3–44, Springer-Verlag Berlin Heidelberg, 2006.

[109] X. Fan, I. M. White, S. I. Shopova, H. Zhu, J. D. Suter, and Y. Sun, "Sensitive optical biosensors for unlabeled targets: A review," *Analytica Chimica Acta*, vol. 620, no. 1-2, pp. 8–26, 2008.

[110] J. Homola, I. Koudela, and S. S. Yee, "Surface plasmon resonance sensors based on diffraction gratings and prism couplers: sensitivity comparison," *Sensors and Actuators B: Chemical*, vol. 54, no. 1-2, pp. 16–24, 1999.

[111] J. Homola, "Present and future of surface plasmon resonance biosensors," *Analytical and Bioanalytical Chemistry*, vol. 377, no. 3, pp. 528–539, 2003.

[112] B. Liedberg, C. Nylander, and I. Lundström, "Biosensing with surface plasmon resonance - how it all started," *Biosensors and Bioelectronics*, vol. 10, no. 8, pp. i–ix, 1995.

[113] E. Kretschmann and H. Raether, "Radiative decay of non radiative surface plasmons excited by light," *Zeitschrift fur Naturforschung - Section A Journal of Physical Sciences*, vol. 23, no. 12, pp. 2135–2136, 1968.

[114] A. Otto, "Excitation of nonradiative surface plasma waves in silver by the method of frustrated total reflection," *Zeitschrift für Physik A Hadrons and nuclei*, vol. 216, no. 4, pp. 398–410, 1968.

[115] J. Homola, S. S. Yee, and G. Gauglitz, "Surface plasmon resonance sensors: review," *Sensors and Actuators B: Chemical*, vol. 54, no. 1-2, pp. 3–15, 1999.

[116] A. D. Taylor, Q. Yu, S. Chen, J. Homola, and S. Jiang, "Comparison of E. coli O157:H7 preparation methods used for detection with surface plasmon resonance sensor," *Sensors and Actuators, B: Chemical*, vol. 107, no. 1 Spec. Iss., pp. 202–208, 2005.

[117] A. D. Taylor, J. Ladd, Q. Yu, S. Chen, J. Homola, and S. Jiang, "Quantitative and simultaneous detection of four foodborne bacterial pathogens with a multi-channel SPR sensor," *Biosensors and Bioelectronics*, vol. 22, no. 5, pp. 752–758, 2006.

[118] N. Masdor, Z. Altintas, and I. Tothill, "Surface plasmon resonance immunosensor for the detection of Campylobacter jejuni," *Chemosensors*, vol. 5, no. 2, p. 16, 2017.

[119] M. Zourob, N. Skivesen, R. Horvath, S. Mohr, M. B. McDonnell, and N. J. Goddard, "Integrated deep-probe optical waveguides for label free bacterial detection," in *Principles of Bacterial Detection: Biosensors, Recognition Receptors and Microsystems* (M. Zourob, S. Elwary, and A. Turner, eds.), pp. 139–168, New York, NY: Springer New York, 2007.

[120] J. Hetch, *City of light: the story of fiber optics*. Oxford University Press, 1999.

[121] E. Hecht, *Optics*. Addison-Wesley, 1998.

[122] S. Lecler and P. Meyrueis, "Intrinsic optical fiber sensor," in *Fiber Optic Sensors* (M. Yasin, S. W. Harun, and H. Arof, eds.), ch. 3, pp. 53–76, InTech, 2012.

[123] H. F. Wolf, *Handbook of fiber optics: theory and applications*, vol. 1. 1979.

[124] J.-P. Goure and I. Verrier, *Optical fibre devices*. Institute of Physics Publishing, 2001.

[125] A. Leung, P. M. Shankar, and R. Mutharasan, "A review of fiber-optic biosensors," *Sensors and Actuators B: Chemical*, vol. 125, no. 2, pp. 688–703, 2007.

[126] R. Narayanaswamy, "Current developments in optical biochemical sensors," *Biosensors and Bioelectronics*, vol. 6, no. 6, pp. 467–475, 1991.

[127] Z. Tian, A. J. Nelson, S. Afroz, V. Srinivasaraghavan, M. Akbar, Z. Li, A. Wang, and M. Agah, "Miniature self-calibrated fiber optic tip temperature and pressure sensor," in *2015 IEEE SENSORS*, pp. 3–6, 2015.

[128] A. Wang, H. Xiao, J. Wang, Z. Wang, W. Zhao, and R. G. May, "Self-calibrated interferometric-intensity-based optical fiber sensors," *Journal of Lightwave Technology*, vol. 19, no. 10, pp. 1495–1501, 2001.

[129] W. Wu, P. Rezai, H. Hsu, and P. Selvaganapathy, "Materials and methods for the microfabrication of microfluidic biomedical devices," in *Microfluidic Devices for Biomedical Applications* (L. Xiujun James and Y. Zhou, eds.), ch. 1, pp. 3–62, Woodhead Publishing Limited, 1st ed., 2013.

[130] D. W. Lübbers and N. Opitz, "Die pCO2-/pO2-optode: eine neue p CO2- bzw. pO2-meßsonde zur messung des pCO2 oder pO2 von gasen und flüssigkeiten / The pCO2-/pO2-optode: a new probe for measurement of pCO2 or pO2 in fluids and gases," *Zeitschrift für Naturforschung C*, vol. 30, no. 7-8, pp. 532–533, 1975.

[131] K. O. Hill, Y. Fujii, D. C. Johnson, and B. S. Kawasaki, "Photosensitivity in optical fiber waveguides: Application to reflection filter fabrication," *Applied Physics Letters*, vol. 32, no. 10, pp. 647–649, 1978.

[132] G. Meltz, W. W. Morey, and W. H. Glenn, "Formation of Bragg gratings in optical fibers by a transverse holographic method," *Optics Letters*, vol. 14, no. 15, p. 823, 1989.

[133] A. M. Vengsarkar, P. J. Lemaire, J. B. Judkins, V. Bhatia, T. Erdogan, and J. E. Sipe, "Long-period fiber gratings as band-rejection filters," *Journal of Lightwave Technology*, vol. 14, no. 1, pp. 58–64, 1996.

[134] A. Kersey, M. Davis, H. Patrick, M. LeBlanc, K. Koo, C. Askins, M. Putnam, and E. Friebele, "Fiber grating sensors," *Journal of Lightwave Technology*, vol. 15, no. 8, pp. 1442–1463, 1997.

[135] M. P. DeLisa, Z. Zhang, M. Shiloach, S. Pilevar, C. C. Davis, J. S. Sirkis, and W. E. Bentley, "Evanescent wave long-period fiber bragg grating as an immobilized antibody biosensor," *Analytical Chemistry*, vol. 72, no. 13, pp. 2895–2900, 2000.

[136] J. Goicoechea, M. Hernáez, C. Zamarreño, and F. Arregui, "Coatings for optical fiber sensors," in *Comprehensive Materials Processing*, vol. 13, pp. 103–119, Elsevier, 2014.

[137] S. W. James and R. P. Tatam, "Optical fibre long-period grating sensors: characteristics and application," *Measurement Science and Technology*, vol. 14, no. 5, pp. R49–R61, 2003.

[138] E. Lindner, M. Becker, M. Rothhardt, and H. Bartelt, "Generation and characterization of first order fiber Bragg gratings with Bragg wavelengths in the visible spectral range," *Optics Communications*, vol. 281, no. 18, pp. 4612–4615, 2008.

[139] E. Chehura, C. C. Ye, S. E. Staines, S. W. James, and R. P. Tatam, "Characterization of the response of fibre Bragg gratings fabricated in stress and geometrically induced high birefringence fibres to temperature and transverse load," *Smart Materials and Structures*, vol. 13, no. 4, pp. 888–895, 2004.

[140] Y. J. Rao, "Recent progress in applications of in-fibre Bragg grating sensors," *Optics and Lasers in Engineering*, vol. 31, no. 4, pp. 297–324, 1999.

[141] B. N. Shivananju, M. Renilkumar, G. R. Prashanth, S. Asokan, and M. M. Varma, "Detection limit of etched fiber Bragg grating sensors," *Journal of Lightwave Technology*, vol. 31, no. 14, pp. 2441–2447, 2013.

[142] C. J. Stanford, G. Ryu, M. Dagenais, M. T. Hurley, K. J. Gaskell, and P. DeShong, "Covalent attachment of carbohydrate derivatives to an evanescent wave fiber Bragg grating biosensor," *Journal of Sensors*, vol. 2009, pp. 1–7, 2009.

[143] E. Chehura, S. W. James, and R. P. Tatam, "Temperature and strain discrimination using a single tilted fibre Bragg grating," *Optics Communications*, vol. 275, no. 2, pp. 344–347, 2007.

[144] V. Mishra, N. Singh, U. Tiwari, and P. Kapur, "Fiber grating sensors in medicine: current and emerging applications," *Sensors and Actuators A: Physical*, vol. 167, no. 2, pp. 279–290, 2011.

[145] K. Zhou, X. Chen, L. Zhang, and I. Bennion, "High-sensitivity optical chemsensor based on etched D-fibre Bragg gratings," *Electronics Letters*, vol. 40, no. 4, p. 232, 2004.

[146] F. Baldini, M. Brenci, F. Chiavaioli, a. Giannetti, and C. Trono, "Optical fibre gratings as tools for chemical and biochemical sensing," *Analytical and Bioanalytical Chemistry*, vol. 402, no. 1, pp. 109–116, 2012.

[147] D. P. Campbell, "Interferometric biosensors," in *Principles of Bacterial Detection: Biosensors, Recognition Receptors and Microsystems* (M. Zourob, S. Elwary, and A. Turner, eds.), pp. 169–211, New York, NY: Springer, 2008.

[148] X. Dong, H. Zhang, B. Liu, and Y. Miao, "Tilted fiber bragg gratings: Principle and sensing applications," *Photonic Sensors*, vol. 1, no. 1, pp. 6–30, 2011.

[149] B. Luo, Y. Xu, S. Wu, M. Zhao, P. Jiang, S. Shi, Z. Zhang, Y. Wang, L. Wang, and Y. Liu, "A novel immunosensor based on excessively tilted fiber grating coated with gold nanospheres improves the detection limit of Newcastle disease virus," *Biosensors and Bioelectronics*, vol. 100, pp. 169–175, 2018.

[150] X. Chen, "Optical fibre gratings for chemical and bio-sensing," in *Current Developments in Optical Fiber Technology* (S. W. Harun and H. Arof, eds.), vol. I, ch. 8, pp. 205–235, InTech, 2013.

[151] T. Guo, F. Liu, B. O. Guan, and J. Albert, "Tilted fiber grating mechanical and biochemical sensors," *Optics and Laser Technology*, vol. 78, pp. 19–33, 2016.

[152] T. Guo, F. Liu, X. Liang, X. Qiu, Y. Huang, C. Xie, P. Xu, W. Mao, B. O. Guan, and J. Albert, "Highly sensitive detection of urinary protein variations using tilted fiber grating sensors with plasmonic nanocoatings," *Biosensors and Bioelectronics*, vol. 78, pp. 221–228, 2016.

[153] C. Ribaut, M. Loyez, J. C. Larrieu, S. Chevineau, P. Lambert, M. Remmelink, R. Wattiez, and C. Caucheteur, "Cancer biomarker sensing using packaged plasmonic optical fiber gratings: Towards in vivo diagnosis," *Biosensors and Bioelectronics*, vol. 92, no. October 2016, pp. 449–456, 2017.

[154] J. R. Guzman-Sepulveda, J. G. Aguilar-Soto, M. Torres-Cisneros, O. G. Ibarra-Manzano, and D. A. May-Arrioja, "Measurement of curvature and temperature using multimode interference devices," in *22nd Congress of the International Commission for Optics: Light for the Development of the World* (R. Rodríguez-Vera and R. Díaz-Uribe, eds.), p. 80115P, 2011.

[155] C. Zhao, L. Ye, X. Yu, and J. Ge, "Continuous fuel level sensor based on spiral side-emitting optical fiber," *Journal of Control Science and Engineering*, vol. 2012, pp. 1–8, 2012.

[156] S. T. Oh, W. T. Han, U. C. Paek, and Y. Chung, "Azimuthally symmetric long-period fiber gratings fabricated with CO2 laser," *Microwave and Optical Technology Letters*, vol. 41, no. 3, pp. 188–190, 2004.

[157] E. Brzozowska, M. Śmietana, M. Koba, S. Górska, K. Pawlik, A. Gamian, and W. J. Bock, "Recognition of bacterial lipopolysaccharide using bacteriophage-adhesin-coated long-period gratings," *Biosensors and Bioelectronics*, vol. 67, pp. 93–99, 2015.

[158] M. Koba, M. Smietana, E. Brzozowska, S. Gorska, M. Janik, P. Mikulic, A. Cusano, and W. J. Bock, "Bacteriophage adhesin-coated long-period grating-based sensor: bacteria detection specificity," *Journal of Lightwave Technology*, vol. 34, no. 19, pp. 4531–4536, 2016.

[159] M. Smietana, W. J. Bock, P. Mikulic, A. Ng, R. Chinnappan, and M. Zourob, "Detection of bacteria using bacteriophages as recognition elements immobilized on long-period fiber gratings.," *Optics Express*, vol. 19, no. 9, pp. 7971–7978, 2011.

[160] A. B. Bandara, Z. Zuo, S. Ramachandran, A. Ritter, J. R. Heflin, and T. J. Inzana, "Detection of methicillin-resistant staphylococci by biosensor assay consisting of nanoscale films on optical fiber long-period gratings," *Biosensors and Bioelectronics*, vol. 70, pp. 433–440, 2015.

[161] S. Korposh, S. James, R. Tatam, and S.-w. Lee, "Optical fibre long-period gratings functionalised with nano-assembled thin films: approaches to chemical sensing," in *Current Trends in Short- and Long-period Fiber Gratings* (C. Cuadrado-Laborde, ed.), ch. 4, pp. 63–86, InTech, 2013.

[162] G. Quero, M. Consales, R. Severino, P. Vaiano, A. Boniello, A. Sandomenico, M. Ruvo, A. Borriello, L. Diodato, S. Zuppolini, M. Giordano, I. C. Nettore, C. Mazzarella, A. Colao, P. E. Macchia, F. Santorelli, A. Cutolo, and A. Cusano, "Long period fiber grating nano-optrode for cancer biomarker detection," *Biosensors and Bioelectronics*, vol. 80, pp. 590–600, 2016.

[163] L. Qi, C. L. Zhao, J. Yuan, M. Ye, J. Wang, Z. Zhang, and S. Jin, "Highly reflective long period fiber grating sensor and its application in refractive index sensing," *Sensors and Actuators, B: Chemical*, vol. 193, pp. 185–189, 2014.

[164] G. Quero, S. Zuppolini, M. Consales, L. Diodato, P. Vaiano, A. Venturelli, M. Santucci, F. Spyrakis, M. Costi, M. Giordano, A. Borriello, A. Cutolo, and A. Cusano, "Long period fiber grating working in reflection mode as valuable biosensing platform for the detection of drug resistant bacteria," *Sensors and Actuators B: Chemical*, vol. 230, pp. 510–520, 2016.

[165] K. Fukuda, M. Tachikawa, and M. Kinoshita, "Allan-variance measurements of diode laser frequency-stabilized with a thin vapor cell," *Applied Physics B: Lasers and Optics*, vol. 77, no. 8, pp. 823–827, 2003.

[166] J. Homola, "Surface plasmon resonance sensors for detection of chemical and biological species," *Chemical Reviews*, vol. 108, no. 2, pp. 462–493, 2008.

[167] N. D. Rees, S. W. James, R. P. Tatam, and G. J. Ashwell, "Optical fiber long-period gratings with Langmuir–Blodgett thin-film overlays," *Optics Letters*, vol. 27, no. 9, p. 686, 2002.

[168] R. Y. N. Wong, E. Chehura, S. E. Staines, S. W. James, and R. P. Tatam, "Fabrication of fiber optic long period gratings operating at the phase matching

turning point using an ultraviolet laser.," *Applied Optics*, vol. 53, no. 21, pp. 4669–74, 2014.

[169] T. Erdogan, "Cladding-mode resonances in short- and long-period fiber grating filters," *Journal of the Optical Society of America A*, vol. 17, no. 11, pp. 2113–2113, 2000.

[170] T. Erdogan, "Cladding-mode resonances in short- and long-period fiber grating filters: errata," *Journal of the Optical Society of America A*, vol. 17, no. 11, pp. 2113–2113, 2000.

[171] D. Gloge, "Weakly guiding fibers," *Applied Optics*, vol. 10, no. 10, p. 2252, 1971.

[172] S. W. James, C. S. Cheung, and R. P. Tatam, "Experimental observations on the response of 1st and 2nd order fibre optic long period grating coupling bands to the deposition of nanostructured coatings.," *Optics Express*, vol. 15, no. 20, pp. 13096–13107, 2007.

[173] V. Bhatia, "Applications of long-period gratings to single and multi-parameter sensing.," *Optics Express*, vol. 4, no. 11, pp. 457–466, 1999.

[174] X. Shu, L. Zhang, and I. Bennion, "Fabrication and characterisation of ultra-long-period fibre gratings," *Optics Communications*, vol. 203, no. 3-6, pp. 277–281, 2002.

[175] C. S. Cheung, S. M. Topliss, S. W. James, and R. P. Tatam, "Response of fiber-optic long-period gratings operating near the phase-matching turning point to the deposition of nanostructured coatings," *Journal of the Optical Society of America B*, vol. 25, no. 6, p. 897, 2008.

[176] L. Marques, F. Hernandez, S. James, S. Morgan, M. Clark, R. Tatam, and S. Korposh, "Highly sensitive optical fibre long period grating biosensor anchored with silica core gold shell nanoparticles," *Biosensors and Bioelectronics*, vol. 75, pp. 222–231, 2016.

[177] M. Verhaegen, P. Orsini, D. Perron, X. Daxhelet, and S. Lacroix, "Long-period grating fabrication techniques," in *Applications of Photonic Technology* (R. A. Lessard and G. A. Lampropoulos, eds.), vol. 4087, pp. 156–161, 2000.

[178] A. Martinez-Rios, D. Monzon-Hernandez, I. Torres-Gomez, and G. Salceda-Delgado, "Long period fibre gratings," in *Fiber Optic Sensors* (M. Yasin, S. W. Harun, and H. Arof, eds.), ch. 11, pp. 275–294, InTech, 2012.

[179] Y. Wang, "Review of long period fiber gratings written by CO2 laser," *Journal of Applied Physics*, vol. 108, no. 8, 2010.

[180] G. Rego, P. V. S. Marques, J. L. Santos, and H. M. Salgado, "Arc-induced long-period gratings," *Fiber and Integrated Optics*, vol. 24, no. 3-4, pp. 245–259, 2005.

[181] Y. Kondo, K. Nouchi, T. Mitsuyu, M. Watanabe, P. G. Kazansky, and K. Hirao, "Fabrication of long-period fiber gratings by focused irradiation of infrared femtosecond laser pulses," *Optics Letters*, vol. 24, no. 10, p. 646, 1999.

[182] S. Savin, M. J. F. Digonnet, G. S. Kino, and H. J. Shaw, "Tunable mechanically induced long-period fiber gratings," *Optics Letters*, vol. 25, no. 10, p. 710, 2000.

[183] L. Su, K. S. Chiang, and C. Lu, "Microbend-induced mode coupling in a graded-index multimode fiber," *Applied Optics*, vol. 44, no. 34, p. 7394, 2005.

[184] Chunn-Yenn Lin, Lon A. Wang, and Gia-Wei Chern, "Corrugated long-period fiber gratings as strain, torsion, and bending sensors," *Journal of Lightwave Technology*, vol. 19, no. 8, pp. 1159–1168, 2001.

[185] M. Fujimaki, Y. Ohki, J. L. Brebner, and S. Roorda, "Fabrication of long-period optical fiber gratings by use of ion implantation," *Optics Letters*, vol. 25, no. 2, p. 88, 2000.

[186] B. J. O'Regan and D. N. Nikogosyan, "Femtosecond UV long-period fibre grating fabrication with amplitude mask technique," *Optics Communications*, vol. 284, no. 24, pp. 5650–5654, 2011.

[187] S. W. James, S. M. Topliss, and R. P. Tatam, "Properties of length-apodized phase-shifted LPGs operating at the phase matching turning point," *Journal of Lightwave Technology*, vol. 30, no. 13, pp. 2203–2209, 2012.

[188] M. Partridge, R. Wong, S. W. James, F. Davis, S. P. J. Higson, and R. P. Tatam, "Long period grating based toluene sensor for use with water contamination," *Sensors and Actuators B: Chemical*, vol. 203, pp. 621–625, 2014.

[189] H. Patrick, C. Askins, R. McElhanon, and E. Friebele, "Amplitude mask patterned on an excimer laser mirror for high intensity writing of long period fibre gratings," *Electronics Letters*, vol. 33, no. 13, p. 1167, 1997.

[190] W. Lu, L. Lu, F. Feng, and J. Shi, "Low-cost amplitude mask for long-period grating fabrication," *Optik*, vol. 125, no. 14, pp. 3462–3464, 2014.

[191] C. Silva, J. M. P. Coelho, P. Caldas, and P. Jorge, "Fibre sensing system based on long-period gratings for monitoring aqueous environments," in *Fiber Optic Sensors* (M. Yasin, S. W. Harun, and H. Arof, eds.), ch. 13, pp. 317–342, InTech, 2012.

[192] A. Iadicicco, D. Paladino, P. Pilla, S. Campopiano, A. Cutolo, and A. Cusano, "Long period gratings in new generation optical fibers," *Recent Progress in Optical Fiber Research*, 2012.

[193] R. Y. N. Wong, E. Chehura, S. W. James, and R. P. Tatam, "A chirped long period grating sensor for monitoring flow direction and cure of a resin," in *Proceedings of SPIE - The International Society for Optical Engineering* (K. J. Peters, W. Ecke, and T. E. Matikas, eds.), vol. 8693, p. 86930E, 2013.

[194] S. J. Buggy, E. Chehura, S. W. James, and R. P. Tatam, "Optical fibre grating refractometers for resin cure monitoring," *Journal of Optics A: Pure and Applied Optics*, vol. 9, no. 6, 2007.

[195] J. M. Estudillo-Ayala, R. I. Mata-Chávez, J. C. Hernández-García, and R. Rojas-Laguna, "Long period fiber grating produced by arc discharges," in *Fiber Optic Sensors* (M. Yasin, S. W. Harun, and H. Arof, eds.), ch. 12, pp. 295–316, InTech, 2012.

[196] Y. Wang, C. Liao, X. Zhong, J. Zhou, Y. Liu, Z. Li, G. Wang, and K. Yang, "Long period fiber gratings written in photonic crystal fibers by use of CO2 laser," *Photonic Sensors*, vol. 3, no. 3, pp. 193–201, 2013.

[197] S. A. Vasiliev and O. I. Medvedkov, "Long-period refractive index fiber gratings: properties, applications, and fabrication techniques," in *Advances in Fiber Optics* (E. M. Dianov, ed.), vol. 4083, pp. 212–223, 2000.

[198] S. Chaubey, S. Kher, J. Kishore, and S. M. Oak, "CO2 laser-inscribed low-cost, shortest-period long period fibre grating in B-Ge co-doped fibre for high-sensitivity strain measurement," *Pramana*, vol. 82, no. 2, pp. 373–377, 2014.

[199] X. Shu, L. Zhang, and I. Bennion, "Sensitivity characteristics of long-period fiber gratings," *Journal of Lightwave Technology*, vol. 20, no. 2, pp. 255–266, 2002.

[200] G. Rego, O. Okhotnikov, E. Dianov, and V. Sulimov, "High-temperature stability of long-period fiber gratings produced using an electric arc," *Journal of Lightwave Technology*, vol. 19, no. 10, pp. 1574–1579, 2001.

[201] M. Smietana, W. J. Bock, P. Mikulic, and J. Chen, "Increasing sensitivity of arc-induced long-period gratings—pushing the fabrication technique toward its limits," *Measurement Science and Technology*, vol. 22, no. 1, p. 015201, 2011.

[202] A. F. Collings and F. Caruso, "Biosensors: recent advances," *Reports on Progress in Physics*, vol. 60, no. 11, pp. 1397–1445, 1997.

[203] A. Sassolas, L. J. Blum, and B. D. Leca-Bouvier, "Immobilization strategies to develop enzymatic biosensors," *Biotechnology Advances*, vol. 30, no. 3, pp. 489–511, 2012.

[204] F. S. Ligler and C. A. R. Taitt, *Optical biosensors: present and future*. Gulf Professional Publishing, 2002.

[205] X. Wang, X. Lu, and J. Chen, "Development of biosensor technologies for analysis of environmental contaminants," *Trends in Environmental Analytical Chemistry*, vol. 2, pp. 25–32, 2014.

[206] C. I. Justino, A. C. Freitas, R. Pereira, A. C. Duarte, and T. A. Rocha Santos, "Recent developments in recognition elements for chemical sensors and biosensors," *TrAC - Trends in Analytical Chemistry*, vol. 68, pp. 2–17, 2015.

[207] C. A. M. McNulty and J. C. Dent, "Rapid identification of Campylobacter pylori (C. pyloridis) by preformed enzymes," *Journal of Clinical Microbiology*, vol. 25, no. 9, pp. 1683–1686, 1987.

[208] S. L. W. On and B. Holmes, "Assessment of enzyme detection tests useful in identification of campylobacteria," *Journal of Clinical Microbiology*, vol. 30, no. 3, pp. 746–749, 1992.

[209] D. J. Monk and D. R. Walt, "Optical fiber-based biosensors," *Analytical and Bioanalytical Chemistry*, vol. 379, no. 7-8, pp. 931–945, 2004.

[210] I. E. Tothill, "Recent advances in the development of sensors for toxicity monitoring," in *Sensors for Chemical and Biological Applications* (M. K. Ram and V. R. Bhethanabotla, eds.), ch. 5, pp. 135–172, CRC Press, 2010.

[211] J. G. Bruno, T. Phillips, M. P. Carrillo, and R. Crowell, "Plastic-adherent DNA aptamer-magnetic bead and quantum dot sandwich assay for campylobacter detection," *Journal of Fluorescence*, vol. 19, no. 3, pp. 427–435, 2009.

[212] G. Keramas, D. D. Bang, M. Lund, M. Madsen, S. E. Rasmussen, H. Bunkenborg, P. Telleman, and C. B. V. Christensen, "Development of a sensitive DNA microarray suitable for rapid detection of Campylobacter spp.," *Molecular and Cellular Probes*, vol. 17, no. 4, pp. 187–196, 2003.

[213] G. Keramas, D. D. Bang, M. Lund, M. Madsen, H. Bunkenborg, P. Telleman, and C. B. V. Christensen, "Use of culture, PCR analysis, and DNA microarrays for detection of Campylobacter jejuni and Campylobacter coli from chicken feces," *Journal of Clinical Microbiology*, vol. 42, no. 9, pp. 3985–3991, 2004.

[214] B. Van Dorst, J. Mehta, K. Bekaert, E. Rouah-Martin, W. De Coen, P. Dubruel, R. Blust, and J. Robbens, "Recent advances in recognition elements of food and environmental biosensors: A review," *Biosensors and Bioelectronics*, vol. 26, no. 4, pp. 1178–1194, 2010.

[215] B. M. Paddle, "Biosensors for chemical and biological agents of defence interest," *Biosensors and Bioelectronics*, vol. 11, no. 11, pp. 1079–1113, 1996.

[216] J. L. McKillip and M. Drake, "Real-time nucleic acid–based detection methods for pathogenic bacteria in food," *Journal of Food Protection*, vol. 67, no. 4, pp. 823–832, 2004.

[217] M. E. A. Downs, "Prospects for nucleic acid biosensors," *Biochemical Society Transactions*, vol. 19, no. Biosensors, pp. 39–43, 1991.

[218] E. Harlow and D. Lane, *Using antibodies: a laboratory manual*. Cold Spring Harbor Laboratory Press, 1999.

[219] S. Patris, M. Vandeput, and J. M. Kauffmann, "Antibodies as target for affinity biosensors," *TrAC - Trends in Analytical Chemistry*, vol. 79, pp. 239–246, 2016.

[220] E. Droz, M. Taborelli, P. Descouts, T. N. C. Wells, and R. C. Werlen, "Covalent immobilization of immunoglobulins G and Fab' fragments on gold substrates for scanning force microscopy imaging in liquids," *Journal of Vacuum Science & Technology B: Microelectronics and Nanometer Structures*, vol. 14, no. 2, p. 1422, 1996.

[221] V. Gaudin, "Advances in biosensor development for the screening of antibiotic residues in food products of animal origin – a comprehensive review," *Biosensors and Bioelectronics*, vol. 90, pp. 363–377, apr 2017.

[222] L. X. Tiefenauer, S. Kossek, C. Padeste, and P. Thiébaud, "Towards amperometric immunosensor devices," *Biosensors and Bioelectronics*, vol. 12, no. 3, pp. 213–223, 1997.

[223] C.-l. Feng, Y.-h. Xu, and L.-m. Song, "Study on highly sensitive potentiometric IgG immunosensor," *Sensors and Actuators B: Chemical*, vol. 66, no. 1-3, pp. 190–192, 2000.

[224] M. I. Prodromidis, "Impedimetric immunosensors—A review," *Electrochimica Acta*, vol. 55, no. 14, pp. 4227–4233, 2010.

[225] M. Hnaiein, W. Hassen, A. Abdelghani, C. Fournier-Wirth, J. Coste, F. Bessueille, D. Leonard, and N. Jaffrezic-Renault, "A conductometric immunosensor based on functionalized magnetite nanoparticles for E. coli detection," *Electrochemistry Communications*, vol. 10, no. 8, pp. 1152–1154, 2008.

[226] S. Kurosawa, J.-W. Park, H. Aizawa, S.-I. Wakida, H. Tao, and K. Ishihara, "Quartz crystal microbalance immunosensors for environmental monitoring," *Biosensors and Bioelectronics*, vol. 22, no. 4, pp. 473–481, 2006.

[227] A. A. Suleiman and G. G. Guilbault, "Recent developments in piezoelectric immunosensors. A review," *The Analyst*, vol. 119, no. 11, p. 2279, 1994.

[228] L. Tedeschi, C. Domenici, A. Ahluwalia, F. Baldini, and A. Mencaglia, "Antibody immobilisation on fibre optic TIRF sensors," *Biosensors and Bioelectronics*, vol. 19, no. 2, pp. 85–93, 2003.

[229] M. Leenaars and C. F. M. Hendriksen, "Critical steps in the production of polyclonal and monoclonal antibodies: evaluation and recommendations," *ILAR Journal*, vol. 46, no. 3, pp. 269–279, 2005.

[230] Thermo Fisher Scientific, "*Campylobacter jejuni* polyclonal antibody." Product data sheet. https://www.thermofisher.com/antibody/product/Campylobacter-jejuni-Antibody-Polyclonal/PA1-7205, Date Accessed: 28/03/2018.

[231] M. Nakazawa, M. Mukumoto, and K. Miyatake, "Production and purification of polyclonal antibodies," in *Immunoelectron Microscopy* (S. D. Schwartzbach and T. Osafune, eds.), vol. 657, ch. 5, pp. 63–74, Humana Press, 2010.

[232] Biorad, "*Campylobacter jejuni* antibody." Product data sheet. https://images.bio-rad-antibodies.com/datasheets/datasheet-1744-9036.pdf, Date Accessed: 28/03/2018.

[233] G. Smith, "Filamentous fusion phage: novel expression vectors that display cloned antigens on the virion surface," *Science*, vol. 228, no. 4705, pp. 1315–1317, 1985.

[234] A. Singh, D. Arutyunov, C. M. Szymanski, and S. Evoy, "Bacteriophage based probes for pathogen detection," *The Analyst*, vol. 137, no. 15, p. 3405, 2012.

[235] A. Ahmed, J. V. Rushworth, N. A. Hirst, and P. A. Millner, "Biosensors for whole-cell bacterial detection," *Clinical Microbiology Reviews*, vol. 27, no. 3, pp. 631–646, 2014.

[236] C. D. Jepson and J. B. March, "Bacteriophage lambda is a highly stable DNA vaccine delivery vehicle," *Vaccine*, vol. 22, no. 19, pp. 2413–2419, 2004.

[237] V. Verma, K. Harjai, and S. Chhibber, "Characterization of a T7-like lytic bacteriophage of Klebsiella pneumoniae B5055: a potential therapeutic agent," *Current Microbiology*, vol. 59, no. 3, pp. 274–281, 2009.

[238] S. Balasubramanian, I. B. Sorokulova, V. J. Vodyanoy, and A. L. Simonian, "Lytic phage as a specific and selective probe for detection of Staphylococcus aureus—a surface plasmon resonance spectroscopic study," *Biosensors and Bioelectronics*, vol. 22, no. 6, pp. 948–955, 2007.

[239] R. Blasco, M. Murphy, M. Sanders, and D. Squirrell, "Specific assays for bacteria using phage mediated release of adenylate kinase," *Journal of Applied Microbiology*, vol. 84, no. 4, pp. 661–666, 1998.

[240] C. R. H. Raetz and C. Whitfield, "Lipopolysaccharide endotoxins," *Annual Review of Biochemistry*, vol. 71, no. 1, pp. 635–700, 2002.

[241] L. Gervais, M. Gel, B. Allain, M. Tolba, L. Brovko, M. Zourob, R. Mandeville, M. Griffiths, and S. Evoy, "Immobilization of biotinylated bacteriophages on biosensor surfaces," *Sensors and Actuators, B: Chemical*, vol. 125, no. 2, pp. 615–621, 2007.

[242] S. Song, L. Wang, J. Li, C. Fan, and J. Zhao, "Aptamer-based biosensors," *TrAC Trends in Analytical Chemistry*, vol. 27, no. 2, pp. 108–117, 2008.

[243] R. Sharma, K. V. Ragavan, M. S. Thakur, and K. S. Raghavarao, "Recent advances in nanoparticle based aptasensors for food contaminants," *Biosensors and Bioelectronics*, vol. 74, pp. 612–627, 2015.

[244] H. P. Dwivedi, R. D. Smiley, and L. A. Jaykus, "Selection and characterization of DNA aptamers with binding selectivity to Campylobacter jejuni using whole-cell SELEX," *Applied Microbiology and Biotechnology*, vol. 87, no. 6, pp. 2323–2334, 2010.

[245] S. H. Ohk, O. K. Koo, T. Sen, C. M. Yamamoto, and A. K. Bhunia, "Antibody-aptamer functionalized fibre-optic biosensor for specific detection of Listeria monocytogenes from food," *Journal of Applied Microbiology*, vol. 109, no. 3, pp. 808–817, 2010.

[246] D. Shangguan, Y. Li, Z. Tang, Z. C. Cao, H. W. Chen, P. Mallikaratchy, K. Sefah, C. J. Yang, and W. Tan, "Aptamers evolved from live cells as effective molecular probes for cancer study," *Proceedings of the National Academy of Sciences*, vol. 103, no. 32, pp. 11838–11843, 2006.

[247] C. K. O'Sullivan, "Aptasensors – the future of biosensing?," *Analytical and Bioanalytical Chemistry*, vol. 372, no. 1, pp. 44–48, 2002.

[248] atdbio, "SELEX." https://www.atdbio.com/img/articles/selex-large.png, Date Accessed: 16/11/2018.

[249] F. C. Dudak and s. H. Boyaci, "Peptide-based surface plasmon resonance biosensor for detection of staphylococcal enterotoxin B," *Food Analytical Methods*, vol. 7, no. 2, pp. 506–511, 2014.

[250] S. W. Lee, S. Korposh, R. Selyanchyn, and T. Kunitake, "Fundamentals and perspectives of molecular imprinting in sensor applications," in *Handbook of Molecular Imprinting: Advanced Sensor Applications* (S. W. Lee and T. Kunitake, eds.), ch. 1, pp. 3–63, Pan Stanford Publishing Pte. Ltd., 2013.

[251] P. Çakir, A. Cutivet, M. Resmini, B. T. S. Bui, and K. Haupt, "Protein-Size Molecularly Imprinted Polymer Nanogels as Synthetic Antibodies, by Localized Polymerization with Multi-initiators," *Advanced Materials*, vol. 25, no. 7, pp. 1048–1051, 2013.

[252] Y. Hu, R. Liu, Y. Zhang, and G. Li, "Improvement of extraction capability of magnetic molecularly imprinted polymer beads in aqueous media via dual-phase solvent system," *Talanta*, vol. 79, no. 3, pp. 576–582, 2009.

[253] B. S. Batlokwa, J. Mokgadi, T. Nyokong, and N. Torto, "Optimal template removal from molecularly imprinted polymers by pressurized hot water extraction," *Chromatographia*, vol. 73, no. 5-6, pp. 589–593, 2011.

[254] P. Fernández-Álvarez, M. Le Noir, and B. Guieysse, "Removal and destruction of endocrine disrupting contaminants by adsorption with molecularly imprinted polymers followed by simultaneous extraction and phototreatment," *Journal of Hazardous Materials*, vol. 163, no. 2-3, pp. 1107–1112, 2009.

[255] S. Korposh, I. Chianella, A. Guerreiro, S. Caygill, S. Piletsky, S. W. James, and R. P. Tatam, "Selective vancomycin detection using optical fibre long period gratings functionalised with molecularly imprinted polymer nanoparticles," *The Analyst*, vol. 139, no. 9, pp. 2229–2236, 2014.

[256] C. Quesada-Molina, B. Claude, A. M. García-Campaña, M. del Olmo-Iruela, and P. Morin, "Convenient solid phase extraction of cephalosporins in milk

using a molecularly imprinted polymer," *Food Chemistry*, vol. 135, no. 2, pp. 775–779, 2012.

[257] E. Turiel, A. Martín-Esteban, and J. L. Tadeo, "Molecular imprinting-based separation methods for selective analysis of fluoroquinolones in soils," *Journal of Chromatography A*, vol. 1172, no. 2, pp. 97–104, 2007.

[258] P. Götz, K. H. Wolf, H. Voß, H. P. Schmauder, and D. Schlosser, "Bioreactor techniques," in *Mehods in Biotechnology* (H. P. Schmauder, ed.), ch. 3, pp. 86–155, Taylor & Francis, 2003.

[259] K. L. Brogan and D. R. Walt, "Optical fiber-based sensors: application to chemical biology," *Current Opinion in Chemical Biology*, vol. 9, no. 5, pp. 494–500, 2005.

[260] R. Gupta and N. Chaudhury, "Entrapment of biomolecules in sol–gel matrix for applications in biosensors: Problems and future prospects," *Biosensors and Bioelectronics*, vol. 22, no. 11, pp. 2387–2399, 2007.

[261] M. D. Trevan, "Enzyme immobilization by entrapment," in *New Protein Techniques* (J. M. Walker, ed.), ch. 36, pp. 491–494, Humana Press, 1988.

[262] A. Subramanian, S. J. Kennel, P. I. Oden, K. B. Jacobson, J. Woodward, and M. J. Doktycz, "Comparison of techniques for enzyme immobilization on silicon supports," *Enzyme and Microbial Technology*, vol. 24, no. 1-2, pp. 26–34, 1999.

[263] B. Abdallah and A. Ros, "Surface coatings for microfluidic-based biomedical devices," in *Microfluidic Devices for Biomedical Applications* (L. Xiujun James and Y. Zhou, eds.), ch. 2, pp. 63–99, Woodhead Publishing Limited, 1st ed., 2013.

[264] L. C. Shriver-Lake, B. Donner, R. Edelstein, K. Breslin, S. K. Bhatia, and F. S. Ligler, "Antibody immobilization using heterobifunctional crosslinkers," *Biosensors and Bioelectronics*, vol. 12, no. 11, pp. 1101–1106, 1997.

[265] A. Gang, G. Gabernet, L. D. Renner, L. Baraban, and G. Cuniberti, "A simple two-step silane-based (bio-) receptor molecule immobilization without additional binding site passivation," *RSC Advances*, vol. 5, no. 45, pp. 35631–35634, 2015.

[266] M. M. F. Choi, "Progress in enzyme-based biosensors using optical transducers," *Microchimica Acta*, vol. 148, no. 3-4, pp. 107–132, 2004.

[267] J. J. Cras, C. A. Rowe-Taitt, D. A. Nivens, and F. S. Ligler, "Comparison of chemical cleaning methods of glass in preparation for silanization," *Biosensors and Bioelectronics*, vol. 14, no. 8-9, pp. 683–688, 1999.

[268] Y. Jung, J. Y. Jeong, and B. H. Chung, "Recent advances in immobilization methods of antibodies on solid supports.," *The Analyst*, vol. 133, no. 6, pp. 697–701, 2008.

[269] N. Herzer, S. Hoeppener, and U. S. Schubert, "Fabrication of patterned silane based self-assembled monolayers by photolithography and surface reactions on silicon-oxide substrates," *Chemical Communications*, vol. 46, no. 31, pp. 5634–5652, 2010.

[270] M. Hijazi, V. Stambouli, M. Rieu, V. Barnier, G. Tournier, T. Demes, J. P. Viricelle, and C. Pijolat, "Synthesis and characterization of tin dioxide thick film modified by APTES in vapor and liquid phases," *Journal of Materials Science*, vol. 53, no. 1, pp. 727–738, 2018.

[271] B. Seed, "Silanizing glassware," in *Current Protocols in Cell Biology*, pp. 2–3, John Wiley & Sons, Inc., 2001.

[272] R. Janissen, L. Oberbarnscheidt, and F. Oesterhelt, "Optimized straight forward procedure for covalent surface immobilization of different biomolecules for single molecule applications," *Colloids and Surfaces B: Biointerfaces*, vol. 71, no. 2, pp. 200–207, 2009.

[273] B. Arkles, *Silane Coupling Agents: Connecting Across Boundaries*. Morrisville, PA: Gelest, Inc, 3rd ed., 2014.

[274] J. A. Camarero, "Recent developments in the site-specific immobilization of proteins onto solid supports," *Biopolymers - Peptide Science Section*, vol. 90, no. 3, pp. 450–458, 2008.

[275] X. C. Chen Liu, "EDC-mediated oligonucleotide immobilization on a long period grating optical biosensor," *Journal of Biosensors and Bioelectronics*, vol. 6, no. 2, pp. 1–6, 2015.

[276] N. S. K. Gunda, M. Singh, L. Norman, K. Kaur, and S. K. Mitra, "Optimization and characterization of biomolecule immobilization on silicon substrates using (3-aminopropyl)triethoxysilane (APTES) and glutaraldehyde linker," *Applied Surface Science*, vol. 305, pp. 522–530, 2014.

[277] A. Jain, G. A. Hirata, M. H. Farías, and F. F. Castillón, "Synthesis and characterization of (3-Aminopropyl)trimethoxy-silane (APTMS) functionalized Gd 2 O 3 :Eu 3+ red phosphor with enhanced quantum yield," *Nanotechnology*, vol. 27, no. 6, p. 065601, 2016.

[278] F. Morhard, J. Pipper, R. Dahint, and M. Grunze, "Immobilization of antibodies in micropatterns for cell detection by optical diffraction," *Sensors and Actuators B: Chemical*, vol. 70, no. 1-3, pp. 232–242, 2000.

[279] C. Oh, J.-H. Lee, Y.-G. Lee, Y.-H. Lee, J.-W. Kim, H.-H. Kang, and S.-G. Oh, "New approach to the immobilization of glucose oxidase on non-porous silica microspheres functionalized by (3-aminopropyl)trimethoxysilane (APTMS)," *Colloids and Surfaces B: Biointerfaces*, vol. 53, no. 2, pp. 225–232, 2006.

[280] R. D. Das, S. Maji, S. Das, and C. RoyChaudhuri, "Optimization of covalent antibody immobilization on macroporous silicon solid supports," *Applied Surface Science*, vol. 256, no. 20, pp. 5867–5875, 2010.

[281] M. Zhu, M. Z. Lerum, and W. Chen, "How To prepare reproducible, homogeneous, and hydrolytically stable aminosilane-derived layers on silica," *Langmuir*, vol. 28, no. 1, pp. 416–423, 2012.

[282] H. D. Duong and J. I. Rhee, "Exploitation of thermo-effect of rhodamine B entrapped in sol-gel matrix and silica gel for temperature detection," *Sensors and Actuators, B: Chemical*, vol. 124, no. 1, pp. 18–23, 2007.

[283] Q. Zhang, C. Xue, Y. Yuan, J. Lee, D. Sun, and J. Xiong, "Fiber surface modification technology for fiber-optic localized surface plasmon resonance biosensors," *Sensors*, vol. 12, no. 3, pp. 2729–2741, 2012.

[284] B. P. Calabia, F. Ninomiya, H. Yagi, A. Oishi, K. Taguchi, M. Kunioka, and M. Funabashi, "Biodegradable poly(butylene succinate) composites reinforced by cotton fiber with silane coupling agent," *Polymers*, vol. 5, no. 1, pp. 128–141, 2013.

[285] Thermo Scientific, "Crosslinking Technical Handbook." https://www.thermofisher.com/content/dam/LifeTech/Images/integration/1602163_CrosslinkingHB_lores.pdf, Date Accessed: 13/07/2018.

[286] ThermoFisher Scientific, "Crosslinking and Photoactivatable Reagents," in *Molecular Probes Handbook*, ch. 5, pp. 170–188, ThermoFisher Scientific, 11th ed., 2010.

[287] V. V. Hira, A. L. de Jong, K. Ferro, M. Khurshed, R. J. Molenaar, and C. J. Van Noorden, "Comparison of different methodologies and cryostat versus paraffin sections for chromogenic immunohistochemistry," *Acta Histochemica*, vol. 121, pp. 125–134, feb 2019.

[288] F. Chiavaioli, P. Biswas, C. Trono, S. Bandyopadhyay, A. Giannetti, S. Tombelli, N. Basumallick, K. Dasgupta, and F. Baldini, "Towards sensitive label-free immunosensing by means of turn-around point long period fiber gratings," *Biosensors and Bioelectronics*, vol. 60, pp. 305–310, 2014.

[289] N. A. Masdor, Z. Altintas, and I. E. Tothill, "Sensitive detection of Campylobacter jejuni using nanoparticles enhanced QCM sensor," *Biosensors and Bioelectronics*, vol. 78, pp. 328–336, 2016.

[290] P. Pilla, V. Malachovská, A. Borriello, A. Buosciolo, M. Giordano, L. Ambrosio, A. Cutolo, and A. Cusano, "Transition mode long period grating biosensor with functional multilayer coatings.," *Optics Express*, vol. 19, no. 2, pp. 512–526, 2011.

[291] J. M. Walker, *Biosensors and biodetection*, vol. 504. Humana Press, 2009.

[292] G. T. Hermanson, *Bioconjugate techniques*. Elsevier Science & Technology, 2nd ed., 2010.

[293] L. McKeen, "Introduction to food irradiation and medical sterilization," in *The Effect of Sterilization on Plastics and Elastomers* (M. Lawrence, ed.), ch. 1, pp. 1–40, Elsevier, 3rd ed., 2012.

[294] L. S. Wong, F. Khan, and J. Micklefield, "Selective covalent protein immobilization: strategies and applications," *Chemical Reviews*, vol. 109, no. 9, pp. 4025–4053, 2009.

[295] M. D. Trevan, "Enzyme immobilization by covalent bonding," in *New Protein Techniques* (J. M. Walker, ed.), ch. 37, pp. 495–510, New Jersey: Humana Press, 1988.

[296] N. G. Welch, J. A. Scoble, B. W. Muir, and P. J. Pigram, "Orientation and characterization of immobilized antibodies for improved immunoassays (Review)," *Biointerphases*, vol. 12, no. 2, p. 02D301, 2017.

[297] B. Lu, M. R. Smyth, and R. O'Kennedy, "Oriented immobilization of antibodies and its applications in immunoassays and immunosensors.," *The Analyst*, vol. 121, no. 3, pp. 29R–32R, 1996.

[298] X. Muñoz-Berbel, N. Godino, O. Laczka, E. Baldrich, F. X. Muñoz, and F. J. del Campo, "Impedance-based biosensors for pathogen detection," in *Principles of Bacterial Detection: Biosensors, Recognition Receptors and Microsystems*, ch. 15, pp. 341–376, New York, NY: Springer New York, 2008.

[299] Y. Mu, H. Zhang, X. Zhao, D. Song, Z. Wang, J. Sun, M. Li, and Q. Jin, "An optical biosensor for monitoring antigen recognition based on surface plasmon resonance using avidin-biotin system," *Sensors*, vol. 1, no. 3, pp. 91–101, 2001.

[300] J. E. Zull, J. Reed-Mundell, Y. W. Lee, D. Vezenov, N. P. Ziats, J. M. Anderson, and C. N. Sukenik, "Problems and approaches in covalent attachment of peptides and proteins to inorganic surfaces for biosensor applications," *Journal of Industrial Microbiology*, vol. 13, no. 3, pp. 137–143, 1994.

[301] A. L. Koch, *The bacteria: their origin, structure, function and antibiosis*. Springer Netherlands, 1st ed., 2006.

[302] P. S. Bisen, "Microbial staining," in *Microbes in Practice*, vol. 1, ch. 6, pp. 139–155, New Delhi: IK International, 2014.

[303] J. R. Lawrence, T. J. Beveridge, and R. G. E. Murray, "Sampling and staining for light microscopy," in *Methods for General and Molecular Microbiology* (C. A. Reddy, T. J. Beveridge, J. A. Breznak, G. A. Marzluf, T. M. Schmidt, and L. R. Snyder, eds.), ch. 2, pp. 19–33, American Society of Microbiology, 3rd ed., 2007.

[304] W. W. Chan, "Staining procedures," in *Clinical Microbiology Procedures Handbook* (D. L. Church, ed.), ch. 3, pp. 3.2.1.1–3.2.3.6, Washington, D.C.: American Society of Microbiology, 4th ed., 2016.

[305] H. Zollinger, *Color chemistry*. Wiley-VCH, 3rd ed., 2003.

[306] B. Bhattacharyya and R. Banerjee, *Environmental Biotechnology*. Oxford University Press, 2007.

[307] M. Rohde, "Microscopy," in *Taxonomy of Prokaryotes* (F. Rainey and A. Oren, eds.), vol. 38, ch. 4, pp. 61–100, Academic Press, 2011.

[308] P. J. Bishop and G. Neumann, "The history of the Ziehl-Neelsen stain," *Tubercle*, vol. 51, no. 2, pp. 196–206, 1970.

[309] C. Lamanna, "The nature of the acid-fast stain.," *Journal of Bacteriology*, vol. 52, no. 1, pp. 99–103, 1946.

[310] V. Annam, M. Kulkarni, and R. Puranik, "Comparison of the modified fluorescent method and conventional Ziehl-Neelsen method in the detection of acidfast bacilli in lymphnode aspirates," *CytoJournal*, vol. 6, no. 1, p. 13, 2009.

[311] T. J. Beveridge, "Use of the Gram stain in microbiology," *Biotechnic and Histochemistry*, vol. 76, no. 3, pp. 111–118, 2001.

[312] C. Jenkins, R. J. Rentenaar, L. Landraud, and S. Brisse, "Enterobacteriaceae," in *Infectious Diseases* (J. Cohen, W. G. Powderly, and S. M. Opal, eds.), ch. 180, pp. 1565–1578.e2, Elsevier, 4th ed., 2017.

[313] D. Claus, "A standardized Gram staining procedure," *World Journal of Microbiology & Biotechnology*, vol. 8, no. 4, pp. 451–452, 1992.

[314] G. M. Carlone, M. J. Valadez, and M. J. Pickett, "Methods for distinguishing Gram-positive from Gram-negative Bacteria," *Journal of Clinical Microbiology*, vol. 16, no. 6, pp. 1157–1159, 1983.

[315] J. A. Hawkins and N. Gubbay, "Cold Ziehl-Neelsen stain for campylobacter in gastric biopsy specimens.," *Journal of Clinical Pathology*, vol. 42, no. 12, p. 1309, 1989.

[316] J. W. Bartholomew and H. Finkelstein, "Relationship of cell wall staining to gram differentiation.," *Journal of Bacteriology*, vol. 75, no. 1, pp. 77–84, 1958.

[317] S. L. Bardy, S. Y. M. Ng, and K. F. Jarrell, "Prokaryotic motility structures," *Microbiology*, vol. 149, no. 2, pp. 295–304, 2003.

[318] R. Lowry, S. Balboa, J. L. Parker, and J. G. Shaw, "Aeromonas flagella and colonisation mechanisms," in *Advances in Microbial Physiology* (R. K. Poole, ed.), vol. 65, ch. 5, pp. 203–256, Elsevier Ltd., 1st ed., 2014.

[319] J. Lowy and J. Hanson, "Electron microscope studies of bacterial flagella," *Journal of Molecular Biology*, vol. 11, no. 2, pp. 293–313, 1965.

[320] E. Leifson, "A method of staining bacterial flagella and capsules together with a study of the origin of flagella," *Journal of Bacteriology*, vol. 20, no. 3, pp. 203–211, 1930.

[321] R. Piccolomini, G. Di Bonaventura, M. Neri, A. Di Girolamo, G. Catamo, and E. Pizzigallo, "Usefulness of Leifson staining method in diagnosis of Helicobacter pylori infection," *Journal of Clinical Microbiology*, vol. 37, no. 1, pp. 199–201, 1999.

[322] E. Leifson, "Staining, shape and arrangement of bacterial flagella.," *Journal of bacteriology*, vol. 62, no. 4, pp. 377–89, 1951.

[323] G. Knaysi, "The endospore of bacteria," *Bacteriology Reviews*, vol. 12, no. 1, pp. 19–77, 1948.

[324] M. D. Lechtman, J. W. Bartholomew, A. Phillips, and M. Russo, "Rapid methods of staining bacterial spores at room temperature," *Journal of Bacteriology*, vol. 89, no. 3, pp. 848–854, 1965.

[325] T. Sandle, *Pharmaceutical microbiology*. Woodhead Publishing, 2015.

[326] E. E. Anthony, "A note on capsule staining," *Science*, vol. 73, no. 1890, pp. 319–320, 1931.

[327] J. H. Barrington, M. Partridge, S. W. James, and R. P. Tatam, "Experimental determination of 2 nd order phase matching turning points in long period gratings," in *2016 IEEE SENSORS*, pp. 1–3, IEEE, 2016.

[328] M. Partridge, S. W. James, J. H. Barrington, and R. P. Tatam, "Overwrite fabrication and tuning of long period gratings," *Optics Express*, vol. 24, no. 20, pp. 1449–1451, 2016.

[329] J. Fulenwider and M. Dakes, "Hand-held tool for optical-fibre end preparation," *Electronics Letters*, vol. 13, no. 19, pp. 578–580, 1977.

[330] N. C. Gallagher and G. L. Wise, "A theoretical analysis of the properties of median filters," *IEEE Transactions on Acoustics, Speech, and Signal Processing*, vol. 29, no. 6, pp. 1136–1141, 1981.

[331] J. J. Davenport, J. Hodgkinson, J. R. Saffell, and R. P. Tatam, "Noise analysis for CCD-based ultraviolet and visible spectrophotometry," *Applied Optics*, vol. 54, no. 27, pp. 8135–8144, 2015.

[332] W. Kern, "The evolution of silicon wafer cleaning technology," *Journal of The Electrochemical Society*, vol. 137, no. 6, p. 1887, 1990.

[333] Aldrich, "Suggestions for cleaning glassware," Tech. Rep. AL-228, Sigma-Aldrich, Milwaukee, WI, USA.

[334] J. M. Bennett, "When is a surface clean?," *Optics and Photonics News*, vol. 1, no. 6, p. 29, 1990.

[335] H. K. Pulker, "Cleaning of substrate surfaces," in *Coatings on Glass*, ch. 4, pp. 60–72, Elsevier Science, 2nd ed., 1999.

[336] T. Putner, "Methods of cleaning glass by vapour degreasing and ultrasonically agitated solvents," *British Journal of Applied Physics*, vol. 10, no. 7, pp. 332–336, 1959.

[337] I. F. Stowers, "Advances in cleaning metal and glass surfaces to micron-level cleanliness," *Journal of Vacuum Science and Technology*, vol. 15, no. 2, pp. 751–754, 1978.

[338] A. Belkind and S. Gershman, "Plasma cleaning of surfaces," tech. rep., Jinghong Vacuum Thin Film (Shenzhen) Co. Ltd., 2008.

[339] M. Castaño-Álvarez, D. F. Pozo Ayuso, M. García Granda, M. T. Fernández-Abedul, J. Rodríguez García, and A. Costa-García, "Critical points in the fabrication of microfluidic devices on glass substrates," *Sensors and Actuators, B: Chemical*, vol. 130, no. 1, pp. 436–448, 2008.

[340] C. A. Goss, D. H. Charych, and M. Majda, "Application of (3-Mercaptopropyl)trimethoxysilane as a molecular adhesive in the fabrication of vapor-deposited gold electrodes on glass substrates," *Analytical Chemistry*, vol. 63, no. 1, pp. 85–88, 1991.

[341] M. J. Roberts, G. A. Lindsay, W. N. Herman, and K. J. Wynne, "Thermally stable nonlinear optical films by alternating polyelectrolyte deposition on hydrophobic substrates," *Journal of the American Chemical Society*, vol. 120, no. 43, pp. 11202–11203, 1998.

[342] University of Cambridge, "Acid Piranha Solution: User Guidance," 2016.

[343] L. Henke, N. Nagy, and U. J. Krull, "An AFM determination of the effects on surface roughness caused by cleaning of fused silica and glass substrates in the process of optical biosensor preparation," *Biosensors and Bioelectronics*, vol. 17, no. 6-7, pp. 547–555, 2002.

[344] J. Keith, L. C. Hess, W. U. Spendel, J. A. Cox, and G. E. Pacey, "The investigation of the behavior of a long period grating sensor with a copper sensitive coating fabricated by layer-by-layer electrostatic adsorption," *Talanta*, vol. 70, no. 4, pp. 818–822, 2006.

[345] D. Kim, Y. Zhang, K. Cooper, and A. Wang, "Fibre-optic interferometric immuno-sensor using long period grating," *Electronics Letters*, vol. 42, no. 6, p. 324, 2006.

[346] W. J. Dressick, C. S. Dulcey, J. H. Georger, G. S. Calabrese, and J. M. Calvert, "Covalent binding of Pd catalysts to ligating self-assembled monolayer films for selective electroless metal deposition," *Journal of The Electrochemical Society*, vol. 141, no. 1, p. 210, 1994.

[347] S. N. Magonov, M.-H. Whangbo, and W. Weiss, *Surface analysis with STM and AFM*. Weinheim (Federal Republic of Germany): VCH, 12th ed., 1997.

[348] E. S. Gadelmawla, M. M. Koura, T. M. A. Maksoud, I. M. Elewa, and H. H. Soliman, "Roughness parameters," *Journal of Materials Processing Technology*, vol. 123, no. 1, pp. 133–145, 2002.

[349] M. Raposo, Q. Ferreira, and P. A. Ribeiro, "A guide for atomic force microscopy analysis of soft-condensed matter," in *Modern Research and Educational Topics in Microscopy* (A. Mendez-Vilas and D. J., eds.), pp. 758–769, Formatex, 2007.

[350] A. Maksumov, R. Vidu, A. Palazoglu, and P. Stroeve, "Enhanced feature analysis using wavelets for scanning probe microscopy images of surfaces," *Journal of Colloid and Interface Science*, vol. 272, no. 2, pp. 365–377, 2004.

[351] J. Corres, I. Matias, J. Bravo, and F. Arregui, "Tapered optical fiber biosensor for the detection of anti-gliadin antibodies," *Sensors and Actuators B: Chemical*, vol. 135, no. 1, pp. 166–171, 2008.

[352] Ultimaker, "PLA." Technical data sheet. https://ultimaker.com/download/74970/UM180821%20TDS%20PLA%20RB%20V11.pdf, Date Accessed: 02/02/2019.

[353] Y. Cheng, S. Deng, P. Chen, and R. Ruan, "Polylactic acid (PLA) synthesis and modifications: a review," *Frontiers of Chemistry in China*, vol. 4, no. 3, pp. 259–264, 2009.

[354] L. Avérous, "Polylactic acid: synthesis, properties and applications," in *Monomers, Polymers and Composites from Renewable Resources* (M. Naceur Belgacem and A. Gandini, eds.), ch. 21, pp. 433–450, Elsevier, 2008.

[355] P. J. Rae and D. M. Dattelbaum, "The properties of poly(tetrafluoroethylene) (PTFE) in compression," *Polymer*, vol. 45, no. 22, pp. 7615–7625, 2004.

[356] Fluoroproducts Dupont, "Teflon® PTFE fluoropolymer resin: Properties Handbook," tech. rep., DuPontTM Technical Report H-37051-3, 1996.

[357] M. Qin, S. Hou, L. Wang, X. Feng, R. Wang, Y. Yang, C. Wang, L. Yu, B. Shao, and M. Qiao, "Two methods for glass surface modification and their application in protein immobilization," *Colloids and Surfaces B: Biointerfaces*, vol. 60, no. 2, pp. 243–249, 2007.

[358] S. Pal, M. J. Kim, and J. M. Song, "Quantitation of surface coverage of oligonucleotides bound to chip surfaces: a fluorescence-based approach using alkaline phosphatase digestion," *Lab on a Chip*, vol. 8, no. 8, p. 1332, 2008.

[359] M. W. Hoffmann, L. Mayrhofer Dr, O. Casals Dr, L. Caccamo, F. Hernez-Ramirez, G. Lilienkamp, W. Daum, M. Moseler, A. Waag, H. Shen, and J. D. Prades, "A highly selective and self-powered gas sensor via organic surface functionalization of p-Si/n-ZnO diodes," *Advanced Materials*, vol. 26, no. 47, pp. 8017–8022, 2014.

[360] S. P. Pujari, L. Scheres, A. T. M. Marcelis, and H. Zuilhof, "Covalent surface modification of oxide surfaces," *Angewandte Chemie International Edition*, vol. 53, no. 25, pp. 6322–6356, 2014.

[361] F. Canfarotta, A. Poma, A. Guerreiro, and S. Piletsky, "Solid-phase synthesis of molecularly imprinted nanoparticles," *Nature Protocols*, vol. 11, no. 3, pp. 443–455, 2016.

[362] Thermo Scientific, "2,4,6-trinitrobenzene sulfonic acid (tnbs)." Product data sheet. https://www.thermofisher.com/document-connect/document-connect.html?url=https://assets.thermofisher.com/TFS-Assets/LSG/manuals/MAN0011392_TNBSA_UG.pdf&title=VXNlciBHdWlkZTogIFROQlNB, Date Accessed: 27/02/2018.

[363] R. Fields, "The rapid determination of amino groups with TNBS," in *Methods in Enzymology* (C. H. W. Hirs and S. N. Timasheff, eds.), vol. 454, ch. 38, pp. 464–468, Academic Press, 1972.

[364] S. Villa, P. Riani, F. Locardi, and F. Canepa, "Functionalization of Fe3O4NPs by silanization: use of amine (APTES) and thiol (MPTMS) silanes and their physical characterization," *Materials*, vol. 9, no. 10, 2016.

[365] S. Khaliq, S. W. James, and R. P. Tatam, "Fiber-optic liquid-level sensor using a long-period grating," *Optics Letters*, vol. 26, no. 16, p. 1224, 2001.

[366] R. R. Coombs, A. E. Mourant, and R. R. Race, "A new test for the detection of weak and "incomplete" RH agglutinins," *The British Journal of Experimental Pathology*, vol. 246, no. 6358, pp. 15–16, 1945.

[367] K. Catt, H. D. Niall, and G. W. Tregear, "Solid phase radioimmunoassay," *Nature*, vol. 213, no. 5078, pp. 825–827, 1967.

[368] K. Catt and G. W. Tregear, "Solid-phase radioimmunoassay in antibody-coated tubes," *Science*, vol. 158, no. 3808, pp. 1570–1572, 1967.

[369] B.-S. Lee, J.-S. Huang, G. D. L. P. Jayathilaka, S. S. Lateef, and S. Gupta, "Production of antipeptide antibodies," in *Immunoelectron Microscopy* (S. Schwartzbach and O. T., eds.), ch. 7, pp. 93–108, Humana Press, 2010.

[370] W. C. Hanly, J. E. Artwohl, and B. T. Bennett, "Review of polyclonal antibody production procedures in mammals and poultry," *ILAR Journal*, vol. 37, no. 3, pp. 93–118, 1995.

[371] M. L. Styers, J. Lowery, and E. Sztul, "Transient expression of epitope-tagged proteins in mammalian cells," in *Immunoelectron Microscopy* (S. Schwartzbach and T. Osafune, eds.), ch. 4, pp. 43–61, Humana Press, 2010.

[372] N. A. Masdor, *Development of immunosensors for the detection of Campylobacter jejuni*. Phd thesis, Cranfield University, 2016.

[373] G. S. Bailey, "The raising of a polyclonal antiserum to a protein," in *Basic Protein and Peptide Protocols* (J. M. Walker, ed.), ch. 40, pp. 381–388, New Jersey: Humana Press, 1994.

[374] D. Otter, "Milk — Physical and chemical properties," in *Encyclopedia of Food Sciences and Nutrition* (L. Trugo and P. M. Finglas, eds.), pp. 3957–3963, Academic Press, 2003.

[375] H. P. Erickson, "Size and shape of protein molecules at the nanometer level determined by sedimentation, gel filtration, and electron microscopy.," *Biological procedures online*, vol. 11, no. 8, pp. 32–51, 2009.

[376] S. Qinghong, Z. Ying, and S. Yan, "Influence of pH and ionic strength on the steric mass-action model parameters around the isoelectric point of protein," *Biotechnology Progress*, vol. 21, no. 2, pp. 516–523, 2008.

[377] Sigma-Aldrich, "Bovine serum albumin (bsa)." BSA. https://www.sigmaaldrich.com/content/dam/sigma-aldrich/product4/071/pbd-id_3v03_2.eps/_jcr_content/renditions/pbd-id_3v03_2-large.jpg, Date Accessed: 11/02/2019.

[378] J. Rangsansarid and K. Fukada, "Factors affecting the stability of O/W emulsion in BSA solution: Stabilization by electrically neutral protein at high ionic strength," *Journal of Colloid and Interface Science*, vol. 316, no. 2, pp. 779–786, 2007.

[379] A. S. Determan, B. G. Trewyn, V. S.-Y. Lin, M. Nilsen-Hamilton, and B. Narasimhan, "Encapsulation, stabilization, and release of BSA-FITC from polyanhydride microspheres," *Journal of Controlled Release*, vol. 100, no. 1, pp. 97–109, 2004.

[380] S. Kaushik, A. Pandey, U. K. Tiwari, and R. K. Sinha, "A label-free fiber optic biosensor for Salmonella typhimurium detection," *Optical Fiber Technology*, vol. 46, pp. 95–103, 2018.

[381] M. Lee and D. R. Walt, "A fiber-optic microarray biosensor using aptamers as receptors," *Analytical Biochemistry*, vol. 282, no. 1, pp. 142–146, 2000.

[382] F. Rusmini, Z. Zhong, and J. Feijen, "Protein immobilization strategies for protein biochips," *Biomacromolecules*, vol. 8, no. 6, pp. 1775–1789, 2007.

[383] S. J. Fowler, "The detection of proteins on blots using gold or immunogold," in *Basic Protein and Peptide Protocols* (J. M. Walker, ed.), ch. 28, pp. 239–256, Humana Press, 1994.

[384] A. Makaraviciute and A. Ramanaviciene, "Site-directed antibody immobilization techniques for immunosensors," *Biosensors and Bioelectronics*, vol. 50, pp. 460–471, 2013.

[385] D. J. Reen, "Enzyme-linked immunosorbent assay (ELISA)," in *Basic Protein and Peptide Protocols* (J. M. Walker, ed.), ch. 47, pp. 461–466, Humana Press, 1994.

[386] K. Rijal, A. Leung, P. M. Shankar, and R. Mutharasan, "Detection of pathogen Escherichia coli O157:H7 AT 70 cells/mL using antibody-immobilized biconical tapered fiber sensors.," *Biosensors and Bioelectronics*, vol. 21, no. 6, pp. 871–80, 2005.

[387] B. T. Wang and Q. Wang, "An interferometric optical fiber biosensor with high sensitivity for IgG/anti-IgG immunosensing," *Optics Communications*, vol. 426, no. May, pp. 388–394, 2018.

[388] Q. Yu, Q. Wang, B. Li, Q. Lin, and Y. Duan, "Technological development of antibody immobilization for optical immunoassays: progress and prospects," *Critical Reviews in Analytical Chemistry*, vol. 45, no. 1, pp. 62–75, 2015.

[389] J. Y. Zheng and L. J. Janis, "Influence of pH, buffer species, and storage temperature on physicochemical stability of a humanized monoclonal antibody LA298," *International Journal of Pharmaceutics*, vol. 308, no. 1-2, pp. 46–51, 2006.

[390] J. Grandke, U. Resch-Genger, W. Bremser, L. A. Garbe, and R. J. Schneider, "Quality assurance in immunoassay performance-temperature effects," *Analytical Methods*, vol. 4, no. 4, pp. 901–905, 2012.

[391] Perkin Elmer^{TM}Life Sciences, "How to optimize rapid and simple immunoassays.." Application notes. http://www.perkinelmer.com/CMSResources/Images/44-73052APP_DELFIAHowToOptimizeRapid.pdf, Date Accessed: 21/03/2019.

[392] IKA, "KS 4000 i control." Technical data sheet. https://www.ika.com/en/Products-Lab-Eq/Shakers-Vortex-mixer-Lab-shakers-csp-179/KS-4000-i-control-Technical-Data-cptd-3510000/, Date Accessed: 03/02/2019.

[393] Y. Han, D. Mayer, A. Offenhäusser, and S. Ingebrandt, "Surface activation of thin silicon oxides by wet cleaning and silanization," *Thin Solid Films*, vol. 510, no. 1-2, pp. 175–180, 2006.

[394] I. Migneault, C. Dartiguenave, M. J. Bertrand, and K. C. Waldron, "Glutaraldehyde: behavior in aqueous solution, reaction with proteins, and application to enzyme crosslinking," *BioTechniques*, vol. 37, no. 5, pp. 790–802, 2004.

[395] J. H. Chua, R.-E. Chee, A. Agarwal, S. M. Wong, and G.-J. Zhang, "Label-free electrical detection of cardiac biomarker with complementary metal-oxide semiconductor-compatible silicon nanowire sensor arrays," *Analytical Chemistry*, vol. 81, no. 15, pp. 6266–6271, 2009.

[396] P. M. Fauchet, "Porous silicon optical label-free biosensors," in *Device Applications of Silicon Nanocrystals and Nanostructures* (N. Koshida, ed.), ch. 10, p. 344, Springer US, 1st ed., 2009.

[397] S. Lepinay, A. Staff, A. Ianoul, and J. Albert, "Improved detection limits of protein optical fiber biosensors coated with gold nanoparticles," *Biosensors and Bioelectronics*, vol. 52, pp. 337–344, 2014.

[398] T. Liu, Y. Zhao, Z. Zhang, P. Zhang, J. Li, R. Yang, C. Yang, and L. Zhou, "A fiber optic biosensor for specific identification of dead Escherichia coli O157:H7," *Sensors and Actuators, B: Chemical*, vol. 196, pp. 161–167, 2014.

[399] S. M. Tripathi, W. J. Bock, P. Mikulic, R. Chinnappan, A. Ng, M. Tolba, and M. Zourob, "Long period grating based biosensor for the detection of Escherichia coli bacteria," *Biosensors and Bioelectronics*, vol. 35, no. 1, pp. 308–312, 2012.

[400] D. R. Karsa, "Biocides," in *Handbook for Cleaning/Decontamination of Surfaces* (I. Johansson and P. Somasundaran, eds.), ch. F.2, pp. 593–623, Elsevier, 2007.

[401] M. A. Hayat, "Glutaraldehyde: role in electron microscopy," *Micron And Microscopica Acta*, vol. 17, no. 2, pp. 115–135, 1986.

[402] K. Pal, A. T. Paulson, and D. Rousseau, "Biopolymers in controlled-release delivery systems," in *Modern Biopolymer Science* (S. Kasapis, J. B. Ubbink, and I. T. Norton, eds.), ch. 16, pp. 519–557, Academic Press, 2009.

[403] K. E. Rasmussen and J. Albrechtsen, "Glutaraldehyde. The influence of pH, temperature, and buffering on the polymerization rate," *Histochemistry*, vol. 38, no. 1, pp. 19–26, 1974.

[404] S. D. Mazumdar, M. Hartmann, P. Kämpfer, and M. Keusgen, "Rapid method for detection of salmonella in milk by surface plasmon resonance (SPR)," *Biosensors and Bioelectronics*, vol. 22, no. 9-10, pp. 2040–2046, 2007.

[405] S. K. Rasmussen, L. K. Rasmussen, D. Weilguny, and A. B. Tolstrup, "Manufacture of recombinant polyclonal antibodies," *Biotechnology Letters*, vol. 29, no. 6, pp. 845–852, 2007.

[406] Acumedia, "Campy Cefex Agar." Technical data sheet. https://foodsafety.neogen.com/pdf/acumedia_pi/7718_pi.pdf, Date Accessed: 18/03/2019.

[407] Acumedia, "*Campylobacter* Supplement." Technical data sheet. https://foodsafety.neogen.com/pdf/acumedia_pi/7981_pi.pdf, Date Accessed: 19/03/2019.

[408] Oxoid, "AnaeroJar." https://assets.thermofisher.com/TFS-Assets/MBD/product-images/F104101~p.eps-650.jpg, Date Accessed: 19/03/2019.

[409] Thermo Scientific, "Bolton selective enrichment broth." http://www.oxoid.com/UK/blue/prod_detail/prod_detail.asp?pr=CM0983&org=154&c=UK&lang=EN, Date Accessed: 19/03/2019.

[410] J. R. Brigati and V. A. Petrenko, "Thermostability of landscape phage probes," *Analytical and Bioanalytical Chemistry*, vol. 382, no. 6, pp. 1346–1350, 2005.

[411] H. Dooley, M. F. Flajnik, and A. J. Porter, "Selection and characterization of naturally occurring single-domain (IgNAR) antibody fragments from immunized sharks by phage display," *Molecular Immunology*, vol. 40, no. 1, pp. 25–33, 2003.

[412] S. Jung, S. Kim, H. Bae, H.-S. Lim, and H.-J. Bae, "Expression of thermostable bacterial β-glucosidase (BglB) in transgenic tobacco plants," *Bioresource Technology*, vol. 101, no. 18, pp. 7144–7150, 2010.

[413] A. Usami, A. Ohtsu, S. Takahama, and T. Fujii, "The effect of pH, hydrogen peroxide and temperature on the stability of human monoclonal antibody," *Journal of Pharmaceutical and Biomedical Analysis*, vol. 14, no. 8-10, pp. 1133–1140, 1996.

[414] R. van der Linden, L. Frenken, B. de Geus, M. Harmsen, R. Ruuls, W. Stok, L. de Ron, S. Wilson, P. Davis, and C. Verrips, "Comparison of physical chemical properties of llama VHH antibody fragments and mouse monoclonal antibodies," *Biochimica et Biophysica Acta (BBA) - Protein Structure and Molecular Enzymology*, vol. 1431, no. 1, pp. 37–46, 1999.

[415] K. Kramer, M. Fiedler, A. Skerra, and B. Hock, "A generic strategy for subcloning antibody variable regions from the scFv phage display vector pCANTAB 5 E into pASK85 permits the economical production of Fab fragments and leads to improved recombinant immunoglobulin stability," *Biosensors and Bioelectronics*, vol. 17, no. 4, pp. 305–313, 2002.

[416] S. A. Khan and J. Iqbal, "Polyclonal-antibody-mediated insolubilization and stabilization of papain," *Biotechnology and Applied Biochemistry*, vol. 32, no. 2, p. 89, 2003.

[417] L. Radoshevich and P. Cossart, "Listeria monocytogenes: towards a complete picture of its physiology and pathogenesis," *Nature Reviews Microbiology*, vol. 16, no. 1, pp. 32–46, 2018.

[418] B. Swaminathan and P. Gerner-Smidt, "The epidemiology of human listeriosis," *Microbes and Infection*, vol. 9, no. 10, pp. 1236–1243, 2007.

[419] R. L. Buchanan, L. G. Gorris, M. M. Hayman, T. C. Jackson, and R. C. Whiting, "A review of Listeria monocytogenes: an update on outbreaks, virulence, dose-response, ecology, and risk assessments," *Food Control*, vol. 75, pp. 1–13, 2017.

[420] S. T. Ooi and B. Lorber, "Gastroenteritis due to Listeria monocytogenes," *Clinical Infectious Diseases*, vol. 40, no. 9, pp. 1327–1332, 2005.

[421] S.-k. Eng, P. Pusparajah, N.-S. Ab Mutalib, H.-l. Ser, K.-g. Chan, and L.-h. Lee, "Salmonella : A review on pathogenesis, epidemiology and antibiotic resistance," *Frontiers in Life Science*, vol. 8, no. 3, pp. 284–293, 2015.

[422] P. F. Teunis, F. Kasuga, A. Fazil, I. D. Ogden, O. Rotariu, and N. J. Strachan, "Dose–response modeling of salmonella using outbreak data," *International Journal of Food Microbiology*, vol. 144, no. 2, pp. 243–249, 2010.

[423] S. B. Zimmerman, "Shape and compaction of Escherichia coli nucleoids," *Journal of Structural Biology*, vol. 156, no. 2, pp. 255–261, 2006.

[424] K. E. Heiman, R. K. Mody, S. D. Johnson, P. M. Griffin, and L. H. Gould, "Escherichia coli O157 outbreaks in the United States, 2003–2012," *Emerging Infectious Diseases*, vol. 21, no. 8, pp. 1293–1301, 2015.

[425] P. F. Teunis, I. D. Ogden, and N. J. Strachan, "Hierarchical dose response of E . coli O157:H7 from human outbreaks incorporating heterogeneity in exposure," *Epidemiology and Infection*, vol. 136, no. 6, pp. 761–770, 2008.

[426] J. A. Davies, G. K. Anderson, T. J. Beveridge, and H. C. Clark, "Chemical mechanism of the gram stain and synthesis of a new electron-opaque marker for electron microscopy which replaces the iodine mordant of the stain," *Journal of Bacteriology*, vol. 156, no. 2, pp. 837–845, 1983.

[427] S. Romero, R. F. Schell, and D. R. Pennell, "Rapid method for the differentiation of Gram-positive and Gram-negative bacteria on membrane filters," *Journal of Clinical Microbiology*, vol. 26, no. 7, pp. 1378–1382, 1988.

[428] A. Popescu and R. J. Doyle, "The Gram stain after more than a century," *Biotechnic & Histochemistry*, vol. 71, pp. 145–151, jan 1996.

[429] A. Katz, A. Alimova, Min Xu, E. Rudolph, M. Shah, H. Savage, R. Rosen, S. McCormick, and R. Alfano, "Bacteria size determination by elastic light scattering," *IEEE Journal of Selected Topics in Quantum Electronics*, vol. 9, no. 2, pp. 277–287, 2003.

[430] A. Brunsting and P. F. Mullaney, "Differential Light Scattering from Spherical Mammalian Cells," *Biophysical Journal*, vol. 14, no. 6, pp. 439–453, 1974.

[431] P. J. Wyatt and D. T. Phillips, "Structure of single bacteria from light scattering," *Journal of Theoretical Biology*, vol. 37, no. 3, pp. 493–501, 1972.

[432] S. J. Webb, "Factors affecting the viability of air-borne bacteria. III The role of bonded water and protein structure in the death of air-borne cells," *Canadian Journal of Microbiology*, vol. 5, pp. 649–669, dec 1959.

[433] P. Y. Liu, L. K. Chin, W. Ser, H. F. Chen, C. M. Hsieh, C. H. Lee, K. B. Sung, T. C. Ayi, P. H. Yap, B. Liedberg, K. Wang, T. Bourouina, and Y. Leprince-Wang, "Cell refractive index for cell biology and disease diagnosis: Past, present and future," *Lab on a Chip*, vol. 16, no. 4, pp. 634–644, 2016.

[434] H. Baccar, M. B. Mejri, I. Hafaiedh, T. Ktari, M. Aouni, and A. Abdelghani, "Surface plasmon resonance immunosensor for bacteria detection," *Talanta*, vol. 82, no. 2, pp. 810–814, 2010.

[435] L. Diéguez, N. Darwish, M. Mir, E. Martínez, M. Moreno, and J. Samitier, "Effect of the refractive index of buffer solutions in evanescent optical biosensors," *Sensor Letters*, vol. 7, pp. 851–855, oct 2009.

[436] D. J. Mason and D. M. Powelson, "Nuclear division as observed in live bacteria by a new technique.," *Journal of Bacteriology*, vol. 71, no. 4, pp. 474–9, 1956.

[437] A. Arcas, F. Dutra, R. Allil, and M. Werneck, "Surface plasmon resonance and bending loss-based U-shaped plastic optical fiber biosensors," *Sensors*, vol. 18(2), no. 648, pp. 1–16, 2018.

[438] M. I. Zibaii, A. Kazemi, H. Latifi, M. K. Azar, S. M. Hosseini, and M. H. Ghezelaiagh, "Measuring bacterial growth by refractive index tapered fiber optic biosensor," *Journal of Photochemistry and Photobiology B: Biology*, vol. 101, no. 3, pp. 313–320, 2010.

[439] B. K. Oh, W. Lee, B. S. Chun, Y. M. Bae, W. H. Lee, and J. W. Choi, "Surface plasmon resonance immunosensor for the detection of Yersinia enterocolitica," *Colloids and Surfaces A: Physicochemical and Engineering Aspects*, vol. 257-258, pp. 369–374, 2005.

[440] K. Zhou, L. Zhang, X. Chen, and I. Bennion, "Optic sensors of high refractive-index responsivity and low thermal cross sensitivity that use fiber Bragg gratings of $>80^{o}$ tilted structures," *Optics Letters*, vol. 31, no. 9, p. 1193, 2006.

[441] I. Buchwalow, V. Samoilova, W. Boecker, and M. Tiemann, "Non-specific binding of antibodies in immunohistochemistry: fallacies and facts," *Scientific Reports*, vol. 1, pp. 1–6, dec 2011.

[442] E. Rigas, J. M. Hallam, H. D. Ford, T. O. H. Charrett, and R. P. Tatam, "Dual-channel OCT for velocity measurement in microfluidic channels," in *26th International Conference on Optical Fiber Sensors*, (Washington, D.C.), p. ThD4, OSA, 2018.

[443] Thermo Fisher Scientific, "ViaGram Red+ Bacterial Gram Stain and Viability Kit (V-7023)." Product information. https://www.thermofisher.com/order/catalog/product/V7023?SID=srch-srp-V7023, Date Accessed: 28/03/2018.

[444] Y. G. Han, B. H. Lee, W. T. Han, U. C. Paek, and Y. Chung, "Fibre-optic sensing applications of a pair of long-period fibre gratings," *Measurement Science and Technology*, vol. 12, no. 7, pp. 778–781, 2001.

[445] S. W. James, I. Ishaq, G. J. Ashwell, and R. P. Tatam, "Cascaded long-period gratings with nanostructured coatings," *Optics Letters*, vol. 30, p. 2197, sep 2005.

[446] S. W. James, S. Korposh, S.-W. Lee, and R. P. Tatam, "A long period grating-based chemical sensor insensitive to the influence of interfering parameters," *Optics Express*, vol. 22, no. 7, p. 8012, 2014.

[447] R. P. Murphy, S. W. James, and R. P. Tatam, "Multiplexing of fiber-optic long-period grating-based interferometric sensors," *Journal of Lightwave Technology*, vol. 25, no. 3, pp. 825–829, 2007.

[448] R. Y. N. Wong, *Advanced fibre optic long period grating sensors; design, fabrication and sensing*. Phd thesis, Cranfield University, 2014.

[449] T. Allsop, F. Floreani, K. Jedrzejewski, P. Marques, R. Romero, D. Webb, and I. Bennion, "Spectral characteristics of tapered LPG device as a sensing element for refractive index and temperature," *Journal of Lightwave Technology*, vol. 24, pp. 870–878, feb 2006.

[450] R. Jarzebinska, C. S. Cheung, S. W. James, and R. P. Tatam, "Response of the transmission spectrum of tapered optical fibres to the deposition of a nanostructured coating," *Measurement Science and Technology*, vol. 20, no. 3, 2009.

[451] A. Iadicicco, S. Campopiano, M. Giordano, and A. Cusano, "Spectral behavior in thinned long period gratings: effects of fiber diameter on refractive index sensitivity," *Applied Optics*, vol. 46, no. 28, p. 6945, 2007.